A UNIFYING MODEL FOR ISOPRENE EMISSION BY PLANTS

Catherine Morfopoulos

A dissertation submitted in fulfillments of the requirements for the Degree of Philosophy of the Imperial College London, Department of Life Sciences.

July 2014

Abstract

Isoprene is the most important biogenic organic volatile compound emitted by terrestrial vegetation into the atmosphere, in term of amount and effects on atmospheric chemistry. Primary environmental drivers of isoprene production are photosynthetic photon flux density (*PPFD*), leaf temperature (*T*) and internal CO_2 concentration (C_i). Robust process-based modelling approaches are needed to assess how future changes in these environmental drivers may affect isoprene emissions and consequently atmospheric chemistry, air quality and (indirectly) the radiative forcing of climate.

I present an original, conceptually simple model for isoprene emission by plants based on the hypothesis that the electron flux available for isoprene biosynthesis depends on the balance between the supply of reducing power generated by the light reactions of photosynthesis and the demand for reducing power in carbon fixation and photorespiration. I explain the physiological reasoning that led me to propose this.

Using various leaf-scale measurements of carbon assimilation and isoprene emission, including a laboratory study I conducted on black poplar, I show that the model can reproduce well the variations of isoprene emission with *PPFD,* temperature, and C_i. The model also reproduces the tendency for the fraction of carbon re-emitted as isoprene to increase with increasing *PPFD*, and for the quantum efficiency of isoprene emission to decrease with increasing CO_2 concentration. The model is shown to systematically outperform mo§dels that are in common use today.

I also analysed the *PPFD* and temperature responses of carbon assimilation and isoprene emission as measured above the forest canopy. The model was upscaled and shown to reproduce key responses shown in two long-term flux monitoring datasets from temperate mixed forests. I discuss future research needs and the potential for this model to be further scaled up for global analyses.

Declaration of Originality

I Catherine Morfopoulos declare that this thesis is my own work and has not been submitted in any form for another degree or diploma at any university or other institute. Information derived from the published and unpublished work of others has been acknowledged in the text and a list of references is given in the bibliography.

Copyright Declaration

The copyright of this thesis rests with the author and is made available under Creative Commons Attribution Non-Commercial No Derivatives licence. Researchers are free to copy, distribute or transmit the thesis on the condition that they attribute it, that they do not use it for commercial purposes and that they do not alter, transform or build upon. For any reuse or redistribution, researchers must clear to others the licence terms of this work.

Catherine Morfopoulos

Department of Life Sciences, Imperial College of London

Acknowledgments

As I put the final touches to my thesis, I realise this work marks not only the end of my PhD but also the end of a big chapter of my life, which started long before this work. I also realise that this is a unique occasion on which to thank a number of people for making it all possible.

First and foremost, I would like to express my deepest gratitude to my supervisor, Colin Prentice, who has given me the opportunity to 'go back to Science'. This was a unique chance for me to do the most exciting and joyful 'job' of my life and I cannot thank him enough for that. Thank you Colin for your guidance and encouragement during this study, for you help finding the perfect words to express my ideas, for the essential freedom you gave me in this work and for helping me achieve this PhD. If a PhD can be seen as a road trip that takes you from a place where you know absolutely nothing to a place where you are an independent scientist, then Colin is the best guide along this path than one could hope for. I wish every PhD student could have the chance to be supervised by someone like Colin.

I also would like to thank my co-supervisor, Josep Peñuelas, for his support and enthusiasm. I realise that I was both lucky and privileged to have Colin and Josep as my mentors during this PhD. Despite having characters as opposed as the weather of their native countries (England and Catalonia), Colin and Josep also have many qualities in common. I have really appreciated their intelligence, their commitment, their true passion for science as well as their unerring curiosity. During this PhD, they have always allowed me to explore and go my own way, yet at the same time they have given me vital support. Thank you both for that!

This work couldn't have seen the light without the Marie Curie International Training Network GREENCYCLESII, funded by the EU FP7 initiative. I would like to acknowledge the tremendous work of writing, reporting and chasing done by Andrew Friend. Thank you Andrew for making this project possible! I also would like to thank all the Greencycles II fellows for making this experience unique: from fieldwork in the pouring rain at Peyresq to experiencing the Northern lights in Abisko. Thanks guys for all these nice souvenirs.

I would like to thank all the members of Imperial College that helped me during these last four years. In particular, my gratitude goes to my Imperial advisor Jo Haigh for her interest in my work, her support and her always-pertinent comments. Thanks also to Maria Martin-Calvo, Diana Anderson, Christine Short, Anthony Fitzgerald, Sally Power, Alexa Lord and Apostolos Voulgarakis.

During this PhD, I also had the occasion to spend some time at the Centre for Ecological Research and Forestry Applications, Barcelona-Spain (CREAF). I would like to thank all the member of CREAF for the warm welcome they gave me. In particular, all my gratitude goes to Dominik Sperlich, Iolanda Fillela, Joan Llusià (and Josep of course!) for saving me from a nervous breakdown after a few instrument/ plant material disasters. Since this experience I have acquired an unbounded respect for experimentalists!

I have been lucky to work on a topic that has been both challenging and fulfilling. This work brought me to meet the 'BVOC community' where I found fantastic support.

Many people have contributed in some way or another to this work, but I wish to express my gratitude especially to Ülo Niinemets for his priceless help and great sense of humor (he never held a grudge against me despite giving a rough ride to his model), Trevor Keenan, Malcolm Possell (his lively emails always cheered me up), Almut Arneth, Michael Barkley, Rüdiger Grote; for kindly sharing their data thanks to Zhihong Sun, Quentin Laffineur, Bernard Heinesch, Karena McKinney, Shelley Pressley; and for their kindness, explanations and patience, Todd Rosenstiel, Russell Monson and Thomas Sharkey.

I would like also to thank all the members of the Geography Department of the University of Bristol and BRIDGE. Special thanks to Paul Valdes and Andy Ridgwell for their *ssss*-support. Thanks also to Jeni, Pru, Angela, Jo and Pati. For their help on large scale modelling, thanks to Renato Spahni, Peter Cox (pleasure meeting you eventually ☺), Stephen Sitch and Lina Mercado. Thanks to Susan Solomon for her help and wisdom when I needed it the most. And going all the way back to the beginning, thanks to Michael Schulz and Yves Balkanski for their warmth humanity and generosity.

I am grateful to both my examiners, Prof Timothy Barraclough (Imperial College London) and Dr Victor Brovkin (Max-Plant Institute) for serving on my examination committee and their interest in my work.

I also would like to thanks my friends and family for their comfort and help during these last years. I feel fortunate to have so many good friends. Thanks to the Bristol Gang Scoob & Lou, Jem & Ses, Dee & Lol, Jo & Ash, Rex & Zoe, and so many others. Thanks to Hannah & Rob, Nicole & Karl, Em & Paul, Steph & Kev. Thanks also to all my lovely French friends Delphine, Michel & Christian, Marie, Béné, Kiki & Jean-Luc, Franck, Véro & Ludo, Beryl &Pat, les Balcons, Mike, Misio…and of course to the Belgium family Pierre, Anne, Béné, Jean-Franc & Fabienne, Renaud, Dré & Zon, Héloise. A big thanks to my cousin Basia. And above all, I am so so grateful for the 'grannies' Alice and Ka, for always being there when I needed them.

As for you Pierre, thank you for your love and patience, and for standing by me through it all. Professionally, it was a joy working with you. Your sharpness, your curiosity and your love for science are delightful. Thank you also for challenging me (despite having to deal with my grumpiness when you do so) and for not shouting 'boring' every time I was talking isoprene at home. As for the rest, no words can express '*tout l'amour que j'ai pour toi'*. How lucky I am to ride on the storm with you. Here's to a lot more fun darling!

Last, but certainly not least, I would like to thank my both sons Zacharie and Milan. Over the last few years they had to bear with two busy parents, missed birthdays, forgotten school plays and a stressed out mummy. Despite this they managed to give me an incredible amount of support and encouragement for such little monkeys. Thanks you Zach and Milan for being such great kids and reminding me what life is really about; after all, this work is dedicated to you.

"Data without models are chaos, but models without data are fantasy."

EG Nisbet, EJ Dlugokencky, and P Bousquet, *Science 31 January 2014: 343 (6170), 493-495*

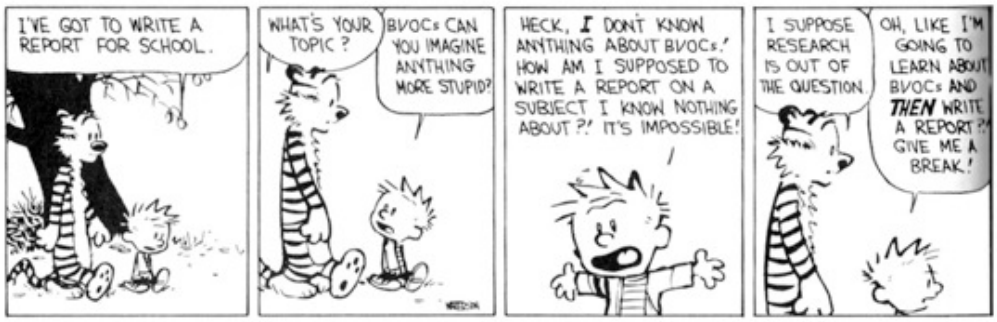


TABLE OF CONTENTS

1 Foreword 9
1.1 Aims and objectives 9
1.2 Introduction 11
1.2.1 Isoprene: what, why and how? 11
1.2.2 Interactions with the atmosphere 21
1.2.3 Observations 23
1.2.4 Existing schemes for isoprene modelling 26
1.2.5 Thesis structure 28

2 The new hypothesis and model 30
2.1 Introduction 30
2.2 Photosynthesis, C_3 Carbon assimilation and the Farquhar model 30
2.3 The Niinemets model 40
2.4 Improving on the Niinemets model 45
2.4.1 Analysis of the Niinemets model 45
2.4.2 The new modelling approach 46
2.5 Conclusions 58

3 A unifying conceptual model for the environmental responses of isoprene emissions from plants 59
Abstract 60
3.1 Introduction 61
3.2 Hypothesis 63
3.3 Tests of the hypothesis 67
3.3.1 Responses to PPFD 67
3.3.2 Responses to C_i 74
3.3.3 Responses to leaf temperature 78
3.3.4 Discussion 82
3.3.5 Conclusion 85
Acknowledgments 85
Annex 3A.1 – Comparison of Model 1 and Model 2 86
Annex 3A.2 – Supplementary table and figure to Chapter III 92

4 Model evaluation at the leaf scale 93
Abstract 94
4.1 Introduction 95
4.2 Materials and methods 100
4.3 Results 109
4.3.1 Experiments varying C_i 109
4.3.2 Experiments varying PPFD 112
4.3.3 Global results 116
4.4 Discussion 117
Annex 4A.1- Comparison Model1 and Model2 122
Annex 4A.2 - Supplementary figures to Chapter IV 124

5 Evaluation of the model at canopy scale using a multi-layer approach 128
Abstract 128
5.1 Introduction 130
5.2 Material and methods 130
5.2.1 Observations/ site description 130
5.2.2 Data treatment /analysis 132

5.2.3 Leaf-level model of photosynthesis 133
5.2.4 Leaf-level models of isoprene 133
5.2.5 Scaling up from leaf to canopy 136
5.2.6 Model evaluation statistics 137
5.3 Results 138
5.3.1 General PPFD- and temperature responses 138
5.3.2 Model evaluation 143
5.4 Discussion 152
Annex 5A.1 – Supplementary figures to chapter V 156

6 Conclusions 158

Bibliography 163

Supplementary material 182
S1. The Guenther *et al.* (1993) algorithm **182**
S2. Model of photosynthetic carbon assimilation (Farquhar *et al.,* 1980) **183**
S3. List of publications **185**

1 Foreword

1.1 Aims and objectives

Volatile isoprenoids are the most important category of Biogenic Volatile Organic Compounds (BVOCs) emitted by terrestrial vegetation, both in terms of the amount of carbon involved and in terms of their impacts on atmospheric chemistry. Despite extensive research on this topic, the great majority of studies still use empirical models to predict how changes in climate and land use affect the emissions of volatile isoprenoids. To predict changes in emissions, empirical models consider the effect of each controlling factor separately. Yet, in reality, factors controlling emissions also influence each other. As an example, leaf temperature (one of the major controls of emission) is partly controlled by shortwave radiation and stomatal aperture; while leaf temperature, light intensity and stomatal aperture together influence BVOC emissions via the leaf-internal CO_2 concentration. Thus, the empirical approach has important limitations as it can potentially neglect unforeseen interactions between environmental drivers. The overall aim of the project was to overcome this problem and thus to propose *a new unifying strategy for process-based modelling of volatile isoprenoid emissions*, with particular attention to the response of emissions to changes in CO_2 concentration. This work focuses on isoprene, the most abundant isoprenoid released by terrestrial vegetation. While keeping in mind that the ultimate objective is improved global modelling (and thus the modelling approach needs to be kept as simple as possible), the study presented here concentrates on processes and observations at the leaf and canopy scales. The prospect of using the new isoprene emission model 'scaled up' in an Earth system modelling framework is addressed in the Conclusions.

The main specific objectives of this thesis are:

i. To improve current process-based modelling of isoprene emission and propose a new modelling approach,
ii. To test the validity of the hypothesis underlying the new modelling approach by revisiting a body of published data,
iii. To conduct, analyse and compare the model with the results of experiments following a specific protocol established to test the hypothesis,
iv. To upscale the model from the leaf to the canopy scale.

The work presented here received funding from the European Community's Seventh Framework Programme (FP7 2007–2013, grant agreement n° 238366), through the European Initial Training Network GREENCYCLES II. The objective of GREENCYCLES II was to *anticipate climate change and biospheric feedbacks within the Earth System to 2200* by improving predictive capability of Earth system models through linked data and modelling activities. In the frame of this thesis, the link between data and modelling activities has been achieved through a close collaboration with experimentalists at Centre for Ecological Research and Forestry Applications, Barcelona-Spain (CREAF).

The topic of isoprene is broad and complex, with many questions remaining. The following text attempts to summarize the different area of interest and to give an overview of the subject.

1.2 Introduction

1.2.1 Isoprene: what, why and how?

What?

With a total emission strength estimated to exceed 1 PgC a^{-1}, volatile isoprenoids (most importantly isoprene and monoterpenes) collectively represent the largest part of the total BVOC emitted by the terrestrial biosphere. Among these, the single most important molecule is isoprene, which accounts for about half of the total BVOC emissions (Laothawornkitkul *et al.*, 2009; Guenther *et al.*, 2012). Isoprene is emitted directly as it is produced (there is no storage in the leaf). It is highly reactive and thus is immediately involved in tropospheric chemistry and physics. A great deal of interest centres on the chemistry of isoprene. Thus it is interesting to start by looking at the molecule *isoprene* itself.

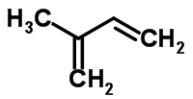
Isoprene, or 2-methyl-1,3-butadiene, is a colourless volatile unsaturated hydrocarbon of formula C_5H_8 (Table 1.1). It was first discovered in 1860 by a British chemist, C. Williams (Williams, 1860). Isoprene has a low boiling point of 34˚C and high vapour pressure of 60.8 kPa (at 20 °C) that explains its high volatility. Isoprene is insoluble in water, but has lipophilic proprieties. Therefore it can interact with lipids, including those constituting the membranes of biological cells. In the leaves, the production of C_5H_8 from CO_2 requires many reduction steps. Consequently, isoprene tends to act as electron donor, and to react in the presence of most oxidizing agents. The two double bonds of the molecule also make it readily polymerized and isoprene is the initial building block for many organic compounds such as terpenes, carotenoids, tocopherol (vitamin E) and natural rubber.

Why?

Global isoprene emissions are estimated to be about 500 $TgCa^{-1}$ (Laothawornkitkul *et al.*, 2009; Guenther *et al.*, 2012). Pike & Young (2009) note that the annual loss of carbon from terrestrial vegetation in the form of isoprene is equivalent to the weight of all human beings. In the same vein, Sharkey (2013) evaluates the annual isoprene release by vegetation as equivalent to '*300 000 Olympic-sized swimming pools*' (Sharkey, 2013). With a energetic cost estimated at 20 ATP and 14 NADPH per isoprene produced (Sharkey and Yeh 2001) and a carbon cost that can amount for more

than 2% of the leaf net carbon assimilation (Sharkey & Loreto, 1993; Lerdau & Throop, 1999) (up to 20% reported for high temperatures), the question of why plants emit isoprene is relevant. The adaptive significance of volatile isoprenoid emissions is still debated but considerable advances have been made during the last few years through the use of genetic manipulation (Sasaki *et al.*, 2005, 2007; Behnke *et al.*, 2007, 2010; Vickers *et al.*, 2009b). The leading hypothesis is that isoprene protects plant from heat damage, in particular during sunflecks, by stabilizing the thylakoid membrane (Sharkey & Singsaas, 1995; Singsaas *et al.*, 1997; Siwko *et al.*, 2007; Velikova *et al.*, 2011). Another well-supported hypothesis is that volatile isoprenoids protect the plant from oxidative stress by quenching Reactive Oxygen Species (ROS). ROS can originate externally through pollution (e.g. high ozone concentrations). But they are also generated internally under conditions of high-temperature or/and high-light stress, so this mechanism may be a principal way in which isoprene serves to protect the plant against heat damage (Velikova *et al.*, 2005; Fares *et al.*, 2006). However, other strategies exist to protect plants from heat and/or oxidative damage; and certain plants emit isoprene while others don't.

Table 1.1: Isoprene properties under the standard state of 25˚C and 100 kPa (except where noted otherwise)

Isoprene Properties	
Chemical structure	
Molecular formula	C_5H_8
Molar Mass	68.12 g mol^{-1}
Density	0.681 g cm^{-3}
Melting point	−143.95 °C
Boiling point	34.67˚C
Vapour pressure	60.8 kPa (20 °C)
Water solubility	0.7 g mL^{-1}

The distribution of plants emitting isoprene is large and doesn't follow any obvious environmental or phylogenetic logic. It is generally assumed that capacity to emit isoprene is mainly found in plants with C_3 carbon fixation metabolic pathway (Box 1.1). According to Pacifico *et al.* (2009), this assumption might result from a lack of measurements on species using other photosynthetic pathways and isoprene emissions have been detected in at least one C_4 plant (*Zea mays*: Evans *et al.*, 1982) and one Crassulacean Acid Metabolism (CAM) plant (*Opuntia lindheimeri*: Archer & Zitser, 1994). A survey of plants emitting isoprene can be found on the web from two compilations: the Sheffield database (Hewitt & Street, 1992; http://www.es.lancs.ac.uk/cnhgroup/download.html); and the University Corporation for Atmospheric Research (UCAR) database (Wiedinmyer *et al.*, 2004; http:// bai.acd.ucar.edu/Data/BVOC/index.shtml). The major groups of land plants (mosses, ferns and fern allies, gymnosperms and angiosperms) all include species that emit isoprene and others that don't. Even in the same genus, some members do produce isoprene and others don't. For instance all North American oaks emit isoprene whereas only a small proportion of European oaks do in significant amounts (Sharkey *et al.*, 2008). However, trees, particularly oak and aspen trees, are generally the biggest isoprene emitters, while most of the crops and desert plants are non-emitters. Thus the question 'why not?' can also be asked. Emerging studies, using the phylogeny of the isoprene synthesis pathway to explore the frequency of gains and losses of the trait (Monson *et al.*, 2013), are beginning to emerge – though not without raising some debate (Sharkey, 2013).

A trade–off seems to exist in the capacity of plants to emit isoprene and monoterpenes (formed of 2 isoprene units). Using data on 192 species from 48 plants families, Harrison *et al.* (2013) shown that isoprene versus monoterpene emission capacity follows a L-shape pattern: moderate to high BVOC emitters tend to emit either isoprene or monoterpenes, or if they emit one, they emit only small quantities of the other (Fig. 1.1). The same study reports a greater tendency to produce isoprene among light-demanding plants (Fig. 1.2). Other leaf traits, such as high photosynthetic capacity (A_{max}), short leaf lifespan, and high specific leaf area (SLA) are also characteristic of '*species with rapid growth in high-resource (including high-light environments)'*. The same association was also recently noted by (Dani *et al.*, 2014).

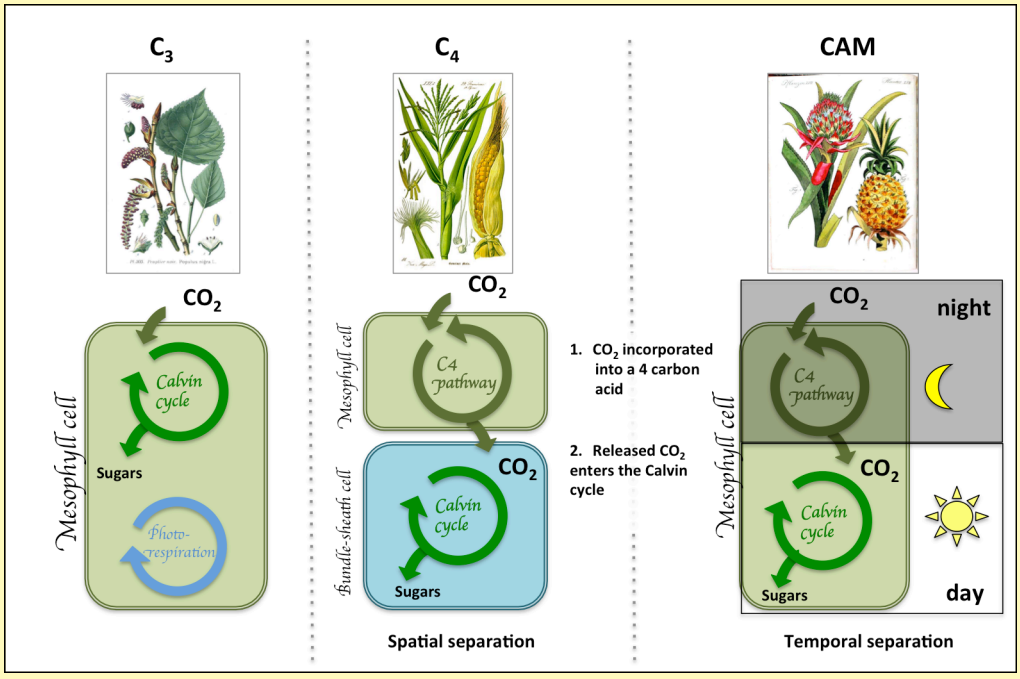
Box 1.1 Carbon fixation metabolic pathways

Carbon assimilation through photosynthesis is achieved differently by different species; the three biochemical mechanisms for carbon assimilation by plants are the C_3, the C_4 and the crassulacean acid metabolism (CAM) pathways. All these pathways transform CO_2 into sugars through the Calvin cycle. However, each pathway has different strategy for incorporating CO_2 to the Calvin cycle.

C_3 plants: C_3 pathway is the most common carbon fixation metabolic pathway and it is present in about 95% of the earth biomass. During the day the leaf stomata (pores at the surface of the leaf) open allowing CO_2 (and O_2) to enter inside the leaf. At the same time water is transpired and escapes outside the leave though the stomata. CO_2 is incorporated into the Calvin cycle and is further reduced to sugar. The first step of this process is a 3-carbon organic acid, and, is catalysed by the enzyme Ribulose-1,5-bisphosphate carboxylase/oxygenase (Rubisco). Because Rubisco has also an affinity for O_2, energy is lost through photorespiration cycles in C_3 plants. Plants with C_3 pathway have also a large water lost through leaf transpiration due to stomata aperture during the day.

C_4 plants: C_4 pathway is present in about 5% of the earth biomass. A large part of C_4 terrestrial plant species is represented by grasses, in particular food crops. C_4 plants developed a CO_2-concentration mechanism to avoid photorespiration. Here, CO_2 is first fixed in a 4-carbon organic acid within mesophyll cells. This organic acid releases CO_2 in a separate cell (the Bundle-sheath cell), where the Calvin cycle transforms CO_2 into sugars in absence of O_2. In comparison with C_3 plants, C_4 plants are characterised by higher water use efficiencies and higher photosynthetic efficiency especially under warmer temperatures where affinity of Rubisco for O_2 increases.

CAM plants: Like the C_4 plants, CAM plants also have a strategy to bypass photorespiration. Here, the CO_2-concentration mechanism is not spatial but temporal. The leaf opens its stomata during the night and atmospheric CO_2 is 'stocked' in the leaf in the form of a 4-carbon organic acid. During the day, the stomata shut, preventing water to be lost and O_2 to enter the leaf; the 4-carbon organic acid releases CO_2, which is transformed into sugar in the Calvin cycle. All these steps occur in the same mesophyll cell. CAM pathway's major advantage is very high water use efficiency due to closure of stomata during the day. This pathway is mainly found in desert plants.



Regionally, the humid tropics are the larger source of isoprene (Sharkey & Yeh, 2001; Guenther *et al.*, 2006; Sharkey *et al.*, 2008; Pacifico *et al.*, 2009). The first reason for that is that humid tropics harbour the greatest number of isoprene-emitting plants. The second reason is that these regions have the largest terrestrial vegetation biomass; or the amount of isoprene emitted at the regional scales on the ecosystem leaf's coverage. Finally, the humid tropical climate is associated with high relative humidity of the air. Under these conditions, where evaporative cooling is reduced due to low atmospheric vapour pressure deficit, the plant is likely to experience higher leaf temperature and consequently higher isoprene emission rate (isoprene steeply increases with increasing temperature) (Sharkey & Yeh, 2001).

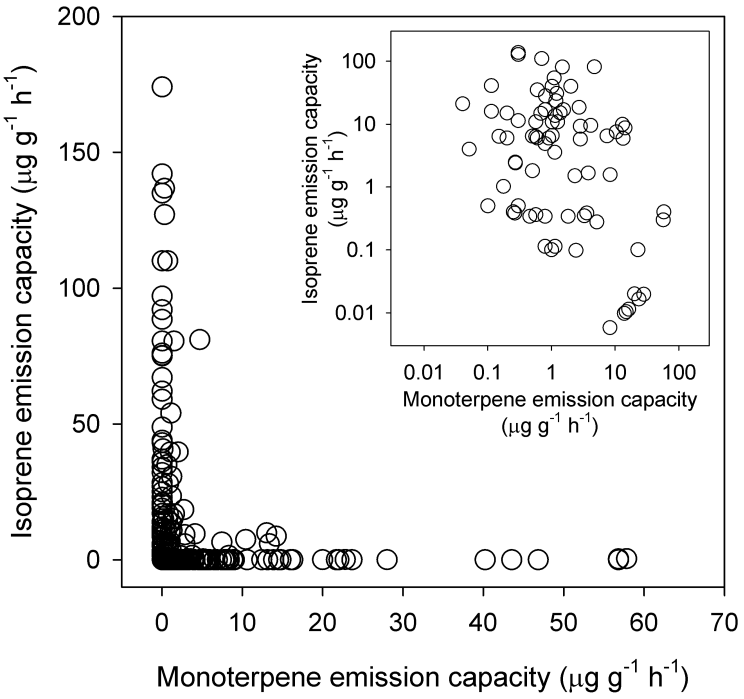


Figure 1.1: Trade-off between isoprene and monoterpene emission capacities. The main plot, the "L-graph", is based on 403 data points representing 192 species from 48 plant families, drawn from 35 individual studies on field-sampled adult plants. Non-zero emissions for *both* isoprene and monoterpene were reported for 80 of 403 cases; these are shown again in the inset panel, on $\log_{10}$-scaled axes. Figure from Harrison *et al*. (2013).

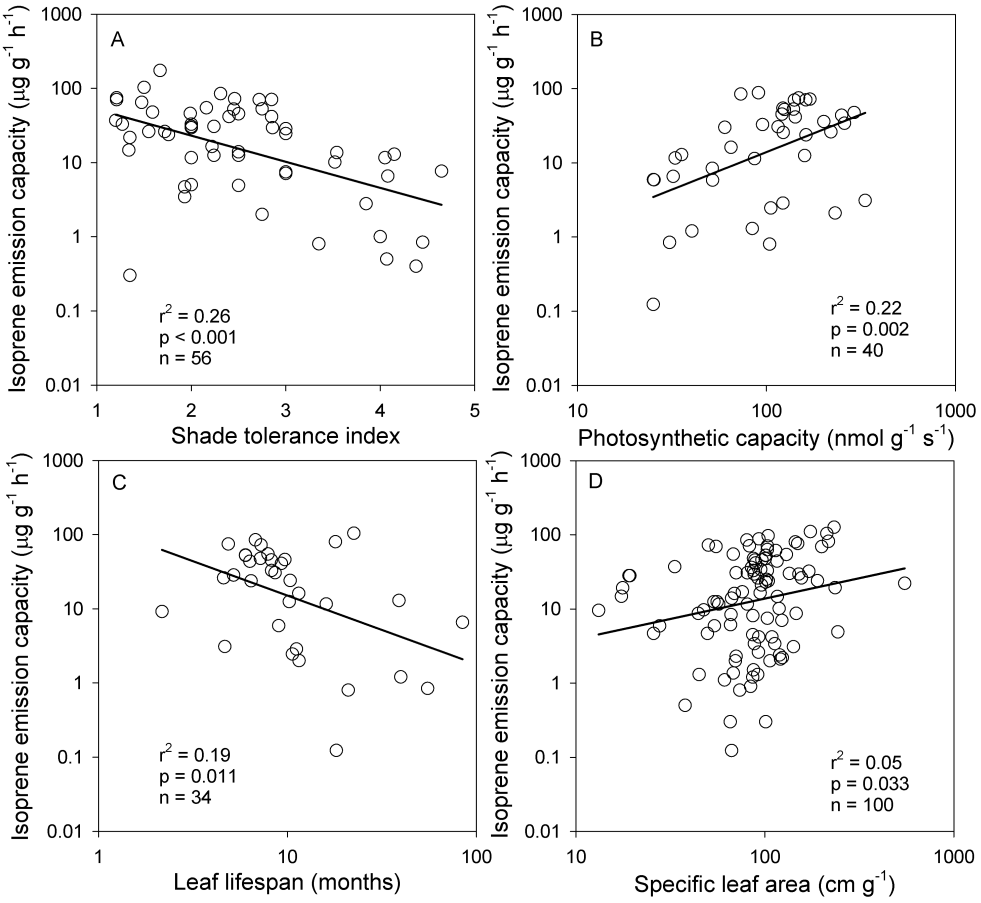


Figure 1.2: Relationship between isoprene emission capacity and traits related to species' ecological strategies: (**A**) shade tolerance index, (**B**) photosynthetic capacity, (**C**) leaf lifespan, (**D**) specific leaf area (SLA). Data are for 134 tree and shrub species from a broad range of families and vegetation types; in each graph each data point represents a different species. SLA data were sourced from the same publications as the emissions data; shade tolerance indices are from Niinemets & Valladares (2006); photosynthesis and leaf lifespan data were derived from a variety of published and unpublished sources. Photosynthetic capacity refers to measurements made in the field under near-optimal light, temperature and soil moisture conditions. Figure from Harrison *et al*. (2013).

How?

Biochemical mechanisms

Two separate metabolic pathways in plants can produce the unsaturated C_5 unit, isopentenyl diphosphate (IDP), and its isomer dimethylallyl diphosphate (DMADP), which is the base of isoprenoid molecules. One is the mevalonic acid (MVA) pathway and takes place in the cytosol. The other, more recently discovered, is the 2-C-methyl-D-erythritol 4-phosphate (MEP) or 1-deoxy-D-xylulose 5-phosphate (DXP) pathway, and takes place in the chloroplast (Lichtenthaler, 1999; Vickers *et al.*, 2009a). It is now known that most of the production of isoprene takes place in the chloroplast, via the

MEP pathway, through the action of isoprene synthase (IspS) on DMADP (Fig. 1.3) (Silver & Fall, 1991).

IspS' main characteristics are i) a low affinity for its substrate DMADP with value of Michaleis constant K_m ranging between 1.2 and 2.45 mM (Silver & Fall, 1995; Schnitzler *et al.*, 2005) and ii) a high temperature optimum with activity maximal between 45 and 48˚C (Monson *et al.*, 1992; Lehning *et al.*, 1999; Niinemets *et al.*, 1999b; Rasulov *et al.*, 2010). The DMADP pool is also used for production of 'essential' isoprenoids, which include carotenoids and sterols. Thus, one additional hypothesis to account for the emission of volatile isoprenoids is that it provides a way for plant to deal with an excess of DMADP, which would lead to unnecessary sequestration of phosphate, after the plants' requirements for essential isoprenoid molecules have been satisfied (Owen & Peñuelas, 2005).

Three reducing steps are needed within the MEP pathway to reduce the initial substrates glyceraldehyde 3-phosphate (G3P, a direct product of photosynthesis) and pyruvate to DMADP. These reducing steps consume one NADPH, and two additional reducing equivalents in the form of either NADPH or ferredoxin (Fd) (Charon *et al.*, 1999; Hecht *et al.*, 2001; Seemann *et al.*, 2006; Li & Sharkey, 2012). These three reduction steps are highlighted in red in the schematic of the MEP pathway in Figure 1.3.

^{13}C labeling experiments show that emitted isoprene mostly originates from photosynthetic products linking the isoprene production with photosynthetic carbon assimilation (Delwiche & Sharkey, 1993; Loreto *et al.*, 2004). This is confirmed by the fact that isoprene emissions are often correlated with net assimilation rate (Monson *et al.*, 1995; Kuhn *et al.*, 2004b). However, in these experiments isoprene doesn't reach 100% of ^{13}C-labelling, suggesting that extra sources of carbon can reach the chloroplasts and be used for isoprene production. The positioning of the unlabelled carbons in isoprene molecules suggests that pyruvate, a precursor of DMADP, has partly cytosolic origins (Karl *et al.*, 2002).

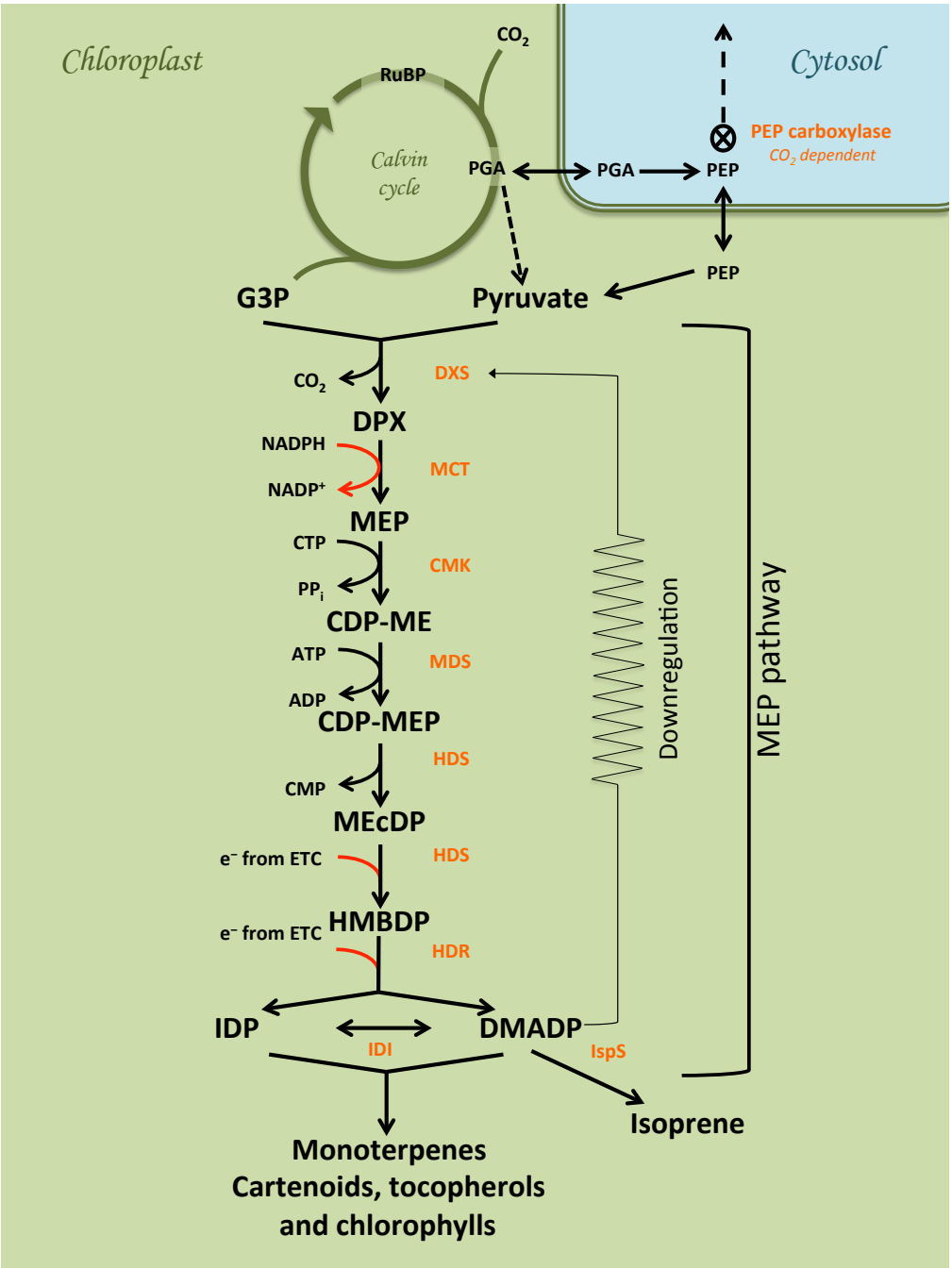


Figure 1.3: The MEP pathway. Metabolytes are in black; enzymes are in orange; reduction steps are in red. RuBP, Ribulose Bisphosphate; PGA, 3-phosphoglycerate; PEP, phosphoenolpyruvate; G3P, glyceraldehyde 3-phosphate; DXS, deoxyxylulose phosphate (DXP) synthase; DXR, DXP reductoisomerase; MEP, methylerythritol phosphate; CTP, cytidine triphosphate; PPi, inorganic diphosphate; MCT, MEP cytidylyltransferase; CDP-ME, diphosphocytidylyl methylerythritol; CMK, CDP-ME kinase; CDP-MEP, CDP-ME phosphate; CMP, cytidine monophosphate; MDS, methylerythritol cyclodiphosphate (MEcDP) synthase; NADPH/NAPD$^+$, nicotinamide adenine dinucleotide phosphate; ADP/ATP, adenosine-di(/tri) phosphate; ETC, electron transport chain; HDS, hydroxymethylbutenyl diphosphate (HMBDP) synthase; HDR, HMBDP reductase; IDP, isopentenyl diphosphate; IDI, IDP isomerase; DMADP, dimethylallyl diphosphate; IspS, isoprene synthase. Based on the work of Li & Sharkey (2012, 2013)

The use of advanced experimental techniques has recently provided new insights on the regulation of the MEP pathway. Profiles of MEP pathway metabolites under different conditions are starting to be identified (Li & Sharkey, 2012), and a possible downregulation of the pathway through the action of DMADP on key enzymes has been discovered (Banerjee *et al.*, 2013).

Controls of isoprene emission

There is no storage of isoprene in plants and emission rates of isoprene are usually correlated with synthesis rates (Affek & Yakir, 2003). However, not all isoprene that is synthesized is emitted, as reaction with ROS within the leaf can lead to the production of other volatile species such as methacrolein (2-Methylprop-2-enal, MAC, C_4H_6O) and methyl vinyl ketone (Butenone, MVK, C_4H_6O) (Jardine *et al.*, 2011). Synthesis of isoprene is mainly controlled by light and temperature (Fig. 1.4). Response to light follows a rectangular hyperbolic shape, similar to the response of photosynthetic assimilation to light, reflecting the link between photosynthesis and isoprene production. However, in the great majority of measurements, light response curves of isoprene saturate at higher light intensities than those of carbon assimilation (Monson *et al.*, 1992; Sharkey & Loreto, 1993; Lerdau & Keller, 1997).

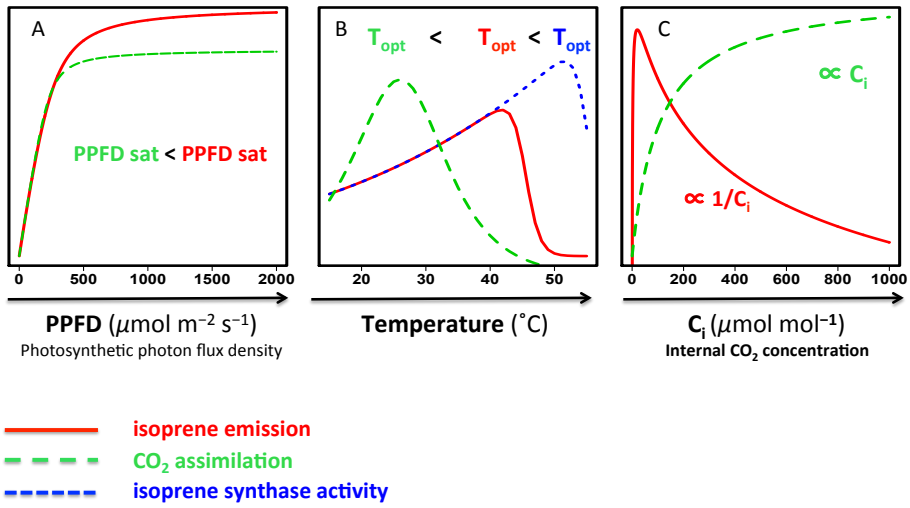


Figure 1.4: Schematic responses of rates of carbon assimilation (dashed green line) and isoprene emission (solid red line) in response to changes in (A) photosynthetic photon flux density (*PPFD*), (B) temperature and (C) internal CO_2 concentration (C_i). In panel (B), the schematic response of isoprene synthase is also represented.

In response to increasing leaf temperature, isoprene emission follows an exponential increase up to an optimum around 38˚C after which emission decreases steeply, reflecting to a certain extend the temperature response of enzymatic activity (Guenther *et al.*, 1993; Niinemets *et al.*, 1999b; Sharkey & Yeh, 2001; Pacifico *et al.*, 2009). This temperature optimum for isoprene emission is higher than the optimum for assimilation. However it is always somewhat lower than the optimum of IspS and therefore cannot be fully explained by enzymatic activity (Monson *et al.*, 1992; Niinemets *et al.*, 1999b; Rasulov *et al.*, 2010) (Fig.1.4 B).

CO_2 concentration also influences the production of isoprene, in the opposite sense to its effect on photosynthesis. Plants grown at high atmospheric CO_2 concentrations emit less isoprene than those grown at lower concentrations (Rosenstiel *et al.*, 2003; Possell *et al.*, 2004; Pacifico *et al.*, 2009; Niinemets, 2010) at least under standard conditions of temperature (30˚C). However, at canopy scale this effect can be offset by a larger plant productivity (Sun *et al.*, 2013b), and higher temperature seems also to suppress this reduction in isoprene emission capacity (Sun *et al.*, 2013a). It has been shown that isoprene emission responds to the leaf-internal CO_2 concentration (C_i), with lower emission rates associated with higher C_i (Wilkinson *et al.*, 2009; Possell & Hewitt, 2011; Sun *et al.*, 2012) (Fig. 1.4 C). There is no generally accepted explanation for this effect, but it has been observed in a variety of plant species, and is persistent – it applies to plants grown in different CO_2 concentrations, as well as in short-term experiments that manipulate ambient CO_2 concentration in order to alter C_i. A few studies (Rosenstiel *et al.*, 2003, 2004; Trowbridge *et al.*, 2012) have hypothesized that an intracellular metabolic competition for phosphoenolpyruvate (PEP; precursor of pyruvate) occurs at higher CO_2 levels leading to lower concentration of DMADP. However, a recent study (Sun *et al.*, 2013a) has questioned the responsiveness of isoprene to changes of C_i at higher leaf temperature. Although not well understood yet, the response of isoprene emissions to atmospheric CO_2 concentrations is fundamental in the context of climate change and needs to be realistically taken in account in models. In particular, the effect of high CO_2 concentration in suppressing isoprene emission may largely negate the previously projected effects of high temperatures in promoting isoprene emission and thus ozone formation (Possell *et al.*, 2005; Young *et al.*, 2009; Heald *et al.*, 2009; Pacifico *et al.*, 2012).

Water stress has a large negative impact on photosynthetic activity, but a very much weaker impact on the emissions of isoprene. Drought can even enhance emissions (Tingey *et al.*, 1981; Sharkey & Loreto, 1993; Fang *et al.*, 1996; Niinemets *et al.*, 1999a; Funk *et al.*, 2005; Brilli *et al.*, 2007). Under sufficiently severe drought, however, emissions collapse.

Finally, plant phenology also influences isoprene emission. A delay is usually observed between the development of photosynthetic capacity and isoprene emission during the early growth of leaves (Sharkey & Loreto, 1993; Monson *et al.*, 1995; Kuhn *et al.*, 2004a). The reason remains unclear: some studies (Loreto *et al.*, 2004; Monson *et al.*, 2007) put forward a shortage of enzyme IspS while a more recent study (Vickers *et al.*, 2010) suggests a lack of DMADP availability in the early stage of leaf development.

1.2.2 Interactions with the atmosphere

The atmospheric lifetime of isoprene is very short, somewhere between 50 min and 1.3 days (Atkinson, 2000). Due to its reactivity, isoprene plays an important role in the oxidation capacity of the atmosphere. If emitted in a high NO_x (NO_2 + NO) regime, sub-products of isoprene oxidation enhance ozone production due to photolysis of NO_2, by regenerating NO_2 from NO (Jenkin & Clemitshaw, 2000) (Fig. 1.5). On another hand, in a low NO_x regime, isoprene acts as a sink for the hydroxyl radical OH (Guenther *et al.*, 1999; Pike & Young, 2009; Archibald *et al.*, 2011) and therefore can increase the lifetime (and thus the concentration) of methane, an important greenhouse gas. The large amount of isoprene emitted by vegetation consumes a large amount of OH, making OH unavailable to oxidise other reduced compounds, including methane. Pike & Young (2008) found (for present-day climate) an increase in the methane lifetime of about 2 years. This result was obtained by comparing atmospheric chemistry model simulations with or without isoprene emissions. However, some recent studies have questioned the real impact of isoprene emission on the tropospheric oxidation capacity, and proposed new pathways for a recycling of OH (Lelieveld *et al.*, 2004, 2008; Guenther, 2008; Fuchs *et al.*, 2013). In a low NO_x regime, due to isoprene nitrate and peroxyacetyl nitrate (PAN) chemistry, isoprene can also reduce the production rate of ozone (Young *et al.*, 2009).

Isoprene may further influence radiative forcing through the formation of secondary organic aerosols (SOA). Sub-products of isoprene oxidation can condense to form particles, which affect the partition between direct and diffuse light, atmospheric albedo and cloud formation. Even if the yield of SOA from isoprene is low (~3%), it may play an important role, due to the sheer amount of isoprene emitted into the atmosphere (Claeys *et al.*, 2004; Edney *et al.*, 2005; Kroll *et al.*, 2006; Heald *et al.*, 2008; Carlton *et al.*, 2009; Carslaw *et al.*, 2010; Nozière *et al.*, 2011).

A warmer climate, changes in land use and higher CO_2 levels are all expected to have an impact on isoprene emissions; and as a key regulator of atmospheric chemistry, changes in isoprene emissions can in turn influence climate (Arneth *et al.*, 2010; Peñuelas & Llusia, 2003). Due to spatial heterogeneity in atmospheric pollutant concentrations (in particular NO_x) and in the distribution of isoprene-emitting vegetation, changes in emissions and thus their feedbacks on climate system may be spatially very variable (Young *et al.*, 2009; Makkonen *et al.*, 2012; Tai *et al.*, 2013; Ashworth *et al.*, 2013; Hardacre *et al.*, 2013). A conceptual scheme of the impact of BVOC emissions, and isoprene in particular, on climate is displayed in Figure 1.5.

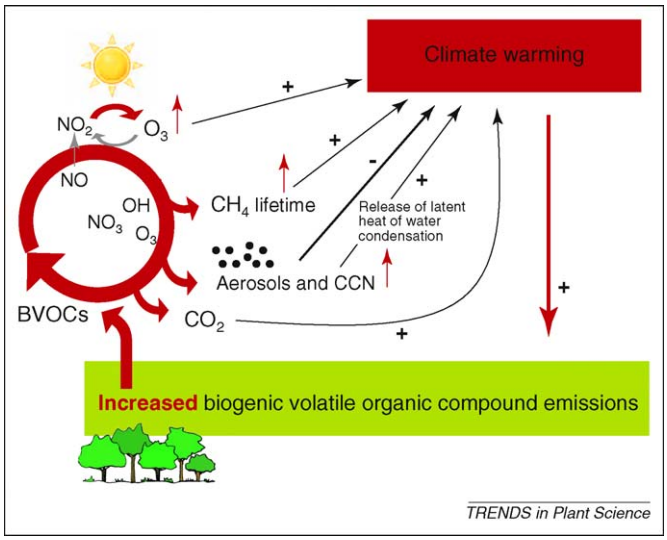


Figure 1.5: Effects of increased BVOC emissions on atmospheric chemistry and climate. Schematic figure of coupling of enhanced BVOC emissions and atmospheric and climatic changes: increased temperature might enhance BVOC emissions (+). Increased BVOC emissions might enhance aerosol formation and growth and therefore also enhance aerosol and cloud condensation nuclei (CCN) concentrations. Enhanced aerosol and CCN concentrations might decrease temperature (–) as a result of increased reflection of sunlight from low clouds back to space. Other positive feedbacks (indirect greenhouse effect through ozone formation and methane lengthening lifetime, CO_2 production) are also represented. Figure from Peñuelas & Staudt (2010).

1.2.3 Observations

Direct observations of isoprene emission can be done at the leaf, canopy and ecosystem level using diverse techniques (Fig. 1.6). However, measurements of other compounds than isoprene, such as (upstream) metabolites of the MEP pathway or (downstream) observations of atmospheric oxidation products, are a mine of information. Each observation gives information at different temporal and spatial scales, and each has its advantages and disadvantages.

Developments in genetics have made it possible to identify the gene sequence and expression for isoprene synthase. Analysis of genomic DNA and IspS mRNA are usually completed with data on the total quantity of the protein isoprene synthase. These combined measurements permit investigation of environmental (heat, light level, ozone level…) and developmental controls on isoprene emission through regulation at the transcriptional level (Sasaki *et al.*, 2005; Fares *et al.*, 2006; Calfapietra *et al.*, 2007; Vickers *et al.*, 2010). On the other hand, large datasets of species DNA sequences combined with information on species-specific isoprene emission capacity (i.e. the Lancaster or NCAR databases) allow the reconstruction of gain and loss events for isoprene emission capacity along phylogenetic pathways (Loreto, 2002; Monson *et al.*, 2013; Sharkey, 2013). Investigation of how this trait has evolved can provide insights on the adaptive response of isoprene emission capacity to the environment.

Purification methods on leaf extracts carried out with high-performance instruments (mass spectrometers and chromatographs) also make it possible to separate, identify and quantify each chemical component along the MEP pathway. These techniques are valuable in determining enzyme activity and/or leaf metabolite content under different environmental conditions. Such analyses are needed in order to better constrain the steps along the MEP pathway and to understand the combined kinetics of processes controlling isoprene production at the plastid level (Silver & Fall, 1995; Lichtenthaler, 1999; Rosenstiel *et al.*, 2004; Li & Sharkey, 2012; Weise *et al.*, 2013; Banerjee *et al.*, 2013).

Observations of isoprene emission rates on individual leaves, branches or entire plants can be done using enclosure measurements. Here, the individual is isolated in a cuvette

or a chamber, and the air is analysed in order to quantify the isoprene fluxes. Isoprene fluxes can be measured i) directly using proton-transfer mass spectrometry (PTR-MS) or the fast isoprene sensor (FIS) based on isoprene/ozone chemiluminescence; or ii) indirectly, using air collected in tubes filled with isoprene adsorbents, and thereafter analysed with various techniques including gas chromatography flame ionization detection (GC-FID) and FIS. Enclosure measurements allow a tight control on relevant aspects of the individual's environment, including temperature, CO_2 concentration, light intensity and ozone concentration. Study of the ^{13}C labelling of isoprene using PTR-MS on individuals exposed to a $^{13}CO_2$ atmosphere can be also done and provides important information on the sources of carbon involved in isoprene production (Karl *et al.*, 2002; Loreto *et al.*, 2004; Trowbridge *et al.*, 2012). The decay of isoprene emission after switching off the light has been used in some studies to evaluate the DMADP pool size (Rasulov *et al.*, 2009a, 2010). Enclosure measurements of isoprene emission can be associated with measurements of net carbon assimilation, chlorophyll fluorescence, leaf dry mass, and observations of leaf anatomy. However, the information given is instantaneous; these techniques do not allow isoprene production rate to be tracked continuously on longer time scales.

Above-canopy observations of isoprene emissions, collected during ground-based or airborne measurements campaigns, give information at the ecosystem scale. As with the enclosure measurements, isoprene emission rates are directly measured. Airborne campaigns provide essential information to understand and constrain isoprene atmospheric chemistry at the ecosystem scale, but the time period covered is usually short (Kuhn *et al.*, 2007). In contrast, static above-canopy observations provide information on the variability in isoprene emission at daily, seasonal and interannual time scales, depending on the duration of the measurement campaign. Here, isoprene concentrations are measured at high frequency using PTR-MS (McKinney *et al.*, 2011; Laffineur *et al.*, 2011, 2013) or FIS (Pressley, 2005). From observed isoprene concentration associated with information on vertical wind velocity, isoprene fluxes are inferred using eddy covariance techniques or even simple gradient and variance techniques (Greenberg *et al.*, 2014). Information on CO_2 fluxes (and thus net ecosystem production), photosynthetic photon flux density (*PPFD*), air temperature, heat and latent fluxes, is usually available as well.

Finally, remotely sensed observations of formaldehyde (HCHO) or more recently glyoxal (CHOCHO), two oxidation products of isoprene, can be used to constrain isoprene emission at a regional scale. However, these observations do not provide a direct measure of either isoprene fluxes or concentration. The errors associated with HCHO and CHOCHO column estimates are rather large, and increase with latitude and cloud cover. Moreover, the contribution of other VOCs and biomass burning to the formation of HCHO and CHOCHO cannot be attributed directly. Nevertheless, information (in particular, seasonal and inter-annual variability) provided by satellite observation of HCHO and CHOCHO, combined with chemistry-transport modelling, is valuable in order to constrain isoprene emissions from regional to global scale, using both bottom-up and top-down approaches (Palmer *et al.*, 2003, 2006; Fu *et al.*, 2008; Barkley *et al.*, 2008, 2011, 2012, 2013; Stavrakou *et al.*, 2009; Marais *et al.*, 2012; Fortems-Cheiney *et al.*, 2012; Foster *et al.*, 2013).

Figure 1.6 summarizes the different type of measurements and their spatio-temporal scales. Evaluation of isoprene emission models commonly uses enclosure and above-canopy measurements as well as remote-sensed observations (e.g. HCHO) in association with chemistry-transport modelling. As isoprene and its immediate oxidation products have a very short lifetime in the atmosphere, no paleo-data are available for isoprene.

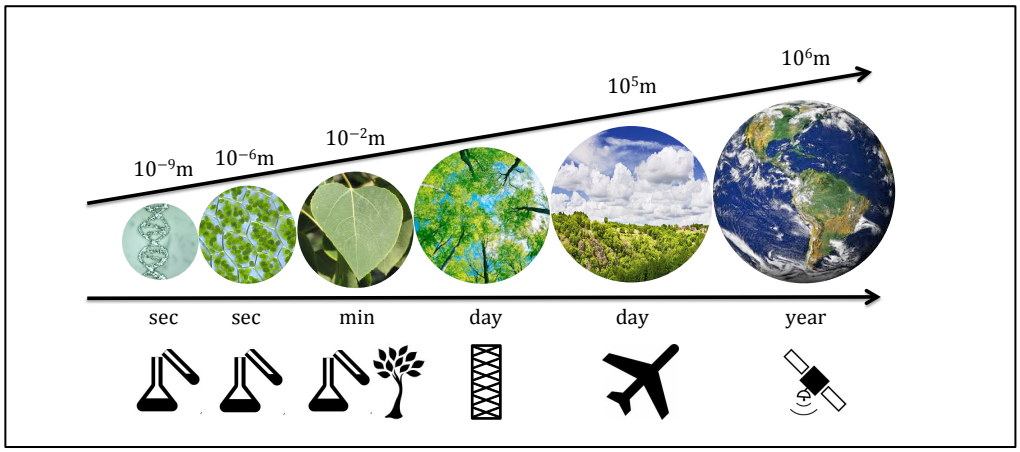


Figure 1.6: Schematic representing space and time scale of isoprene related observations.

1.2.4 Existing schemes for isoprene modelling

Due to the complexity of the biochemistry involved, modelling isoprene emissions is a challenge. All models of isoprene emissions mimic, to a certain extent, models of photosynthesis. Early isoprene models were developed by Guenther and co-workers (Guenther *et al.*, 1991, 1993, 1995). The algorithms proposed by Guenther and co-workers for isoprene and monoterpene emissions depended on previous observational studies, which had pointed out similarities between the light responses of isoprene emission rate and carbon assimilation. Using similar mathematical approaches as for photosynthesis to describe light- and temperature response curves, Guenther and co-workers proposed the following empirical algorithm:

$$E = E_s f\left(D_1\right) f\left(D_2\right) f\left(D_3\right) \cdots f\left(D_n\right) \quad (1.1)$$

where E is the BVOC emission rate, E_S is the BVOC emission rate under standardised conditions, and $f(D_i)$ for (i = 1..n) are functions describing how changes in the environmental driver D_i affect the standard emission rate E_S. Initially the environmental variables driving the isoprene emissions were light and temperature alone. However, the algorithm evolved, and now includes activity factors accounting for emission responses to past temperature, leaf age, soil moisture, leaf area index (LAI) and CO_2 inhibition (Guenther *et al.*, 2012). This empirical approach has two major advantages. The first is that it is extremely simple to compute and the principle of a standard emission factor modulated by a succession of functions can be easily extended to any other biogenic volatile compound. The second advantage is simply that this was the only available model for isoprene emission (and this is still true for most BVOCs other than isoprene) for about 10 years. Thus, large datasets of E_s are now available. The downside of this approach however is that isoprene species-dependent emission capacities have usually been measured without additional information on photosynthetic capacities. Yet, as described later, process-based models of isoprene emission by plants all build on models of photosynthetic carbon assimilation. In a process-based modeling approach, information on both isoprene emission and photosynthetic capacities is essential.

The initial algorithm of Guenther and co-worker evolved into a larger BVOC model called MEGAN (Model of Emissions of Gases and Aerosols from Nature: http://bai.acd.ucar.edu/MEGAN/; Guenther *et al.* (2012)). The latest version of MEGAN

included almost 150 compounds and is freely accessible. Thus, the great majority of studies analysing impact of BVOC on air quality and global environment use MEGAN. In this work (Chapter III, IV, V), I used the simplest version of this algorithmic as proposed by Guenther *et al.* (1993) and detailed in the Supplementary Material section (note S1).

Almost a decade after the publication of first algorithms for calculation of isoprene production, Niinemets *et al.* (1999b) proposed a first mechanistic approach to simulating isoprene emission. The model is based on energetic requirements for isoprene production. The basic idea is that a certain proportion of electrons generated by Photosystem II are used in the MEP pathway. This model received wider attention in the regional- and global-scale modeling community thanks to the work of Arneth and co-workers (Arneth *et al.*, 2007a,b, 2008a,b, 2011). This model is described more details in Chapter II.

Shortly afterwards, Martin *et al.* (2000) proposed another mechanistic approach for the calculation of isoprene emission. As in the standard model of photosynthesis, the rate of emission is governed by the slowest of three processes in the production pathway of isoprene:

– The production of pyruvate in the chloroplast;

– The production of ATP by phosphorylation;

– The maximum capacity of isoprene synthase.

The Martin *et al.* (2000) model has been used in regional studies (Keenan *et al.*, 2009, 2011), but never at the global scale.

Zimmer and co-workers (Zimmer *et al.*, 2000, 2003) developed a more complex process-based approach whereby the entire production pathway (and associated metabolite pools) was represented. This model was coupled with a photosynthetic model (the seasonal isoprene synthase model–biochemical isoprenoid biosynthesis model, SIM-BIM), and expanded to cover monoterpene emissions (Grote *et al.*, 2006). The representation of the cascade of biochemical reactions occurring along the isoprene production pathway requires knowledge of the maximum reaction velocity and

Michaelis-Menten constants (K_m) at each step. In practice, some parameters describing reaction velocities were obtained using inversion, whereby parameters are estimated to best fit the data rather than being measured directly. The rest of the parameters were either measured or taken from the literature, but parameter values taken from literature largely referred to different species from those under consideration. All enzymatic maximum reaction rates were further adjusted in time by a factor determined experimentally from reaction rates of isoprene synthase extracts from the studied species. Due to its complexity, this model has never been applied at regional- or global scale.

Finally, Niinemets *et al.* (2013) proposed very recently a new model named the C-Ratio model. Here, gross assimilation rates are multiplied by the 'C-ratio', which is the ratio between isoprenoid emission and CO_2 gross assimilation. This ratio is modulated by light- and temperature-dependent function. An additional function accounts for seasonal variation in the C-ratio.

More detailed reviews of isoprene emission modelling can be found in the literature (Arneth *et al.*, 2007b; Monson *et al.*, 2012; Pacifico *et al.*, 2009; Grote *et al.*, 2013) .

1.2.5 Thesis structure

In the following chapter (Chapter II), after describing the Farquhar model for carbon assimilation (Farquhar *et al.*, 1980) and the Niinemets model for isoprene emission by plants (Niinemets *et al.*, 1999b), I explain the motivations for developing a new model for isoprene emissions. I also expound my hypothesis that isoprene production is controlled by reductant availability. I explain why I consider that the energetic balance between assimilation needs and reductant supply from light reactions controls reductant availability for secondary pathways.

Chapter III describes how I tested the validity of my working hypothesis by investigating published observed responses of isoprene emission to changes in its main environmental drivers (light, temperature and CO_2), and comparing these responses to the ones predicted by my model. In particular, I examined whether, when environmental conditions vary, observed changes in the ratio of assimilated carbon lost in the form of isoprene follow predicted changes. To my knowledge, this is the first time that a

modeling study has considered together the variations (and the empirical mis-match) between assimilation rate and isoprene emission.

In Chapter IV, I describe leaf-scale experiments I conducted at CREAF on *Populus nigra* L., a high isoprene emitter. The experiments were designed explicitly to test my hypothesis by changing environmental conditions, following a specific protocol. Then, I detail how I tested my model against this new dataset as well as an additional dataset from the study of Sun *et al*. (2012) on hybrid aspen (*Populus tremula* L. x *P. tremuloides* Michx).

Chapter IV reports how I upscaled my new isoprene model from leaf to canopy scale using long-term above-canopy flux measurements of both isoprene and CO_2 fluxes. The upscaling technique I used is a simple multi-layer approach, which allows model behaviour to be tested at larger scales without adding (uncontrolled) complexity.

Finally, in the Conclusions, I discuss the advantages of my new model and the possibility of extending it to global-scale applications. I also highlight secondary environmental controls on isoprene emissions, which are still missing from the model. I discuss how recent experimental studies question aspects of our knowledge of the controls of isoprene emission. I conclude the thesis with an outlook on what is still lacking in term of experimental and modelling studies of isoprene emission.

2 The new hypothesis and model

2.1 Introduction

All process-based models of isoprene emissions are tightly linked to models of photosynthetic carbon assimilation in leaves. Thus, understanding the logic behind process-based isoprene models requires a fundamental knowledge of the logic that photosynthetic models follow, along with a basic comprehension of the processes underlying carbon assimilation. In this section, I describe key processes taking place in the chloroplast, leading to the assimilation of atmospheric CO_2 by C_3 plants (Box 1.1). I also describe succinctly, but still with some essential process-dependent details, the standard model for photosynthetic carbon assimilation for C_3 leaves developed by Farquhar and co-workers (Farquhar et al., 1980; Brooks & Farquhar, 1985).

The model of isoprene emission developed by Niinemets and co-workers (Niinemets *et al.*, 1999b; Niinemets, 2004) is also described here in detail. This is an essential step as my work has explicitly attempted to improve this model. The Niinemets model is, as far as I know, the only process-based model for isoprene emission that has been used at the global scale for studying the potential impact of future environmental change on emissions.

The hypothesis underlying my new modelling approach is then described, along with a proposed physiological explanation.

2.2 Photosynthesis, C_3 Carbon assimilation and the Farquhar model

Photosynthetic carbon assimilation by plants is a complex and highly evolved natural biochemical process by which carbon dioxide and water are combined and reduced to produce carbohydrates. Photosynthesis takes place in the chloroplasts (also called plastids), bodies present in the leaf and/or outer stem cells of all green plants. The processes comprise an enzymatic phase (dark reactions) and a photo-activated phase (light reactions). The Farquhar model describes processes occurring in both of these phases and assumes that the most limiting process drives the final rate of carbon assimilation.

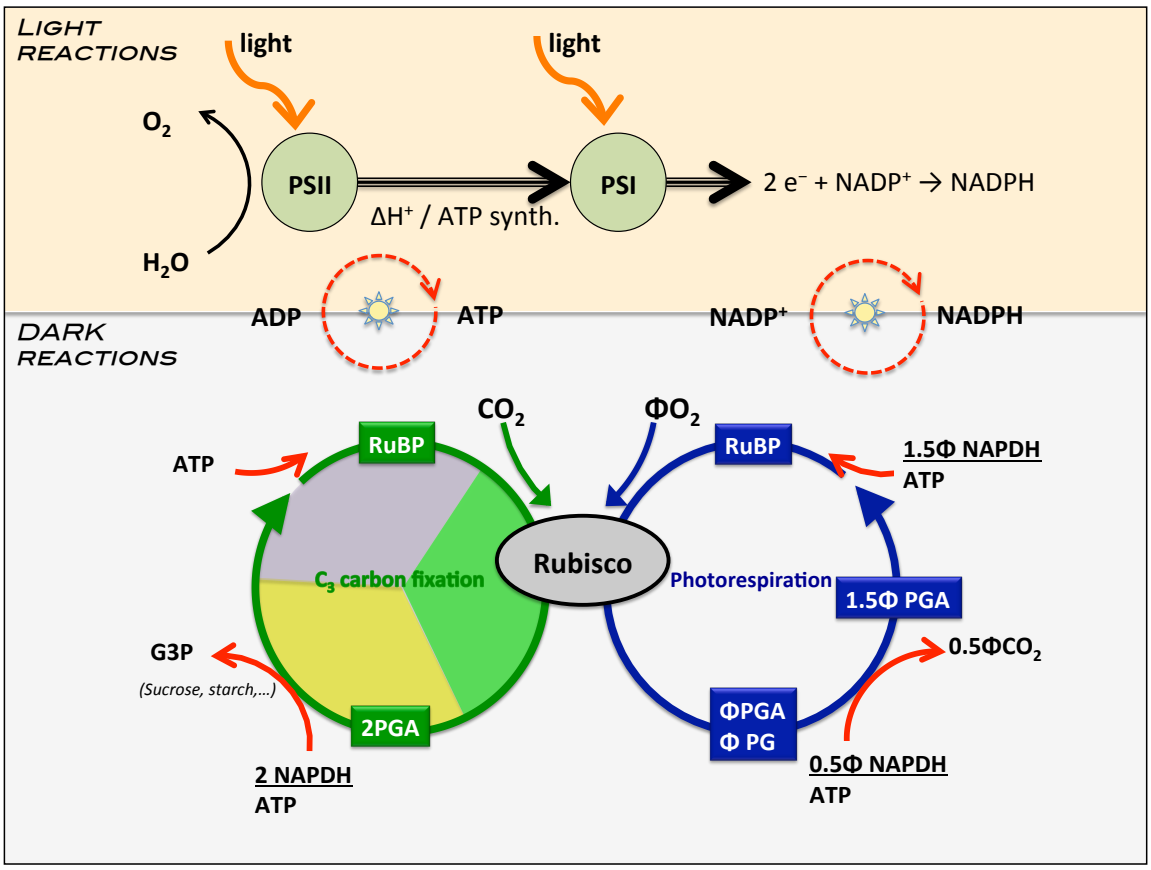
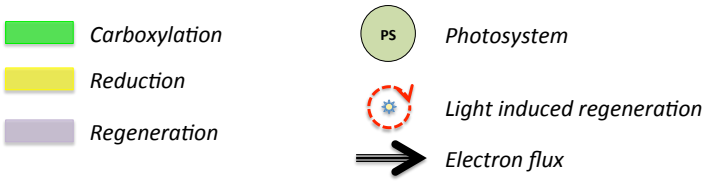


Figure 2.1: Schematic representing processes occurring in photosynthetic carbon assimilation and associated photorespiration.



PGA 3-phosphoglycerate; **G3P** glyceraldehyde-3-phosphate **;** **PG** 2-phosphoglycolate; **NADPH/NAPD⁺** nicotinamide adenine dinucleotide phosphate; **ADP/ATP** adenosine-di(/tri) phosphate **;** **RuBP** *Ribulose Bisphosphate* **;** **Rubisco** Ribulose bisphosphate carboxylase/ oxygenase

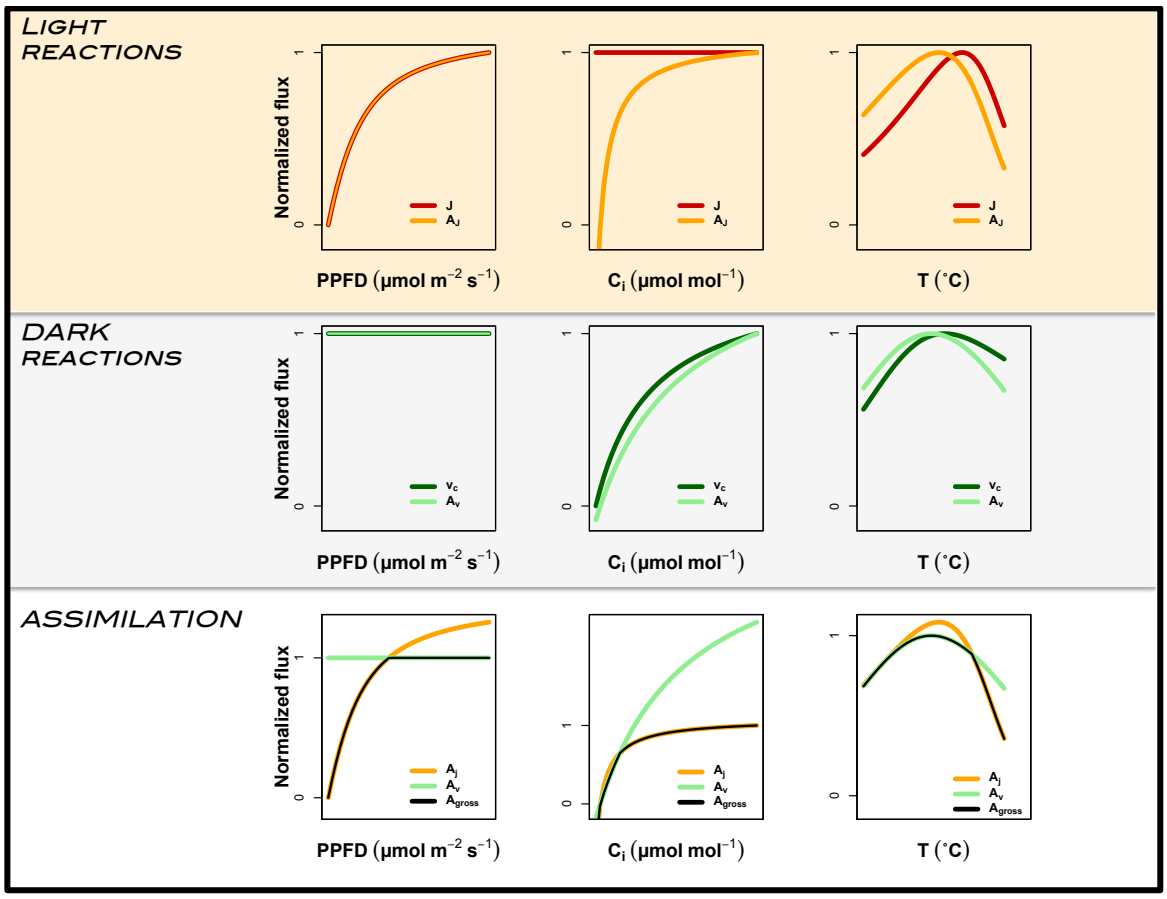


Figure 2.2: Schematic of the normalized responses to increase in photosynthetic photon flux density (*PPFD*), internal CO_2 concentration (C_i), and temperature (T) of electron flux (J) in red and associated light-limited gross assimilation rate (A_j) in orange; carboxylation rate (V_c) in dark green and associated Rubisco-limited gross assimilation rate (A_v) in light green; and gross assimilation rate (A_{gross}) in black. Simulations were done using the Farquhar model as modified by Medlyn *et al.* (2002, 2005) (Supplementary Material, note S2).

DARK REACTIONS

The Calvin cycle

The Calvin cycle, discovered by Calvin and co-workers in the 1950s, involves three phases, which allow plants to transform inorganic CO_2 molecules into organic compounds. The three stages are described in Figure 2.1:

1. *Carboxylation* of the five-carbon molecule Ribulose Bisphosphate (RuBP). By reacting with RuBP, CO_2 enters the cycle, giving two three-carbon molecules of 3-phosphoglycerate (PGA). This first step is catalysed by the key enzyme ribulose bisphosphate carboxylase/oxygenase, referred to as Rubisco.

2. *Reduction and phosphorylation* of PGA into gyceraldehyde-3-phosphate (G3P). G3P constitutes the base for sucrose or starch production. It is also one of the two initial substrates for isoprene synthesis.
3. *Regeneration* of the acceptor RuBP from G3P. Approximately 1/6th of G3P is used for sugar production. The rest of G3P is combined and *phosphorylated* in order to regenerate RuBP and complete the cycle.

The Farquhar model describes limitation of CO_2 assimilation in the carboxylation phase and controlled by Rubisco enzymatic kinetics. The carboxylation stage can be described using Michaelis–Menten kinetics:

$$V_c = V_{cmax} \cdot \frac{C_i}{\left(k_c + C_i\right)} \tag{2.1}$$

where V_c is the rate of carboxylation; V_{cmax} is the maximum rate of carboxylation attained when all enzymes are bound to substrate; k_c is the Michaelis–Menten constant for carboxylation and represents the substrate concentration at which the reaction rate is half of V_{cmax}; and C_i is the internal CO_2 concentration, i.e. the concentration inside the leaf. C_i is controlled by both atmospheric CO_2 concentration and aperture of the microscopic pores on the surface of the leaf (stomata) that permit diffusion of water out of and CO_2 into the leaf. k_c indicates the affinity of Rubisco for CO_2 while V_{cmax} depends mostly on the concentration of Rubisco in the chloroplast. Both k_c and V_{cmax} vary with temperature. Thus V_c varies with temperature and CO_2 concentration (Fig. 2.2). To first order photosynthetic photon flux density (*PPFD*) has no impact on V_c.

Photorespiration

A limitation of CO_2 assimilation, particularly in C_3 plants (which have no CO_2 concentration mechanism), comes from the affinity of the key enzyme Rubisco to bind with O_2 and catalyse oxygenation of RuBP into PGA and the two-carbon molecule 2-phosphoglycolate (PG). A complex pathway, taking place among three different organelles (chloroplast, peroxisome and mitochondrion) follows this first step. Along this pathway, 0.5 mole of CO_2 per mole of O_2 is lost; and 0.5 mole of inorganic ammonium (NH_4^+) is released and refixed. This latter process requires the use of the equivalent of one mole of NADPH per mole of NH_4^+ (not detailed in Figure 2.1). Thus

reduction steps occurring along the pathway include reduction reactions for re-fixation of NH_4^+ and regeneration of RuBP.

Like carboxylation, oxygenation can be described using Michaelis–Menten kinetics:

$$V_o = V_{omax} \cdot \frac{O_i}{\left(k_o + O_i\right)} \tag{2.2}$$

where V_o is the rate of oxygenation; V_{omax} is the maximum rate of oxygenation; k_o Michaelis–Menten constant for oxygenation and O_i is the internal O_2 concentration.

Thus O_2 competes with CO_2 for the common substrate RuBP and for each carboxylation, a number Φ of oxygenation occurs, with Φ defined as the ratio of oxygenation to carboxylation ($\Phi = V_o/V_c$). Competition between O_2 and CO_2 for RuBP affects the 'apparent' Michaelis–Menten constants for carboxylation and oxygenation. In other words, the internal concentration of the substrate (CO_2 or O_2) necessary to reach half of the maximum reaction rate (V_{cmax} or V_{omax}) needs to be greater than in absence of the competitive substrate. The increase of the concentration necessary to reach half of the maximum reaction rate depends on the competitive substrate concentration. This effect can be taken into account by introducing modified Michaelis–Menten constants:

$$k_c^{'} = k_c (1 + \frac{O_i}{k_o}) \tag{2.3}$$

and

$$k_o^{'} = k_o (1 + \frac{C_i}{k_c}) \tag{2.4}$$

In presence of both substrates, carboxylation and oxygenation rates become:

$$V_c = V_{cmax} \cdot \frac{C_i}{\left(k_c^{'} + C_i\right)} = V_{cmax} \cdot \frac{\left(\frac{C_i}{k_c}\right)}{\left(1 + \frac{O_i}{k_o} + \frac{C_i}{k_c}\right)} \tag{2.5}$$

and

$$V_o = V_{omax} \cdot \frac{O_i}{\left(k_o^{'} + O_i\right)} = V_{omax} \cdot \frac{\left(\frac{O_i}{k_o}\right)}{\left(1 + \frac{O_i}{k_o} + \frac{C_i}{k_c}\right)} \tag{2.6}$$

and

$$\phi = \frac{V_o}{V_c} = \left(\frac{V_{omax}}{V_{cmax}}\right) \cdot \frac{\left(\frac{O_i}{k_o}\right)}{\left(\frac{C_i}{k_c}\right)} \tag{2.7}$$

As one carboxylation of RuBP incorporates one CO_2 in the cycle and one oxygenation is accompanied by the loss of 0.5 CO_2, the rate of gross CO_2 assimilation (A_{gross}) is related to rate of carboxylation and oxygenation thus:

$$A_{gross} = V_c - 0.5V_o \tag{2.8}$$

The ingenuity of the Farquhar model comes from the introduction of the term Γ^*, which is the compensation point in absence of dark respiration. In other words Γ^* is the CO_2 internal concentration for which A_{gross} is equal to zero (and $\Phi = 2$). Replacing C_i by Γ^* in equation 2.7 when $A_{gross} = 0$ gives:

$$\Gamma^* = \left(\frac{V_{omax}}{V_{cmax}}\right) \cdot \left(\frac{O_i}{k_o}\right) \cdot \left(\frac{k_c}{2}\right) \tag{2.9}$$

Rearranging equations 2.7, 2.8 and 2.9:

$$\phi = \frac{2\Gamma^*}{C_i} \tag{2.10}$$

and

$$A_{gross} = A_v = V_c(1 - 0.5\phi) = V_c\left(1 - \frac{\Gamma^*}{C_i}\right) = V_{cmax} \cdot \frac{(C_i - \Gamma^*)}{(C_i + k_c^{'})} \tag{2.11}$$

This is the 'Rubisco-limited' assimilation rate (A_v) and represents the assimilation driven by enzymatic reactions dictated by Rubisco kinetics (dark reactions). A_v is limited by Rubisco availability (V_{cmax}), substrate availability (C_i) and competition for substrate with O_2 (Γ^*). The response of A_v with increasing *PPFD*, C_i and temperature (T) is shown in Figure 2.2. As for the carboxylation rate, changes in *PPFD* do not affect A_v. As shown in Figure 2.2, differences between V_c and A_v in response to changes in C_i and T are due to the effect of the Rubisco affinity for O_2. Farquhar model temperature dependencies, as used within this study, are described in the supplementary material (S2).

LIGHT REACTIONS

Reduction and phosphorylation steps of the Calvin cycle are essential for the conversion of carbon dioxide into sugar and for the CO_2 assimilation pathway to operate as a cycle. *Reduction* reactions use electrons provided by the oxidation of the reduced form of nicotinamide adenine dinucleotide phosphate (NADPH) into $NADP^+$:

$$NADPH \rightarrow NADP^+ + H^+ + 2\ e^-$$

Phosphorylation steps use the phosphate and energy provided by the loss of an inorganic phosphate (P_i) occurring in the transformation of adenosine-triphosphate (ATP) into adenosine-diphosphate (ADP):

$$ATP \rightarrow ADP + P_i + energy$$

NADPH and ATP are produced in the thylakoid membranes of the chloroplast where light reactions occur. Their production uses energy provided by *PPFD*, making light a limiting factor for carbon assimilation. NADPH molecules trap electrons extracted from photolysis of water, and permit export of electrons from the thylakoid membrane to the rest of the cell. Water splitting and the production of NADPH generate a gradient of protons, which in turn provides the energy necessary to produce ATP by photophosphorylation of ADP. The Farquhar model takes into account light limitation of assimilation on the basis of NAPDH limitation.

The rate of NADPH consumption is equal to the rate of PGA produced in the carboxylation and oxygenation pathways (RuBP regeneration) plus the rate of NH_4^+ re-fixation associated with photorespiration:

$$\begin{aligned} \textit{Rate of consumption of } \text{NADPH} &= (2V_c + 1.5V_o) \\ &= V_c \cdot (2 + 2\phi) \\ &= V_c \cdot \left(2 + \frac{4\Gamma^*}{C_i}\right) \end{aligned} \tag{2.12}$$

Photosynthetic photon flux density (*PPFD*) is the part of the light spectrum (mainly visible) absorbed by the chloroplast. Two photons are needed to move an electron from its energy state in H_2O to the higher energy state in $NADP^+$ (Box 2.1). Accompanying this increase in energy level, the electron is transferred from compounds of high reduction-oxidation (redox) potential (oxidant) to compounds of low redox potential (reductant). One photon, absorbed by Photosystem II (PSII), extracts an electron from water, and a second photon, absorbed by the Photosystem I (PSI), brings this electron to a energy state strong enough to reduce $NAPD^+$ to NAPDH (Box 2.1). Thus, 4 photons, corresponding to 2 electrons, are necessary for one $NADP^+$ to be reduced into NAPDH. Note that the NAPDH requirement per CO_2 assimilation is equal to 2 in the carboxylation pathway. Electron transport rate (J) can be described to first order by:

$$J = \alpha PPFD \tag{2.13}$$

where α in the quantum yield in mol electron mol photon^{-1}. The quantum yield depends on leaf absorptance, quantum yield of PSII and the fraction of *PPFD* reaching PSII (0.5) (von Caemmerer, 2000) (Fig 2.3). This linear relationship between *PPFD* and J however applies only for low *PPFD*. For higher *PPFD*, due to thylakoid membranes properties, J saturates, approaching a maximum rate of electron transport J_{max}. Thus the electron transport rate can be represented by a non-rectangular hyperbola:

$$J = \frac{(\alpha PPFD + J_{max}) - \sqrt{(\alpha PPFD + J_{max})^2 - 4\alpha\theta PPFD J_{max}}}{2\theta} \tag{2.14}$$

where θ is a curvature parameter and J_{max} is the maximum electron transport rate. To first order, J_{max} varies with temperature only; J varies with T and *PPFD*, but not C_i (Fig. 2.2).

As reduction of $NADP^+$ to NADPH requires 2 electrons, the rate of NAPDH production is equal to:

$$\text{NADPH } production = \frac{J}{2} \tag{2.15}$$

Therefore if production of NAPDH limits carbon assimilation, then the rate of the consumption of NAPDH equal the rate of production of NADPH and assimilation is found to be in a so-called light-limited regime. Gross assimilation is calculated by rearranging equations 2.8, 2.12 and 2.15:

$$A_{\text{gross}} = A_{\text{j}} = \left(\frac{J}{4}\right) \cdot \frac{(C_{\text{i}} - \Gamma^*)}{(C_{\text{i}} + 2\Gamma^*)} \tag{2.16}$$

This is the light-limited gross assimilation (A_{j}). It is mainly determined by *PPFD*, leaf structure and thylakoid membranes proprieties (α, J_{max}). However, A_{j} is also dependent on the distribution of NAPDH between the carboxylation and oxygenation pathways (C_{i}, Γ^*). Consequently, calculation of A_{j} includes a component associated with properties of Rubisco. There are differences between the responses of J and A_{j} to changes to C_{i} and T, as shown in Figure 2.2.

A_{v} and A_{j} represent 'potential' CO_2 assimilation rates by leaves. Effective gross assimilation is controlled by the most limiting factor and gross assimilation is calculated as the minimum of Rubisco- and light-limited gross assimilation (Fig. 2.2):

$$A_{\text{gross}} = \min\left\{A_{\text{v}}, A_{\text{j}}\right\} \tag{2.17}$$

The net assimilation rate of CO_2 (A_{net}) is always somewhat lower than A_{gross} as CO_2 is lost through mitochondrial respiration (R_{d}):

$$A_{\text{net}} = A_{\text{gross}} - R_{\text{d}} \tag{2.18}$$

Mostly, it is A_{net} (not A_{gross}) that is measured by commonly used gas-exchange measurement techniques.

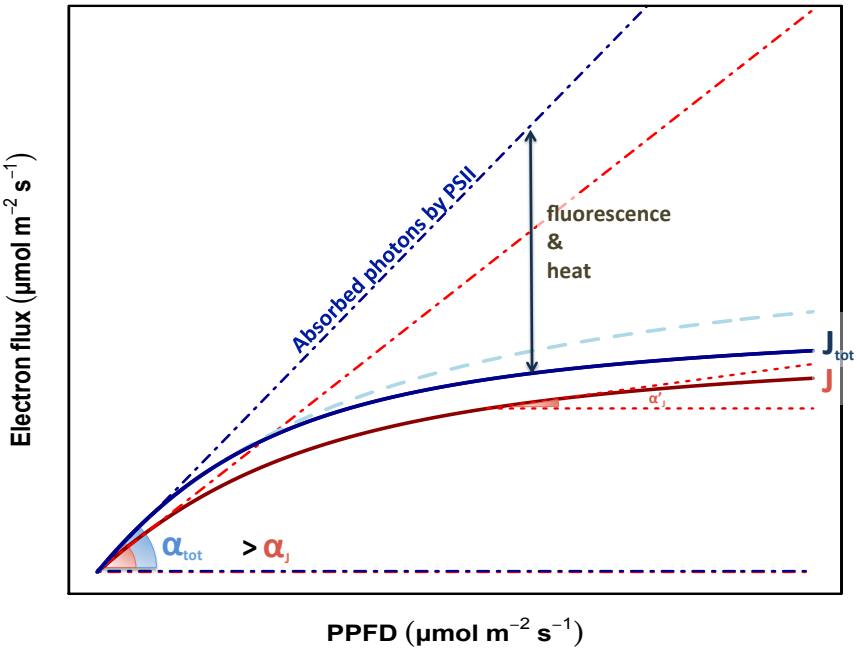


Figure 2.3: Schematic representing, in blue, the total electron flux generated by photosystem II (J_{tot}) and, in red, the total electron flux as computed from assimilation curves using the Farquhar model (J) versus photosynthetic photon flux density (*PPFD*). Differences between the two fluxes that can be observed are represented with higher quantum efficiencies (α) for J_{tot} or saturation of J_{tot} at higher light intensity than J (light blue dashed line). The dotted-dashed line in blue represents the total photons absorbed by the chloroplast. Differences between the total electrons flux and the total of photon absorbed are due to transfer of energy to heat dissipation and florescence. This figure is only illustrative and scales are not respected.

2.3 The Niinemets model

'A biochemical model of isoprene emission based on the electron requirement for isoprene synthesis'

Niinemets and co-workers (Niinemets *et al.*, 1999b; Niinemets, 2004) were the first to attempt to model isoprene emission in a process-based way. Before the study of (Niinemets *et al.*, 1999b), available models of isoprene emission were based on empirical algorithms (Guenther *et al.*, 1991, 1993, 1995). Temperature response function based on equations developed by Johnson *et al.* (1942) describing the temperature dependency of enzymatic catalysed reactions, and a hyperbolic relationship with *PPFD* calculate rates of isoprene emission in relation to changes in leaf temperature and *PPFD*. However, Niinemets and co-workers found that a unique set of *PPFD* and temperature dependencies for isoprene emission (*I*), was restrictive – variation in the *PPFD* and temperature responses between species was considerable. Thus, they proposed a new process-based model, based on the energetic requirement for isoprene synthesis and leaf photosynthetic properties. The model was developed using experiments on *Liquidambar* and *Quercus* species and has been expanded to larger scales (Arneth *et al.*, 2007a,b, 2008b; Keenan *et al.*, 2009; Young *et al.*, 2009; Pacifico *et al.*, 2011, 2012; Unger *et al.*, 2013).

The Niinemets model was built on two foundations. The first foundation comes from observations. Despite the general correlation between *I* and net assimilation rate, there are differences in their responses: *i) I* saturates at higher *PPFD* than A_{net}, *ii)* the A_{net} to *I* ratio declines with increasing temperature, and *iii)* decreases in stomatal conductance reduce A_{net} but not *I*. In all these situations A_{net} is affected in a different manner from photosynthetic electron transport (*J*). Thus, these observations suggest that the electron flux *J*, rather than carbon assimilation rates, limits *I*.

The second foundation is more physiological and comes from the (then novel) research on production pathways of isoprene, which revealed that foliar isoprene is mainly produced in the chloroplast by the MEP pathway. Knowledge of the MEP pathway available at that time is summarized in Figure 2.4.

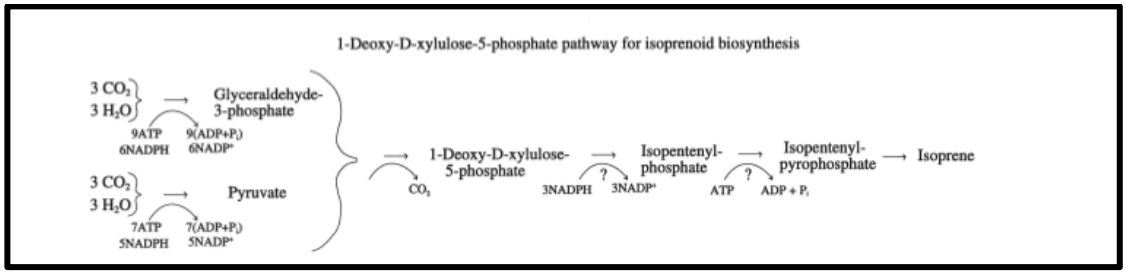


Figure 2.4: The DPX (or MEP) pathway as illustrated in Niinemets *et al.* (1999b). Taken from Figure A1 of Niinemets *et al.* (1999b) with the permission of the authors.

Therefore, Niinemets and co-workers developed a model based on leaf electron transport rate and the electron requirement for isoprene synthesis. This model proposes that a fraction of the total electrons (ε_N) is involved in the isoprene synthesis pathway, with the hypothesis that ε_N is controlled by both competition for electrons between isoprene and carbon assimilation and photorespiratory pathways, and enzymatic (IspS) activity. ε_N is defined by:

$$\varepsilon_N = \frac{J_I}{J_{tot}} \tag{2.19}$$

where J_I is the electron flux required in order to generate a production rate of isoprene I and J_{tot} is the total photosynthetic electron flux produced by photosystem II, approximated by J (equation 2.14). J can be computed from leaf gas-exchange measurements (under RuBP regeneration limitation) using the Farquhar model (Eq. 2.16 and 2.18):

$$J_{tot} \approx J = \left(A_{net} + R_d\right) \cdot \frac{(4C_i + 8\Gamma^*)}{(C_i - \Gamma^*)} \tag{2.20}$$

The total electron flux produced by photosystem II (J_{tot}) is always somewhat larger than J, the electron flux used for carbon assimilation and photorespiration, as additional electrons are used for other redox reactions in the leaf, including nitrate reduction and isoprene synthesis (Fig. 2.3).

With the newly available knowledge of the MEP pathway, Niinemets *et al.* (1999b) estimated a total cost of 14 NAPDH (equivalent to 28 electrons) per molecule of isoprene emitted (Fig. 2.4). The production of one molecule of isoprene (C_5H_8) requires the assimilation of six molecules of CO_2 (one CO_2 is lost in the pathway). Thus the requirement of NADPH is 2.33 per assimilated CO_2 for the synthesis of one molecule of isoprene. This energetic cost is compared with the cost for sugar synthesis, which (in the absence of energetic loss in photorespiration) is two NAPDH per CO_2. Hence, Niinemets *et al.* (1999b) made a parallel between effective electron cost for sugar synthesis and for isoprene synthesis in order to calculate the electron flux (J_I) required to produce isoprene at a rate I:

$$J_I = 6I.\left(\frac{2.33}{2}\right).\frac{(4C_i + 8\Gamma^*)}{(C_i - \Gamma^*)} = 6I.\frac{(4.67C_i + 8\Gamma^*)}{(C_i - \Gamma^*)} \qquad (2.21)$$

Combining equations 2.19 and 2.21, gives the model isoprene emission rate:

$$I = \varepsilon_N J \frac{(C_i - \Gamma^*)}{6\,(4.67C_i + 9.33\Gamma^*)} \qquad (2.22)$$

or on a dry mass basis

$$I = \varepsilon_N J_m M_A \frac{(C_i - \Gamma^*)}{6\,(4.67C_i + 9.33\Gamma^*)} \qquad (2.22')$$

where J_m is the rate of photosynthetic electron transport per unit of leaf dry mass (μmol g^{-1} s^{-1}), and M_A is the leaf dry mass per unit area (g m^{-2}).

The second hypothesis of the Niinemets model is that the strength of the demand for electrons used for isoprene synthesis is proportional to the activity of isoprene synthase (S_S). Thus, and based on equation 2.19, the temperature response of ε_N is given by:

$$\varepsilon_N = d\frac{S_S}{J_m} \qquad (2.23)$$

where S_S is the specific activity of isoprene synthase (μmol isoprene (g isoprene synthase)$^{-1}$ s^{-1}), d is a scaling constant in ((μmol electron) (g isoprene synthase) (μmol

isoprene)$^{-1}$ (g leaf dry mass)$^{-1}$). S_S and J_m both have temperature dependencies of the form

$$\frac{\exp\left(c - \frac{\Delta H_a}{R T_k}\right)}{1 + \exp\left(\frac{(\Delta S T_k - \Delta H_d)}{R T_k}\right)}$$

Here c is a scaling constant, ΔH_a and ΔH_d are the activation and deactivation energies, ΔS is the entropy term, T_k is absolute temperature and R is the gas constant (8.314 J mol^{-1} K^{-1}). Specific values of these parameters are given for S_S and J_m in Table 2.1. Figure 2.5 shows the form of the response to temperature of ε_N, S_S and J_m. It has to be noted that for a given C_i, the overall temperature dependency of the Niinemets model follows the temperature response of enzymatic activity only, as by replacing equation 2.23 in equation 2.22:

$$I = d\, S_S\, M_A \frac{(C_i - \Gamma^*)}{6\,(4.67 C_i + 9.33 \Gamma^*)} \qquad (2.24)$$

The loss of the temperature response of the electron flux is an issue, which was recognised by Niinemets *et al.* (1999b). The authors also pointed out that the drop-off of isoprene emissions at temperature below temperature optimum of IspS suggests an influence of the temperature dependency of J. Consequently, they set up an upper limit to ε_N. This temperature response of isoprene emissions has been transcribed into a larger-scale model, by using the simplified function of Arneth *et al.* (2007b) which mimics the one from Niinemets *et al*. (1999b):

$$f(T) = \min\left\{\exp(a_T (T - T_{st})); 2.3\right\} \qquad (2.25)$$

T_{st} is the temperature of standard conditions (30˚C), and a_T is a scaling parameter set to 0.1 ˚C^{-1}.

Table 2.1: Parameters used for temperature response of ε_N taken from Niinemets *et al.* (1999b)

Parameter	Symbol	Units	Value for S_S	Value for J_m
Scaling constant	c	unitless	35.478	10.19
Activation energy	ΔH_a	kJ mol^{-1}	83.129	24.998
Deactivation energy	ΔH_d	kJ mol^{-1}	284.6	299.69
Entropy term	ΔS	kJ K^{-1} mol^{-1}	0.8875	0.9437

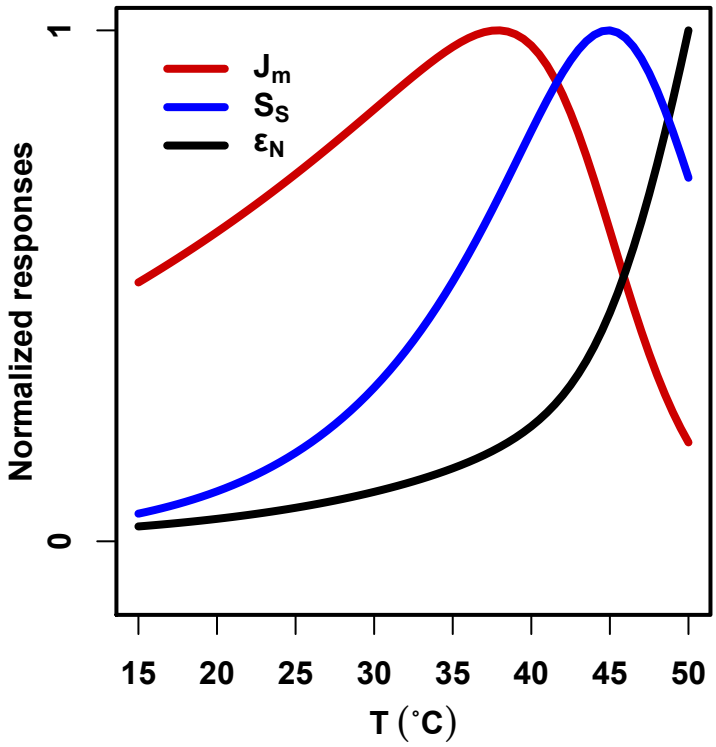


Figure 2.5: Normalised temperature responses of enzymatic activity (S_S), photosynthetic electron transport per unit of leaf dry mass (J_m) and fraction of electron (ε_N) as modelled by the Niinemets model using values from Niinemets *et al.* (1999b) (Table 2.1).

2.4 Improving on the Niinemets model

My working hypothesis originates from inconsistencies noticed in the Niinemets model. Hence, I start this paragraph by explaining those inconsistencies.

2.4.1 Analysis of the Niinemets model

The first contradiction is the importance implicitly assigned by the Niinemets model to pathways other than the MEP (or DXP) pathway for isoprene synthesis. In particular, the model strongly links isoprene emissions to the production of G3P. By comparing Figure 2.4 and equation (2.22), we see that the cost in NADPH for isoprene synthesis in the Niinemets model is primarily linked to NADPH cost related to the Calvin cycle and associated photorespiration pathways, while the cost in NADPH along the MEP pathway itself is neglected. Moreover, due to the parallelism between the Niinemets model and the Farquhar model, the extra NADPH cost needed in order to reduce G3P and Pyr into DMADP is tightly linked with the specificity of Rubisco and its affinity to both CO_2 and O_2 through the use of the term Γ^*. The hypothesis underlying the Niinemets model could be considered not a substrate limitation but as a competition for electrons between the isoprene synthesis pathway and the Calvin and photorespiratory cycles. Thus, I conjectured that the cost of electrons involved in the MEP pathway should be represented with more accuracy in a different way, and be decoupled from specific electron cost of CO_2 assimilation.

The second problem I found with the Niinemets model comes from equation (2.22), which can be rewritten as:

$$
\begin{aligned}
I &= \varepsilon_N J \frac{(C_i - \Gamma^*)}{6\,(4.67 C_i + 9.33 \Gamma^*)} \\
&= \varepsilon_N J \frac{(C_i - \Gamma^*)}{6\left(\frac{2.33}{2}\right)\cdot\left(4C_i + 8\Gamma^*\right)} \\
&= \left[\frac{\varepsilon_N}{6\left(\frac{2.33}{2}\right)}\right]\cdot\underbrace{\left[\left(\frac{J}{4}\right)\cdot\frac{(C_i - \Gamma^*)}{(C_i + 2\Gamma^*)}\right]}_{A_j} \\
I &= \varepsilon'_N \cdot A_j
\end{aligned}
\qquad (2.22'')
$$

with ε'_N a constant expressed in ($(\mu$mol isoprene) (μmol $CO_2)^{-1}$). The Niinemets model thus describes a substrate-limited situation even when assimilation is actually light-limited.

A supplementary issue arises from this: when the assimilation of CO_2 is Rubisco-limited, A_j becomes hypothetical. The original idea of Niinemets and co-authors was certainly to link I to J (rather than A_j), and A_j versus $PPFD$ follows the response of J under constant conditions of C_i and T as shown in Figure 2.2. However, the majority of studies using Niinemets *et al.* (1999b)'s approach have related I to A_j (Arneth *et al.*, 2007a,b; Young *et al.*, 2009; Pacifico *et al.*, 2011, 2012; Unger *et al.*, 2013).

2.4.2 The new modelling approach

The hypothesis underlying the Niinemets model clearly stipulates a competition for electrons between isoprene synthesis and other biochemical pathways, including nitrate reduction. Niinemets *et al*. (1999b) also discussed in their original paper the fact that the total electron flux produce by Photosystem II (J_{tot}) is always somewhat larger than necessary for sugar synthesis (Figs 2.3, 2.6). This has to be so in order to feed other pathways' energetic requirements. A parallel is made between isoprene and nitrate reduction, which also is found to saturate at higher light intensities and to increase with decreasing C_i (Bloom *et al.*, 1989; Holmes *et al.*, 1989). However, the mathematical approach of the Niinemets model does not exactly represent this idea.

In order to fill the gaps in the Niinemets model and in an attempt to represent the NADPH and associated electron fluxes involved in the MEP pathway alone, I analysed the available studies that have quantified J_{tot} in comparison to J (as used in Calvin and photorespiratory cycles and computed from carbon assimilation measurements). The difference is important because the MEP pathway has to find additional reducing power to move the reduction state of carbon in sugars up to the level of isoprene. The 'excess' of electrons can be represented by $[J_{tot} - J]$ or more precisely $[J_{tot} - J_{CO2+O2}]$. J_{CO2+O2} represents the electrons used in the Calvin and photorespiratory cycles and $J_{CO2+O2} = J$, when assimilation is under light-limited conditions (Fig. 2.5). Unfortunately, it is commonly assumed that $J_{tot} = J$. There is very little information about the differences between J_{tot} and J. Although it is common (and generally true) to assume than J_{tot} and J vary together, some difference between the two electrons fluxes has been be observed

(schematically represented in Fig.2.3). Differences in quantum efficiencies of J_{tot} and J have been measured using O_2 evolution and gas exchange techniques. These differences can be partially but not fully explained by the additional electrons needed for nitrate assimilation (Singsaas *et al.*, 2001). J_{tot} has been found to saturate at the same light fluxes as J for plants fed with ammonium, but J_{tot} has been found to saturate at higher light fluxes than J for plant fed with nitrate (note that nitrate reduction to ammonium occurs mainly in the cytoplasm and consumes NAPDH) (Bloom *et al.*, 1989). This observation suggests that the leaf has the ability to adapt its photosynthetic capacity to its need for reducing power.

New techniques, based on chlorophyll fluorescence, are now commonly used to measure the total electron flux produced by Photosystem II. The principle of chlorophyll fluorescence is that light energy absorbed in the chloroplast can (i) drive photosynthesis (photochemistry); (ii) be dispersed as heat; or (iii) be re-emitted as light (fluorescence) (Fig. 2.3, Box 2.1). However, the relative ease of fluorescence measurements (a number of commercial manufacturers provide a fluorimeter designed to be attached to standard gas exchange chambers) hides the fact that the theory behind these measurements is not simple. Although measurements using fluorescence techniques give information on Photosystem II activity, absolute values of J_{tot} should be interpreted with caution (Baker, 2008; Murchie & Lawson, 2013). Investigation of $[J_{tot} - J]$ is further complicated by uncertainties in the measurement of J. J is usually estimated from gas exchange measurement of leaf net assimilation. But gas exchange measurements do not give a direct observation of J. Hence, calculations of J from gas exchange techniques suffer from unavoidable assumptions e.g. about leaf absorptance, activation and de-activation energies and respiration rates.

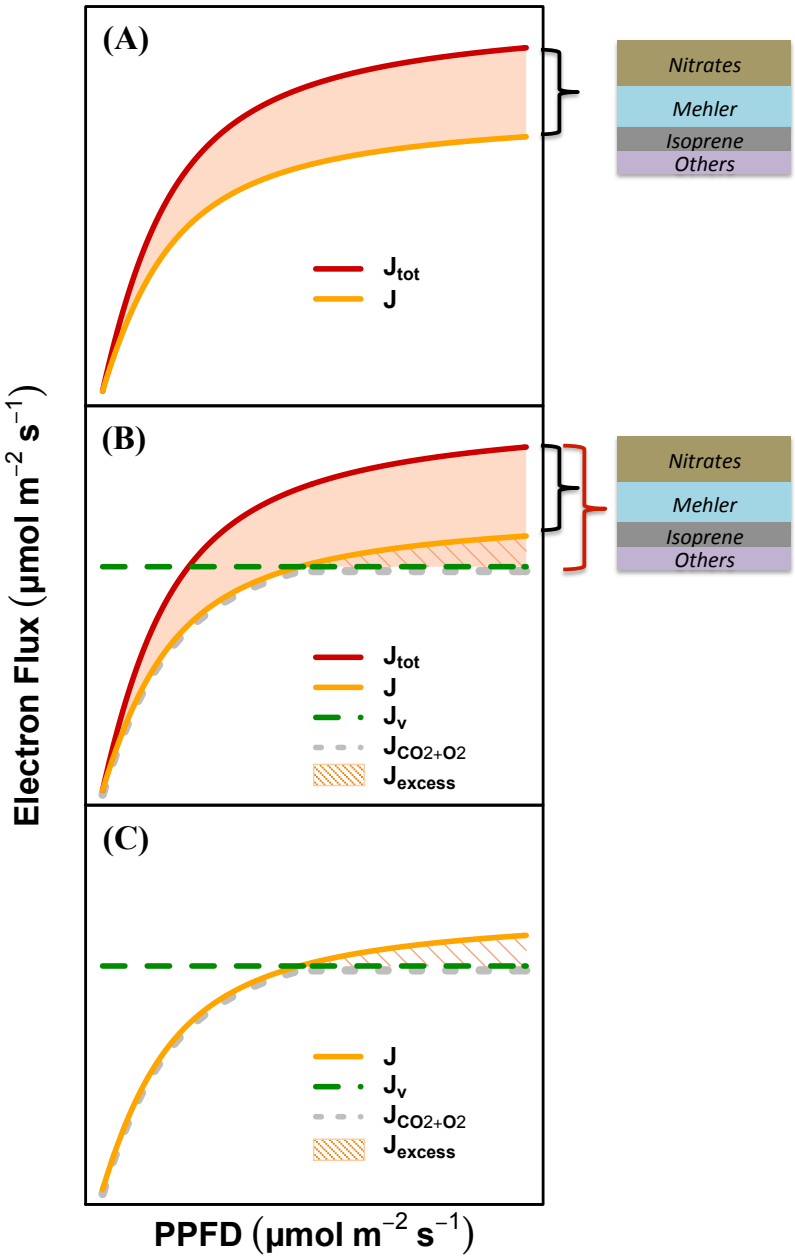
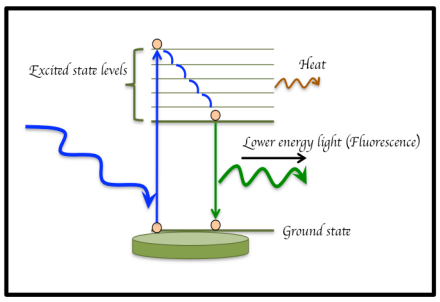


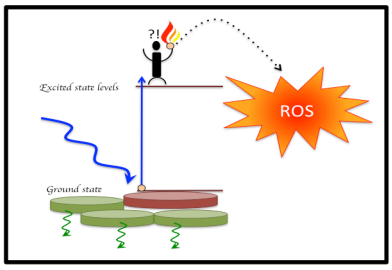
Figure 2.6: Schematic representation of electrons fluxes versus photosynthetic photon flux density (*PPFD*) assuming constant conditions of temperature and internal CO_2 and O_2 concentration. In red, the total electron flux generated by photosystem II (J_{tot}); in orange, total electron flux as computed from assimilation curve using the Farquhar model (J); in dashed green, electron flux required to satisfy the Rubisco capacity, (J_v); in dotted grey, electron flux used for CO_2 assimilation and associated photorespiration (J_{CO2+O2}); The light orange area represents the pool of electrons available for other purposed than carbon assimilation and photorespiration; the orange dashed area represents the knowledge available on the electrons in excess using Farquhar equations. Panel (A) shows the situation when assimilation is always light limited; Panel (B) shows the situation when assimilation becomes Rubisco-limited at high PPFD. Panel (C) shows the modelling tools available for modelling the pool of available electrons for other purposes than carbon assimilation and photorespiration. Graphs are only figurative and scales, in particular for the differences between electron fluxes, are not representative.

Box 2.1 (1/3) Overall picture of processes involving photon capture in the chloroplast

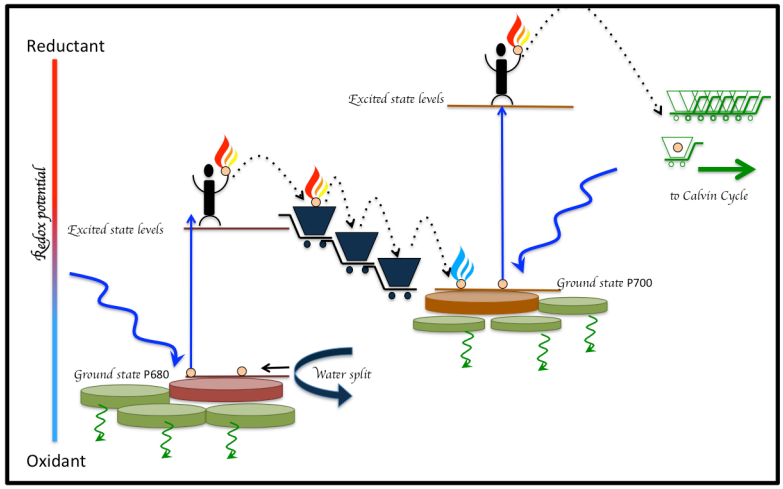


In the absence of reaction centres, a photon absorbed by chlorophyll brings an electron from its ground-level energy state to a higher-energy state. Relaxation of the excited state to its lowest vibrational level occurs with heat dissipation. From there, the electron relaxes to its ground state by emitting a photon of lower energy than the photon absorbed. This light emission is called fluorescence.

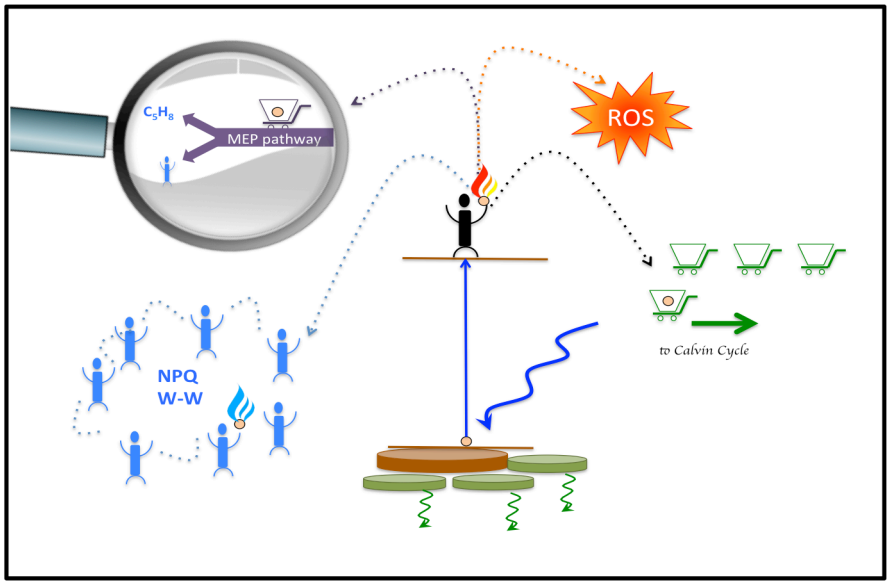
In the presence of reaction centres, excited chlorophyll becomes unstable and generates reactive oxygen species (ROS), which are damaging for the plant. ROS are produced through the transfer of energy or electrons to oxygen species. The most common ROS found in the chloroplast are superoxide (O_2^-), singlet oxygen ($^1O_2^*$) and hydrogen peroxide (H_2O_2).



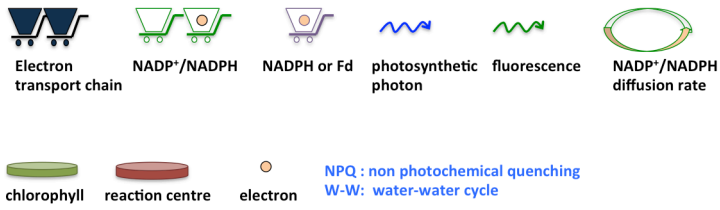
The best way of dealing with the photon energy absorbed by the reaction centres is by using this energy for photosynthesis. A photon absorbed by Photosystem II (PSII; functional and structural units with a reaction centre at their heart) excites the reaction center P680. Excited P680 is a very strong biologic oxidant. It snatches an electron from water, and passes its excited electron (at a high energy level) to the electron transport chain (ETC). A chain of redox reactions brings this electron to the ground-state energy level of PSI. Another photon absorbed by P700 brings the electron to a level of higher energy. Excited P700 is a very strong biological reductant. It reduces Ferrodoxin (Fd), which in turn reduces $NAPD^+$ to NAPDH. NAPDH is further exported to the Calvin cycle and used to produce sugar from CO_2.



Box 2.1 (2/3) Overall picture of processes involving photon capture in the chloroplast

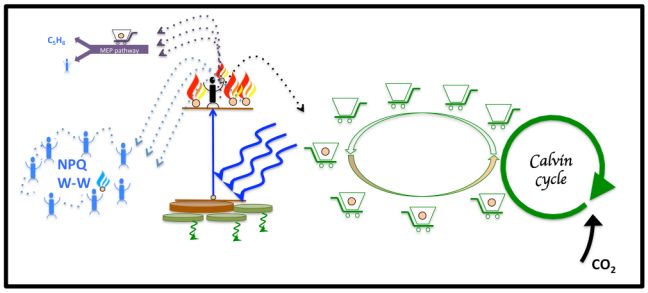


A large part of the photon energy absorbed by chlorophyll is re-emitted as light (fluorescence). Thanks to the reaction centres and ETC, a part of this energy is quenched and used in photochemistry. To avoid the production of damaging ROS, plants have developed strategies to deal with the excess of energy absorbed and electrons produced. Among those, the Mehler reaction or water-water cycle (W-W) efficiently uses electrons in excess to reduce oxygen to water. Non-photochemical quenching (NPQ) also deals with excess energy. The general concept of NPQ can be described as a transfer of energy from excited chlorophyll to molecules having the ability to dissipate this energy as heat (non-radiative relaxation). The major mechanism of NPQ is called the xanthophyll cycle and involves three carotenoids: violanxanthin, antheraxanthin and zeaxanthin.
Finally, some of the electrons generated by the complex PSII-ETC-PSI are used in the MEP pathway. The MEP pathway produces isoprene and also carotenoids involved in NPQ.



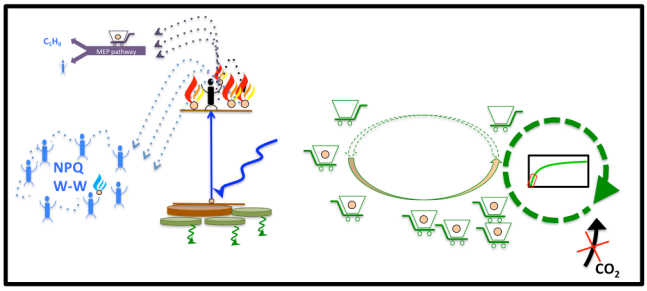
Box 2.1 (3/3) Overall picture of processes involving photon capture in the chloroplast

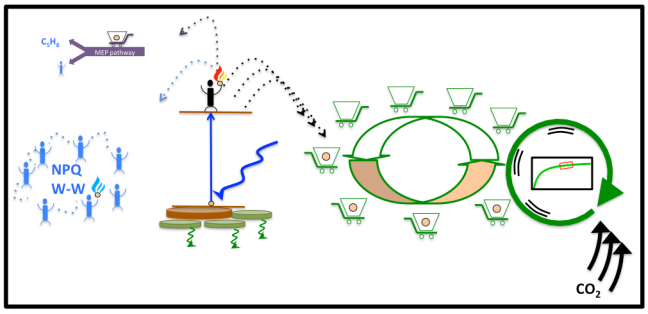
The production of ROS, and associated photoprotective mechanisms are enhanced under conditions where the photon intensity is in excess to what can be absorbed by carbon assimilation. It is logic to assume that the intensity of the electron flux available for the MEP pathway is influenced in the same way.



If photon intensity increases; the electron flux that can be generated by the photosystems goes over what can be absorbed by CO_2 assimilation. Energy and electrons are in excess. NPQ increases to dissipate excess of energy into heat. More electrons are used in the W-W cycle and in the MEP pathway.

Low CO_2 concentration causes another situation where photon intensity is greater than can be used in the Calvin cycle. Less substrate availability (CO_2) leads to lower carboxylation velocity (highlighted in red in the Michaelis-Menten kinetics curve). This reduction in the velocity of carboxylation causes an over-reduction of the NADP pool. Again, energy and electrons are in excess. NPQ increases to dissipate excess of energy into heat. More electrons are used in the W-W cycle and in the MEP pathway.





On the other hand, high CO_2 concentration leads to higher carboxylation velocity (highlighted in red in the Michaelis-Menten kinetics curve) and the rate of electron consumption in the Calvin cycle increases. More photon energy is used in photochemistry processes. In this situation, electrons are in deficit. NPQ decreases to allow more energy to be used in photochemistry. Fewer electrons are used in the W-W cycle and in the MEP pathway.

Process-based models that can simulate total electron transport rate are in an early stage of development (Ye *et al.*, 2013); the quantities involved in the MEP pathway are small (nanomole scale); and quantitative models of other pathways consuming reducing power do not exist. Therefore we have no choice but to work with the commonly used Farquhar model, a decision that requires some assumptions to be made.

J_{max} is commonly found to be larger than V_{cmax} (Medlyn *et al.*, 2002; Kattge & Knorr, 2007). Consequently, carbon assimilation rate usually saturates at lower light than electron flux (Figs. 2.2, 2.6) and there is an observed threshold in assimilation drivers (*PPFD*, *T* and C_i) for which carbon assimilation switches from a light-limited to a Rubisco-limited regime. The electron flux (J_v) required to support Rubisco-limited assimilation can be estimated by substituting A_v (Eq. 2.11) in equation 2.16:

$$J_v = 4V_{cmax} \cdot \frac{(C_i + \Gamma^*)}{(C_i + k_c')} \qquad (2.26)$$

As for assimilation, the electron flux J_{CO2+O2} required to satisfy the energetic need of net assimilation follows the minimum of J and J_v. The different responses of electron fluxes J_{tot}, J and J_v to increasing light intensity (for a given T and C_i) are schematically represented in Figure 2.6. As shown in Figure 2.6, the MEP pathway finds necessary reducing power to reduce G3P and Pyr into DMADP in the electron pool represented by [$J_{tot} - J$] (shaded in light orange in Fig. 2.6). This pool of 'available' electrons increases when the assimilation becomes Rubisco-limited, as the requirement of electron for carbon assimilation then becomes equal to J_v. The dashed area in Figure 2.6 represents this increase of the electron pool available for other purposes than carbon assimilation. From a modelling point of view, information about ([$J_{tot} - J_{CO2+O2}$]) is not available; what we have to work with is limited to the mathematical representation of J and J_v. However, as shown in Figure 2.6, for high light (or low C_i) we can extract some information about [$J_{tot} - J_{CO2+O2}$] from carbon assimilation curves as we can assume that under Rubisco-limited conditions [$J_{tot} - J_{CO2+O2}$] is at least equal to [$J - J_v$].

The general form of [$J_{tot} - J$] versus *PPFD* could follow any of four patterns: i) [$J_{tot} - J$]~ constant J; ii) [$J_{tot} - J$] narrows with increasing *PPFD*, iii) [$J_{tot} - J$] increases with *PPFD* or vi) [$J_{tot} - J$] varies randomly. Assuming that [$J_{tot} - J_{CO2+O2}$] does not show a

sharp slope break when assimilation becomes Rubisco-limited, but rather a gradual increase following the extent to which the NADPH requirements of the Calvin-Benson and photorespiratory cycles are satisfied, I proposed that [$J_{tot} - J_{CO2+O2}$] increases with *PPFD* in proportion to the leaf energetic status. The leaf energetic status is defined here as the balance (or imbalance) between the supply of photosynthetically generated reducing power and the demands of carbon fixation and photorespiration, which can be approximated by the difference between the light- and Rubisco-limited electron fluxes for carbon assimilation [$J - J_v$].

This hypothesis of a gradual increase of that [$J_{tot} - J_{CO2+O2}$] with the energetic status of the leaf can be viewed as parallel to non-photochemical quenching (NPQ); a photoprotective mechanism where energy is dissipated as heat mostly by the enzymatic conversion of the carotenoid violaxanthin to zeaxanthin (the xanthophyll cycle). Indeed energetic quenching, by florescence and heat lost, increases gradually with the energetic status of the leaf in light response curves, rather than suddenly when assimilation is light-saturated (Box 2.1). A recent study by J. Peñuelas and co-workers supports this hypothesis by showing for *Populus nigra L.* and *Quercus ilex L*. a strong negative relationship between isoprenoid emissions (isoprene plus monoterpenes) and light use efficiency (Peñuelas *et al.*, 2013) .

To represent the idea that the pool size of available electrons for isoprene synthesis is proportional to the degree to which requirement of electron for carbon assimilation are satisfied, I tested two models.

Model1

In the first model, the rate of isoprene emission is linearly related to the "energetic status" [$J - J_v$] of the leaf.

$$I = a J + b(J - J_v) \qquad (2.27)$$

The total electron flux J_{tot} is approximated by J (as in the Niinemets model), the rate of isoprene emission I is calculated as an emission baseline represented by a fraction of the total electron flux ($a J$) modulated by a term which accounts for the electron availability for isoprene production b ($J - J_v$); This model was first introduced in (Harrison *et al.*, 2013). This version was used to further test the validity of my hypothesis by comparing

the behaviour of the model with key observed responses of isoprene emission (Morfopoulos *et al.*, 2013) (Chapter III).

However, this model can generate unrealistic negative values, especially under low light. Under light-limited conditions, with a high demand of NAPDH by the Calvin cycle, the term b ($J - J_v$) can reach large enough negative values to create overall negative emissions. This is an obvious limitation of Model 1.

Model 2

In Model 2 the *fraction* of electrons allocated to isoprene biosynthesis is linearly related to the energetic status of the plant:

$$\varepsilon = c_1 + c_2 (J - J_v) \quad (2.28)$$

and

$$I = \varepsilon J \quad (2.29)$$

As in Model 1, the total electron flux J_{tot} is approximated by J. The term ε, which represents the fraction of J allocated to isoprene emission, is not constant but has a magnitude depending on the energetic status of the leaf. c_1 and c_2 are constants. My hypothesis however poses that the *magnitude* of the electron flux available (and not the *fraction* of electrons allocated) for isoprene synthesis becomes larger with the energetic status of the leaf. Using variation of the fraction of electron allocated into the MEP pathway ε, instead of variation of electron fluxes, is a pragmatic way to compensate for the lack of modelling tools to simulate J_{tot}. In Chapter IV, this model is further explained and tested, using data and on hybrid aspen (*Populus tremula* L. x *P. tremuloides Michx*) from (Sun *et al.*, 2012) and on *Populus nigra* L. (Morfopoulos *et al.,* 2014).

Both formulations (Models 1 and 2) represent processes associated with DMADP production. The transformation of [DMADP] to isoprene also depends on the activity of IspS. This responds primarily to changes in temperature. For a constant T, changes in isoprene emission rates are thus proportional to changes in [DMADP]. But with changes in T, isoprene emission rate responds to changes of both DMADP concentration and activity of IspS. And for a constant [DMADP] pool size, emissions are expected to increase with temperature up to the temperature optimum of IspS. To represent this behaviour, I include a function of temperature in the model:

$$f(T) = \frac{S_S}{S_{Ss}} \quad (2.30)$$

where S_S is the IspS activity, as introduced by Niinemets *et al.* (1999b) (Table 2.1) and S_{Ss} is the IspS activity for a standard T (30˚C). Consequently, with a normalised enzymatic temperature response, the model's parameters (a, b) or (c_1, c_2) must apply to standard temperature conditions. In this thesis, the temperature responses of the model(s) with additional function for enzymatic response have been expounded theoretically (Morfopoulos *et al.*, 2013) and tested at the canopy scale (Chapter V). However, in the frame of collaboration with the Institute for Advanced Sustainability Studies (IASS, Germany), modelled effects of temperature have been tested against observations. The paper resulting from this collaborative study has been published in *Plant, Cell and Environment* (Grote *et al.*, 2014).

On the other hand, for a given temperature, the low affinity of IspS for its substrate DMADP, implied by the high value of Michaelis constant ($1.2 < K_m < 2.45$ mM) (Silver & Fall, 1995; Schnitzler *et al.*, 2005), ensures linearity between [DMADP] and isoprene emissions. Thus, in the case of constant T, the model describing processes involved in the MEP pathway and associated production of DMADP can be related directly to emissions.

The physiological hypothesis

Many studies have proposed a link between isoprene emission and leaf energetic status to account for the diverse observed behaviour of isoprene emission in response to T, C_i and *PPFD* (Niinemets *et al.*, 1999b; Rasulov *et al.*, 2009b, 2010; Li & Sharkey, 2012). Yet the basic concept that isoprene emission is controlled by NAPDH availability is still strongly debated in the isoprene community. The idea of the MEP pathway acting as a safety valve to get rid of excess of energy (and DMADP) has been previously proposed (Owen & Peñuelas, 2005; Rosenstiel *et al*., 2004). The concept of an energy security valve can be criticised because the amount of energy engaged in the MEP pathway alone is small; it does not have the capacity to absorb all of the excess energy that can generated in the chloroplast. Nevertheless, even if the pathway does not act as a safety valve, it is still physiologically plausible that the flux of electrons through the pathway could be controlled by changes in energetic status of the leaf.

Here, I propose a theoretical concept as to how chemical processes control electron/NADPH fluxes in the cell and in turn influence the entrainment of electrons into the MEP pathway. Movements of NADPH and $NADP^+$ inside the cell have to be driven by diffusion generated by gradients of concentration. NADPH, which is produced in the thylakoid membranes, should preferentially diffuse towards the location of NADPH sinks. Oxidation-reduction reactions in the cell, such as those involved in the Calvin/photorespiratory cycles and the isoprene synthesis pathway, act as NAPDH sinks and thus create NADPH concentration gradients. These concentration gradients – from the thylakoid membrane to location in the cell when reduction reactions take place – generate fluxes of NAPDH from thylakoids toward reaction centres. Accompanying these NADPH fluxes, reverse fluxes of $NADP^+$ are also generated from oxidation-reduction reaction centres ($NADP^+$ production) toward the thylakoids ($NADP^+$ sinks) (Box 2.1). Thus, an analogy with an electrical circuit can be drawn (Fig. 2.8), with thylakoids acting as anodes and biochemical pathways including oxidation-reduction steps acting as cathodes. In this analogy the main circuit is the one associated with carbon assimilation. This main circuit has a very low resistance due to the extensive use of NADPH in the carbon assimilation and photorespiration cycles (large sink strength). The resistance of the Calvin Cycle pathway can however increase in situations of reduced substrate availability (C_i) and/or the degree of engagement of Rubisco and NADPH in the reduced form (higher light). The isoprene synthesis pathway could be considered as one of many parallel circuits, with higher resistances limiting the fraction of the electron flux through these minor circuits. The current flowing through the pathway must nonetheless increase in proportion to the applied voltage, and must be sensitive to changes in the resistance of the main circuit. The high resistance of the MEP pathway could be due to i) low substrate availability (Pyr), ii) low concentrations of enzymes involved in the MEP pathway, or iii) down-regulation of the MEP pathway by DMADP (Trowbridge *et al.*, 2012; Banerjee *et al.*, 2013).

Two of the three reduction steps occurring along the MEP pathway can use electrons directly from the electron transport chain, using Ferredoxin (Fd) as the reductant (Fd is an intermediate in the electron transfer chain from PSII to $NAPD^+$, and has a redox potential strong enough to reduce $NADP^+$ to NAPDH). This fact, along with the location of the MEP pathway – which is presumed to be close to the thylakoid membrane, as IspS is possibly bound to the thylakoid membrane (Wildermuth & Fall, 1996;

Lichtenthaler, 1999) – further supports the hypothesis that the MEP pathway can be sensitive to changes in the degree of engagement of electrons in the Calvin cycle.

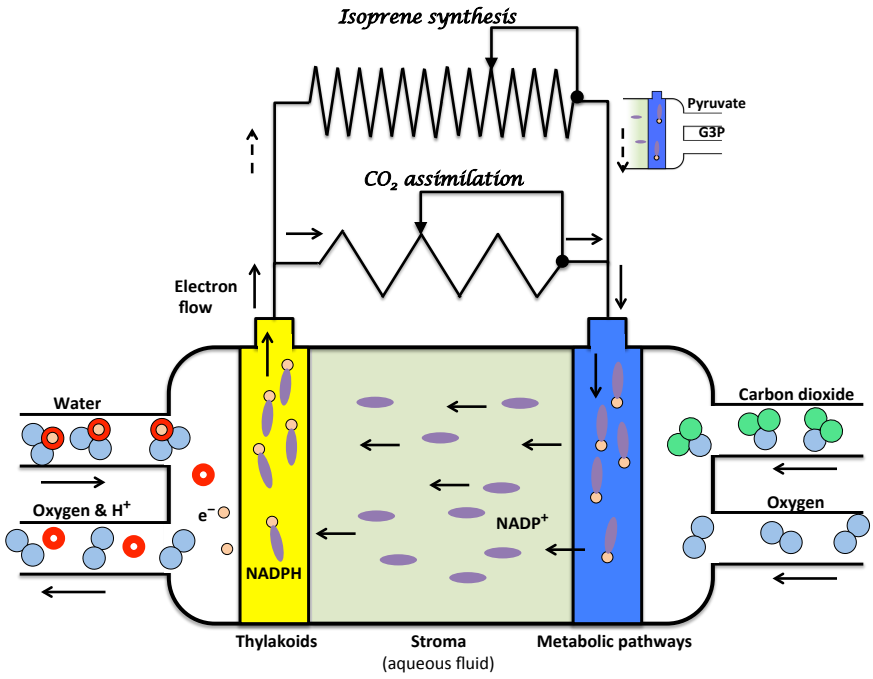


Figure 2.7: Schematic of the parallel between electrolyte circuit and processes involved in the oxydo-reduction reactions and nicotinamide adenine dinucleotide phosphate (NADPH/$NAPD^+$) fluxes. *(Inspired by the schematic of molten carbonate fuel cell* http://www.doitpoms.ac.uk/tlplib/fuel-cells/mcfc_electrolyte.php*; University of Cambridge)*

Unexplained bursts of isoprene emission have been observed a few minutes after the leaf is put in the dark. The intensity of the observed burst of isoprene in the dark is found to be proportional to the light intensity (and thus energetic status) applied to the leaf before the light is switched off (Rasulov *et al.*, 2011). One of the possible explanations for this observed burst is the use of residual post-illuminated NADPH by the MEP pathway (Thomas Sharkey, personal communication 2013). This observation tends to support the

idea of the MEP pathway being sensitive to the cell reductant sinks and reductant availability, whether in the form of Fd or NADPH.

Behnke *et al.* (2007) showed that transgenic grey poplar with isoprene synthase suppressed developed higher non-photochemical quenching capacity than isoprene-emitting individuals. This observation too is in line with the idea of a connection between the intensity of the MEP pathway and the energetic status of the leaf.

2.5 Conclusions

An analysis of the Farquhar and Niinemets models, along with examination of the processes involved in both carbon assimilation related cycles and isoprene production pathway, led to the hypothesis that isoprene production rates are primarily controlled by the excess or deficit of electrons generated by Photosystem II, relative to the needs of carbon fixation. To embody this hypothesis isoprene emission rate are proposed to be proportional to the energetic status of the leaf evaluated using the difference in the light- and Rubisco electron fluxes for carbon assimilation [$J - J_v$]. Two model versions are proposed. In Model 1, the rate of isoprene emission is linearly related to the energetic status of the leaf. In Model 2, the *fraction* of electrons allocated to isoprene biosynthesis is linearly related to the electron excess. A possible physiological underpinning of these models was suggested. It was shown that several lines of evidence make it plausible that the flux of electrons through the isoprene synthesis pathway is related to the energetic status of the leaf.

The following chapters show how this new modelling approach considerably improves the form of the response of isoprene emission to its environmental drivers when compared to the Niinemets model. Moreover the new modelling approach represents the original idea of Niinemets and co-authors, of a competition for electrons between isoprene and the Calvin cycle, more accurately than the original Niinemets model. The mathematical form is simple, but novel, and proves to have considerable predictive power.

The following chapters describe how the new hypothesis is sufficient to reproduce widely observed responses of isoprene emission to changes in *PPFD*, temperature, CO_2 concentration and drought.

3 A unifying conceptual model for the environmental responses of isoprene emissions from plants

This chapter describes how the new model hypothesis (previously described in detail in chapter II), that isoprene production rates are primarily controlled by the excess or deficit of electrons generated by Photosystem II, relative to the needs of carbon fixation, has been tested. A body of published data has been revisited, paying particular attention to how the isoprene/carbon assimilation ratio (I/A) varies in response to light. The systematic increase of I/A with light, at both leaf and canopy scales, confirms the importance of electron availability in determining isoprene emission rates. This chapter also describes how the new hypothesis alone is sufficient to reproduce widely observed responses of isoprene emission to changes in light, temperature, CO_2 concentration and drought.

Results presented in this chapter have been published in the journal *Annals of Botany* (Morfopoulos *et al.*, 2013) using Model 1, where the rate of isoprene emission is linearly related to the leaf energetic status as approximated by the difference between light- and Rubisco- limited electron fluxes (equation 2.27 in Chapter II). After the publication of Morfopoulos *et al.* (2013), Model 2 was developed, in which the *fraction* of electrons allocated to isoprene biosynthesis is linearly related to the energetic status; this was found to fit observations better and avoids a problem of potentially negative emissions that afflicts Model 1. Additional figures that redraw key figures from Morfopoulos *et al.* (2013), but using Model 2, are accordingly displayed in annex 3A.1.

Abstract

Isoprene is the most important volatile organic compound emitted by land plants in terms of abundance and environmental effects. Controls on isoprene emission rates include light, temperature, water supply and CO_2 concentration. A need to quantify these controls has long been recognized. There are already models that give realistic results, but they are complex, highly empirical, and require separate responses to different drivers. I set out to find a simpler, unifying principle.

I present a simple model based on the idea of balancing demands for reducing power (derived from photosynthetic electron transport) in primary metabolism versus the secondary pathway that leads to the synthesis of isoprene. I assess this model's ability to account for key features in a variety of experimental data sets.

The model simultaneously predicts the fundamental responses observed in short-term experiments: (1) the decoupling between carbon assimilation and isoprene emission; (2) a continued increase in isoprene emission with photosynthetic photon flux density (*PPFD*) at high *PPFD*, after carbon assimilation has saturated; (3) a maximum of isoprene emission at low internal CO_2 concentration (C_i) and an asymptotic decline thereafter with increasing C_i; (4) maintenance of high isoprene emissions when carbon assimilation is restricted by drought; and (5) a temperature optimum higher than that of photosynthesis, but lower than that of isoprene synthase activity.

I used a simple model to test the hypothesis that reducing power available to the synthesis pathway for isoprene varies according to the extent to which the needs of carbon assimilation are satisfied. Despite its simplicity the model explains much in terms of the observed response of isoprene to external drivers as well as the observed decoupling between carbon assimilation and isoprene emission. The concept has the potential to improve global-scale modelling of vegetation isoprene emission.

3.1 Introduction

Isoprene (2-methyl-1,3-butadiene; C_5H_8) is a highly volatile and reactive unsaturated hydrocarbon that is produced continuously in daylight by many terrestrial plants, and in great abundance by broad-leaved trees. On a mass basis, it is the most important biogenic volatile organic compound (BVOC) emitted by vegetation, with an annual global emission of approximately 0.5 x 10^{15} g C. This is similar in magnitude to the total annual emission of the greenhouse gas methane (CH_4) from all natural sources combined (Guenther *et al.*, 1995, 2006; Laothawornkitkul *et al.*, 2009). Although not a greenhouse gas itself, isoprene reacts in the atmosphere with oxidants, including hydroxyl radicals (OH) and ozone (O_3) (Fan & Zhang, 2004), and consequently influences the atmospheric lifetime and concentration of CH_4 (Poisson *et al.*, 2000; Collins *et al.*, 2002, 2010; Pike & Young, 2009). The influence of isoprene on atmospheric oxidation capacity has been proposed as one of the controls of the glacial-interglacial variations of atmospheric CH_4, as recorded in ice cores (Valdes *et al.*, 2005; Singarayer *et al.*, 2011). Isoprene also enhances the production of tropospheric ozone (O_3), a potent greenhouse gas and toxic pollutant, under high-NO_x conditions (Sanderson *et al.*, 2003; Hauglustaine *et al.*, 2005), and can significantly affect the atmosphere's radiative balance through the generation of secondary organic aerosols (Claeys *et al.*, 2004; Heald *et al.*, 2008; Carlton *et al.*, 2009; Nozière *et al.*, 2011).

Isoprene emissions by plants at the leaf scale respond to changes in photosynthetic photon flux density (*PPFD*), temperature, ambient CO_2 concentration, and drought (Sharkey & Yeh, 2001; Laothawornkitkul *et al.*, 2009; Pacifico *et al.*, 2009; Niinemets, 2010). Despite general agreement between models under the present climate, simulations of future isoprene emissions, and their potential impact on atmospheric chemistry, change dramatically depending on the temperature and light responses of the model (Keenan *et al.*, 2009) and whether or not the model includes a physiological response of isoprene emission to CO_2 (Young *et al.*, 2009; Heald *et al.*, 2009; Pacifico *et al.*, 2012). Given the continuously increasing atmospheric CO_2 concentration and its impact on future temperature, we need to understand the processes behind observed responses, and use that understanding to build better models.

The adaptive significance of isoprene emission is thought to be connected with enhancing membrane stability at high temperatures, and protection against oxidative

stress – including that induced by high temperatures (Sharkey & Yeh, 2001; Vickers *et al.*, 2009a; Velikova *et al.*, 2011, 2012). On time scales of weeks to years, acclimation mechanisms acting at the level of gene transcription may operate, possibly in such a way as to match isoprene synthase activity to adaptive requirements (Grote & Niinemets, 2008; Monson *et al.*, 2012; Harrison *et al.*, 2013). Here however I focus on the immediate responses of isoprene emission to environmental variations, as observed in experiments conducted over a time scale of minutes to hours, and the basic metabolic mechanisms that may be responsible for them.

The biosynthesis of isoprene occurs via the chloroplastic methylerythritol 4-phosphate (MEP) pathway (Lichtenthaler, 1999; Logan *et al.*, 2000; Sharkey *et al.*, 2008). ^{13}C labelling experiments have shown that the majority of the C in isoprene comes directly from photosynthesis, with the remainder coming from cytosolic C pools depending upon the environmental conditions (Delwiche & Sharkey, 1993; Kreuzwieser *et al.*, 2002; Karl *et al.*, 2002; Affek & Yakir, 2003; Loreto *et al.*, 2004). However, the metabolic controls of the MEP pathway are only beginning to be elucidated (Li & Sharkey, 2012). With incomplete understanding of the metabolic controls of the pathway, models have been developed on the basis of experimental studies of the relationships between isoprene emission and environmental variables. The approach with the longest pedigree combines empirically derived functions for each environmental effect: this is the principle of the MEGAN model (Guenther *et al.*, 2006), developed from the pioneer work of Guenther *et al.* (1993). Other approaches have made more direct use of the limited available information at the biochemical process level, e.g. SIM-BIM (Zimmer *et al.*, 2000, 2003) and the models of Niinemets *et al.* (1999b) and Martin *et al.* (2000). Aside from the model from Martin *et al.* (2000), which has an ATP limitation for isoprene production at high C_i, all these models need an empirical parameterization in order to reproduce the observed CO_2 response. This is potentially quite a severe limitation because there may be unforeseen interactions between the effects of different environmental drivers. Empirical models such as MEGAN include a multiplicity of functions for each environmental response of isoprene emission. More mechanistic approaches such as SIM-BIM, on the other hand, require information on many parameters. This might also be an issue because there is a generally accepted trade-off between the multiplicity of required parameter values and model robustness. I set out to identify a unifying principle that might transcend these limitations.

My starting point was the model of Niinemets *et al.* (1999b), which is based on quantifying the NADPH requirement of isoprene synthesis. Niinemets *et al.* (1999b) assumed that a certain fraction of the total electron flux generated by Photosystem II is allocated to this function. The model I present here, initially proposed in Harrison *et al.* (2013), builds on Niinemets' work but differs in one fundamental respect: it links isoprene emission to the electron availability for isoprene emission, relative to the needs of CO_2 assimilation. Therefore, the model predicts higher isoprene emissions when absorbed radiant energy (leading to the 'supply' of NADPH) exceeds the 'demand' for CO_2 assimilation. An excess of energy arises because of a mismatch between light availability and carboxylation capacity, which typically occurs daily – especially at high *PPFD*, associated high temperature and under water stress. I compare the model's predictions of observed, published environmental responses of isoprene emission to changes in *PPFD* and the leaf-internal concentration of CO_2 (C_i) with those obtained with the Guenther *et al.* (1993) algorithm, hereafter called G93, which is the basis of the widely used MEGAN model (Guenther *et al.*, 2006, 2012); and the model of Niinemets *et al.* (1999b), hereafter called the Niinemets model. I also compare the theoretical temperature responses of my model with G93 and the Niinemets model. I focus on these two models as they have been widely used at the global scale (Guenther *et al.*, 2006; Lathière *et al.*, 2010; Arneth *et al.*, 2011; Pacifico *et al.*, 2012). However, other isoprene models have been developed. Reviews can be found in Arneth *et al.* (2007b), Grote & Niinemets (2008) and Monson *et al.* (2012).

3.2 Hypothesis

In isoprene-emitting plants with the C_3 pathway of photosynthesis, over 90% of isoprene production takes place in the chloroplast via the MEP pathway (Lichtenthaler *et al.*, 1997; Sharkey *et al.*, 2008). The final stage is the enzymatic synthesis of isoprene from its precursor, dimethylallyl diphosphate (DMADP). On a per-molecule basis, isoprene synthesis is energetically expensive, and has a high requirement for reducing power (14 NADPH for one molecule of isoprene). For comparison, only six NADPH are needed to synthesize glyceradehyde 3-phosphate (G3P), and only five for pyruvate. NADPH consumption for G3P and pyruvate synthesis takes place within the Calvin cycle and therefore is linked to the electron cost for carbon assimilation. Three additional reducing steps are needed within the MEP pathway in order to reduce G3P and pyruvate to

DMADP. These supplementary reducing steps consume one further NADPH, and two additional reducing equivalents in the form of either NADPH or ferredoxin (Fd) *(Charon et al.,* 1999*; Hecht et al., 2001; Seemann et al.*, 2006; Li & Sharkey, 2012). My hypothesis focuses on these additional reduction steps, which are directly linked to the production of isoprene.

Isoprene production is typically measured in nanomoles per second while photosynthesis and respiration rates (to which G3P and pyruvate production are linked) are measured in micromoles per second. Hence, the major consumption of reducing power takes place within the Calvin cycle and associated photorespiration while the diversion of reducing power to the MEP pathway is very small. Yet there is abundant circumstantial evidence for a link between the availability of reducing power (after the requirements of carbon assimilation have been accounted for) and the magnitude of this diversion. The MEP pathway is tightly linked to the photosynthetic apparatus and involves light-dependent reactions and takes place in the chloroplast. Higher isoprene emission capacity is encountered under conditions when photoinhibition occurs, including high light intensities, low C_i and high temperatures. Isoprene emissions decrease if plants are fed with nitrate (note that nitrate reduction to ammonia occurs mainly in the cytoplasm and consumes NAPDH) instead of being fed with ammonia directly (Rosenstiel *et al.*, 2004; Campbell, 1988). Li & Sharkey (2012) measured extremely high level of the intermediate metabolite, methylerythritol cyclodiphosphate (MEcDP), in a N_2 atmosphere, where the carbon assimilation and photorespiration sinks for NADPH are blocked. Thus, it might be that the MEP pathway acts as a 'branch circuit' with the amount of NAPDH allocated to it increasing in proportion to the amount of reducing power to spare from other functions.

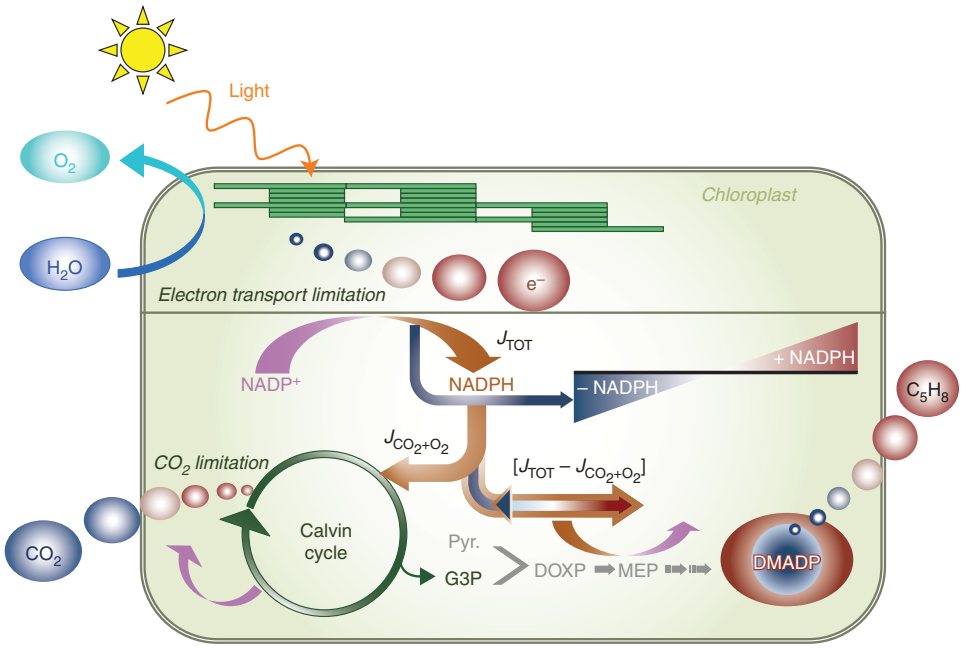


Figure 3.1 Schematic of the processes underlying the model of isoprene emissions. The availability of reducing power (NADPH) for CO_2 assimilation is represented by a colour scheme, from dark blue (deficit of NADPH) to dark red (excess of NADPH). Symbols: NADPH and $NADP^+$, nicotinamide adenine dinucleotide phosphate; DMADP, dimethylallyl diphosphate; Pyr, pyruvate; G3P, glyceraldehyde 3-phosphate; DOXP, 1-deoxy-D-xylulose 5-phosphate; MEP, 2-C-methyl-D-erythritol 4-phosphate.

Thus I hypothesize that isoprene emission is regulated in the short term by variations of the DMADP pool size, linked to the excess or deficit of electrons (and so also reducing power) relative to the needs of carbon assimilation. Figure 3.1 provides a schematic of the processes involved. When the chloroplast is illuminated, light absorbed by the thylakoids generates the electron flux (J_{tot}) that finally reduces $NADP^+$ to NADPH. Most of the NADPH is used in the Calvin cycle for carbon fixation, but the total NADPH thus generated ($\approx 0.5\ J_{tot}$) exceeds the amount consumed in the Calvin Cycle ($\approx 0.5\ J_{CO2+O2}$). When assimilation is light-limited (at high C_i and/or low *PPFD*) there is still some NADPH available for other functions, which include nitrate reduction (Canvin & Atkins, 1974; Niinemets, 2004; Eichelmann *et al.*, 2011) and DMADP synthesis. When assimilation is Rubisco-limited (at low C_i and/or high *PPFD*) this excess of NADPH becomes larger, allowing more NADPH to be used in DMADP synthesis. This reasoning suggests the following simple model:

$$I = \max([a\,J + b(J - J_v)].f(C_i), 0) \qquad (3.1)$$

where I is the rate of isoprene emission; $f(C_i)$ is a function of internal CO_2 concentration; J is an estimate of the total electron flux, taken to be a non-rectangular hyperbolic function of absorbed *PPFD* and the maximum electron flux J_{max}, following Farquhar *et al.* (1980); and ***a*** and ***b*** are parameters. The electron flux required to support carbon assimilation is derived as follows. From Farquhar *et al.* (1980),

$$A_j = \left(\frac{J}{4}\right) \cdot \frac{(C_i - \Gamma^*)}{(C_i + 2\Gamma^*)} \tag{3.2}$$

where A_j is the gross (light-limited) assimilation rate and Γ^* is the CO_2 compensation point in the absence of dark respiration. Hence

$$J = 4A_j \cdot \frac{(C_i + 2\Gamma^*)}{(C_i - \Gamma^*)} \tag{3.3}$$

When Rubisco limits photosynthesis, then

$$A_v = V_{cmax} \cdot \frac{(C_i - \Gamma^*)}{(C_i + k_c')} \tag{3.4}$$

where A_v is the gross (Rubisco-limited) assimilation rate, V_{cmax} is the Rubisco capacity and $k_c' = k_c(1 + [O_2]/k_o)$ where k_c and k_o are the Michaelis coefficients of Rubisco for CO_2 and O_2 respectively (Farquhar *et al.*, 1980). Substituting this into equation (3.3) gives:

$$J_v = 4V_{cmax} \cdot \frac{(C_i + \Gamma^*)}{(C_i + k_c')}, \tag{3.5}$$

It should be noted that J in equation (3.1) is used as an estimate of J_{tot} and could be an underestimate (Singsaas *et al.*, 2001; Niinemets, 2004). More details of the photosynthetic model, as used in this thesis, can be found the supplementary material (S2). The term **a**J in equation (1) represents a 'baseline' of isoprene emission under the equilibrium conditions for carbon assimilation ($J = J_v$, energy supply = Rubisco demand), while **b**$(J - J_v)$ represents variation in isoprene emission due to the disequilibrium between supply and demand. The function $f(C_i)$ in equation (3.1) is

chosen to take the value C_i/Γ^* when $C_i \leq \Gamma^*$ and 1 otherwise. On account of this function, the model slightly differs from the one I proposed in Harrison *et al.* (2013). The function $f(C_i)$ reflects the idea that a minimum rate of supply of carbon chains is required for isoprene synthesis, and the common observation that isoprene emission ceases abruptly when $C_i < \Gamma^*$ (Wolfertz *et al.*, 2003; Rasulov *et al.*, 2009b, 2011; Monson *et al.*, 2012; Sun *et al.*, 2012). This fall-off of isoprene at low C_i is not always observed: emission of isoprene in CO_2-free air have been reported in a few studies (Monson & Fall, 1989; Affek & Yakir, 2003; Li & Sharkey, 2012), but comparable conditions are not found in natural environments.

Although based conceptually on the NADPH requirements of isoprene synthesis and the Farquhar photosynthesis model, my approach differs from that of Niinemets *et al.*, (1999b) where isoprene production was assumed to be closely linked to the light-limited carbon assimilation rate (A_j). This difference has important consequences, as I will show.

3.3 Tests of the hypothesis

I consider the observed environmental responses of isoprene emission (I) and also the ratio of isoprene emission to carbon gross assimilation (I/A_{gross}), which is a sensitive indicator of the allocation of reducing power to the MEP pathway versus the Calvin cycle. I will also consider changes in the ratio of isoprene emission to carbon net assimilation (I/A_{net}).

3.3.1 Responses to PPFD

Equation (3.1) predicts an increase of isoprene emission with *PPFD*, but also an increase of the ratio I/A_{gross} (Fig. 3.2A). The predicted behaviour of I/A_{net} ($A_{net} = A_{gross} - R_d$, where R_d is mitochondrial respiration) is substantially different at low *PPFD*, as shown in Figure 3.2A. At saturating *PPFD*, the difference becomes less important. This is due to the introduction of the R_d term, which affects the assimilation independently from the allocation of reducing power between carbon fixation and secondary metabolism. Most laboratory experiments have reported only A_{net}; this should be kept in mind while interpreting the results.

The response of normalised I/A_{gross} (and I/A_{net}) with *PPFD* is predicted to take place in three stages (Fig. 3.2A).

Stage 1: light-limited carbon assimilation This stage occurs when *PPFD* absorbed is insufficient to generate an electron flux to satisfy Rubisco capacity. It is characterized by an initial steep increase of I/A_{gross} with *PPFD*, becoming gradually less steep at higher *PPFD*. For I/A_{net} the form of the response at low *PPFD* depends on the magnitude of R_d.

Stage 2: transition between light- and Rubisco-limited carbon assimilation This stage is characterized by a discontinuity (abrupt increase) in the slope of I/A_{gross} (and I/A_{net}) versus *PPFD*.

Stage 3: Rubisco-limited carbon assimilation When the electron requirement for carbon assimilation is fully satisfied, the additional reducing power generated by increasing *PPFD* allows I/A_{gross} to continue increasing while A_{gross} remains constant. In this stage, I/A_{net} follows a similar pattern of the I/A_{gross} and increases with *PPFD*. With still further increases in *PPFD* I/A_{gross} and I/A_{net} eventually saturates, as J tends to its maximal value (J_{max}).

Note that the *PPFD* flux where the transition between light- and Rubico limited assimilation occurs (*Stage 2*), as well as the rate of increase of I/A_{gross} with increasing *PPFD*, are dependent of both the photosynthetic and the isoprene model parameters.

I also examined the normalised responses of I/A_{gross} and I/A_{net} to changes in *PPFD* in the G93 and Niinemets models (Fig. 3.2B, C). Under light-limited conditions (Stage 1), the picture differs dramatically depending on the model. In the Niinemets model, isoprene emissions are tightly linked to A_j (see Chapter II) and therefore the response of I to *PPFD* necessarily has the same shape as that of A_j, irrespective of the chosen values of V_{cmax} or J_{max}. As a result, the ratio I/A_{gross} in this model is always constant under light-limited conditions, where carbon assimilation is equal to A_j. The ratio I/A_{net}, when simulated with the Niinemets model, always decreases with *PPFD* under light-limited conditions. In G93, by contrast, changes in I/A_{gross} with *PPFD* are strongly dependent on V_{cmax}, J_{max} and temperature under light-limited conditions. Consequently, the increase followed by a decrease of I/A_{gross} under light-limited conditions, shown in Figure 3.2B, is one of the possible responses of I/A_{gross} for G93, obtained for the temperature and

photosynthetic parameters chosen for this simulation. Changing those parameters changes the shape of the response, and I/A_{gross} can decrease or increase at low *PPFD*. Introducing a dark respiration term affects the shape of the response of I/A_{net} with *PPFD*, as represented by the dashed lines in Figure 3.2B. Hence, G93 can potentially show an *I*/*A* response to *PPFD* similar to that of my model.

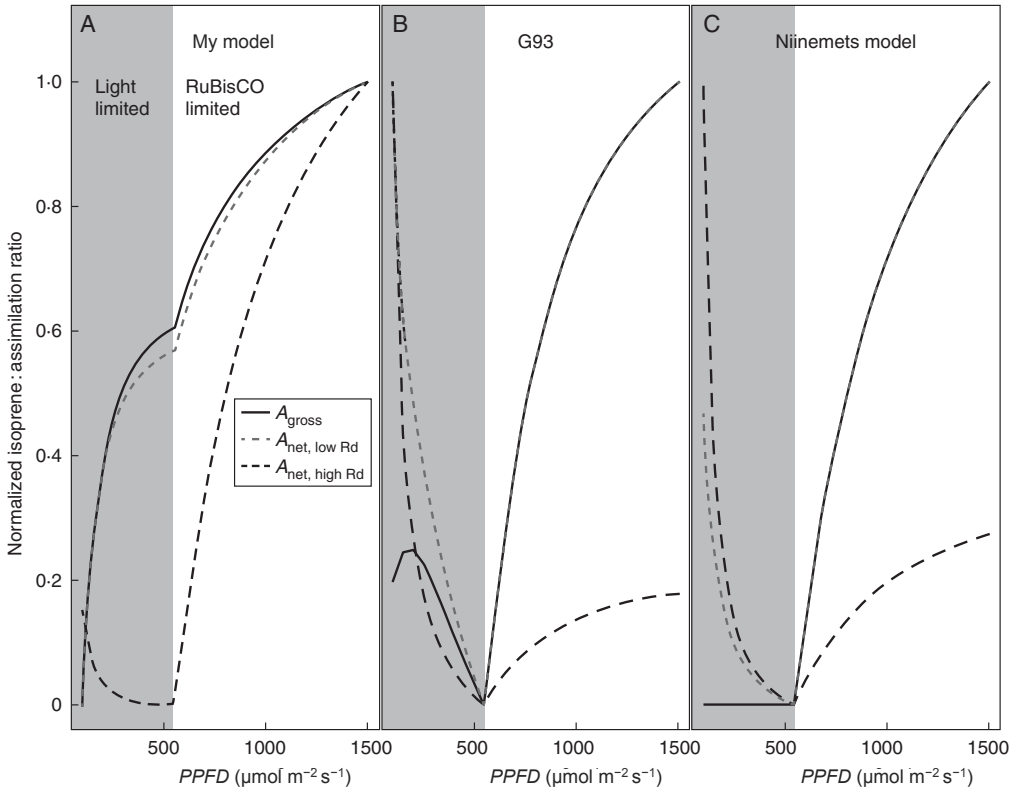


Figure 3.2 Modelled responses of the normalised ratio of isoprene to CO_2 assimilation to changes in *PPFD* for (A) my model, (B) G93, (C) the Niinemets model. T = 30˚C, C_i = 273 μmol mol^{-1}. $V_{cmax\text{-}25^{\circ}C}$ = 70 μmol m^{-2} s^{-1}, $J_{max\text{-}25^{\circ}C}$ = 130 μmol m^{-2} s^{-1} based on values from Arneth *et al.* (2007b)'s study. The solid line represents the ratio of isoprene emission to gross assimilation, the dashed line to net assimilation. Normalised ratio of isoprene to CO_2 net assimilation were simulated for two extreme values of dark respiration in order to illustrate the potential effect of the magnitude of R_d on how I/A_{net} varies with *PPFD*; grey short-dashed line, low R_d; $R_{d\text{-}25^{\circ}C}$ = 0.5 μmol m^{-2} s^{-1}; black long-dashed line, high R_d; $R_{d\text{-}25^{\circ}C}$ = 2 μmol m^{-2} s^{-1}. Isoprene model parameters **a** and **b** (Eq. 3.1) are based on data of Possell & Hewitt (2011) (Fig. 3.6).

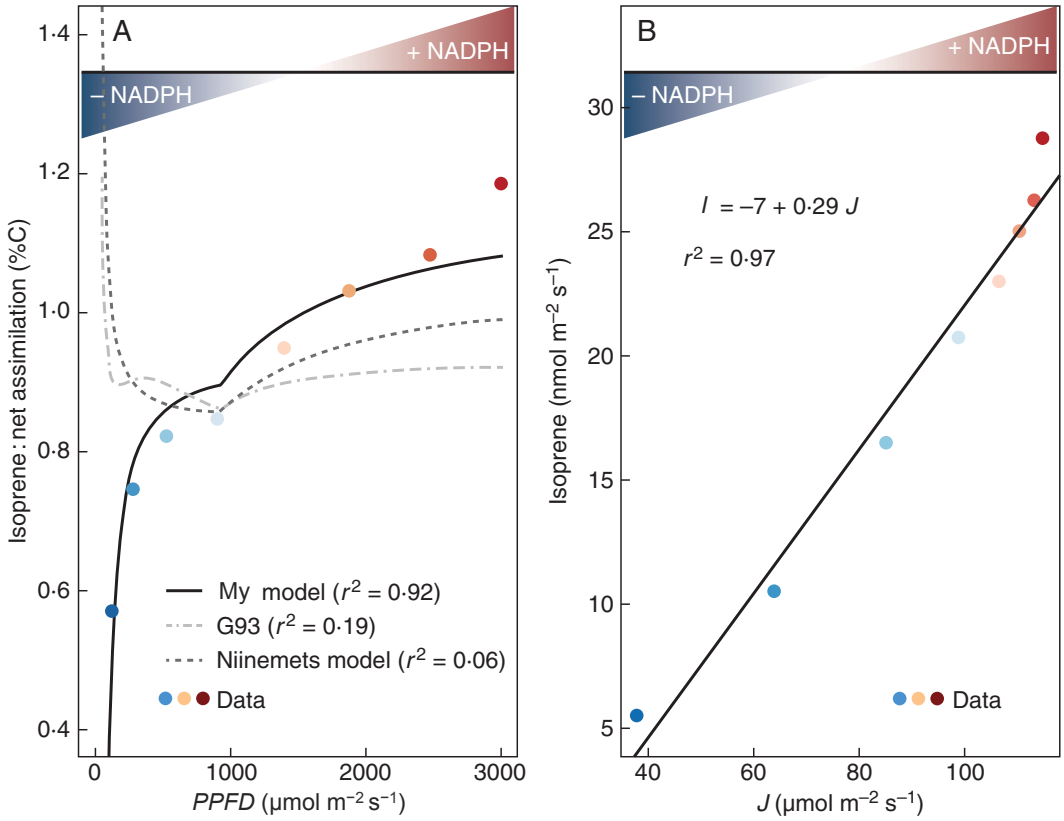


Figure 3.3 The relationship between isoprene emission and NADPH availability for carbon assimilation with changing *PPFD*. (A) Increasing values of the isoprene to CO_2 net assimilation ratio with increasing *PPFD*, based on data digitized from Figure 2 in Sharkey & Loreto (1993). The solid line, the dot-dashed light grey line and the dashed dark grey lines represent simulations made with my model, G93, and the Niinemets model, respectively. (B) the linear regression between isoprene data and the light-limited electron flux (*J*). Plant-specific isoprene parameters (a, b) are estimated from this linear regression and parameters for assimilation (V_{cmax}, J_{max}) were fitted to the assimilation observations by minimizing the residual sum of squares (RSS). In both panels, the availability of reducing power (NADPH) for CO_2 assimilation is illustrated by a colour scheme, from dark blue (deficit) to dark red (excess).

All three models predict increasing I/A_{gross} with *PPFD* under Rubisco-limited conditions. Indeed, in the Niinemets model, as isoprene emissions are linked to A_j, they must continue to increase even when carbon assimilation is Rubisco-limited. In that sense, the Niinemets model implicitly allows consumption of extra NADPH above the needs for carbon assimilation (for the *PPFD* response only). For G93, isoprene emission approaches an asymptotic value at high *PPFD*, while the Farquhar model fully saturates under Rubisco-limited condition at high *PPFD*.

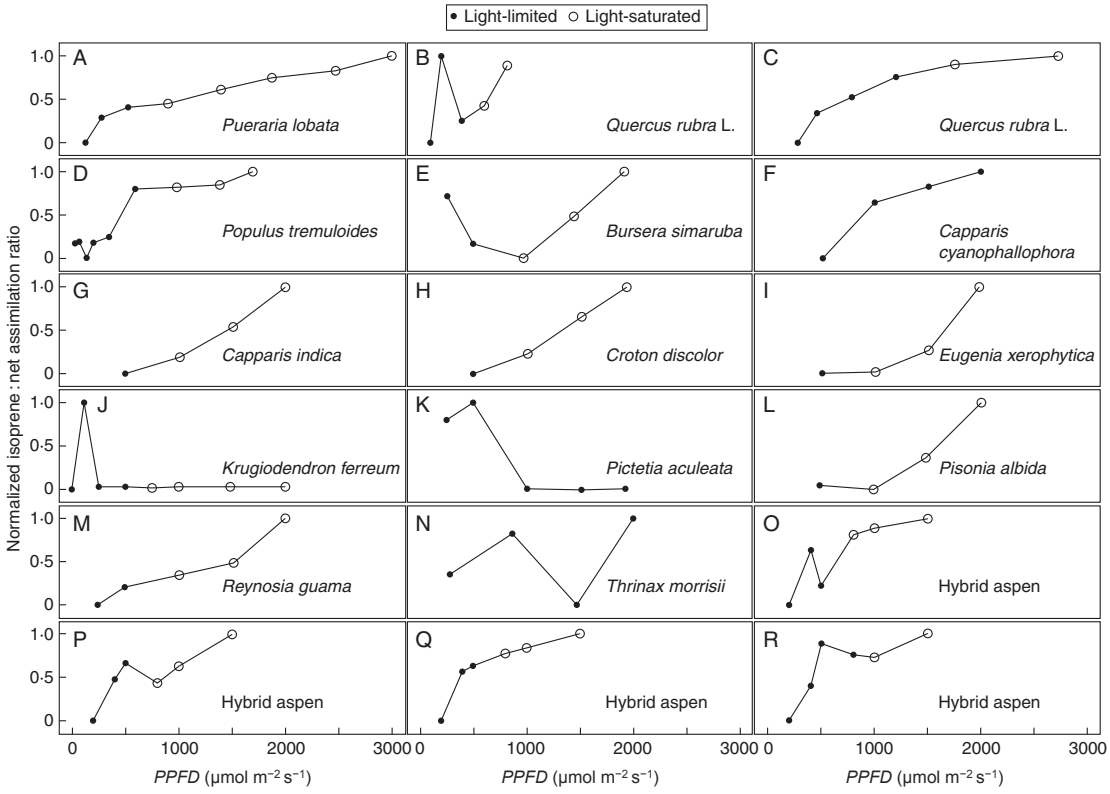


Figure 3.4 Observed responses of the normalised ratio (isoprene emission/ net CO_2 assimilation) to changes in *PPFD*. Closed circles show where carbon assimilation is light-limited, open circles where it is light-saturated. Data digitized from (A) Sharkey & Loreto (1993), (B, C) Loreto & Sharkey (1990), (D) Monson & Fall (1989), (E-N) Lerdau & Keller (1997), (O-R) Sun *et al.* (2012). (O) Plants grown at ambient CO_2, chamber [CO_2] = 380 μmol mol^{-1}. (P) Plants grown at ambient CO_2, chamber [CO_2] = 780 μmol mol^{-1}. (Q) Plants grown at elevated CO_2, chamber [CO_2] = 380 μmol mol^{-1}. (R) Elevated CO_2, chamber [CO_2] = 780 μmol mol^{-1}.

Most studies reporting the fraction of assimilated carbon that is re-emitted as isoprene have found that it increases with *PPFD*, in line with my predictions (Sharkey & Loreto, 1993; Harley *et al.*, 1996; Lerdau & Keller, 1997; Niinemets *et al.*, 2010a). However one study (Lerdau & Throop, 1999) found no significant increase in I/A_{net} with *PPFD* for most of the tropical taxa they investigated.

Figure 3.3A compares the relationships of I/A_{net} to *PPFD* in my model and in digitised data from Sharkey & Loreto (1990) on kudzu leaves (*Pueraria lobata*). Assuming J_v is constant (no variation in C_i; Fig. 3.3B), the observed isoprene emissions show a strong positive linear relationship with J (r^2 = 0.97). The model parameters **a** and **b** (Eq.3.1) have been estimated from this linear regression. The Farquhar model parameters were

estimated with a best data/model fit by minimizing the residual sum of squares (RSS). The comparison between my model and the data for I/A_{net} shows excellent agreement (r^2 = 0.92). In comparison, G93 and the Niinemets model both show poor agreement (r^2 = 0.19 and r^2 = 0.06 respectively). Yet the three models have a good agreement of the modelled isoprene alone (I) with data (my model: r^2 = 0.97; G93: r^2 = 0.92; Niinemets: r^2 = 0.97; results not shown).

I also compiled data on the response of I/A_{net} to *PPFD* from the limited number of published studies in order to assess the generality of the pattern (Fig. 3.4). The publications reported A_{net} rather than A_{gross}, and did not typically provide measurements of R_d. As the predicted response of I/A_{net} for low *PPFD* is dependent on R_d, it is not surprising to observe an initial decline in I/A_{net} with *PPFD* for some of the 18 experiments. More importantly, the great majority of the studies show increasing I/A_{net} up to the highest *PPFD* fluxes, especially when photosynthesis saturates (open circles in Fig. 3.4). In some studies a drop in assimilation rate at high *PPFD* contributed to this increase in I/A_{net} at high *PPFD*; this was probably due to stomatal closure at high *PPFD*, resulting in reduced C_i.

As shown in Figure 3.2, the Niinemets model cannot reproduce the positive response of I/A_{net} to *PPFD* that is generally observed under low *PPFD*. My model, along with G93, fully captures the shape of the observed response of I/A_{net} to *PPFD* over the full range of *PPFD*. But my model also provides a process-based explanation for this response.

In collaboration with T.F. Keenan (Macquarie University, Australia), I also examined the relationship between I/A_{gross} and *PPFD* at the canopy scale, at which isoprene emission is more likely to be controlled by the DMADP pool size than by isoprene synthase activity (Vickers *et al.*, 2010). We used simultaneous CO_2 and isoprene flux measurements made at Harvard Forest, Massachusetts, USA (42.54˚ N, 72.17˚ W) (Urbanski *et al.*, 2007; McKinney *et al.*, 2011). Data used were obtained during the 2007 growing seasons using eddy covariance, with Proton Transfer Reaction Mass Spectrometry used to measure the isoprene mixing ratio (McKinney *et al.*, 2011). Daytime data were selected for temperatures above 23˚C where variations in isoprene emission were no longer significantly driven by temperature (Fig. 3A.2.1). Ecosystem respiration, estimated from night-time CO_2 flux measurements, was used to convert the daytime measured net ecosystem CO_2 exchanges into canopy-scale gross assimilation

rates. Canopy-scale carbon assimilation shows a typical rectangular hyperbolic response to *PPFD*, but the response of isoprene emission to *PPFD* is closer to linearity, and emissions do not saturate at high *PPFD* (Fig. 3.5A, B). Thus, above a *PPFD* threshold of ~300 μmol m^{-2} s^{-1}, I/A_{gross} increases with *PPFD* even at high *PPFD*, where assimilation is light-saturated, consistently with my hypothesis.

Scaling from leaf to canopy involves additional processes, such as within-canopy chemistry and canopy structure effects (Grote, 2007; Keenan *et al.*, 2011; Bryan *et al.*, 2012). Therefore, a canopy model is needed to fully account for these results, especially for low *PPFD* where deposition processes can influence the observed above-canopy isoprene emissions and possibly explain the observed drop in I/A_{gross}. Nevertheless these results, along with those of laboratory experiments, corroborate the notion that isoprene emission is related to the availability of electrons generated in photosynthesis, relative to the demand for them to be used in carbon assimilation.

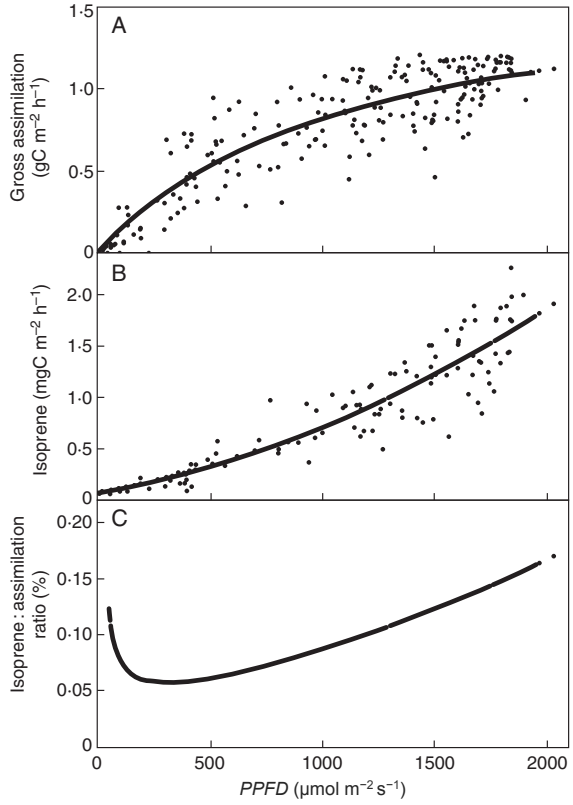


Figure 3.5 Above canopy gross assimilation (A), isoprene emissions (B) and isoprene emission/gross assimilation (C), in relation to *PPFD*. From flux measurements at Harvard Forest.

3.3.2 Responses to C_i

Responses of isoprene emission to ambient CO_2 concentration have been widely reported. Plants grown at high atmospheric CO_2 concentrations generally emit less isoprene than those grown at lower CO_2 concentrations. On short time scales, isoprene emission has also been shown to respond strongly and rapidly to C_i, with lower emission rates at higher C_i (Rosenstiel *et al.*, 2003; Wilkinson *et al.*, 2009; Possell & Hewitt, 2011; Sun *et al.*, 2012). The fact that rapid changes in C_i evoke instantaneous responses in isoprene emission suggests that the driving mechanism must be tightly linked to processes in the chloroplast.

The mechanisms behind the decoupling between isoprene emission and carbon assimilation in the response to C_i are not well established. Niinemets *et al.* (1999b) hypothesized that the dependency of isoprene emission on C_i might be due to the partitioning of reducing power and ATP into the MEP pathway. However the model of Niinemets *et al.* (1999b) does not allow for any greater partitioning of reducing power to the MEP pathway at low C_i. Isotopic labelling studies have provided evidence for the existence of extra-chloroplastic sources of carbon to support isoprene production. Hence, competition for phosphoenolpyruvate (PEP) between cytosolic and chloroplastic processes has been proposed as an explanation for the drop in isoprene emission at high C_i due to the CO_2-dependence of PEP carboxylase activity (Karl *et al.*, 2002; Rosenstiel *et al.*, 2003; Possell & Hewitt, 2011; Trowbridge *et al.*, 2012). But these experiments compared plants grown at different CO_2 concentrations. Gene expression involving changes in enzyme quantities cannot explain the observed fast (about 10-minute) responses to changes in C_i. I focus here only on the short-term responses to C_i, in which isoprene emission appears to be tightly coupled to changes in the pool size of DMADP (Rasulov *et al.*, 2009b). Specifically, I examine whether the fast responses of isoprene emission to C_i could be explained in a simple way by my model, based on the same mechanisms I have proposed to explain the response to *PPFD*.

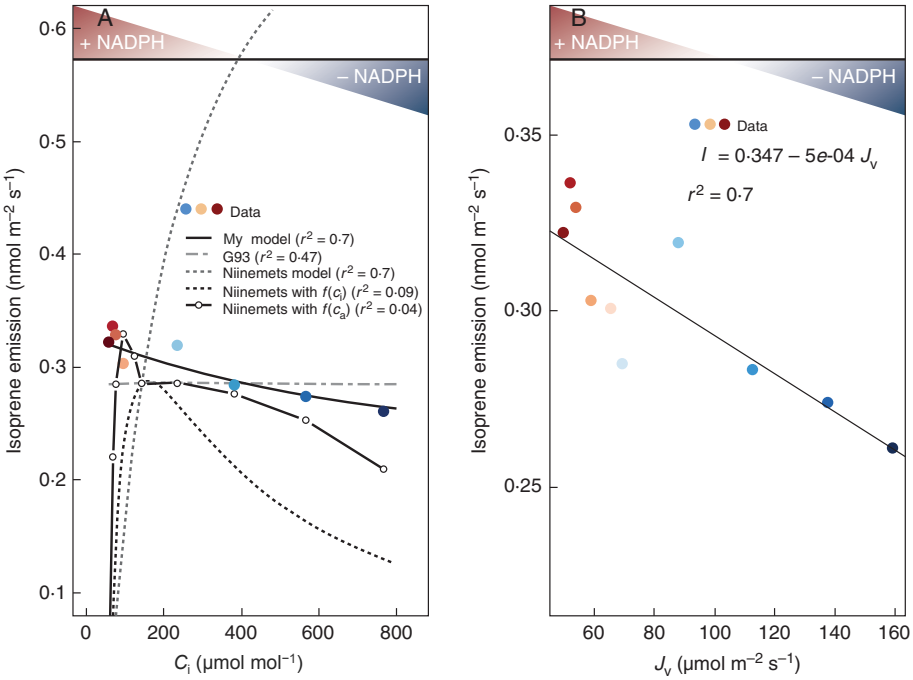


Figure 3.6 The relationship between isoprene emission and NADPH availability for carbon assimilation with changing internal CO_2 concentration C_i. (A) Decreasing isoprene emissions with increasing leaf-internal CO_2 concentration (C_i) (data from Possell and Hewitt (2011); T = 30°C, $PPFD$ = 1000 μmol m^{-2} s^{-1}). The solid line, the dot-dashed light grey line and the dashed dark grey lines represent simulations made with my model, G93, and the Niinemets model, respectively. The dashed black line represent the Niinemets model with an additional CO_2 effect represented by $f(C_i)$= C_i [C_a = 390 μmol mol^{-1}]/ C_i, where C_a is the atmospheric CO_2 concentration. The plain grey line represent the Niinemets model with an alternative additional CO_2 effect represented by f(C_a)= [C_a = 390 μmol mol^{-1}]/ C_a. The terms $f(C_i)$ and $f(C_a)$ are adapted from (Arneth *et al.,* 2007b). Standard isoprene emission factor (I_s) is taken as the observed emission at C_a = 390 μmol mol^{-1}. (B) Linear regression between isoprene data and the electron flux required for carbon assimilation by Rubisco (J_v). Plant-specific isoprene parameters (a, b) are estimated from this linear regression and parameters for assimilation (V_{cmax}, J_{max}) were fitted to the observations by minimizing the residual sum of squares (RSS). In both panels, the availability of reducing power (NADPH) for CO_2 assimilation is represented by a colour scheme, from dark blue (deficit) to dark red (excess).

At low C_i, carbon fixation is Rubisco-limited, resulting in an excess of NADPH (Fig. 3.1; Fig. 3.6A). The excess of NADPH can be smaller or larger depending on *PPFD*. This provides a simple explanation for why isoprene responses to changes in C_i are light-dependent (Loreto & Sharkey, 1990) (Fig. 3.7D) . Moreover, my model can indeed reproduce the isoprene emission response to changes in C_i. This is shown in Figure 3.6A using data on *Acacia nigrescens* from Possell & Hewitt (2011). Here, isoprene emission shows a strong negative linear relationship with the Rubisco-limited electron flux, J_v (r^2 = 0.70), as shown in Figure 3.6B. The parameters **a** and **b** (Eq. 3.1) of my model were estimated from this linear regression (Table 3A.2.1). When plotted against C_i, my model

shows a good agreement with the data ($r^2 = 0.70$). Figure 3.6A also shows the response of the G93, and the Niinemets model with and without a CO_2 inhibition effect (Arneth *et al.*, 2007b; Pacifico *et al.*, 2011). It is obvious from Figure 3.6A that these models do not reproduce the observed response of isoprene emission to C_i. Without an additional empirical function for CO_2 inhibition, isoprene emissions simulated with the Niinemets model are quite out of range. Instead the model shows a strong negative correlation with the data ($r^2 = 0.7$). The negative relationship can be explained by the fact that although the *PPFD* and therefore the light-limited electron flux (J) are constant, light-limited assimilation (A_j) is strongly C_i -dependent. Adding an empirical function to represent the CO_2 inhibition effect, as in Arneth *et al.* (2007b), changes the shape of the response (allowing a decrease at high C_i) but still the simulated emissions agree poorly with the data.

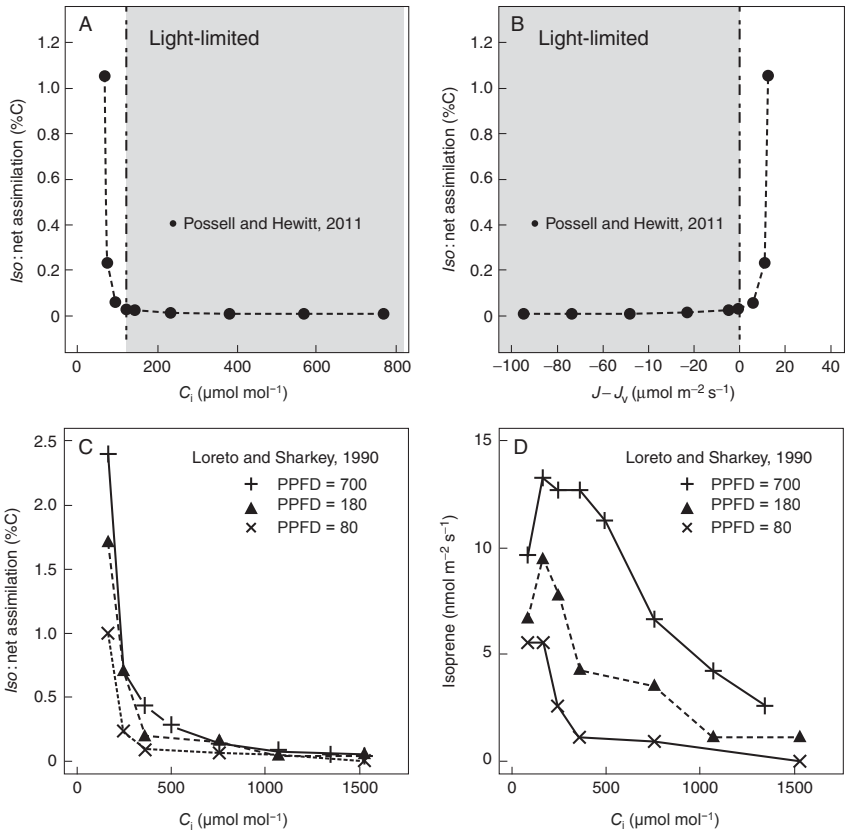


Figure 3.7 Observed changes in the ratio of isoprene emission to net carbon assimilation with changes in (A) leaf-internal CO_2 concentration (C_i), (B) electron excess ($J - J_v$) (data from Possell & Hewitt (2011)). Observed changes with C_i of (C) the ratio of isoprene emission to carbon assimilation and (D) isoprene emission, for three *PPFD* fluxes. Data digitized from Loreto & Sharkey (1990).

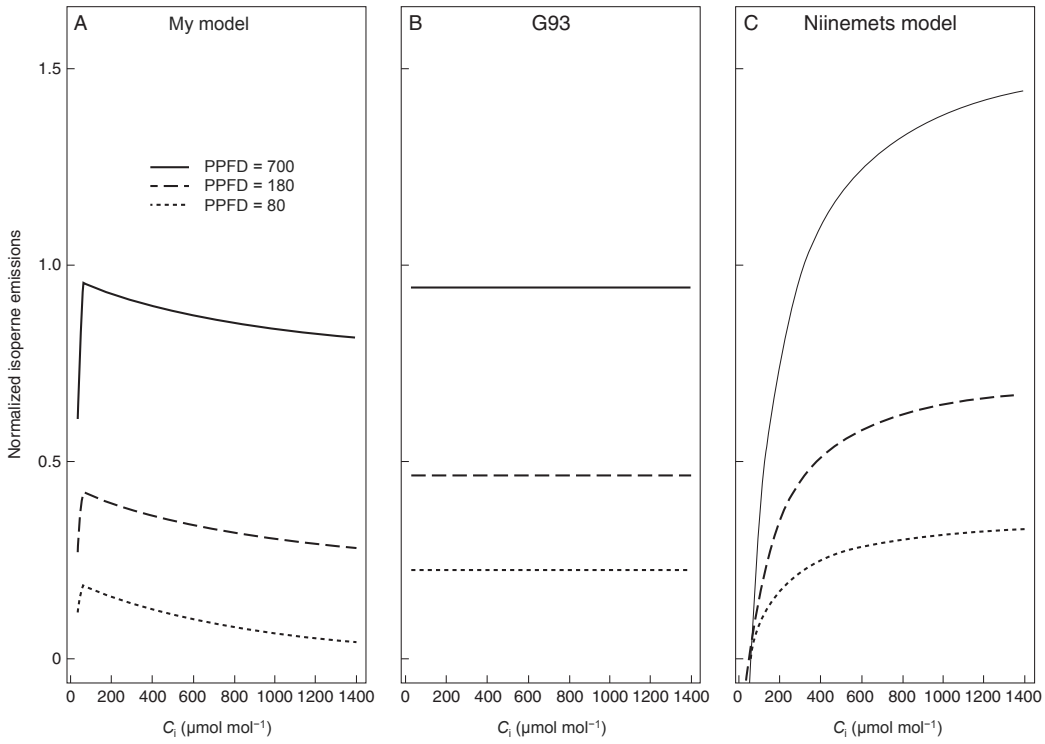


Figure 3.8 Modelled responses of isoprene emission versus C_i for three *PPFD* fluxes (80, 180, 700 μmol $m^{-2} s^{-1}$). (A) My model, (B) G93, (C) the Niinemets model. Parameters values as in Fig. 3.2. Emissions were normalised to a standard emission rate at T = 30˚C, C_i = 273 μmol mol^{-1}, *PPFD* = 1000 μmol m^{-2} s^{-1}.

Again using the data from Possell & Hewitt (2011), I plotted I/A_{net} versus C_i (Fig. 3.7A) and $[J - J_v]$ (Fig. 3.7B). These plots confirm that the fraction of assimilated carbon allocated to isoprene production increases under conditions of NADPH excess. This provides a simple explanation for the response of isoprene emission to C_i. The extremely steep rise in I/A_{net} when $[J - J_v]$ becomes positive is due to the combination of steeply increasing isoprene emission with decreasing assimilation rate as C_i declines.

Loreto & Sharkey (1990) measured changes in isoprene emission with changing C_i at different *PPFD* fluxes in *Quercus rubra*. Both I/A_{net} and isoprene emission are shown (Fig. 3.7C, D) to increase with *PPFD*, consistent with a dependence on NADPH availability, at all values of C_i. I compared the responses of G93 and the Niinemets model to C_i at different *PPFD* fluxes, together with my model (Fig. 3.8). Note that both G93 and the Niinemets model are applied here in their original formulations (see Chapter II for details), and therefore do not include additional parameterizations of the

CO_2 effect. A number of studies have used these same models with additional empirical functions, introduced specifically to account for the observed CO_2 inhibition (Arneth *et al.*, 2007b; Heald *et al*., 2009; Pacifico *et al*., 2011). G93 in its original formulation simulates no change at all in isoprene emission with changes in C_i, although it has isoprene emission depending on *PPFD* (Fig. 3.8B). The Niinemets model in its original formulation also simulates increasing isoprene emission with *PPFD*, but here the modelled emissions *increase* with increasing C_i, due to the fact that this model tightly links isoprene emission to light-limited assimilation (Fig. 3.8C). Thus, additional functions are required in both models to account for the observed effects of varying C_i. In contrast, my model (Fig. 3.8A) can reproduce the form of the C_i response shown in the data (Fig. 3.7D), as well as the effects of combined changes in C_i and *PPFD* (Fig. 3.7D), without the need for any additional function.

3.3.3 Responses to leaf temperature

The temperature dependence of isoprene emission differs from that of photosynthesis. Temperature optima for carbon assimilation are usually ≤ 30˚C in C_3 plants, while isoprene emission peaks at ≈ 40˚C (Guenther *et al*., 1993; Niinemets *et al.*, 1999b; Sharkey & Yeh, 2001; Pacifico *et al.*, 2009). An increase of *I/A* with temperature is usually observed (Sharkey & Loreto, 1993; Harley *et al.*, 1996; Sharkey *et al*., 1996; Niinemets *et al*., 1999b; Sharkey & Yeh, 2001). The optimum for isoprene emissions rarely exceeds 40˚C, so the temperature dependence of isoprene emission cannot be fully explained by the temperature dependence of isoprene synthase, which is maximally active between 45˚C and 48˚C (Monson *et al.*, 1992; Lenhing *et al.*, 1999; Niinemets *et al.,* 1999b; Rasulov *et al.*, 2010). The decrease in isoprene emissions above 40˚C has long been considered to be linked to the behaviour of the photosynthetic electron transport rate (Guenther *et al.*, 1991; Niinemets *et al.*, 1999b). Rasulov *et al.* (2010) found that this decrease is associated with decline in the DMADP pool size and the energetic status of the leaf.

In G93 the temperature dependency of isoprene emission is fixed with a temperature optimum around 38˚C. In the Niinemets model, it is assumed to be primarily controlled by IspS activity, with the fraction of electrons used for isoprene production exponentially increasing with temperature. The temperature optimum for isoprene

emissions in the Niinemets model is thus close to the optimum for IspS. Some global-scale studies have set an upper limit for the increase of ε with temperature, thereby reducing the temperature optimum to a value closer to 38˚C (Pacifico *et al.,* 2011).

My model is based on the hypothesis that the production of DMADP depends on photosynthetic electron flux and variations in electron availability for functions other than carbon assimilation. Thus my modelled optima for isoprene emissions are primarily driven by the behaviour of the light-limited electron flux. Figures 3.9 and 3.10 illustrate how a temperature response arises in my model. Carbon assimilation follows the lower of the temperature response curves of the Rubisco and light-limited assimilation rates. Rubisco activity usually has a higher temperature optimum than electron transport (Crafts-Brandner & Salvucci, 2000; Medlyn *et al.*, 2002; Cen & Sage, 2005; Kattge & Knorr, 2007). At high *PPFD* an excess of NADPH can arise for temperatures below the optimum for electron transport (*J*), so isoprene emissions increase. Above this optimum (T_{opt_J}), J_v still increases even if assimilation is reduced, due to the higher affinity of Rubisco for O_2 at high temperatures. Both J and $[J - J_v]$ decrease for temperatures higher than T_{opt_J} (as illustrated in Fig. 3.9B). My model thereby predicts a temperature optimum of isoprene emissions that is closer to the temperature optimum of the electron transport rate. Beyond this optimum, my model predicts a drop in the availability of reducing power, leading to a decrease of DMADP and consequently isoprene emissions. At low *PPFD* (light-limited condition), however, $[J - J_v]$ decreases with increasing temperature, compensating the increase of *J*. Predicted emissions are thus almost insensitive to temperature or even decrease with temperature (Fig. 3.10A, B). This behaviour is not realistic, so the model may be overestimating the effect of $[J - J_v]$ at low *PPFD*.

I infer that energetic control alone is insufficient to fully explain the observed temperature dependency of isoprene emission. In principle the activities of enzymes along the MEP pathway should also influence the production rate of DMADP, but very little is known about their temperature responses (Zimmer *et al.*, 2000). Temperature optima for isoprene production are shifted toward higher temperature than T_{opt_J} most likely because a decrease in DMADP pool size is compensated by an increase in IspS activity (Rasulov *et al*., 2010). Taking into account the temperature response of IspS, I can reproduce this shift (Figs. 3.9C, 3.10C). So I suggest that temperature effects on

enzyme activity may need to be considered, as well as temperature effects on electron availability.

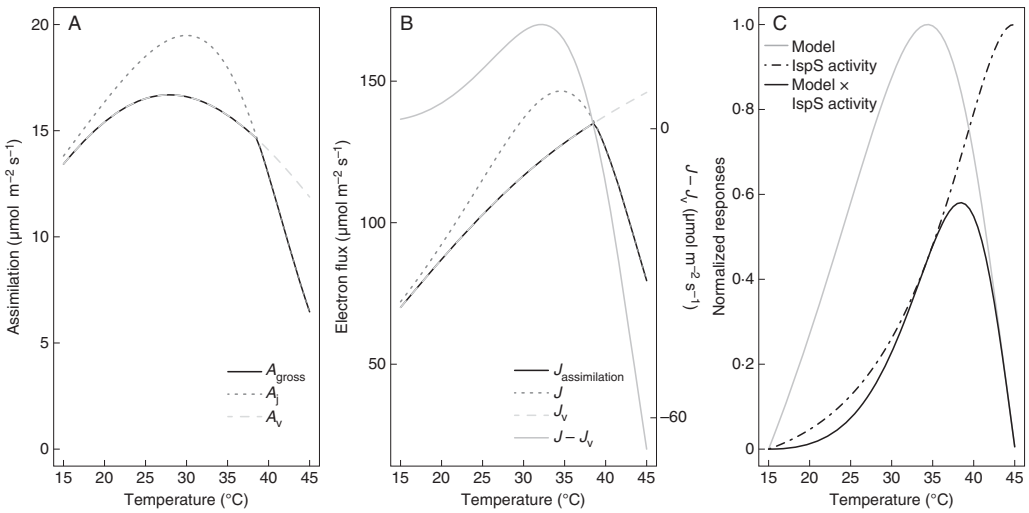


Figure 3.9 Explanation of the predicted temperature dependency of isoprene emissions. (A) Responses to temperature of the light-limited A_j (dark grey short-dash line), the Rubisco limited A_v (light grey long-dash line) and the gross assimilation A_{gross} (solid black line); (B) associated electrons fluxes (left hand axis) and the associated electrons availability ($J - J_v$) (solid grey line; right hand axis). (C) Normalised responses to temperature of my model (solid grey line), normalised IspS activity (dotted-dashed black line) and the resulting product (solid black line). Temperature dependency of IspS is as described in Niinemets *et al.* (1999b) (Table 2.1). Parameters values of the model are taken as in Figure 3.2.

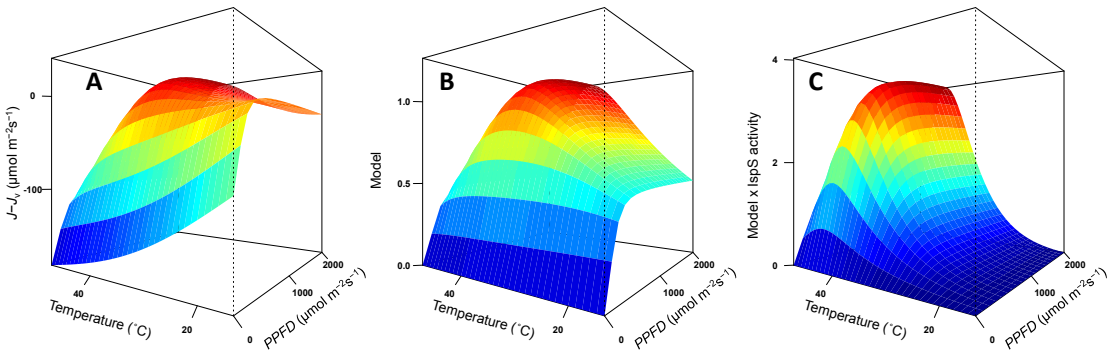


Figure 3.10 Responses to variation in temperature (in ˚C) and *PPFD* (in μmol m^{-2} s^{-1}) of electrons availability ($J - J_v$) (in μmol m^{-2} s^{-1}) (A), my model (B), and my model simulations multiply by a normalised function of enzymatic activity (C). Farquhar model parameters are for *Quercus robur*, as described in Medlyn *et al*. (2002). Isoprene model parameters **a** and **b** (Eq. 3.1) are based on data of Possell & Hewitt (2011) (Fig. 3.6). Model outputs in panel (B) and (C) are normalised to be unity at T =30˚C and *PPFD*=1000 μmol m^{-2} s^{-1}.

A further limitation of my model is the paucity of available information on the temperature responses of J_{max} and V_{cmax} (Medlyn *et al.*, 2002; Kattge & Knorr, 2007). The experiments needed to quantify these responses are time–consuming, and in particular, few studies have included temperatures > 40˚C. In general we would expect a decline in DMADP production for temperatures > 40˚C due to thylakoid damage, while at temperatures above 45-48˚C, irreversible damage to enzyme function will cause isoprene emission to cease.

Using data from Medlyn *et al.* (2000) and references therein, I checked variations with temperature of electron availability among isoprene emitting species at 1000 μmol m^{-2} s^{-1} *PPFD* (Fig. 3.11). I also tested the influence of the temperature response parameterization of V_{cmax} by contrasting an Arrhenius function with a peak function, as described in Medlyn *et al.* (2000). The temperature optima for the selected species are all higher for V_{cmax} than J_{max} (Medlyn *et al*., 2002; Kattge & Knorr, 2007). Consequently I predicted a decline in DMADP pool size above T_{opt_J}, due to the decline of J being accompanied by a decline in $[J - J_v]$, but the shape of the decline depended on the parameterization adopted.

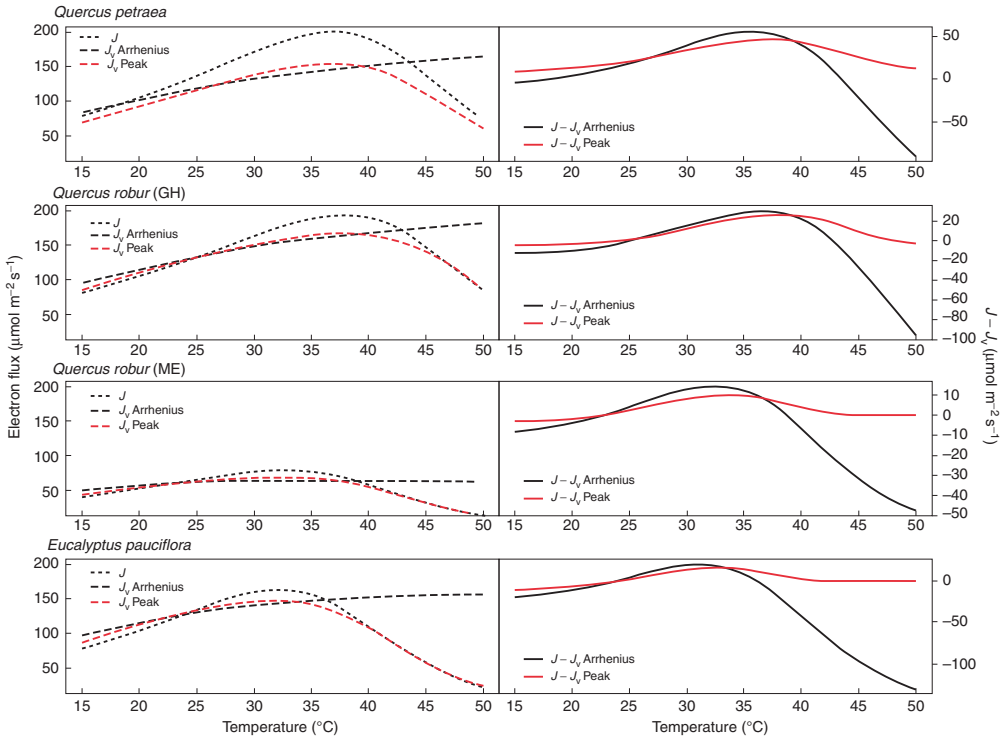


Figure 3.11 Left: temperature responses for different species of the light-limited electron flux (J) (dark grey dotted line), the Rubisco-limited electron flux (J_v) using an Arrhenius function for V_{cmax} (J_v Arrhenius, light grey dashed line), and the Rubisco-limited electron flux using a peak function for V_{cmax} (J_v peak, red dashed line). Right side: resulting temperature responses of ($J - J_v$), using an Arrhenius function for V_{cmax} (light grey solid line, left side y-axis), and a peak function for V_{cmax} (red solid line, right side y-axis). Farquhar parameters and calculation of V_{cmax} are as described in Medlyn *et al.* (2000). For *Quercus robur*: GH, greenhouse experiment; ME, mini-ecosystem experiment (Medlyn *et al.*, 2000). Simulations are done for $C_i = 273$ μmol mol^{-1} and $PPFD$=1000 μmol m^{-2} s^{-1}.

3.3.4 Discussion

I have used a conceptual model to ask whether variation in the availability of NADPH in the chloroplast can plausibly account for observed changes in isoprene emission with *PPFD*, C_i and leaf temperature. The answer is yes. By modelling isoprene emission as proportional to a simple metric of the excess or deficit of electrons relative to the demands of carbon assimilation, I have provided a unifying explanation for the lack of close coupling of isoprene emission with carbon assimilation, the disparities in carbon allocated into isoprene production, high isoprene emissions at low C_i, and the shift of the temperature optimum for isoprene emission above that of carbon assimilation but below that of isoprene synthase.

To my knowledge, this is the first study that has attempted to model the flux of reducing power into the MEP production pathway based on the idea of a balance between electron supply and demand. My hypothesis invokes mechanisms that are incompletely understood and thus is to some extent speculative. Nevertheless, it appears to have significant predictive power in explaining the already documented responses of isoprene emission to *PPFD*, C_i and (with some caveats) temperature. Moreover, this hypothesis provides a parsimonious explanation for the response of isoprene emission to drought. Under moderate to mild drought where the photosynthetic apparatus is not damaged (Cornic & Briantais, 1991), carbon assimilation is first reduced by stomatal closure (and thus reduced C_i). Under higher drought severity, this reduction is greatly increased by decreased ATP in water-deficient leaves (Lawlor & Tezara, 2009), which reduces the photosynthetic metabolic potential (A_{pot}), even if C_i increases due to light respiration. The resulting oversupply of reducing power ensures that isoprene emissions continue at a high rate, although carbon assimilation is reduced (Niinemets, 2010). However, a decrease in ATP could also reduce isoprene emissions. Under extreme drought, however, damage to the photosynthesis apparatus eventually results in the cessation of both carbon assimilation and isoprene emission.

A strong diurnal cycle is observed in isoprene emission at canopy scales. Low emissions during early morning and late afternoon contrast with high emissions during the midday period (Hewitt *et al.*, 2011; Keenan & Niinemets, 2012). My hypothesis explains this as a consequence of higher *PPFD* and temperature, and lower C_i due to partial stomatal closure associated with higher evaporative demand in the midday period. This simple explanation does not require the intervention of a circadian clock, as had been proposed by Hewitt *et al.* (2011).

It should be noted that I am *not* advocating a function of isoprene emissions as an 'electron sink' as was earlier proposed (e.g. Logan *et al.*, 2000). It is clear from the findings of Li & Sharkey (2012) that the quantity of electrons used in isoprene synthesis is far too small for this function to be plausible. The low affinity of IspS for DMADP already argues strongly against this notion (Silver & Fall, 1995; Schnitzler *et al.*, 1997). My model implies that the allocation of reducing power to this pathway occurs under those conditions when electron availability is in excess, which fortuitously occurs during

stress events when isoprene biosynthesis and emission is advantageous to the plant (e.g. Sharkey *et al*., 2001; Vickers *et al*., 2009a).

My results provide an alternative, robust approach to modelling isoprene emissions for global change applications. But more work is needed before implementing the model in a global context. Particular attention should be given to the influence of enzymatic activity on temperature responses of the modelled rates of isoprene. The values of the parameters **a** and **b** (Eq. 3.1), and their potential species and environmental dependencies, also call for further investigation at several scales:

1) For leaves, by setting up experiments that could test interactions among the short-term responses of isoprene emission to different environmental drivers, and associated variations in the excess of electrons (i.e. isoprene/assimilation responses to C_i at different *PPFD* fluxes, together with isoprene/assimilation response to *PPFD* at different C_i); and the influence of growth conditions on the parameters. Note that, as most of the process-based models are closely linked to photosynthesis models, information on the values of V_{cmax} and J_{max} associated with the isoprene standard emission rate would be valuable.

2) For ecosystems, by upscaling the model from the leaf scale to the canopy, with particular attention to the response of I/A_{gross}. This step would require a representation of the canopy structure and vertical mixing as well as the canopy chemistry accounting for isoprene oxidation, deposition and OH regeneration.

3) At the global scale, with the possibility of using remotely sensed formaldehyde column concentrations to better constrain model parameters for different plant function types and environments. Formaldehyde is a product of isoprene oxidation. As it is observed by satellite, with global coverage, numerous studies have used formaldehyde data to investigate isoprene emission at larger scales (Palmer *et al.*, 2003, 2006; Stavrakou *et al.*, 2008; Barkley *et al.*, 2008; Fortems-Cheiney *et al.*, 2012).

A comprehensive approach to isoprene modelling would also have to account for longer-term acclimation over a time scale of weeks to months, including responses to antecedent temperatures (Guenther *et al.*, 2006, 2012), phenological stages and differences between the short-term and acclimated responses to CO_2 (Sun *et al.*, 2012), which are presumably mediated by transcriptional control of the MEP pathway

enzymes. It would be of particular interest to examine whether these acclimatory changes in isoprene emission are correlated with acclimatory changes in reducing power. However, some acclimatory shifts are unlikely to be able to be explained by a model based on reducing power alone. For example, growth at higher temperatures leads to increased emission rates measured at a common temperature (Pétron *et al.*, 2001; Niinemets *et al*., 2010b), whereas reducing power at a given temperature tends to be reduced by high growth temperatures due to a decline in the J_{max}:V_{cmax} ratio (Hikosaka *et al*., 1999; Onoda *et al.*, 2005). Longer-term responses of isoprene emission to changes in growth temperature are therefore presumably governed by other factors, including transcriptional control of the MEP pathway enzymes.

3.3.5 Conclusion

A simple model of the biochemistry and physiology of isoprene emissions has been developed and used to test the hypothesis that the reducing power available to the synthesis pathway for isoprene varies according to demands of carbon assimilation. The model explains the observed response of isoprene production to environment and the coupling/decoupling between carbon assimilation and isoprene emission. The model has the potential to improve global-scale modelling of vegetation isoprene emissions, as well as emissions of isoprenoids that do not origin from storages.

Acknowledgments

I thank Karena McKinney for providing the original isoprene data for the Harvard forest site. I thank Russell Monson and Rüdiger Grote for their helpful and constructive comments on the *Annals of Botany* manuscript.

Annex 3A.1 – Comparison of Model 1 and Model 2

Here key figures from Morfopoulos *et al.* (2013) are redrawn using the latest version of the isoprene model, referred to as Model 2. In Model 2, the *fraction* of electrons allocated to isoprene biosynthesis is linearly related to the energetic status of the plant:

$$\varepsilon = c_1 + c_2 (J - J_v) \quad (3A.1.1)$$

and

$$I = \varepsilon J \quad (3A.1.2)$$

J and J_v are the light- and Rubisco-limited electron fluxes, respectively, calculated using the Farquhar equations; ε represents the fraction of J allocated to isoprene emission, and has a magnitude depending on $[J - J_v]$; c_1 and c_2 are constants.

Figure 3A.1.1 compares the relationships of the isoprene emission/net assimilation ratio (I/A_{net}) to photosynthetic photon flux density (*PPFD*) using digitized data from Sharkey & Loreto (1993) on kudzu leaves (*Pueraria lobata*). Assuming J_v is constant (no variation in C_i; Fig. 3A.1.1B), observed isoprene emissions show a quadratic response in relationship with J ($r^2 = 0.99$), as implied by Model 2. A quadratic function characterises the response of isoprene emission versus light better than the linear response previously assumed in Morfopoulos *et al.* (2013). Using Model 2 improves the agreement with data for I/A_{net} versus *PPFD* (Model 2: $r^2 = 0.98$; Model 1: $r^2 = 0.92$).

Figure 3A.1.2 illustrates the short-term response of isoprene emission to changes in C_i using Model 2 and data on *Acacia nigrescens* from Possell and Hewitt (2011). Here, parameters c_1 and c_2 were obtained from a linear regression between $\varepsilon = I/J$ and $[J - J_v]$. When plotted against C_i, model 2 shows a good agreement with the data ($r^2 = 0.70$). The response of Model 2 is close to that of Model 1. This is not surprising as the two models are equivalent when C_i varies under constant temperature and light flux. Indeed, at constant T and *PPFD*, the light-limited electron flux (J) is constant. Thus, and under these conditions only, both models take the form:

$$I = Constant1 - Constant2 . J_v \quad (3A.1.3)$$

Figures 3A.1.3, 3A.1.4, 3A.1.5, and 3A.1.6 are redrawn versions of Figures from Morfopoulos *et al.* (2013), showing normalised responses of the model to changes of the key drivers (*PPFD*,*T*, C_i) of isoprene emission using Model 2. Very few changes are detected between the shapes of the responses of Model 2 compared to Model 1. The key characteristics (decrease of emission with C_i, increase of I/A with increasing *PPFD*, temperature optimum for isoprene emission close to what is usually observed) are retained in the new formulation.

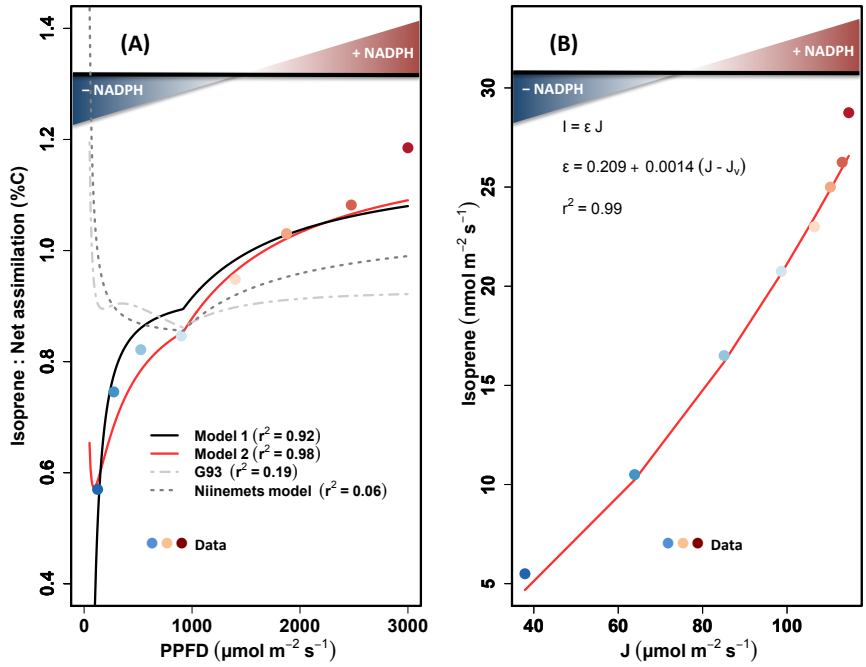


Figure 3A.1.1: The relationship between isoprene emission and NADPH availability for carbon assimilation with changing *PPFD*. (A) Increasing values of the isoprene to CO_2 net assimilation ratio with increasing *PPFD*, based on data digitized from figure 2 in Sharkey and Loreto (1993). Simulations made with Model 1 [$I = a\,J + b\,(J - J_v)$], Model 2 [$I = \varepsilon J$; $\varepsilon = c_1 + c_2\,(J - J_v)$], G93, and the Niinemets model are as indicated in the key. (B) 2nd degree polynomial fit between isoprene data and the light-limited electron flux (J). Plant-specific isoprene parameters (c_1, c_2) are estimated from this polynomial fit and parameters for assimilation (V_{cmax}, J_{max}) were fitted to the assimilation data by minimizing the residual sum of squares (RSS). In both panels, the availability of reducing power (NADPH) for CO_2 assimilation is illustrated by a colour scheme, from dark blue (deficit) to dark red (excess).

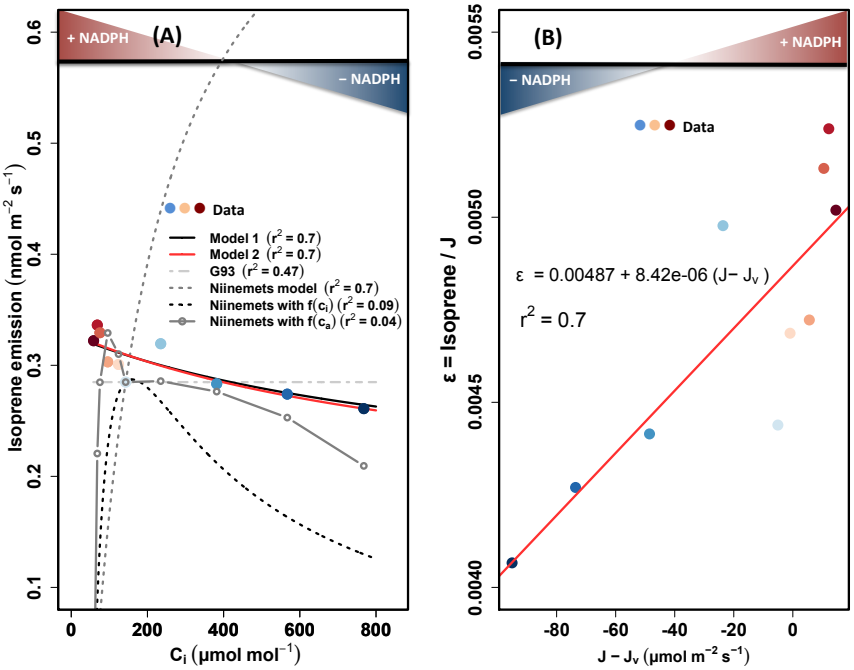


Figure 3A.1.2: The relationship between isoprene emission and NADPH availability for carbon assimilation with changing internal CO_2 concentration C_i. (A) Decreasing isoprene emissions with increasing leaf-internal CO_2 concentration, C_i (data from Possell and Hewitt, 2011); T = 30 °C, $PPFD$ = 1000 μmol m^{-2} s^{-1}. Simulations made with Model 1 [$I = a\,J + b\,(J - J_v)$], Model 2 [$I = \varepsilon\,J$; $\varepsilon = c_1 + c_2\,(J - J_v)$], G93 and the Niinemets model are as indicated in the key. The dashed black line represent the Niinemets model with an additional CO_2 effect represented by $f(C_i) = C_i\,[C_a = 390\ \mu\text{mol mol}^{-1}]\,/C_i$, where C_a is the atmospheric CO_2 concentration. The plain grey line represent the Niinemets model with an alternative additional CO_2 effect represented by $f(C_a) = [C_a = 390\ \mu\text{mol mol}^{-1}]\,/C_a$,. The terms $f(C_i)$ and $f(C_a)$ are adapted from Arneth *et al.* (2007b). Standard isoprene emission factor (I_s) is taken as the observed emission at C_a = 390 μmol mol^{-1}. (B) The linear regression between $\varepsilon = I/J$ and energetic status of the leaf, approximated by the difference between light- and Rubisco limited electron fluxes [$J - J_v$]. Plant-specific isoprene parameters (c_1, c_2) are estimated from this linear regression and parameters for assimilation (V_{cmax}, J_{max}) were fitted to the observations by minimizing the residual sum of squares (RSS). In both panels, the availability of reducing power (NADPH) for CO_2 assimilation is represented by a colour scheme, from dark blue (deficit) to dark red (excess).

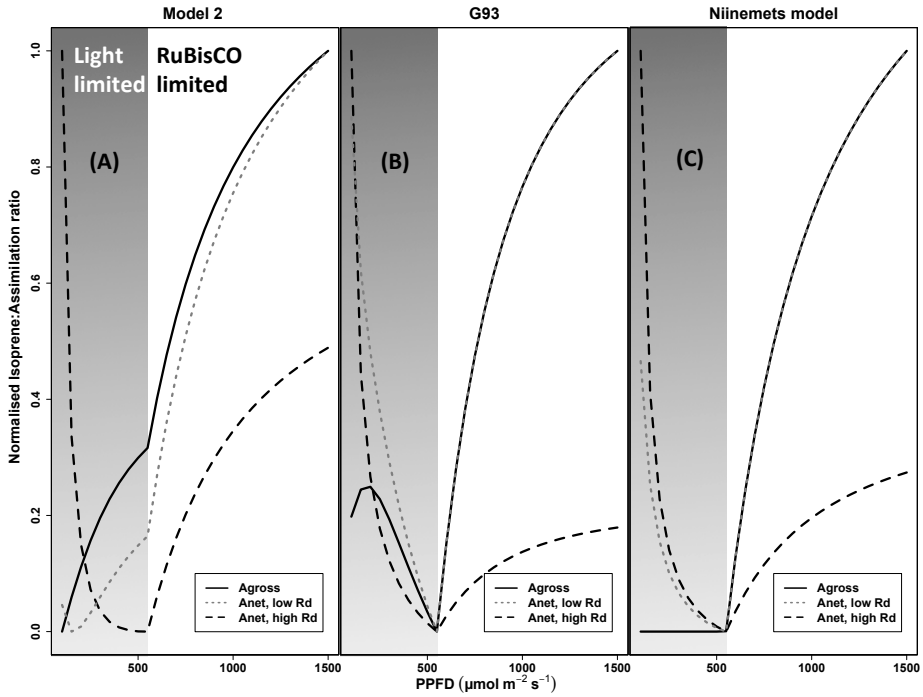


Figure 3A.1.3: Modelled responses of the normalised ratios of isoprene to CO_2 assimilation to changes in *PPFD* for (A) Model 2 *[*$I = \varepsilon J$; $\varepsilon = c_1 + c_2 (J - J_v)$*]*, (B) G93, (C) the Niinemets model. $T = 30^{\circ}C$, $C_i = 273$ μmol mol^{-1}. $V_{cmax_25^{\circ}C} = 70$ μmol m^{-2} s^{-1}, $J_{max_25^{\circ}C} = 130$ μmol m^{-2} s^{-1} based on values from Arneth *et al.* (2007b)'s study. The solid line represents the ratio of isoprene emission to gross assimilation, the dashed line to net assimilation. Normalised ratios of isoprene to CO_2 net assimilation were simulated for two extreme values of dark respiration in order to illustrate the potential effect of the magnitude of R_d on how I/A_{net} varies with *PPFD*: grey short-dashed line, low $R_{d;}$ $R_{d_25^{\circ}C} = 0.5$ μmol m^{-2} s^{-1}; black long-dashed line, high $R_{d;}$ $R_{d_25^{\circ}C} = 2$ μmol m^{-2} s^{-1}. Isoprene model parameters c_1 and c_2 are based on data of Possell and Hewitt (2011) (Fig. 3A.1.2).

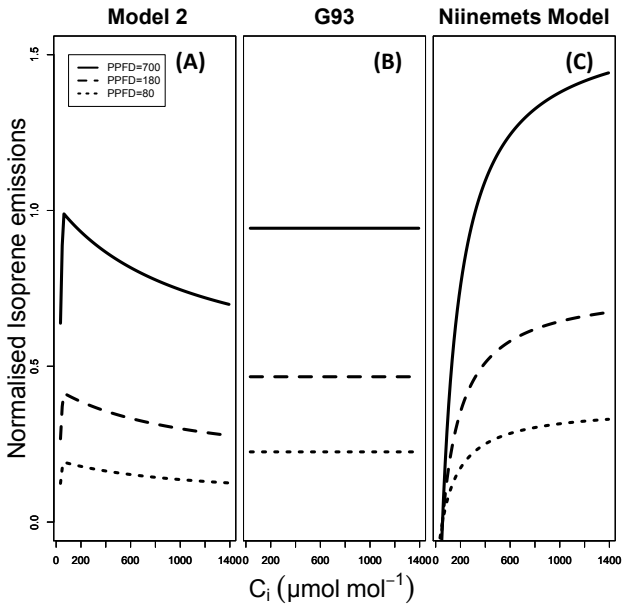


Figure 3A.1.4: Modelled responses of isoprene emission versus C_i for three *PPFD* (80, 180, 700 μmol m^{-2} s^{-1}). (A) Model 2 *[*$I = \varepsilon J$; $\varepsilon = c_1 + c_2 (J - J_v)$], (B) G93, (C) the Niinemets model. Parameters values as in Fig. 3A.1.3. Emissions were normalised to a standard emission rate at T = 30˚C, C_i = 273 μmol mol^{-1}, *PPFD* = 1000 μmol m^{-2} s^{-1}.

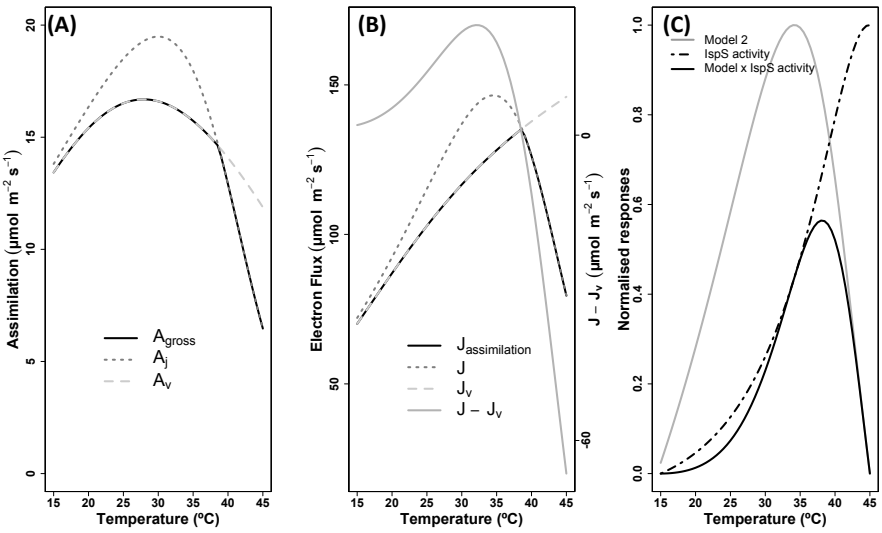


Figure 3A.1.5: Explanation of the predicted temperature dependency of isoprene emissions. (A) Responses to temperature of the light-limited A_j (dark grey short-dash line), the Rubisco limited A_v (light grey long-dash line) and the gross assimilation A_{gross} (solid black line); (B) associated electrons fluxes (left hand axis) and the associated electrons availability ($J - J_v$) (solid grey line; right hand axis). (C) Normalised responses to temperature of model 2 *[*$I = \varepsilon J$; $\varepsilon = c_1 + c_2 (J - J_v)$] (solid grey line), normalised IspS activity (dotted-dashed black line) and the resulting product (solid black line). Temperature dependency of IspS is as described in Niinemets *et al*. (1999b). Parameters values of the model are taken as in Fig. 3A.1.3.

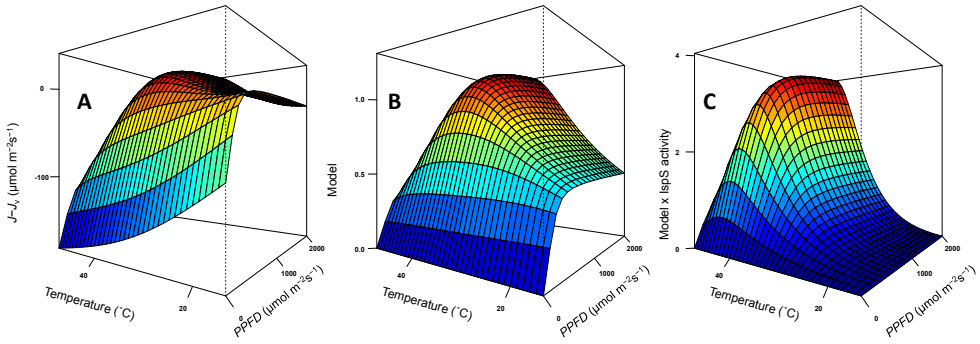


Figure 3A.1.6: Responses to variation in temperature (in ˚C) and *PPFD* (in μmol m^{-2} s^{-1}) of electron availability ($J - J_v$) (in μmol m^{-2} s^{-1}) (A), Model 2 *[*$I = \varepsilon J$; $\varepsilon = c_1 + c_2 (J - J_v)$] (B), Model2 simulations multiplied by a normalised function of enzymatic activity (C). Farquhar model parameters are for *Quercus robur*, as described in Medlyn *et al.* (2002). Parameters values of the model are taken as in Fig. 3A.1.3.Model outputs in panel (B) and (C) are normalised to be unity at T = 30˚C and *PPFD* = 1000 μmol m^{-2} s^{-1}.

Annex 3A.2 – Supplementary table and figure to Chapter III

Table A3.1 Values of the parameters of Farquhar and isoprene models for Fig. 3.3 and Fig.3.6

Symbol	Unit	Value (Fig. 3.3)	Value (Fig. 3.6)
J_{max25}	μmol m^{-2} s^{-1}	99.53	54.32
V_{cmax25}	μmol m^{-2} s^{-1}	62.8	56.9
a	unitless	$2.2\ 10^{-4}$	$4.86\ 10^{-5}$
b	unitless	$7\ 10^{-5}$	$5\ 10^{-6}$

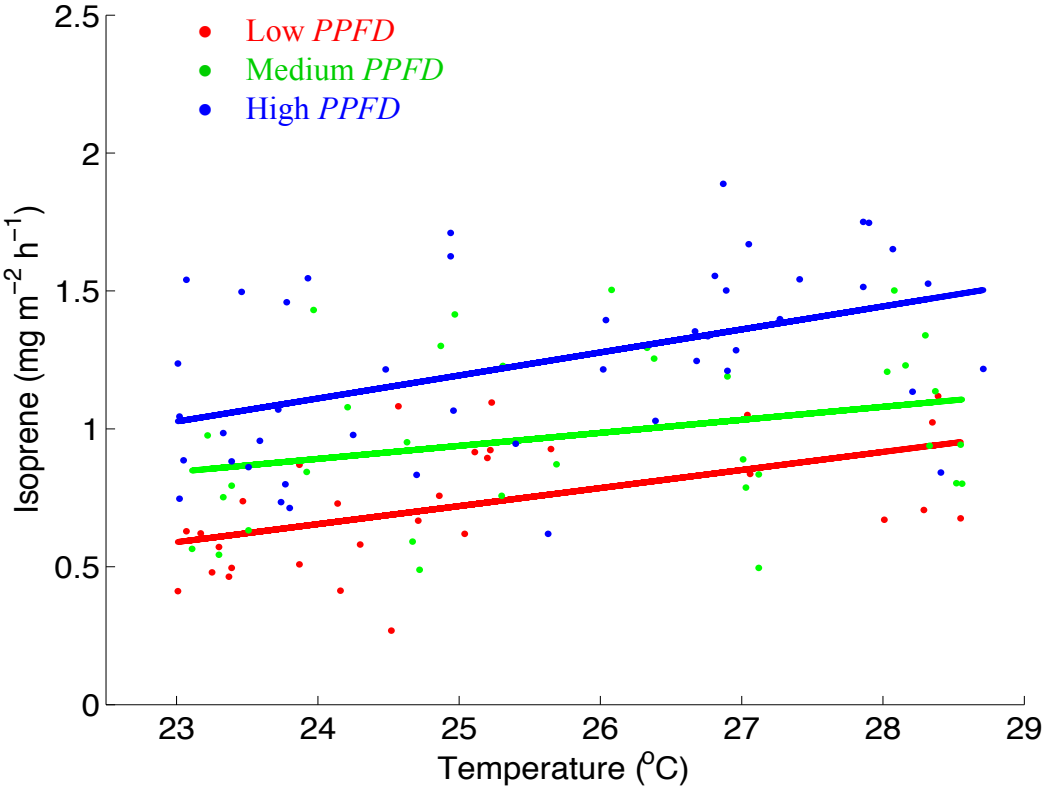


Figure A1.8: Above canopy isoprene emissions in relation to air temperature for three ranges of *PPFD* - Low (1000-1250 μmol m^{-2} s^{-1}), Medium (1250-1500 μmol m^{-2} s^{-1}) and High (1500-1750 μmol m^{-2} s^{-1}). Data from flux measurements at Harvard Forest.

4 Model evaluation at the leaf scale

This chapter describes the development of Model 2 following experiments conducted at CREAF (Spain) on *Populus nigra* L. The protocol of these experiments was designed to test the hypothesis that isoprene production rates are primarily controlled by the excess or deficit of electrons generated by Photosystem II, relative to the needs of carbon fixation. Changes in the balance between energy provided and energy required for carbon assimilation were obtained by varying CO_2 concentration and light intensity during the experiments.

The results presented in this chapter have been published in *New Phytologist*. After describing the data protocol, I explain how Model 2 was tested against the CREAF data, and additional data on hybrid aspen from Sun *et al.* (2012)'s study.

Using data acquired at CREAF, Model 1 was also tested. Model 1 captures well the observed CO_2 responses but it fails to reproduce the observed light responses by producing negative values at low light. This deficiency is described in the Annex to this chapter (Annex 4A.1).

Abstract

I present a unifying model for isoprene emission by photosynthesizing leaves based on the hypothesis that isoprene biosynthesis depends on a balance between the supply of photosynthetic reducing power and the demands of carbon fixation.

I compared the predictions from my model, as well as from two other widely-used models, with measurements of isoprene emission from leaves of *Populus nigra* L. and hybrid aspen (*Populus tremula* L. x *P. tremuloides* Michx.) in response to changes in leaf-internal CO_2 concentration (C_i) and photosynthetic photon flux density (*PPFD*) under diverse ambient CO_2 concentrations (C_a).

My model reproduces the observed changes in isoprene emissions with C_i and *PPFD*, and also reproduces the tendency for the fraction of fixed carbon allocated to isoprene to increase with increasing *PPFD*. It also provides a simple mechanism for the previously unexplained decrease in the quantum efficiency of isoprene emission with increasing C_a.

Experimental and modelled results support my hypothesis. My model can reproduce the key features of the observations and has the potential to improve process-based modelling of isoprene emissions by land vegetation at the ecosystem and global scales.

4.1 Introduction

Isoprene (2-methyl-1,3-butadiene; C_5H_8) is released into the atmosphere by its main source, the terrestrial vegetation. With a total annual emission around 0.5 Pg C a^{-1} (Guenther *et al.*, 2006, 2012; Arneth *et al.*, 2008a), this extremely volatile and reactive molecule is the most important biogenic volatile organic compound (BVOC) produced by plants.

Why do certain plants emit isoprene and others not? What is the advantage for emitters in losing 2% or more of their assimilated carbon in the form of isoprene? What are the controls over isoprene production and emission? These questions remain largely unresolved. However, some indications have emerged in recent years thanks to advances in diverse fields from cell physiology to phylogeny (Li & Sharkey, 2012; Monson *et al.*, 2013; Niinemets & Monson, 2013; Sharkey, 2013). Isoprene appears to protect the photosynthetic apparatus from heat and oxidative damage by enhancing membrane stability at high temperatures, and by quenching reactive oxygen species (Sharkey & Yeh, 2001; Vickers *et al.*, 2009b; Velikova *et al.*, 2011, 2012; Possell & Loreto, 2013). Isoprene is produced in the chloroplast from its immediate precursor dimethylallyl diphosphate (DMADP), which is synthesized via the methylerythritol 4-phosphate (MEP) pathway (Lichtenthaler, 1999; Logan *et al.*, 2000; Sharkey *et al.*, 2008). Isoprene production is therefore controlled by the supply of DMADP, and by the activity of isoprene synthase (Rasulov *et al.*, 2009a,b, 2010; Vickers *et al.*, 2010; Li *et al.*, 2011; Monson, 2013). The metabolic controls of the MEP pathway, in relation to isoprene biosynthesis are just beginning to be understood (Li & Sharkey, 2012; Banerjee *et al.*, 2013; Weise *et al.*, 2013), and the whole pathway controls cannot yet be included in isoprene emission models in a wholly mechanistic manner (Grote *et al.*, 2013; Li & Sharkey, 2013).

In addition to its physiological interest, isoprene has sparked attention in climate science because of its impact on atmospheric chemistry and climate. Because of its abundance and reactivity, isoprene emission substantially affects the atmospheric content of tropospheric ozone, methane, and secondary organic aerosols (Poisson *et al.*, 2000; Sanderson *et al.*, 2003; Claeys *et al.*, 2004; Heald *et al.*, 2008; Pike & Young, 2009; Nozière *et al.*, 2011; Paasonen *et al.*, 2013). To investigate the potential impact of isoprene on air quality and climate, models for isoprene emission have been developed

(Grote & Niinemets, 2008; Monson *et al.*, 2012; Grote *et al.*, 2013). Many recently published studies have used the MEGAN model (Guenther *et al.*, 2012), which is based on the pioneering work of Guenther and co-workers (Guenther *et al.*, 1991, 1993). In MEGAN, a species-specific standard isoprene emission (I_s) is modified by empirical functions that account for the observed variations in isoprene emissions due to various environmental controls. Although simple, this approach is vulnerable to model overparameterization due to interactions among environmental drivers (Niinemets *et al.*, 2010a; Sun *et al.*, 2012). Other models have been developed based upon the available knowledge about the underlying biochemical processes. These include the models of Niinemets *et al.* (1999b) and Martin *et al.* (2000), and the SIM-BIM model (Zimmer *et al.*, 2000, 2003). Nevertheless, all isoprene emission models remain largely empirical, and the mechanistic content of current models admits considerable scope for improvement (Monson *et al.*, 2012; Grote *et al.*, 2013).

Although often invoked as a potential driver of isoprene production (Niinemets *et al.*, 1999b; Rasulov *et al.*, 2010; Li & Sharkey, 2012), few studies have quantitatively explored the impact of leaf energetic status on isoprene emissions. I define the leaf energetic status as the balance (or imbalance) between the supply of photosynthetic induced reducing power and the demands of carbon fixation and photorespiration. Here, I investigate the hypothesis that the rate of isoprene biosynthesis depends on the leaf energetic status. I used observations from *Populus nigra* L. grown in full sun (this study) and hybrid aspen (*Populus tremula* L. x *P. tremuloides* Michx.) grown at two CO_2 concentrations (Sun *et al.*, 2012). For each dataset, the experimental protocol allowed us to study short-term variations of isoprene emission, and associated variations of the electron balance between photosynthetic supply and carbon assimilation requirements. Changes in both isoprene emission and energy balance were obtained by modifying the light and CO_2 conditions of the experiments. I used these datasets to test a new modelling framework, in which changes in leaf energetic status are approximated by the difference between the light- and Rubisco-limited electron fluxes for carbon assimilation. I use the same data to test the responses of two of the better-known among published isoprene models: the Guenther *et al.* (1993) algorithm that underlies MEGAN, and the "process-based" model developed by Niinemets *et al.* (1999b), Niinemets (2004) and modified by Arneth *et al.* (2007b).

Hypothesis

Isoprene is produced in the chloroplast by the 2-*C*-methyl-D-erythritol 4-phosphate (MEP) pathway, in which glyceraldehyde 3-phosphate (G3P) and pyruvate (Pyr) are transformed into dimethylallyl diphosphate (DMADP). The process involves reduction steps that require reducing power in the form of NADPH and/or ferredoxin (Fd) (Charon *et al.*, 1999; Hecht *et al.*, 2001; Seemann *et al.*, 2006; Li & Sharkey, 2012). DMADP is further transformed into isoprene by the enzyme isoprene synthase. Therefore, isoprene production is co-driven by enzymatic activity and NADPH and/or ATP availability (Lichtenthaler, 1999).

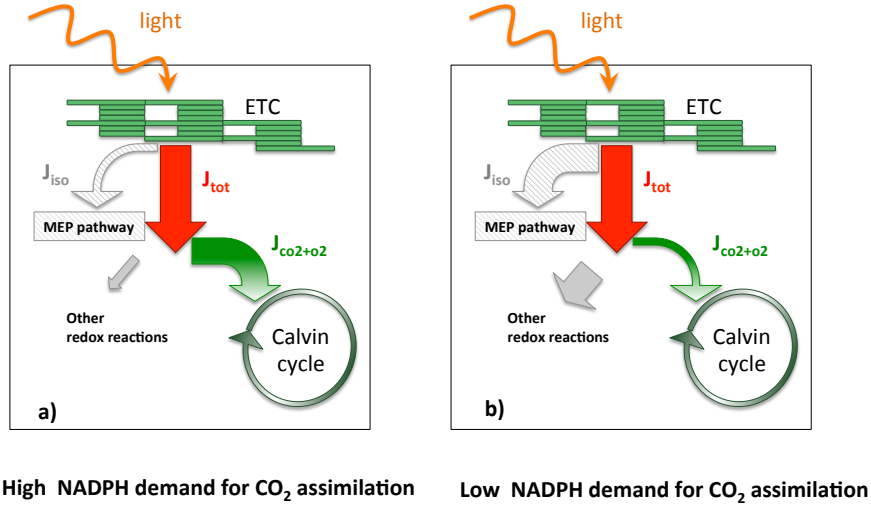


Figure 4.1: Schematic of the processes underlying the proposed hypothesis for isoprene emission modelling. The arrow colour scheme is as follow: red, total electron flux generated by light reaction in photosystem II (J_{tot}); green, electron flux used in reactions associated with carbon assimilation and photorespiration (J_{CO2+O2}); dashed grey, electron flux used in the MEP pathway (J_{iso}); dark grey, electron flux used for other redox reaction. Changes in fluxes intensities in situation of (a) high and (b) low demand for carbon assimilation are symbolically represented by changes in the arrows width. This schematic is illustrative only and the arrows are not fitted to scale. Symbols: ETC, electron transport chain; MEP, 2-C-methyl-D-erythritol 4-phosphate; NADPH, nicotinamide adenine dinucleotide phosphate.

Plastid NADPH is provided by the electron transport flux generated by the light reactions of Photosystem II. As reduction steps in carbon assimilation and photorespiration consume almost all of the NADPH generated, it is common to assume that the total electron flux (J_{tot}, Fig. 4.1) is the same as the total electron flux used in carbon assimilation (J_{CO2+O2}). However, in reality J_{tot} is always somewhat larger than J_{CO2+O2}. It has to be so in order to supply NADPH for additional redox reactions in the leaf (Niinemets *et al.*, 1999b; Singsaas *et al.*, 2001; Niinemets, 2004). The reduction steps along the MEP pathway constitute some of these additional reactions. Thus, J_{tot} can be expressed as $J_{tot} = J_{CO2+O2} + J_{iso} + J_{other}$, where J_{iso} and J_{other} represent electron fluxes involved respectively in isoprene production and other redox reactions in the leaf. I hypothesize accordingly that the additional reducing power available for isoprene production is dependent on the extent to which the NADPH requirements of the Calvin-Benson and photorespiratory cycles are satisfied (Harrison *et al.*, 2013; Morfopoulos *et al.*, 2013). As illustrated in Figure 4.1, the MEP pathway could be envisioned to act like a small branch circuit, with greatest influx occurring when the demand of carbon assimilation for reducing power is least (Rosenstiel *et al.*, 2004; Owen & Peñuelas, 2005). But the MEP pathway alone does not have the capacity to absorb all of the excess of energy generated. Thus, my hypothesis also suggests that isoprene emissions might co-vary with other, more effective energy-quenching processes, including the Mehler reaction and the xanthophyll cycle.

Although the biochemical mechanisms controlling the partitioning of the NADPH fluxes inside the plastid are incompletely understood, the nature of the responses of isoprene emission to different environmental drivers suggest that this hypothesis is well founded (Morfopoulos *et al.*, 2013). Indeed, the literature shows a persistent tendency for plants to increase isoprene emission (and the fraction of assimilated carbon transformed to isoprene) with increasing leaf energetic status. For example:

1) Isoprene emissions increase with decreasing CO_2 concentration (Rosenstiel *et al.*, 2003; Wilkinson *et al.*, 2009; Possell & Hewitt, 2011; Sun *et al.*, 2012).
2) The fraction of assimilated carbon transformed to isoprene increases with increasing light intensity (Sharkey & Loreto, 1993; Harley *et al.*, 1996; Lerdau & Keller, 1997).

3) The temperature optimum for isoprene emissions is lower than that of isoprene synthase (IspS) activity, and apparently co-controlled by the temperature dependencies of the electron transport rate and IspS activity (Monson *et al.*, 1992, 2012; Rasulov *et al.*, 2010).
4) Isoprene emissions decrease in plants fed with nitrate (which consumes NADPH in the process of nitrate reduction to ammonium), but increase if fed with ammonium directly (Rosenstiel *et al.*, 2004).
5) Isoprene emissions increase when light use efficiency decreases (Peñuelas *et al.*, 2013).

These observations all support the hypothesis that isoprene emissions are influenced by the balance of reducing power between what can be produced by light reactions, and what is needed for carbon assimilation and other major NADPH sinks.

Ideally, to represent this hypothesis quantitatively, I should model the total electron flux and the dynamics of all relevant electron sinks. But in reality, (i) process-based models that can simulate total electron transport rate (J_{tot}) are in an early stage of development (Ye *et al.*, 2013), (ii) the partitioning of the additional reducing power between J_{other} and J_{iso} remains enigmatic, and (iii) the nanomole scale at which isoprene emission occurs (compared to the micromole scale of electron flux) makes it unrealistic to attempt a full mass balance of the competing processes. Accordingly, my pragmatic approach is to model the energetic status of the leaf using the Farquhar model (Farquhar *et al.*, 1980) for photosynthetic carbon assimilation, thus approximating the energetic status of the leaf as the difference between the light-limited electron flux (J) and the electron flux required to support Rubisco-limited photosynthesis (J_v). J is an approximation of the amount of reductant that light reactions can supply, while J_v represents the capacity of Rubisco to absorb this reducing power. Therefore energy transfers to other processes than carbon assimilation [$J_{tot} - J_{CO2+O2} = J_{other} + J_{iso}$] should be correlated to the magnitude of the difference [$J - J_v$]. Based on this proxy, I build a model of isoprene emissions that I will describe further in the text. I test the model with data on isoprene emission as a function of internal CO_2 concentration (C_i) and photosynthetic photon flux density (*PPFD*).

I further test my hypothesis by examining observed and modelled changes in the fraction of assimilated carbon allocated to isoprene production. The ratio of isoprene emission to gross carbon assimilation (I/A_{gross}) is a sensitive indicator of the allocation of reducing power to the MEP pathway versus the Calvin-Benson cycle (Niinemets *et al.*, 2013). Under a constant leaf temperature and CO_2 concentration, we would expect the fraction of assimilated carbon re-emitted as isoprene to be constant, if only enzymatic limitations were involved. But if indeed isoprene production depends on the energetic status of the leaves then I/A_{gross} would be expected to increase with increasing *PPFD* (Niinemets *et al.*, 2013), as carboxylation becomes progressively Rubisco-limited, while electron transport continues to increase.

Finally, I examine changes in the quantum efficiency of isoprene emission (Φ_{iso}). Previous studies have reported changes with environmental conditions (Monson *et al.*, 1992; Logan *et al.*, 2000; Sun *et al.*, 2012). Changes in the quantum efficiency of CO_2 assimilation (Φ_{CO2}) cannot explain changes in Φ_{iso}. The processes controlling quantum yields for isoprene are not fully understood. I postulate that differences in the quantum efficiency of isoprene emission (Φ_{iso}) are driven by the energetic status of the leaves, and can thus be related to variation of $[J - J_v]$. Thus I expect the quantum yield of isoprene emission to be lower when the NADPH demand for carbon assimilation is higher.

I will show that my energetic status model is able to reproduce i) changes in isoprene emission induced by changes in C_i and *PPFD*, ii) the observed tendency of (I/A_{gross}) to increase with increasing *PPFD* and iii) the observed increase in Φ_{iso} with decreasing CO_2 concentration.

4.2 Materials and methods

Plant material and growing conditions

In this study I examine results from experiments conducted on two different species: *Populus nigra* L. and hybrid aspen *(Populus tremula* x *P. tremuloides*).

The first set of experiments was conducted on three saplings of *Populus nigra*, grown in 15 L pots with a substrate composed of peat and sand (2:1) in a nursery (Tres Turons S.C.P., Castellar del Vallès, Catalonia, Spain). Plants were grown in a sunny

environment under Mediterranean ambient conditions outdoors for 2 months prior to the measurement (2nd May to 7th July 2012). Typical Mediterranean climate is characterized by seasonal summer drought with warm temperatures and mild winters. This is reflected by the average monthly temperature of 22.8°C in August and 7.9°C in January. Mean annual precipitation and temperature are 723 mm and 15.1°C (1951-2010) (Ninyerola *et al.*, 2000). Due to high temperature and low precipitation the plants were under conditions of high evaporative demand. However, regular irrigation ensured that the substrate was held at field capacity throughout this period. Here I used data from one leaf of each sapling, giving an overall dataset of three sun- adapted individuals.

The second set of experiments was conducted with two-year old saplings of hybrid aspen *(Populus tremula* x *P. tremuloides*) grown under two different ambient CO_2 concentrations (380 and 780 μmol mol^{-1}). These experiments, along with a full description of the materials and methods used, are reported in Sun *et al.* (2012, 2013b), and here only a brief summary of the methods is provided. The plants were grown in a custom-made four-chamber open gas-exchange system. Each individual chamber experienced 12 h photoperiod at levels of light between 500 and 800 μmol m^{-2} s^{-1}, day-night air temperature between 28-30/23 ˚C and air relative humidity of 60%. Two chambers (chamber 1 and 3) were kept at an ambient CO_2 concentration of 380 μmol mol^{-1} (HA-G380), while the other two chambers were treated with an elevated CO_2 concentration of 780 μmol mol^{-1} (HA-G780). Here I used data from three leaves of each chambers, giving an overall dataset of six individuals grown at ambient CO_2 concentration and six individuals grown at elevated CO_2 concentration.

For each dataset, results shown are averaged values across individuals.

Foliage Gas Exchange Analyses and Isoprene Emission Rates

Gas exchange measurements were conducted on individuals of *Populus nigra* using a Li-Cor LI-6400 portable photosynthesis system (an open gas exchange analyser using a 6 cm^2 clamp-on leaf cuvette (LI 6400; LI-COR, Inc., Lincoln, NE, USA)). The calibration of the infrared gas analyser (IRGA) was done by the manufacturer less than one year prior to the measurements.

The exhaust tube of the IRGA measure head was connected to a Proton-Transfer-Reaction Mass Spectrometer (PTR-MS) system (Ionicon Analytik, Innsbruck, Austria),

using tubing material made of Siltek-passivated stainless steel (Restek, Bellefonte, PA, USA). Analyses of emission rates for isoprene were done simultaneously with gas exchange measurements with the PTR-MS. The PTR–MS technique is based on chemical ionisation, specifically non-dissociative proton transfer from H_3O^+ ions to most of the common BVOCs, and has been fully described elsewhere (Lindinger *et al.*, 1998). In my experiment on *Populus nigra* the PTR–MS drift tube was operated at 2.1 mbar and 60ºC, with an E/N (electric field/molecule number density) of around 130 Td (Townsend) (1 Td = 10^{-17} V cm^2). The primary ion signal (H_3O^+) was maintained at ~6 × 10^6 counts per second. The instrument was calibrated using an aromatic mix standard gas (TO-14A, Restek, Bellefonte, PA, USA) and isoprene standard gas with 100 nmol mol^{-1} isoprene in N_2 (Abelló-Linde SA, Barcelona). Prior to data acquisition, the leaf cuvette was left empty in order to analyse the background concentrations of isoprene, and thereafter calculate the foliar emission rates. No significant drift in the background of isoprene was found during the experiments.

Foliage gas exchange analyses and isoprene emission rates on hybrid aspen were obtained using a Walz GFS-3000 portable gas-exchange system and a Fast Isoprene Sensor (FIS, Hills Scientific, Boulder Colorado, USA). More information about the methods can be found in Sun *et al.* (2012, 2013b).

Before each experiment, the leaf was enclosed in the gas- exchange system and left under baseline conditions until net assimilation (A_{net}), stomatal conductance (g_s) and C_i stabilised (typically 20-30 min). For *Populus nigra,* baseline conditions were of *PPFD* of 1000 μmol m^{-2} s^{-1}, leaf temperature of 30 °C, relative humidity of 50% (± 10%) and ambient CO_2 concentration of the leaf chamber (C_a) of 390 μmol mol^{-1}. For hybrid aspen*,* baseline conditions were of *PPFD* of 500 μmol m^{-2} s^{-1}, leaf temperature of 30 °C, relative humidity of 60%, C_a of 380 μmol mol^{-1} for HA-G380 and C_a of 780 μmol mol^{-1} for HA-G780. After preconditioning the leaf as explained above, two types of response curves were created, (i) the leaf net assimilation versus internal CO_2 concentration (A_{net}/C_i) and (ii) the leaf net assimilation versus *PPFD* (A_{net}/ *PPFD*).

CO_2 response curves of net assimilation and isoprene emissions

C_i response curves were obtained at a leaf temperature of 30°C and a quantum flux density of 1000 μmol m^{-2} s^{-1} for *Populus nigra* and 500 μmol m^{-2} s^{-1} for hybrid aspen. The C_a values used to generate the *Anet*-C_i response curve were:

50 → 150 → 200 → 250 → 350 → 390 → 500 → 700 → 800 → 900 → 1200 → 2000 (μmol mol^{-1}), for *Populus nigra*;

380 → 200 → 150 → 100 → 50 → 20 → 0 → 380 → 780 → 1000 → 1500 → 2000 (μmol mol^{-1}), for HA-G380;

780 → 380 → 200 → 150 → 100 → 50 → 20 → 0 → 780 → 1000 → 1500 → 2000 (μmol mol^{-1}), for HA-G780.

At every C_a, values of A_{net}, isoprene emission rate (I) and stomatal conductance (g_s) were recorded when the gas-exchange rates were stable, typically 5–10 min after the change of C_a.

PPFD response curves of net assimilation and isoprene emissions

By applying sequential changes in *PPFD*, light response curves at different C_a were obtained. Three different C_a (200, 390 and 1000 μmol mol^{-1}) were applied for *Populus nigra,* and two different C_a (380 and 780 μmol mol^{-1}) were applied for hybrid aspen.

The following sequence of *PPFD* was applied:

2500 → 2000 → 1750 → 1500 → 1250 → 1000 → 700 → 500 → 250 → 150 → 75 → 0 (μmol m^{-2} s^{-1}) for *Populus nigra;*

500 → 1500 → 1000 → 800 → 400 → 200 → 120 → 60→ 30 → 12 → 0 (μmol m^{-2} s^{-1}) for hybrid aspen.

The waiting time between each light intensity was approximately 10 min. The data were logged when the rate of A_{net}, g_s, C_a and I were in the steady state, except for hybrid aspen at *PPFD* higher than 1500 μmol m^{-2} s^{-1} where the values were recorded after 5 to 8 min to avoid the development of photoinhibition.

Energetic status model

My isoprene model is modified in one small (but important) way from the one introduced in Harrison *et al.* (2013) and Morfopoulos *et al.* (2013) and deals with the issue of negative values for isoprene emission generated using the first version of the model (annex 4A.1). In these earlier papers, isoprene emission rate was assumed to be linearly related to the energy status of the leaf, whereas here the *fraction* of electrons allocated to isoprene biosynthesis is linearly related to the energetic status of the leaf:

$$\varepsilon = c_1 + c_2 (J - J_v) \tag{4.1}$$

and

$$I = \varepsilon J \, f(C_i) \, f(T) \tag{4.2}$$

where I is isoprene emission; $f(C_i)$ is a function of internal CO_2 concentration; $f(T)$ is a function of temperature taking in account response of enzymatic activity to temperature; J is the light-limited electron flux, taken to be a non-rectangular hyperbolic function of absorbed *PPFD* and the maximum electron flux J_{max}, following Farquhar *et al.* (1980), and

$$J_v = 4V_{cmax} \cdot \frac{(C_i + \Gamma^*)}{(C_i + k_c^{'})} \tag{4.3}$$

which is the electron flux required to support Rubisco-limited carbon assimilation. Γ^* is the CO_2 compensation point in the absence of mitochondrial respiration in the light, V_{cmax} is the Rubisco carboxylation capacity, and $k_c^{'} = k_c(1 + [O_2]/k_o)$ where k_c and k_o are the Michaelis coefficients of Rubisco for CO_2 and O_2 respectively (Farquhar *et al.*, 1980). The term ε in equation (4.2) is not constant but varies depending on the energetic status of the leaf, estimated by $[J - J_v]$. The function $f(C_i)$ in equation (4.2) is chosen to take the value C_i / Γ^* when $C_i \leq \Gamma^*$ and 1 otherwise and reflects the common observation that isoprene emission ceases when $C_i < \Gamma^*$ due to a minimum supply of carbon chains required for isoprene synthesis and/or to inhibition of electron transport rate below Γ^* (Dietz *et al.*, 1985; Wolfertz *et al.*, 2003; Rasulov *et al.*, 2009b, 2011; Monson *et al.*, 2012; Sun *et al.*, 2012) This fall-off of isoprene at low C_i is not fully understood and not always observed: emission of isoprene in CO_2-free air has been reported in a few studies (Monson & Fall, 1989; Affek & Yakir, 2003; Li & Sharkey, 2012). However,

comparable conditions are not found in natural environments. Using the C_i response curves, changes in the fraction ε of the light limited electron flux (J) allocated to isoprene production (Eq. 4.1-4.2) were plotted against the corresponding difference between light- and Rubisco-limited electron fluxes [$J - J_v$]. Parameters c_1 and c_2 were obtained from a linear regression between ε and [$J - J_v$] when $C_i > \Gamma^*$ (Fig. 4.2a; Fig. 4.3a-b). Because all the experiments were conducted at a leaf temperature of 30˚C, I neglect here the temperature dependency due to IspS activity, and $f(T)$ is accordingly set equal to 1. Quantum efficiencies for isoprene production (Φ_{iso}) were calculated as the initial slope of isoprene emission versus *PPFD*, for *PPFD* lower than 250 μmol m^{-2} s^{-1}. The uncertainties bounds of the energetic status model displayed in the figures represent uncertainties in the estimated values of V_{cmax} and J_{max} in the Farquhar model.

The G93 algorithm

The algorithm developed by Guenther and co-workers (Guenther *et al.*, 1993), which is the basis of the isoprene module of the MEGAN model (Guenther *et al.*, 2012), is the most widely used algorithm for prediction of isoprene emission by plants. Hereafter this algorithm is referred to as G93. In G93 the emission rates of isoprene are calculated by multiplying a species-specific standard emission rate (I_s) by a set of empirical equations taking into account changes in environmental variables. The standard conditions for I_s are a leaf temperature of 30˚C and an incident *PPFD* of 1000 μmol m^{-2} s^{-1}. Because in this study all the experiments were conducted at a constant leaf temperature of 30˚C, I consider only changes driven by light intensity:

$$I = I_s C_L \tag{4.4}$$

with

$$C_L = \frac{\alpha C_{L1} PPFD}{\sqrt{(1 + \alpha^2 PPFD^2)}} \tag{4.5}$$

where C_{L1} and α are empirical coefficients. For each light response curve, in order to take into account the CO_2 effect on standard emission rates, the value of I_s was taken as the observed emission rate at a *PPFD* of 1000 μmol m^{-2} s^{-1}, under the CO_2 conditions of the experiment.

The Niinemets model

The Niinemets model (Niinemets *et al.*, 1999b) is based on quantifying the NADPH cost for isoprene synthesis. It builds on the Farquhar model of photosynthesis. The general concept is that a temperature-dependent fraction of the electron flux (ε_N) is used for isoprene production:

$$\varepsilon_{\mathrm{N}} = \frac{J_I}{J_{\mathrm{tot}}} \tag{4.6}$$

where J_{I} is the electron flux required in order to produce a quantity of isoprene and J_{tot} is the total photosynthetic electron flux, approximated by J, using the Farquhar model:

$$J_{\mathrm{tot}} \approx J = A_{\mathrm{j}} \cdot \frac{(4C_{\mathrm{i}} + 8\Gamma^*)}{(C_{\mathrm{i}} - \Gamma^*)} \tag{4.7}$$

where A_{j} is the gross assimilation under electron transport-limited conditions, C_i is the internal CO_2 concentration and Γ* is the compensation point.

The total NADPH cost for isoprene production per mole CO_2 assimilated is 1.17 times higher for isoprene (2.33 NADPH per CO_2) than for sugar synthesis (2 NADPH per CO_2); and six molecules of CO_2 must be assimilated to produce one isoprene molecule. Drawing a parallel with the Farquhar model, J_{I} is thus estimated as:

$$J_{\mathrm{I}} = 6I.\left(\frac{2.33}{2}\right) \cdot \frac{(4C_{\mathrm{i}} + 8\Gamma^*)}{(C_{\mathrm{i}} - \Gamma^*)} = 7.02I. \frac{(4C_{\mathrm{i}} + 8\Gamma^*)}{(C_{\mathrm{i}} - \Gamma^*)} \tag{4.8}$$

Combining (6), (7) and (8), the overall model for isoprene emission becomes:

$$I = \varepsilon_{\mathrm{N}} J \frac{(C_{\mathrm{i}} - \Gamma^*)}{7.02\,(4C_{\mathrm{i}} + 8\Gamma^*)} = \frac{\varepsilon_{\mathrm{N}}}{7.02} \cdot A_{\mathrm{j}} \tag{4.9}$$

Because all the experiments were conducted at a leaf temperature of 30˚C, I neglect the temperature dependency of ε_{N}. The effect of changes in CO_2 concentration on ε_{N} is adapted from Arneth *et al.* (2007b):

$$\varepsilon_{\mathrm{N}} = \varepsilon_{\mathrm{Ns}} \frac{C_{\mathrm{a_s}}}{C_a} \tag{4.10}$$

where $\varepsilon_{\mathrm{Ns}}$ is the fraction of electrons used for isoprene production under the standard conditions of leaf temperature T_s = 30°C, *PPFD* = 1000 μmol m^{-2} s^{-1}, and $C_{\mathrm{a_s}}$ = 390 μmol mol^{-1} . In this study, $\varepsilon_{\mathrm{Ns}}$ was estimated from experiment varying *PPFD* at a C_a of 390 μmol mol^{-1} for *Populus nigra* and 380 μmol mol^{-1} for hybrid aspen.

The Farquhar model

The Farquhar *et al.* (1980) photosynthesis model describes the limitations on the C_3 net photosynthetic rate (A_{net}) by two main equations representing the limitations imposed by Rubisco-catalyzed carboxylation (V_{cmax}) and RuBP regeneration, which is limited by *PPFD* and by the maximum electron transport rate (J_{max}). Under Rubisco limited conditions, A_{net} is expressed as:

$$A_{\mathrm{net}} = A_{\mathrm{v}} - R_{\mathrm{d}} = V_{\mathrm{cmax}} \cdot \frac{(C_{\mathrm{i}} - \Gamma^*)}{(C_{\mathrm{i}} + k_{\mathrm{c}}^{'})} - R_{\mathrm{d}} \tag{4.11}$$

A_{v} is the gross assimilation under Rubisco-limited conditions, R_{d} is the mitochondrial respiration in the light and was assumed to be equal to dark respiration divided by 2 (Niinemets *et al.*, 2005; Misson *et al.*, 2010; St. Paul *et al.*, 2012). Under electron transport limitation, A_{net} is expressed as

$$A_{\mathrm{net}} = A_{\mathrm{j}} - R_{\mathrm{d}} = \left(\frac{J}{4}\right) \cdot \frac{(C_{\mathrm{i}} - \Gamma^*)}{(C_{\mathrm{i}} + 2\Gamma^*)} - R_{\mathrm{d}} \tag{4.12}$$

where J is the potential rate of electron transport. J in turn depends on *PPFD* up to a maximum J_{max} (de Pury & Farquhar, 1997). For each C_{a}, the averaged value of observed C_{i} was used for the model simulations. Values of Michaelis-Menten constants, activation and de-activation energies, specificity for Rubisco and their temperature dependencies were taken from Bernacchi *et al.* (2002) and Medlyn *et al.* (2005) (supplementary material S2).

For the experiment on *Populus nigra*, probably due to the growing conditions of the plants (Mediterranean summer sunshine), the plants adapted their maximum Rubisco capacity (V_{cmax}) to the prevailing high levels of irradiance and temperature. As a result,

under most of the experimental conditions (including a large part of the A_{net}/C_i curve), the carbon assimilation was found to be limited by electron transport and not by Rubisco capacity. In order to estimate V_{cmax}, I therefore used the light response curve for assimilation, at a C_a of 200 μmol mol^{-1} and $PPFD \geq 1500$ μmol m^{-2} s^{-1}, where A_{net} was saturating. I calculated V_{cmax} by minimizing the residual sum of squares (RSS) between the Rubisco-limited equation and the observations. The capacity for photosynthetic electron transport (J_{max}) was obtained similarly by minimizing RSS between the light limited equation and the assimilation data from all experiments. For hybrid aspen, J_{max} and V_{cmax} were estimated from A_{net}-C_i curves by minimizing RSS between the Farquhar model and the observations.

Model parameters are summarized in Table 4.1. Statistical analyses were performed using the software R version 2.15.0.

Table 4.1: Model parameter values at a leaf temperature of 30˚C.

Data	Model	Parameter	Value	Units
Populus nigra	**Farquhar**	J_{max}	111(+20 −15)	μmol m^{-2} s^{-1}
		V_{cmax}	169 (+35 −32)	μmol m^{-2} s^{-1}
		α _co2	0.27 (+0 −0.03)	mol electron mol^{-1} photon
		θ	0.01 (+0.36 −0)	unitless
	Energetic status	c_1	0.309 × 10^{-3}	unitless
	model	c_2	8.648 × 10^{-7}	m^2 s μmol^{-1}
Hybrid Aspen	**Farquhar**	J_{max}	88(+39 −15)	μmol m^{-2} s^{-1}
HA-G380		V_{cmax}	56 (+6 −17)	μmol m^{-2} s^{-1}
		α_co2	0.385*	mol electron mol^{-1} photon
		θ	0.7*	unitless
	Energetic status	c_1	0.193 × 10^{-3}	unitless
	model	c_2	2.87 × 10^{-6}	m^2 s μmol^{-1}
Hybrid Aspen	**Farquhar**	J_{max}	95(+29 −24)	μmol m^{-2} s^{-1}
HA-G780		V_{cmax}	59 (+15 −0)	μmol m^{-2} s^{-1}
		α_co2	0.385*	mol electron mol^{-1} photon
		θ	0.7*	unitless
	Energetic status	c_1	0.219 × 10^{-3}	unitless
	model	c_2	8.648 × 10^{-7}	m^2 s μmol^{-1}
All	**G93**	α	0.0027*	unitless
		C_{L1}	1.066*	unitless

Farquhar model uncertainties (in brackets) were obtained by fitting the model to the maximum and minimum bounds of the assimilation curves. *Parameters not fitted to data; J_{max}, maximum electron flux; V_{cmax}, maximum Rubisco carboxylation capacity; α_co2, quantum yield of electron transport; θ, curvature parameter of the light response curve; c_1 and c_2, parameters of my energetic status model; α and C_{L1} parameters of the G93 algorithm.

4.3 Results

4.3.1 Experiments varying C_i

For each plant type, isoprene emissions showed a strong negative response to changes in C_i (Fig. 4.2b; Fig. 4.3c-d). For *Populus nigra* maximum isoprene emissions were approximately 33 nmol m^{-2} s^{-1} at low C_i (73 – 174 μmol mol^{-1}), declining to 8 nmol m^{-2} s^{-1} at high C_i (1280 μmol mol^{-1}). Maximum isoprene emission rates (at low C_i) represented up to 2.24% of assimilated carbon (Fig. 3A.2.1); this percentage drops to 0.17% at high C_i. For hybrid aspen, averaged isoprene emissions peaked at low C_i (105 – 140 μmol mol^{-1}) with maxima about 21 nmol m^{-2} s^{-1} for HA-G380 and 25 nmol m^{-2} s^{-1} for HA-G780, declining below 4 nmol m^{-2} s^{-1} at high C_i (1400 μmol mol^{-1}). A decline in isoprene emissions for very low value of C_i was observed whatever the growing conditions. As highlighted in Sun *et al.* (2012), isoprene emissions reached higher rates for individuals grown under elevated CO_2 concentrations, in contradiction to what is usually assumed. Maximum emission rates represented a loss of assimilated carbon into isoprene of 5.6% for HA-380 and 6.6% for HA-G780; this percentage drops to 0.09% for high value of C_i.

For all experiments, a very strong, linear correlation was found between [J– J_v] and the number of electrons ε engaged in the isoprene production pathway, with $r^2 > 0.89$ (Fig. 4.2a; Fig. 4.3a-b). Yet the response of ε versus [J– J_v] seems to start saturating at very negative values of [J– J_v] in each dataset. This behaviour might be due to an overall saturation of redox sate of Q_A (the primary acceptor of Photosystem II) associated with a limitation of capacity of J_{tot} that can be observed under high C_i (Dietz *et al.*, 1985).

With parameters obtained from linear regression of ε versus [J– J_v], my model simulated isoprene emissions in response to changes C_i with an excellent agreement to the observations (r^2 = 0.94, 0.87 and 0.93 for *Populus nigra*, HA-G380 and HA-G780 respectively) (Fig. 4.2b; Fig. 4.3c-d).

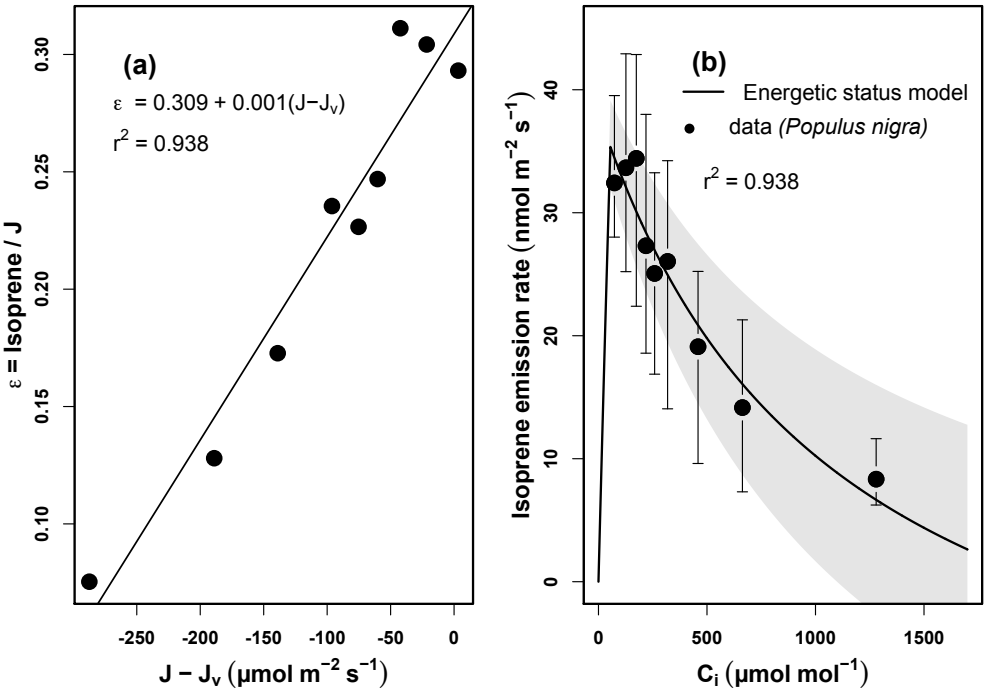


Figure 4.2: Isoprene emissions versus internal CO_2 concentration (C_i) at a leaf temperature of 30˚C and a photosynthetic photon flux density of 1000 μmol m^{-2} s^{-1} for *Populus nigra* L. (a) Observed changes in the fraction of electrons used for isoprene production taken as the ratio of isoprene emission rate to light-limited electron flux for carbon assimilation ($\varepsilon = I/J$) in response to changes in the energetic status of the leaf taken as the difference between the light- and Rubisco-limited electron fluxes for carbon assimilation [$J - J_v$]. (b) Observed (black circles) and modelled (solid line) isoprene emission rates in response to changes in C_i. The grey shadowed area represents uncertainties of the isoprene model due to uncertainties in the values of the maximum Rubisco carboxylation capacity (V_{cmax}) and maximum electron flux (J_{max}) in the Farquhar model. Errors bars represent the maximum and minimum bounds of the isoprene curve.

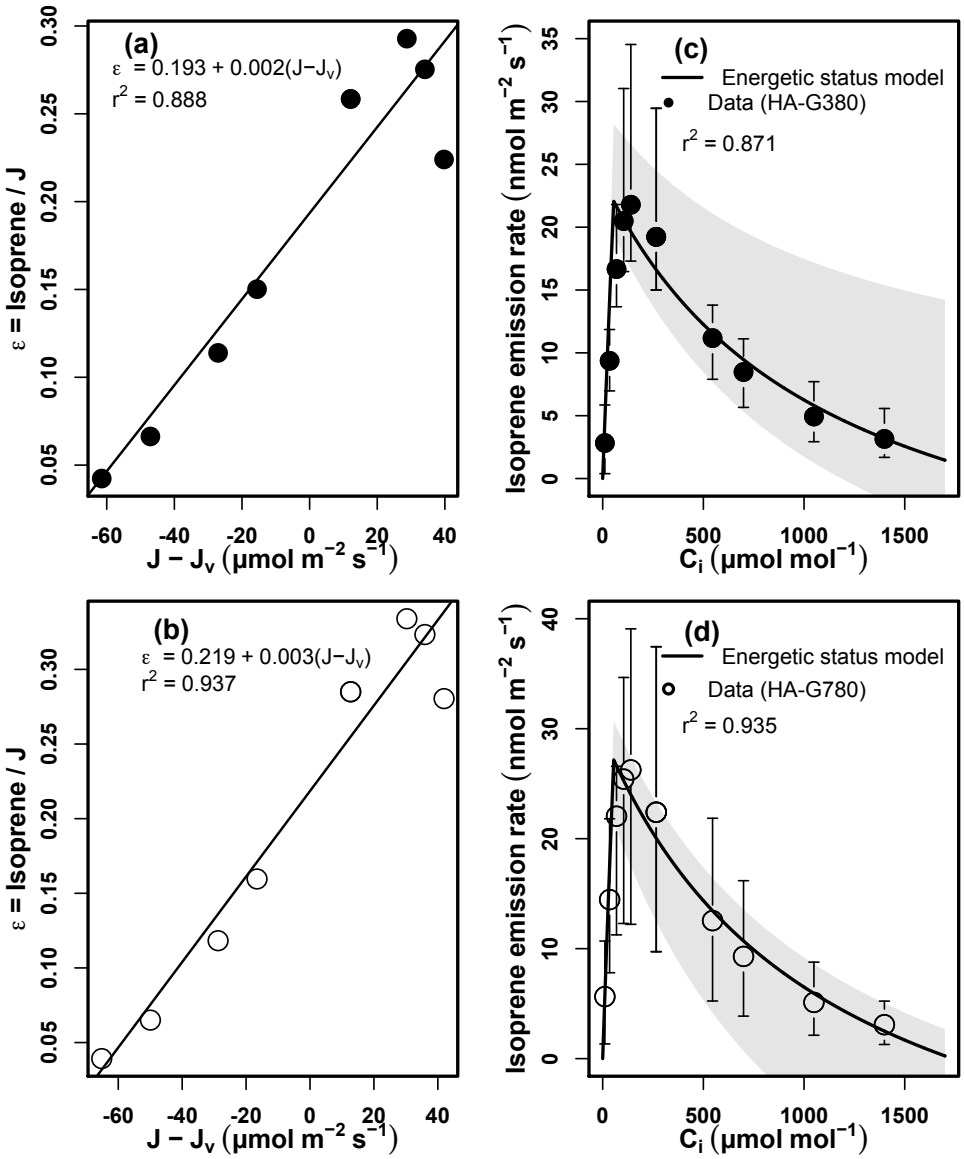


Figure 4.3: Isoprene emissions internal CO_2 concentration (C_i) at a leaf temperature of 30˚C and a photosynthetic photon flux density of 1000 μmol m^{-2} s^{-1} for hybrid aspen. Observed changes in the fraction of electrons used for isoprene production taken as the ratio of isoprene emission rate to light-limited electron flux for carbon assimilation ($\varepsilon = I/J$) in response to changes in the energetic status of the leaf taken as the difference between the light- and Rubisco-limited electron fluxes for carbon assimilation [$J - J_v$] for hybrid aspen (*Populus tremula* L. x *P. tremuloides* Michx.) grown under (a) ambient CO_2 concentration (HA-G380; solid circles) and (b) elevated CO_2 concentration (HA-G780; open circles). Observed (circles) and modelled (solid line) isoprene emission rates in response to changes in C_i for hybrid aspen grown under (c) ambient CO_2 concentration (solid symbols) and (d) elevated CO_2 concentration (open symbols). The grey shadowed area represents uncertainties of the isoprene model due to uncertainties in the values of the maximum Rubisco carboxylation capacity (V_{cmax}) and maximum electron flux (J_{max}) in the Farquhar model. Errors bars represent the maximum and minimum bounds of the isoprene curves. The experimental details are reported in Sun *et al.* (2012; 2013b)

I also tested the response versus C_i of the Niinemets model corrected by the empirical CO_2 response function proposed by Arneth *et al.* (2007b) (Fig. 4A.2.2). The Niinemets model reproduced the data reasonably well but tended to underestimate isoprene emissions for *Populus nigra*, while it tended to overestimate isoprene emissions for the hybrid aspen experiments. It has also to be noted that without the CO_2 response function proposed by Arneth *et al.* (2007b) , the Niinemets model would show an increase of isoprene emissions with increasing C_i, imitating the response of A_j.

4.3.2 Experiments varying PPFD

Isoprene emissions

For all experiments, isoprene emissions rates increased with increasing *PPFD*, with observed maxima for isoprene emissions inversely related to C_a (and consequently to C_i) – opposite to the net assimilation rates. Observed isoprene emissions versus *J* are found to have a quadratic type of response, in line with my model (shown for hybrid aspen in Fig. 4A.2.3).

For Populus nigra at each C_a, my model captured variations of isoprene emissions extremely well with $r^2 > 0.99$ (Fig. 4.4, Table 4.2). For C_a of 200 μmol mol^{-1}, however, my model systematically underestimated the observed values. The Niinemets model showed comparable r^2 values (Table 4.2) consistent with the fact that isoprene emission, both in my model and in the Niinemets model, is proportional to *J*. G93 was the only model with a component (I_s) fitted directly to the observations, yet G93 performed less well than the other two models. All models underestimated isoprene emission rates at the highest *PPFD* of 2500 μmol m^{-2} s^{-1}.

For hybrid aspen, all models captured well the variation of isoprene emissions with *PPFD* with $r^2 > 0.88$. Yet my model tended to systematically underestimate isoprene emission for HA-G380 (Fig. 4.5).

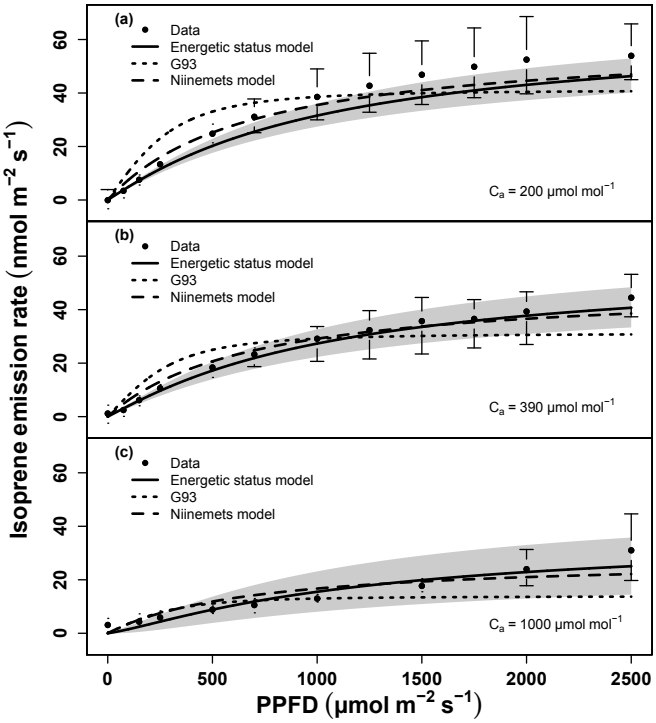


Figure 4.4: Isoprene emission rates of *Populus nigra* versus photosynthetic photon flux density (*PPFD*) at a leaf temperature of 30˚C, and three atmospheric CO_2 concentrations (C_a): (a) 200 μmol mol^{-1}, (b) 390 μmol mol^{-1}, (c) 1000 μmol mol^{-1}. The grey shadowed area represents uncertainties of the isoprene model due to uncertainties in the values of the maximum Rubisco carboxylation capacity (V_{cmax}) and maximum electron flux (J_{max}) in the Farquhar model. Errors bars represent the maximum and minimum bounds of the isoprene curves.

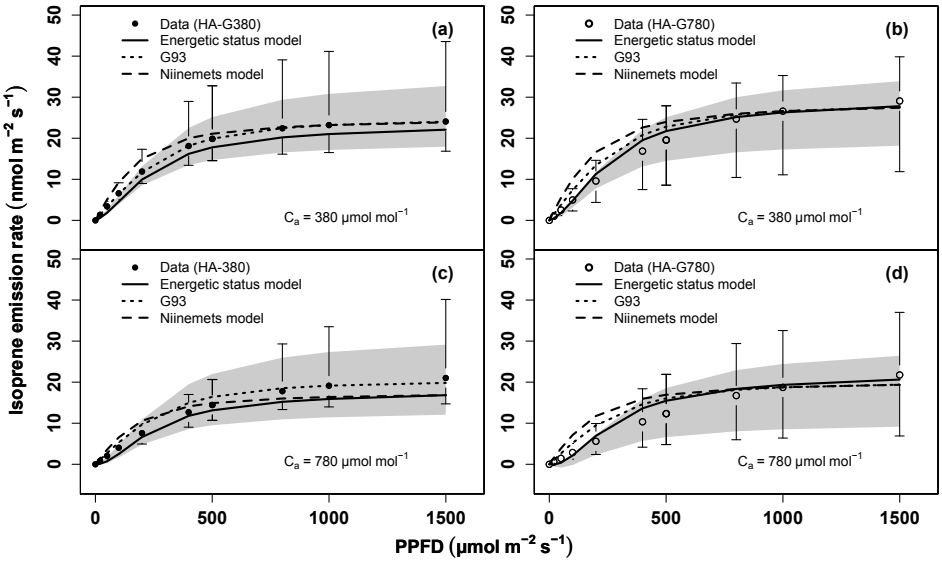


Figure 4.5: Isoprene emission rates for hybrid aspen (*P. tremula* x *P. tremuloides*) versus photosynthetic photon flux density (*PPFD*) at a leaf temperature of 30˚C, at two atmospheric CO_2 concentrations (C_a): C_a = 380 μmol mol^{-1} for individuals grown under (a) ambient (HA-G380) and (b) elevated (HA-G780) CO_2 concentrations; C_a = 780 μmol mol^{-1} for individuals grown under (c) ambient (HA-G380) and (d) elevated (HA-G780) CO_2 concentrations. The grey shadowed area represents uncertainties of the isoprene model due to uncertainties in the values of the maximum Rubisco carboxylation capacity (V_{cmax}) and maximum electron flux (J_{max}) in the Farquhar model. Errors bars represent the maximum and minimum bounds of the isoprene curves.

Table 4.2: Isoprene emissions versus changes in photosynthetic photon flux density (*PPFD*) at different CO_2 concentrations (C_a).

Data	C_a	Energetic status model		G93		Niinemets model	
	(μmol mol^{-1})	r^2	P	r^2	P	r^2	P
	200	~1	<1e-5	0.88	<1e-5	0.99	<1e-5
Populus n.	**390**	~1	<1e-5	0.86	<1e-4	0.98	<1e-5
	1000	0.92	<1e-4	0.56	0.311	0.81	<1e-3
HA-G380	**380**	~1	<1e-5	~1	<1e-5	0.99	<1e-5
	780	0.99	<1e-5	0.98	<1e-5	0.94	<1e-5
HA-G780	**380**	0.98	<1e-5	0.97	<1e-5	0.93	<1e-5
	780	0.96	<1e-5	0.93	<1e-5	0.88	<1e-4

Isoprene: assimilation ratios (I/A_{gross})

Observed mean I/A_{gross} increased with increasing *PPFD* regardless of the C_a, plant type or grown conditions. However, the range of I/A_{gross} across individuals is considerable. The fraction of assimilated carbon re-emitted as isoprene was inversely related to the CO_2 concentration. The high ratios of I/A_{gross} at low C_a were due to a combination of high isoprene emission rates and low carbon assimilation rates.

My energetic status model can reproduce an increase of the fraction of carbon allocated to isoprene emission with increasing *PPFD* (Fig. 4.6; Fig. 4.7). It fails to reproduce absolute values of I/A_{gross}; however, note that the simulated I/A_{gross} includes combined uncertainties of the isoprene model and the Farquhar model.

G93 shows versatility in the simulation of carbon allocated to isoprene emission with simulated I/A_{gross} decreasing with *PPFD* for *Populus nigra*, while increasing for hybrid aspen.

With the exception of hybrid aspen at C_a = 380 μmol mol^{-1}, the Niinemets models failed to capture the changes in I/A_{gross} with changing *PPFD*, showing no relationship between I/A_{gross} and *PPFD*.

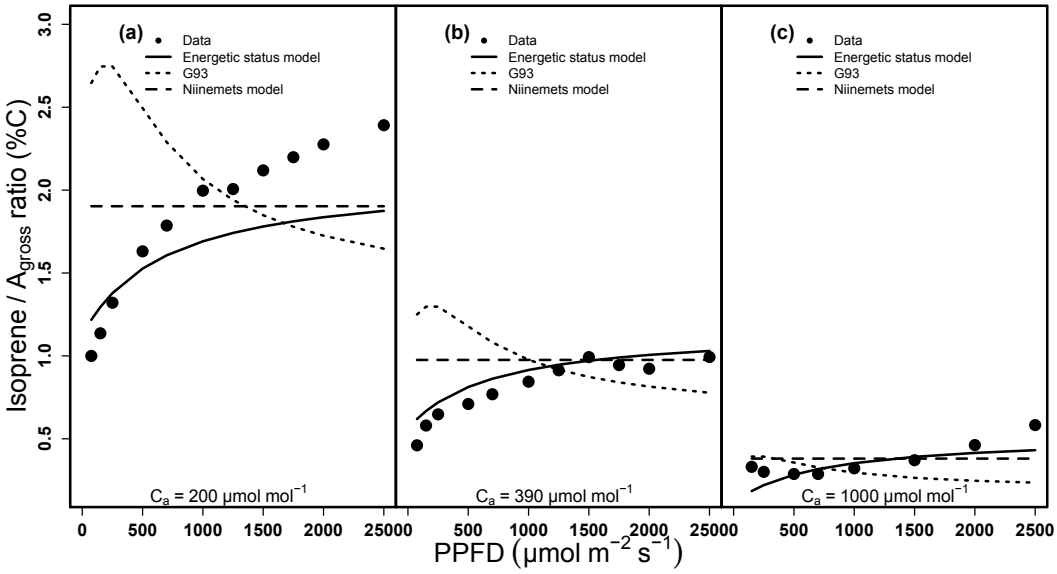


Figure 4.6: Ratios of isoprene emission to gross assimilation (A_{gross}) versus photosynthetic photon flux density (*PPFD*) at leaf temperature of 30˚C for *Populus nigra* at atmospheric CO_2 concentration of (a) 200 μmol mol^{-1}, (b) 390 μmol mol^{-1}, (c) 1000 μmol mol^{-1}.

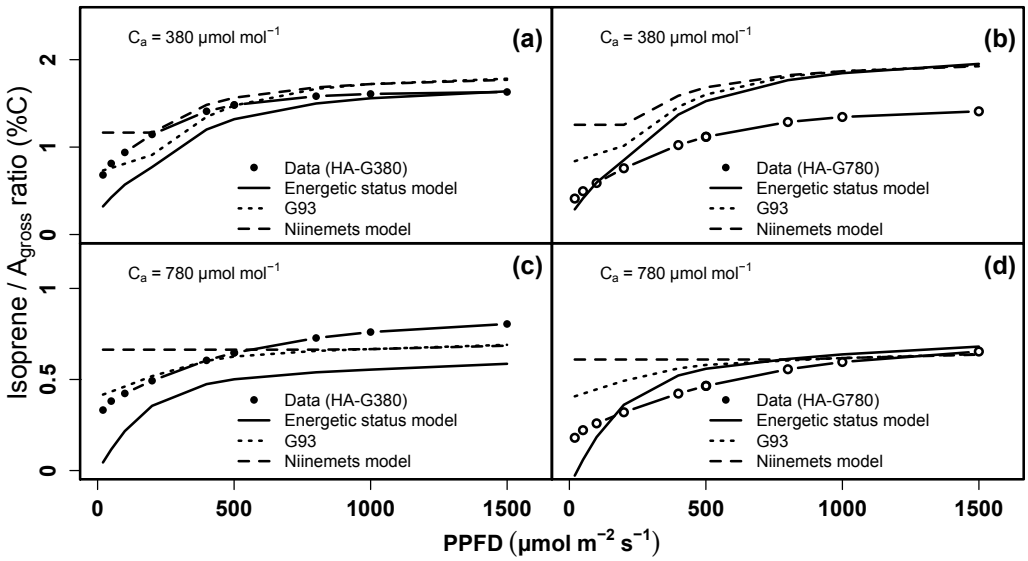


Figure 4.7: Ratios of isoprene emission to gross assimilation (A_{gross}) versus photosynthetic photon flux density (*PPFD*) at leaf temperature of 30˚C for hybrid aspen (*P. tremula* x *P. tremuloides*) at atmospheric CO_2 concentration of 380 μmol mol^{-1} for individuals grown under (a) ambient (b) elevated CO_2 concentration; and atmospheric CO_2 concentration of 780 μmol mol^{-1} for individuals grown under (c) ambient and (d) elevated CO_2 concentration.

Isoprene quantum efficiencies

As predicted by my hypothesis, the observed quantum efficiencies for isoprene production were dependent on the CO_2 concentration (Fig. 4.8). Higher quantum efficiencies correspond to lower C_a, at which the demand for reductant by the Calvin-Benson cycle is lower. My model captured the observed decrease of Φ_{iso} with increasing C_a. However, the model overestimated Φ_{iso} at high C_a and underestimated Φ_{iso} at low C_a for *Populus nigra*. The model overestimated Φ_{iso} for HA-G380 and underestimated Φ_{iso} for HA-G780.

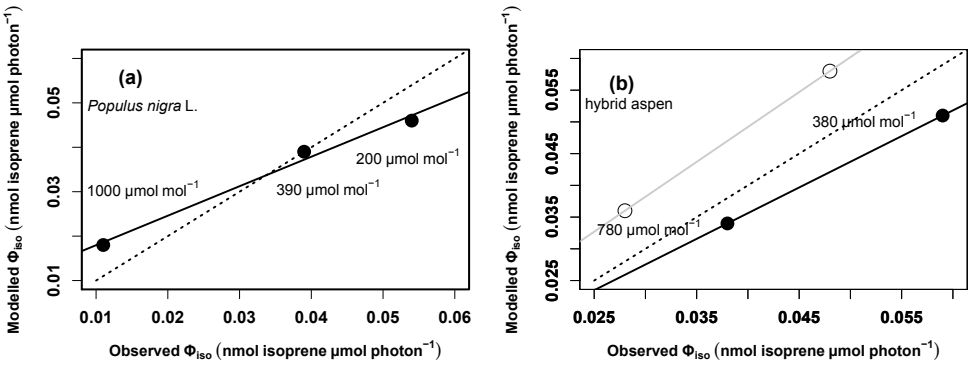


Figure 4.8: Quantum efficiencies for isoprene emission (Φ_{iso}): modelled versus observed values at different atmospheric CO_2 concentrations for (a) *Populus nigra* and (b) hybrid aspen (*P. tremula* x *P. tremuloides*) grown under CO_2 conditions of 380 μmol mol^{-1} (solid circles) and of 780 μmol mol^{-1} (open circles). The solid line represents the best linear fit between the model and the data; the dashed line represents the 1:1 line.

4.3.3 Global results

The overall performance of each model is illustrated in Figures 4.9 and 4.10. My energetic status model gave excellent results overall (r^2 = 0.97 for *Populus nigra*, r^2 = 0.94 for hybrid aspen). No major pattern was detected in the residuals although the model has the tendency to underestimate the observations (Fig. 4A.2.4; Fig. 4A.2.5). Moreover this model could reproduce the following key features of the observations:

1) A decrease in isoprene emissions with increasing C_i.
2) An increase in isoprene emissions with increasing *PPFD*, with maxima inversely proportional to CO_2 concentration.
3) An increase of the proportion of assimilated carbon diverted to isoprene production (I/A_{gross}) with increasing *PPFD*.
4) A decrease in the quantum efficiency of isoprene production with increasing CO_2 concentration.

With I_s adjusted for each experiment, G93 reproduces very well the observed variations of isoprene emission with *PPFD*, especially for hybrid aspen (C_i experiments are not included for G93). For *Populus nigra*, the bell-shape pattern observed in the residuals versus fitted values plot (Fig. 4A.2.4) suggests that the standard light response of the G93 is not adapted to fit the observations.

With no empirical adjustment included to account for the CO_2 effect, the Niinemets model (r^2 = 0.09 to 0.14) failed to reproduce the observed variations of isoprene emission with *PPFD* and C_i. Including a CO_2 effect in this model however caused major improvements (r^2 = 0.97 to 0.89).

4.4 Discussion

I used the C_i and *PPFD* response curves of assimilation and isoprene emissions for *Populus nigra* (this study) and *P. tremula* x *P. tremuloides* (hybrid aspen) (Sun *et al.*, 2012), where changes in balance between electron supply and electron demand for carbon assimilation purpose were driven by different environmental variables. I tested against these data a new model in which isoprene production is a function of the energetic status of the leaves, alongside two widely used isoprene models: the G93 algorithm (Guenther *et al.*, 1993) and the Niinemets model (Niinemets *et al.*, 1999b; Arneth *et al.*, 2007b). My new model showed excellent results and a visible improvement relative to the original Niinemets model (Figs. 4.9 and 4.10).

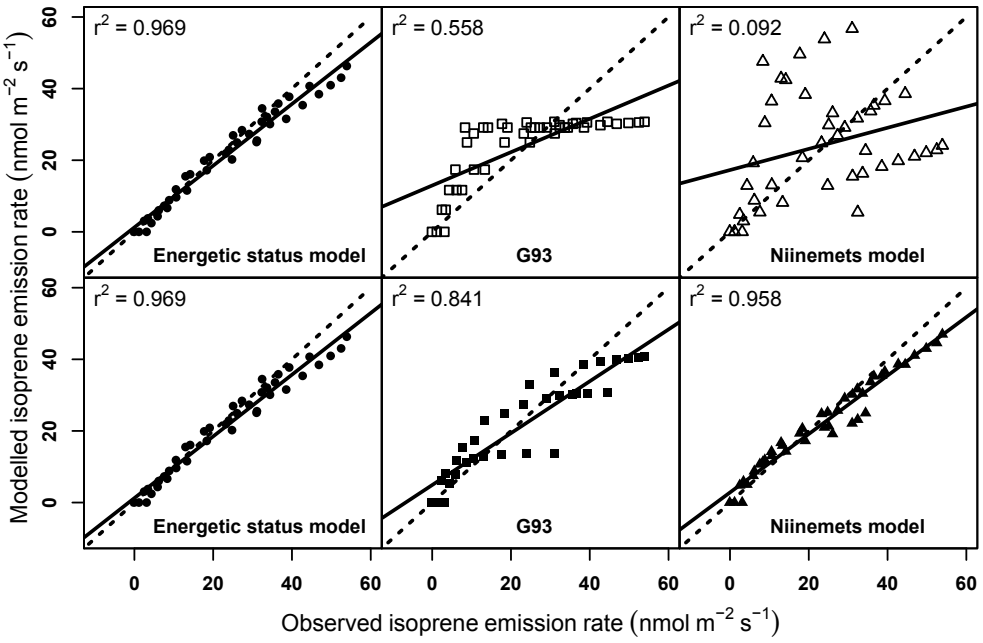


Figure 4.9: *Populus nigra* modelled isoprene emission rates versus observed isoprene emission rates for all the experiments. The solid line represents the best linear fit between the model and the data; the black dashed line is the 1:1 line. Solid circles represent my energetic status model. Squares represent the G93 algorithm, without (open) and with (solid) an adjustment of the standard emission rate to account for CO_2 concentration effects. Triangles represent the Niinemets model, without (open) and with (solid) a CO_2 effect based on Arneth *et al.* (2007b). Only experiments varying photosynthetic photon flux density are represented for G93 with adjustment of the standard emission rate to account for CO_2 concentration effects.

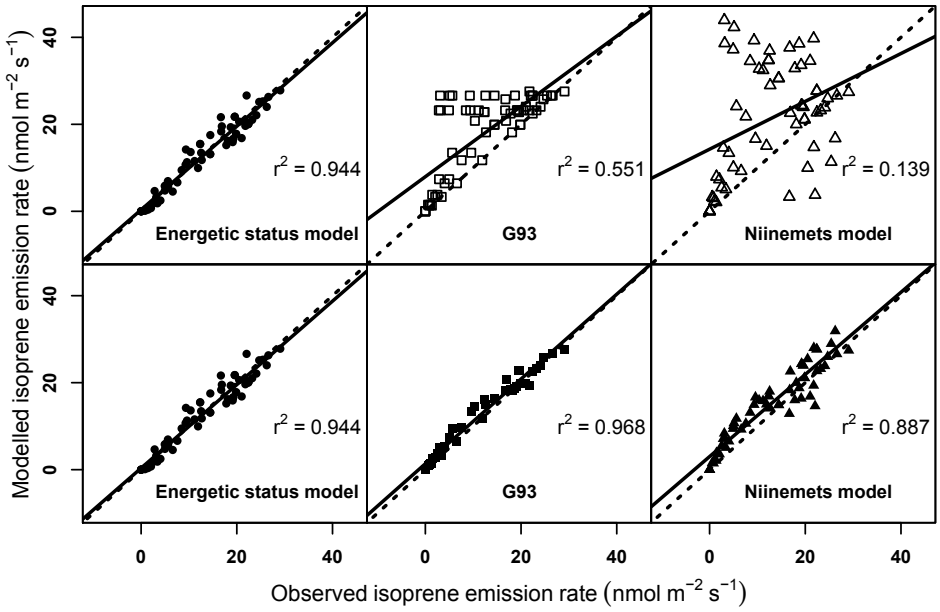


Figure 4.10: Hybrid aspen (*P. tremula* x *P. tremuloides*) modelled isoprene emission rates versus observed isoprene emissions rates for all the experiments. The solid line represents the best linear fit between the model and the data; the black dashed line is the 1:1 line. Solid circles represent my energetic status model. Squares represent the G93 algorithm, without (open) and with (solid) an adjustment of the standard emission rate to account for CO_2 concentration effects. Triangles represent the Niinemets model, without (open) and with (solid) a CO_2 effect based on Arneth *et al.* (2007b). Only experiments varying photosynthetic photon flux density are represented for G93 with adjustment of the standard emission rate to account for CO_2 concentration effects.

My model finds its origin in the Niinemets model based on 'energetic requirements for isoprene synthesis and leaf photosynthetic properties'. It keeps the major advantage of its simplicity and thus the evident potential for its use in large-scale modelling, where excessive complexity is to be avoided wherever possible. Yet, my new model diverges from its prototype in two fundamental ways. First, it links isoprene emission directly to the electron flux (J) rather than to light-limited assimilation. Second, it links isoprene emission to reductant availability and thus transcribes the original idea of (Niinemets *et al.*, 1999b) of a '*competition for electrons between isoprene synthesis and Calvin and photorespiratory cycles*'. The component of electron flux generated by photosystem II and not used for carbon assimilation and photorespiration is extremely hard to investigate experimentally (Singsaas *et al.*, 2001). Nevertheless, my hypothesis is supported by (i) the high positive correlations found between the observations and simulations made with my energetic status model, (ii) the fact that measured I/A_{gross} increases with increasing *PPFD*, (iii) the fact that observed Φ_{iso} is inversely proportional

to C_a, iv) strong linearity between the flux of electrons engaged in the isoprene production and $[J - J_v]$ and v) a quadratic type response of isoprene emission to J.

In fact, the first derivation of the Niinemets *et al.* (1999b) model predicted that the fraction of electrons going into isoprene synthesis varies with CO_2 concentration, but this variation was not explicitly formalized. In the later development of this model, Arneth *et al.* (2007b) included this effect empirically in the emission model. Still, reduction of isoprene emissions at intercellular CO_2 concentrations between 0-150 μmol mol^{-1} (Loreto & Sharkey, 1990; Rasulov *et al.*, 2009b, 2011; Sun *et al.*, 2012) was not considered. Wilkinson *et al.* (2009), also included CO_2-dependence of isoprene emission, but did not consider the declining part of isoprene emission at low CO_2 concentrations. It has been shown that this reduction is associated with reduced availability of dimethylallyl diphosphate (DMADP) and suggested to indicate limited NADPH or ATP availability (Rasulov *et al.*, 2009b, 2011). Here the model based on NADPH-limitation described well the entire CO_2-response curve (Fig. 4.2; Fig. 4.3), in line with the experimental observations of variation of DMADP pool size with $[CO_2]$.

A limitation of the present study is that experiments were conducted under constant temperature. This has the advantage of decoupling effects related to NADPH production from effects of enzyme kinetics. However, isoprene emissions also respond strongly to temperature, both instantaneously and over longer periods (Guenther *et al.*, 1991; Pacifico *et al.*, 2009; Laffineur *et al.*, 2011; Sun *et al.*, 2013a). Improved understanding of the controls on isoprene emission for global or regional modelling purposes thus also requires that the hypothesis presented here be tested and analysed under variations of temperature, as well as *PPFD* and C_i.

Following the logic of the G93 algorithm, many studies (including mine) have examined isoprene emission under the standard conditions of a leaf temperature of 30 ˚C and a *PPFD* of 1000 μmol m^{-2} s^{-1}. This might be a limitation, as interactions between different drivers are then neglected. As an example of the importance of this limitation, the recent study of Sun *et al.* (2013a) showed cancellation of the isoprene response to rapid changes in C_i at higher temperature. Thus, there is a need for a more complete experimental studies focusing on the interactions between the effects of simultaneous changes in temperature, *PPFD* and C_i.

In future model development it will also be important to consider the adaptation of model parameters to long-term variation in temperature and CO_2, and effects of changes due to leaf ontogeny – all of which could modify the expression of the isoprene synthase gene (Monson, 2013; Rajabi Memari *et al.*, 2013; Rosenkranz & Schnitzler, 2013) and the pool size of DMADP (Sun *et al.*, 2012; Rasulov *et al.*, 2013). Consideration of such changes is needed to allow the inclusion of acclimation in isoprene emission on time scales from days to months, and thus eventually allow the responses of isoprene emissions to global change to be modelled in a more explicitly process-based manner than has been possible so far.

Annex 4A.1- Comparison Model1 and Model2

Here I describe tests of the first version of the isoprene model (Model 1) against data collected at CREAF on *Populus nigra* L. In Model 1, the rate of isoprene emission is linearly related to the energetic status $[J - J_v]$ of the leaf.

$$I = a\,J + b\,(J - J_v) \qquad (4A.1.1)$$

J and J_v are the light- and Rubisco-limited electron fluxes, respectively, calculated using the Farquhar equations*; a* and *b* are constants.

For the C_i experiments, isoprene emission shows a strong negative linear relationship with the Rubisco-limited electron flux, J_v (r^2 = 0.938), as shown in Fig. 4A.1.1.a. Parameters ***a*** and ***b*** (Eq. 4A.1.1) were estimated from this linear regression. When plotted against C_i, Model1 shows excellent agreement with the data (r^2 = 0.938) (Fig. 4A.1.1.b).

Using parameters ***a*** and ***b*** from C_i experiments, Model 1 was tested against observed isoprene light curves under three CO_2 concentrations (200, 390, 1000 μmol mol^{-1}). The results of the comparison of Model 1 versus data are shown in Table 4A.1.1 and Figure A4.2. Although Model 1 manages to capture variations of observed isoprene emissions as suggested by the high correlation with the data ($r^2 > 0.8$), it generates negative values at low *PPFD*, as revealed by Figure 4A.1.2. Therefore, this version of the model was discarded and replaced by Model 2.

Table 4A.1.1: Isoprene emissions versus changes in *PPFD* at different CO_2 concentrations.

Data	**C_a**	**Model1**		**Model2**		**G93**		**Niinemets model**	
	(μmol mol^{-1})	r^2	P	r^2	P	r^2	P	r^2	P
	200	0.99	<1e-5	~1	<1e-5	0.88	<1e-5	0.99	<1e-5
Populus n.	**390**	0.98	<1e-5	~1	<1e-5	0.86	<1e-4	0.98	<1e-5
	1000	0.81	<1e-3	0.92	<1e-4	0.56	0.311	0.81	<1e-3

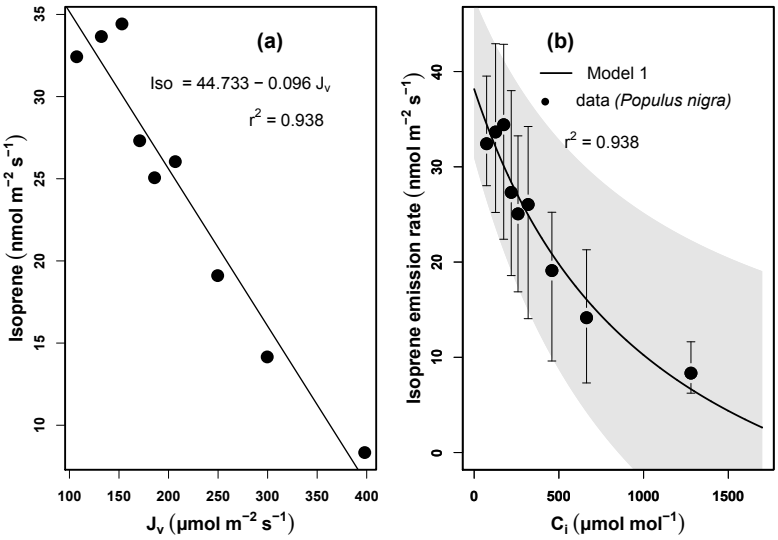


Figure 4A.1.1: Isoprene emissions versus internal CO_2 concentration (C_i) at a leaf temperature of 30˚C and a photosynthetic photon flux density of 1000 μmol m^{-2} s^{-1} for *Populus nigra* L and using the conceptual model from Morfopoulos *et al.* (2013). (a) Observed changes in isoprene emission in response to changes in Rubisco-limited electron flux (J_v) (b) Observed (black circles) and modelled (solid line) isoprene emission rates in response to changes in C_i. The grey shadowed area represents uncertainties of the conceptual model from Morfopoulos *et al.* (2013) (Model1) due to uncertainties in the values of the maximum Rubisco carboxylation capacity (V_{cmax}) and maximum electron flux (J_{max}) in the Farquhar model. Errors bars represent the maximum and minimum bounds of the isoprene curves.

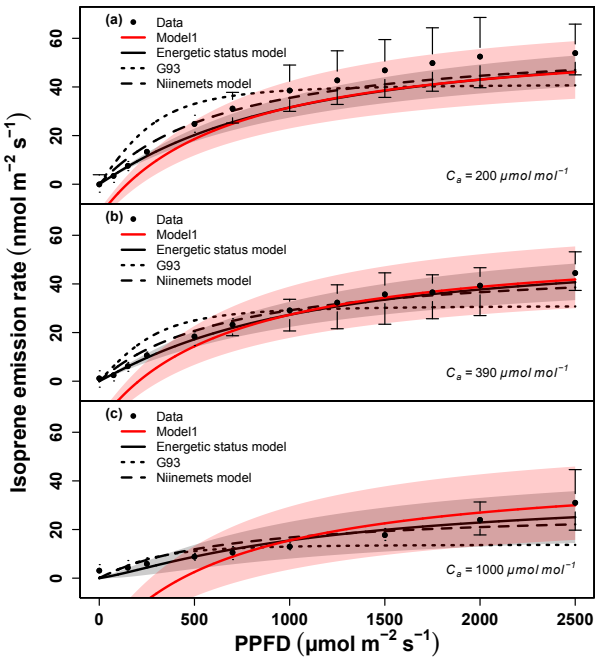


Figure 4A.1.2: Isoprene emission rates of *Populus nigra* versus photosynthetic photon flux density (*PPFD*) at a leaf temperature of 30˚C, and three atmospheric CO_2 concentrations (C_a): (a) 200 μmol mol^{-1}, (b) 390 μmol mol^{-1}, (c) 1000 μmol mol^{-1}. The shadowed area represents uncertainties of the isoprene models due to uncertainties in the values of the maximum Rubisco carboxylation capacity (V_{cmax}) and maximum electron flux (J_{max}) in the Farquhar model: in grey for the energetic status model (this study), and in red for conceptual model from Morfopoulos *et al.* (2013) (Model1). Errors bars represent the maximum and minimum bounds of the isoprene curves.

Annex 4A.2 - Supplementary figures to Chapter IV

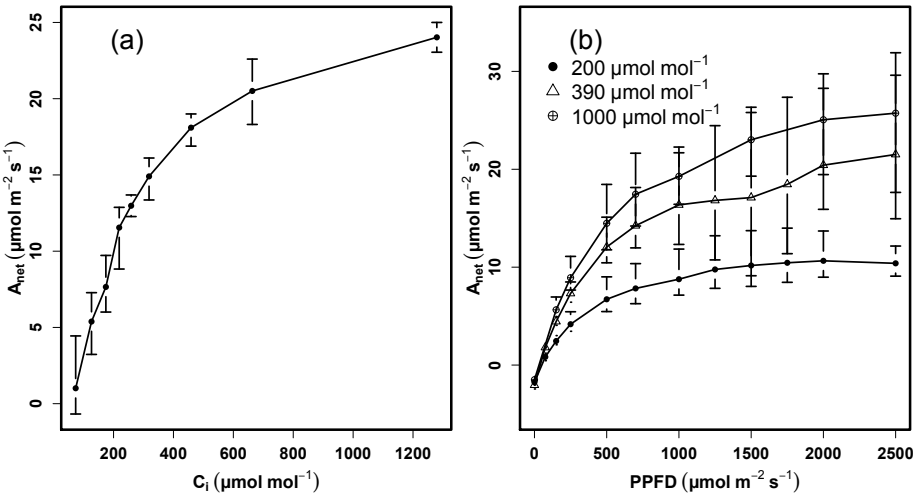


Figure 4A.2.1: *Populus nigra* net CO_2 assimilation rate (A_{net}) versus (a) internal CO_2 concentration (C_i) and (b) photosynthetic photon flux density (*PPFD*) for three atmospheric CO_2 concentrations (200, 390 and 1000 μmol mol^{-1}) at 30˚C.

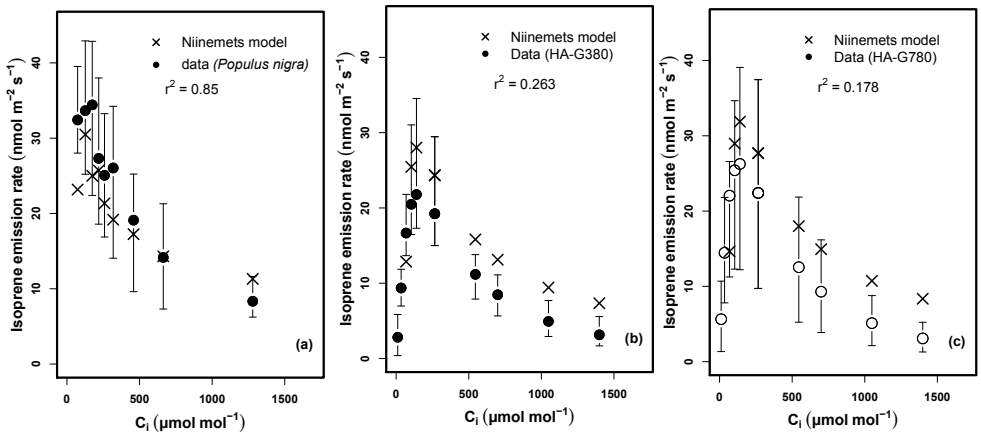


Figure 4A.2.2: Observed (circles) and modeled (crosses), using the Niinemets model modified by Arneth *et al.* (2007b), isoprene emission rate changes in response to changes in internal CO_2 concentration (C_i) for (a) *Populus nigra* and hybrid aspen grown under CO_2 atmospheric concentration of (b) 380 μmol mol^{-1} and (c) 780 μmol mol^{-1}. For hybrid aspen, the poor correlation between model and data is mainly due to negative values (down to – 384 nmol m^{-2} s^{-1}) simulated by the model for $C_i < \Gamma^*$.

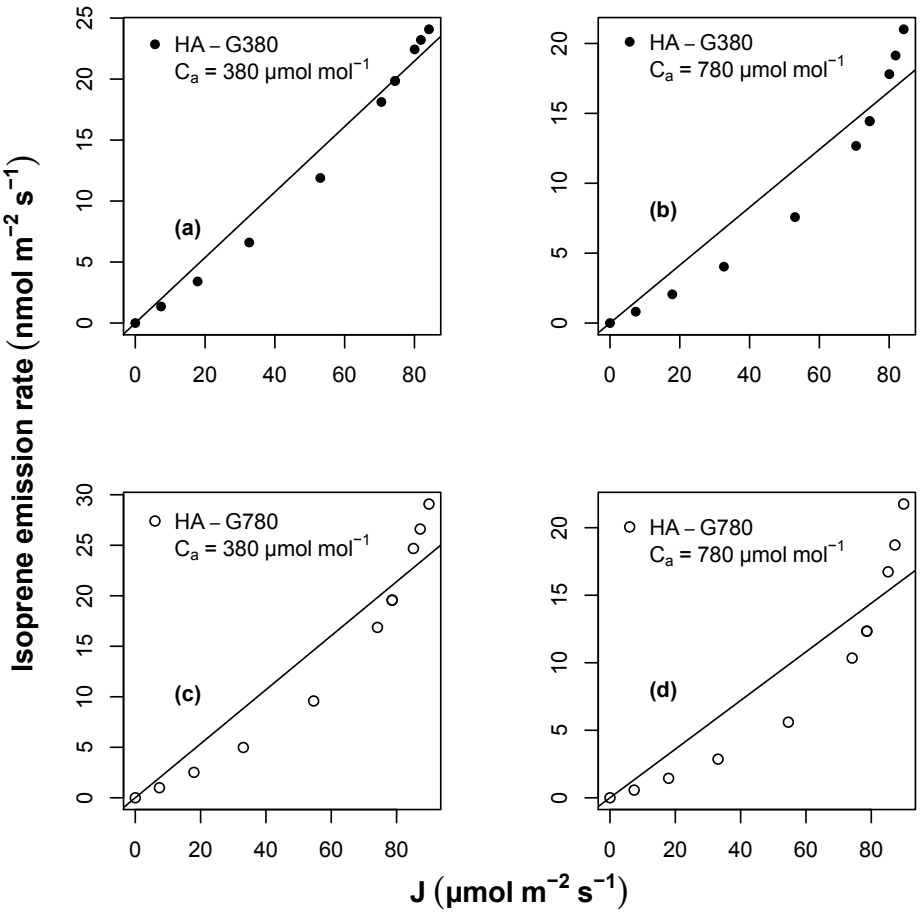


Figure 4A.2.3: Observed isoprene emission rates versus light limited electron flux (*J*) for hybrid aspen grown under CO_2 concentration of 380 μmol mol^{-1} and measured at a CO_2 concentration (C_a) of (a) 380 μmol mol^{-1} and (b) 780 μmol mol^{-1}; hybrid aspen grown under CO_2 concentration of 780 μmol mol^{-1} and measured at a CO_2 concentration of (c) 380 μmol mol^{-1} and (d) 780 μmol mol^{-1}.

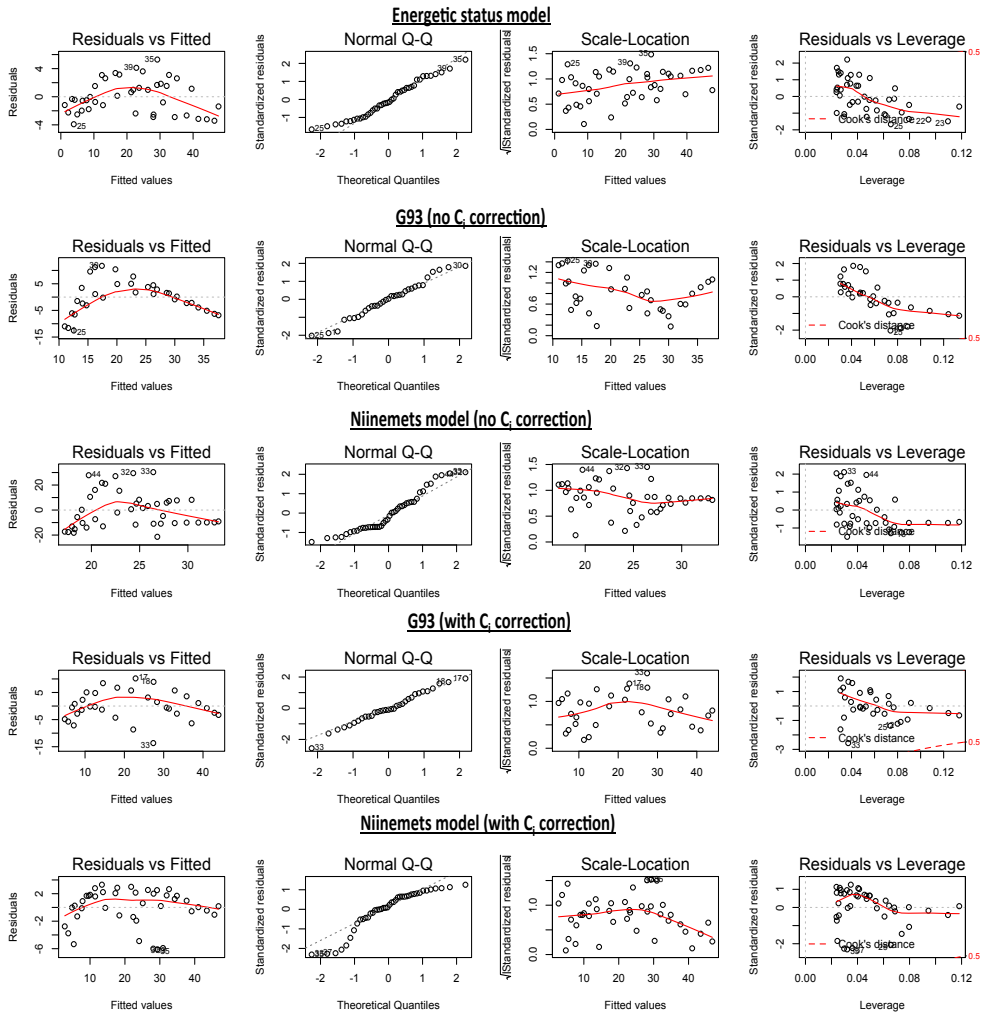


Figure 4A.2.4: Residuals against fitted values, normal Q-Q plot, square root of the standardized harvarhhCook's distance for *Populus nigra* (using Model 2).

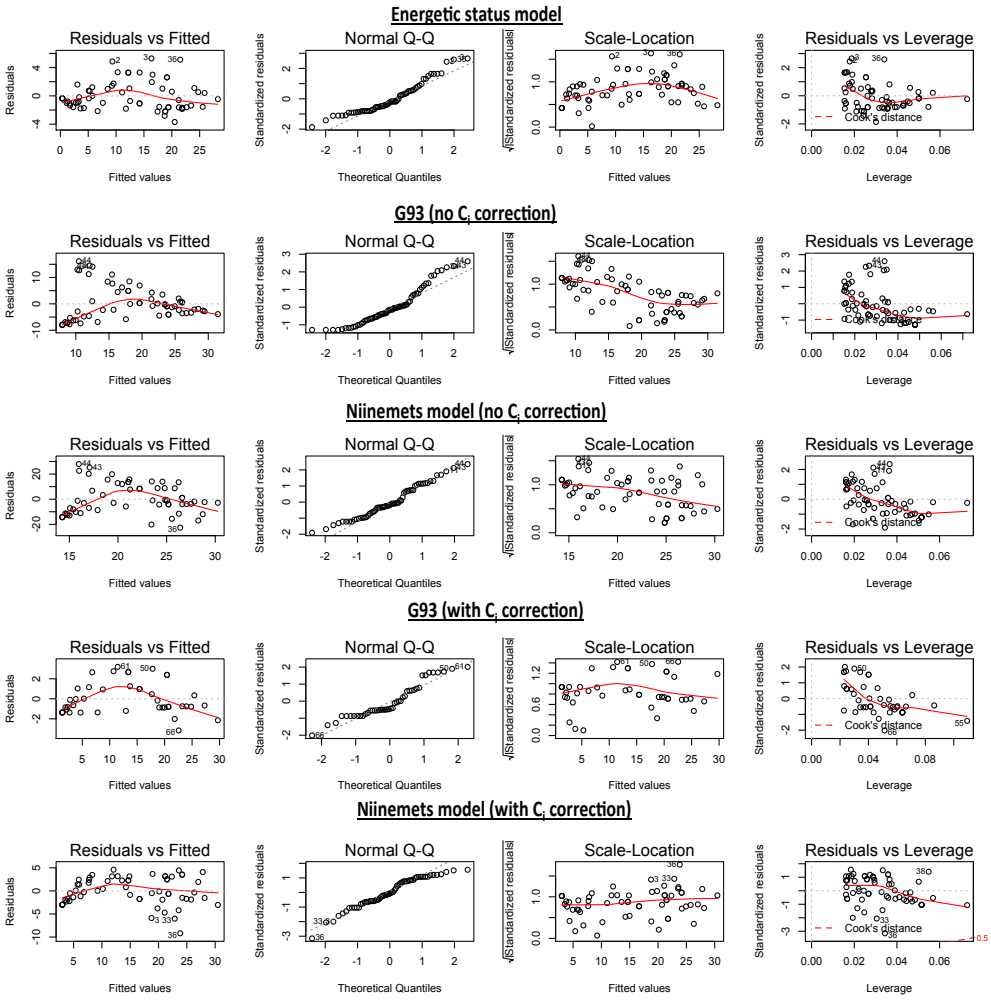


Figure 4A.2.5: Residuals against fitted values, normal Q-Q plot, square root of the standardized residuals against the fitted values and standardized residuals as a function of leverage, along with Cook's distance for hybrid aspen (using Model 2).

5 Evaluation of the model at canopy scale using a multi-layer approach

Abstract

Having successfully tested the new model for isoprene emission at the leaf scale (Chapter IV, Morfopoulos *et al*., 2014), I investigate here the model's ability to reproduce above-canopy isoprene emissions. Long-term time series of above-canopy fluxes of CO_2 and isoprene, measured continuously at two mixed-temperate forest sites located at the University of Michigan Biological Station, USA (UMBS) (Pressley *et al*., 2005, 2006) and Vielsalm, Belgium (Laffineur *et al.*, 2011, 2013), are analysed. A simple approach is used to investigate responses of gross primary production (*GPP*) and isoprene emission rates to changes in photosynthetic photon flux density (*PPFD*) and air temperature (T_a). *GPP* was found be controlled primarily by *PPFD* while isoprene emissions showed equally strong responses to *PPFD* and T_a. This finding is consistent with the isoprene production being jointly controlled by the energetic status of the leaf and by enzymatic activity. *GPP* showed almost no response (UMBS), or even a decreasing response (Vielsalm), to increasing T_a. The percentage of carbon lost into the form of isoprene tended to increase with increasing *PPFD*, supporting the idea that the availability of reducing power influences isoprene emission.

Using a multi-layer method, I compared the global responses of *GPP* to those of the Farquhar model (Farquhar *et al.,* 1980) and the general responses of isoprene emission to those of three leaf-level isoprene emission models: the Guenther *et al.* (1993) algorithm, the Niinemets *et al.* (1999b) model and the new model I developed based on the energetic status of the leaf (Morfopoulos *et al*., 2013, 2014). The Farquhar model reproduces well the variation in *GPP*, with the exception of the temperature responses at the Vielsalm site. All three isoprene-emission models reproduce well the general responses of isoprene emission to changes in *PPFD* and T_a. The isoprene emission model based on the energetic status of the leaf, however, captures best how the ratio of isoprene emission to *GPP* changes in response to changes in *PPFD*. This model improves the simulated responses of isoprene emissions when compared to the original

Niinemets *et al.* (1999b)'s model, confirming the advance made by this new modelling approach.

5.1 Introduction

This chapter explores the possibility of upscaling the new energetic status model from leaf to canopy. Only the second version of the model (Model 2) has been employed. To investigate whether the model still holds at the canopy scale, a simple multi-layer method is used. Long-term above-canopy measurements of both isoprene and CO_2 fluxes are rare. But information on CO_2 fluxes is essential for process-based isoprene emission modelling. To my knowledge, only three sites: Harvard forest (USA), the University of Michigan Biological Station (USA) and Vielsalm (Belgium) cover several growing seasons giving substantial datasets of both isoprene and CO_2 fluxes. Data at the University of Michigan Biological Station and Vielsalm have been used here, with the following questions in mind:

1- Can it be confirmed that the ratio of isoprene emission to carbon assimilation increases with light intensity, as observed at Harvard forest (Chapter III, Fig 3.5)?

2- How do the observed isoprene emission responses to changes in the main drivers (light and temperature) scale up from leaf to canopy?

3- Can the new modelling approach account for features of the data that are not reproduced by other isoprene emission models?

The work presented here is currently in the form of a thesis chapter only. I plan to include in this study analysis of the above-canopy measurements at Harvard forest as well, and later to submit this work as a co-authored journal article to *Biogeosciences* with the following co-authors: S. Pressley, Q. Laffineur, B. Heinesch, K.A. McKinney (for the data) and P.M. Cox, R. Grote, T.F. Keenan, L.M. Mercado, J. Peñuelas, I.C. Prentice, N. Unger.

5.2 Material and methods

5.2.1 Observations/ site description

I used long-term measurements of above-canopy isoprene and CO_2 fluxes recorded continuously at two temperate forest sites, University of Michigan Biological Station (Pressley *et al.*, 2005, 2006) (UMBS) and Vielsalm (Laffineur *et al.*, 2011, 2013).

The UMBS site is located near Pellston, Michigan, USA (45°30'N, 84°42'W). Its climate is continental and its vegetation consists of a mixture of bigtooth aspen (*Populus grandidentata* Michx.), quaking aspen (*P. tremuloides* Michx.), American beech (*Fagus grandifolia* Ehrh.), paper birch (*Betula papyrifera* Marsh.), maple (*Acer rubrum* L., *A. saccharum* Marsh.) and red oak (*Quercus rubra* L.) (Schmid *et al.*, 2003) – all deciduous broadleaved tree species. Eddy covariance flux measurements of isoprene, CO_2, momentum, latent and sensible flux, were performed continuously for the 1999 to 2003 and 2005's growing seasons. In parallel, above-canopy air temperature (T_a) and photosynthetic photon flux density (*PPFD*) were recorded. CO_2 and H_2O mixing ratios were measured with an open-path infrared gas analyzer (IRGA) (Auble & Meyers, 1992) and isoprene mixing ratios were analysed with a fast isoprene sensor (FIS) (Hills & Zimmerman, 1990). Mixing ratios were converted to 30-min averaged CO_2 and isoprene fluxes using eddy covariance techniques. Estimates of vegetation area index (*VAI*) for the years 2000 to 2002 ranged between 3.2 and 3.7 m^2 m^{-2} (Pressley *et al.*, 2005). At UMBS, isoprene was primarily emitted by aspen (76%) and red oak (24%), which represented about 69% of the living biomass within 1km radius from the measurement flux tower. More information about the materials and methods of the measurements at UMBS can be found in (Pressley *et al.*, 2005, 2006).

The Vielsalm site is located in the Ardennes, Belgium (50°18'N, 5°59'E). The climate is temperate maritime and the vegetation consists of a mixture of coniferous and deciduous species, mainly (non-native) Douglas fir (*Pseudotsuga menziesii* Mirb.), Norway spruce (*Picea abies* L.), silver fir (*Abies alba* Miller) and European beech (*Fagus sylvatica* L.). Isoprene fluxes were measured continuously above canopy using the disjunct eddy covariance technique by mass scanning with proton transfer reaction- mass spectrometry (PTR- MS) for the 2009 to 2011 growing seasons. Simultaneously, momentum, CO_2, latent and sensible fluxes, above-canopy T_a and *PPFD* were also recorded. The source of isoprene emission has been attributed to *P. abies* using footprint model techniques. More information on the measurements at Vielsalm can be found in Laffineur *et al.* (2011, 2013).

At both sites, gross primary productivity (*GPP*) was deduced by subtracting the total ecosystem respiration (*TER*) from the net ecosystem exchange (*NEE*) as measured by eddy covariance. Nighttime *TER* was estimated from nighttime *NEE* data, when *GPP* is

considered equal to zero (no carbon assimilation at night). Response to changes in soil temperature of *TER* during the day was back-calculated following the algorithm of Reichstein *et al*. (2005).

5.2.2 Data treatment /analysis

At both measurement sites, I investigated the overall above-canopy responses of *GPP* and isoprene fluxes to changes in temperature and *PPFD*. I selected, for all years of measurements, data from the period when foliage cover was fully developed but not senescent (June, July and August), in order to attenuate the bias that seasonal acclimation of both isoprene emission and photosynthetic capacities can induce. Since *PPFD* and T_a are not fully independent, I studied general responses of *GPP* and isoprene emission versus *PPFD* (or T_a) in narrow ranges of T_a (or *PPFD*). In this way, I expect the influence of one parameter in the observed response of *GPP* or isoprene to changes in the other parameter to be minimized. *PPFD*-responses were plotted for T_a increasing from 15˚C to 25˚C by increments of 5˚C; similarly, T_a-responses were obtained for *PPFD* increasing from 100 to 1700 μmol m^{-2} s^{-1} by increments of 100 μmol m^{-2} s^{-1}. Figs. 5.1 and 5.2 give an example of the methodology used shown for the UMBS site. After binning the data in this way, smooth response curves were estimated using Michaelis-Menten type functions for *GPP* and isoprene *PPFD*-curves; and exponentials for isoprene T_a-curves. Ratios of isoprene emission on *GPP* to *PPFD* were calculated from those fitted functions.

I also tested the influence of the canopy temperature (T_c) on the results by processing the data the same way that described above but using T_c instead of T_a (Figs. 5A.1 – 5A.2), with T_c estimated as (Hoyaux *et al.*, 2008):

$$T_c = T_{ak} + \frac{HU}{\rho C_p u_*^2} \qquad (5.1)$$

where T_{ak} is the air temperature in K, H is the above-canopy heat flux in Wm^{-2}, u_* and U are respectively the friction and average wind velocity in m s^{-1}, ρ is the air density in kg m^{-3} and C_p is the mass air heat capacity in J kg^{-1} K^{-1}.

5.2.3 Leaf-level model of photosynthesis

I used the Farquhar *et al.* (1980) model for carbon assimilation by photosynthesis as modified by Medlyn *et al.* (2002, 2005). Gross carbon assimilation is calculated as the minimum of light-limited or Rubisco-limited assimilation rates. Gross light-limited assimilation (A_j) is computed from electron flux (J) as:

$$A_j = \left(\frac{J}{4}\right) \cdot \frac{(C_i - \Gamma^*)}{(C_i + 2\Gamma^*)} \tag{5.2}$$

where C_i is the CO_2 concentration inside the chloroplast and Γ^* is the compensation point in absence of dark respiration. The electron flux is dependent on *PPFD* and approximated as:

$$J = \frac{(\alpha_{CO2}\, PPFD + J_{max}) - \sqrt{(\alpha_{CO2}\, PPFD + J_{max})^2 - 4\alpha_{CO2}\,\theta\, PPFD\, J_{max}}}{2\theta} \tag{5.3}$$

where J_{max} is the saturating electron flux, α_{co2} is the quantum efficiency for electron transport rate (ETR) in mol electron mol^{-1} photon and θ is a curvature parameter of the light response.

Gross Rubisco-limited assimilation (A_v) rate is calculated as:

$$A_v = V_{cmax} \cdot \frac{(C_i - \Gamma^*)}{(C_i + k_c^{'})} \tag{5.4}$$

where V_{cmax} is the Rubisco capacity and $k'_c = k_c\,(1 + [O_2]/k_o)$ where k_c and k_o are the Michaelis-Menten coefficients of Rubisco for CO_2 and O_2 respectively. The resulting gross assimilation (A_{gross}) is thus equal to:

$$A_{gross} = \min\left(A_j, A_v\right) \tag{5.5}$$

Γ^*, J_{max}, V_{cmax} and K vary with temperature. The temperature dependencies of these components are detailed in the supplementary material (S2).

5.2.4 Leaf-level models of isoprene

Here, I analysed the responses of three leaf-level isoprene emission models and their capacity to catch the general trend of emission responses to changes in *PPFD* and T_a.

The Guenther *et al.* (1993) *algorithm (G93)*

The G93 algorithm estimates isoprene emission (I) from a species-dependent standardised isoprene emission rate (I_s, leaf temperature of 30˚C and *PPFD* of 1000 μmol m^{-2} s^{-1}). I_s is modulated by temperature- and *PPFD*- dependent functions to estimate I at a given temperature and *PPFD*. Thus, isoprene emission rate is determined as:

$$I = I_s C_L C_T \tag{5.6}$$

The *PPFD*- and temperature- dependencies (C_L and C_T) are computed as:

$$C_L = \frac{\alpha C_{L1} PPFD}{\sqrt{(1+\alpha^2 PPFD^2)}} \tag{5.7}$$

and,

$$C_T = \frac{\exp\left(\frac{C_{T1}(T_k - T_{ks})}{R T_k T_{ks}}\right)}{C_{T3} + \exp\left(\frac{C_{T2}(T_k - T_{ks})}{R T_k T_{ks}}\right)} \tag{5.8}$$

where T_k and T_{ks} are the leaf temperature in Kelvin under ambient and standard conditions, with T_{ks} = 303.15 K. α, C_{L1}, C_{T1}, C_{T2} and C_{T3} are empirical components characterising the *PPFD*- and temperature response shapes. These components were kept constant at α = 0.0027, C_{L1} = 1.066, C_{T1} = 95 000, C_{T2} = 230 000 J mol^{-1} and C_{T3} = 0.961 (Guenther, 1997).

Since the study of Guenther *et al.* (1993), this algorithm has been updated many times to take into account effects of seasonality, CO_2, past temperature- and past light- regimes, canopy depth on isoprene emissions (Guenther *et al.*, 1995, 2006, 2012; Guenther, 1997). Here, I choose to use the simplest version of the model and thus neglect improvements that these updates can bring to the model.

The Niinemets *et al.* (1999b) *model (N99)*

The model proposed by Niinemets and co-workers built on the idea that isoprene emissions are co-limited by available energetic metabolites (NADPH) and isoprene synthase (IspS) activity. Here, a temperature-dependent fraction ε_N of the electron transport rate (J) is used for isoprene production. Isoprene emission rate is computed as:

$$I = \varepsilon_N J \alpha_N, \text{ where } \alpha_N = \frac{(C_i - \Gamma^*)}{6\,(4.67 C_i + 9.33 \Gamma^*)} \quad (5.9)$$

The fraction of electrons ε_N involved in isoprene synthesis has a temperature dependency taken as a combination of the temperature responses of both isoprene synthase activity and J. Here, I use the temperature function proposed by Arneth *et al.* (2007b) and based on the work of Niinemets *et al.* (1999b):

$$\varepsilon_N = \varepsilon_{Ns} \exp(a_T (T - 30)) \quad (5.10)$$

where T is the leaf temperature in ˚C, ε_{Ns} is the fraction of electron for isoprene at the standard conditions of T at 30˚C and $PPFD$ at 1000 μmol m^{-2} s^{-1}, and a_T is a scaling parameter set to 0.1 $^{\circ}C^{-1}$.

The energetic status model (Morfopoulos *et al.,* 2013, 2014)

This model built on N99 keeping the original idea that isoprene emissions are co-limited by DMADP (the immediate precursor of isoprene) and IspS activity. The DMADP pool size is posited to be dependent on NADPH (reducing power) availability. The model differs from N99 by mathematically incorporating the idea of a competition for electrons between primary and secondary metabolites. Accordingly, the proportion of electrons ε involved into the production of isoprene depends on the energetic balance between the energy produced through light reactions (supply) and the demand for energy of the Calvin and photorespiratory cycles (demand). Therefore, an energetic-status dependent fraction (ε) of J is diverted into DMADP production. An additional function takes into account the temperature dependency of IspS and consequently the transformation of the DMADP pool into isoprene. Overall the model expresses isoprene emission as:

$$I = \varepsilon J f(T), \text{ where } \varepsilon = c_1 + c_2 (J - J_v) \quad (5.11)$$

and c_1 and c_2 are constants, J and J_v are respectively the light- and Rubisco- electron transport rate. $f(T)$ is a function taking into account the normalised temperature response of IspS activity:

$$f(T) = \frac{S_S}{S_{Ss}} \tag{5.12}$$

where S_S describes IspS activity using values reported in Niinemets *et al.* (1999b) (Table 2.1 in Chapter II). S_{Ss} is the IspS activity for a given standard T (here taken at 25˚C). The standard temperature is set to be the one for which parameters c_1 and c_2 were estimated. J_v is computed from the Farquhar model as:

$$J_v = 4V_{cmax} \cdot \frac{(C_i + \Gamma^*)}{(C_i + k_c^{'})} \tag{5.13}$$

5.2.5 Scaling up from leaf to canopy

I use a multi-layer modelling approach and assume that light penetrates into the canopy in the standard way, following the Beer-Lambert law:

$$PPFD_z = PPFD_0 \exp(-k L_z) \tag{5.14}$$

where L_z is the leaf area index above canopy level z, $PPFD_0$ is the *PPFD* at the top of the canopy and k is an extinction coefficient set to 0.5, based on the assumption of a spherical leaf angle distribution.

Similar to light, the extinction of the maximum Rubisco capacity is assumed to follow a Beer-Lambert extinction law through the canopy:

$$V_{cmax_z} = V_{cmax_0} \exp(-k_v L_z) \tag{5.15}$$

where V_{cmax_0} is the maximum Rubisco capacity at the top of the canopy and k_v represents the extinction of V_{cmax} through the canopy. The extinction of V_{cmax} through the canopy is usually found to be less that the one of the light and k_v was set equal to 0.15 (Lloyd *et al.*, 2010).

The relationship between J_{max} and V_{cmax} at 25˚C is usually found to be nearly constant across diverse species in the same environment. I assumed a constant ratio J_{max}/V_{cmax} of 1.67 at 25˚C throughout the canopy (Medlyn *et al.*, 2002). However, the ratio J_{max}/V_{cmax} is not constant for temperatures other than 25˚C. Changes in the ratio with temperature were ruled by temperature dependencies of both J_{max} and V_{cmax} (note S2). In the interest of simplicity, and in the absence of direct observations, the following assumptions were made: the internal CO_2 concentration (C_i) was kept constant through the canopy and set at 266 μmol mol^{-1}; leaf temperature was assumed to be equal to air temperature (T_a) and kept constant through the canopy; and, with the exception of J_{max} and $V_{cmax,}$ all model parameters were kept constant through the canopy. The leaf area index (*LAI*) at the bottom of the canopy was set to 3 at UMBS and 5 at Vielsalm. Integration through the canopy was performed in *LAI* increments of 0.1 m^2 m^{-2}. Parameters of the photosynthetic and isoprene emission models were estimated by minimizing the residual sum of squares (*RSS*) between the models and the Michaelis-Menten type estimates of the observed *PPFD*-curves with T_a ranging from 24.5-25˚C. These parameters are reported in Table 5.1. Results showing *GPP* or *I* modelled at different canopy depth (i.e. *PPFD*-curves reported in the *canopy profile* section) were obtained by forcing the *PPFD* and T_a conditions while keeping the Farquhar parameters constant at the canopy depth considered.

5.2.6 Model evaluation statistics

Explained variance of the linear regression between measured and predicted variables (r^2) is not enough to assess the performance of a model (Niinemets *et al.*, 2013). Indeed, if (r^2) evaluates how well predictions and data vary together, it could mask a systematic bias. To reinforce model evaluation, I choose to use two additional statistical tools, which taken together cover model evaluation from different perspectives. Here, I describe briefly these statistics.

The first additional statistic I used is the Nash-Sutcliffe modelling efficiency (Nash & Sutcliffe, 1970) (N_E):

$$N_E = 1 - \frac{\sum_{i=1}^{n}(y_i - P_i)^2}{\sum_{i=1}^{n}(y_i - \bar{y})^2} \quad (5.16)$$

where y_i is the i[th]-observation, P_i is the i[th]-prediction and $\bar{y}$ is the mean of observations. A prefect model would have a N_E of one; a value of zero indicates that the model predictions are as good as $\bar{y}$; negative values indicates that $\bar{y}$ is a better predictor that the proposed model. As pointed out by Niinemets *et al*. (2013), N_E suffers from being strongly influenced by model behaviour at high values of y_i.

Other model evaluation statistic is the mean absolute error:

$$\sigma_A = \frac{1}{n}\sum_{i=1}^{n}|y_i - P_i| \quad , \quad (5.17)$$

σ_A, measures the average magnitude of the errors in a set of predictions, without considering their direction and thus provides information on the deviance of the predicted values compared to the observations.. All statistics were performed using the software R version 2.15.0.

5.3 Results

5.3.1 General PPFD- and temperature responses

I analysed *PPFD*- and T_a-curves of *GPP* and isoprene emission at the UMBS and Vielsalm sites (Figs. 5.1- 5.4). The UMBS site experiences larger *GPP* and isoprene emission compared to the Vielsalm site presumably due to lower latitude (and associated higher *PPFD*) and differences in species. Median *GPP* was equal to 21.6 μmol m^{-2} s^{-1} at the UMBS site in comparison with 16 μmol m^{-2} s^{-1} at the Vielsalm site. Similarly, isoprene emission median values were higher at UMBS (6.9 nmol m^{-2} s^{-1}) than at the Vielsalm site (0.8 nmol m^{-2} s^{-1}).

PPFD-curves across T_a

At both sites, *GPP* and isoprene emission *PPFD*-curves were fitted using Michaelis-Menten type fits. Statistics related to these fits are displayed in Table 5.2. These fits

explain 51% and 47% of the variance in *GPP* and isoprene emission, at the UMBS site; and 77% and 71% at the Vielsalm site.

Estimated *PPFD*-curves of both *GPP* and *I* are presented in Figs. 5.3A,B for UMBS and Figs. 5.4A,B for Vielsalm. At both sites, isoprene *PPFD*-curves show an almost linear response and a strong influence of T_a. Maxima of isoprene emissions show a clear increase with T_a, and, *I* increases by 37% at UMBS and 43% at Vielsalm when T_a increases from 15 to 24˚C at a *PPFD* of 1000 μmol m^{-2} s^{-1}. In comparison, T_a has a lesser influence on the *GPP* responses to *PPFD*. At UMBS, at a *PPFD* of 1000 μmol m^{-2} s^{-1}, the maximum increase in *GPP* is 11% for T_a increasing from 16˚C to 21˚C; at Vielsalm, the maximum increase in *GPP* is 13% for T_a decreasing from 24 to 15˚C. This latter observation is notable as for the temperature range considered here, observed instantaneous responses of assimilation increase with increasing temperature (Medlyn *et al*., 2002).

The observed decrease in *GPP* with increasing temperature for a given *PPFD* at Vielsalm (Fig. 5.4A) could be partly explained by a reduction in the ratio of internal on ambient CO_2 concentration (C_i/ C_a) driven by higher vapour water deficit at higher temperature that are likely to occur in summer under a European continental climate.

Table 5.1: Parameters of the models at UMBS and Vielsalm; G93, the Guenther *et al.* (1993)'s algorithm; N99, the Niinemets et al (1999b)'s model; Energetic status model, this study.

Model	Parameter	Units	UMBS	Vielsalm
Farquhar	α_{co2}	mol electron mol^{-1} photon	0.23	0.2
	θ	-	0.13	0.13
	V_{cmax}	μmol m^{-2} s^{-1}	90	30
G93	I_s	nmol m^{-2} s^{-1}	13.81	3.4
N99	ε	-	12.12×10^{-3}	6.13×10^{-3}
Energetic status model	c_1	μmol isoprene μmol^{-1} electron	1.3×10^{-4}	6.10×10^{-4}
	c_2	μmol isoprene m^2 s μmol^{-2} electron	6.9×10^{-7}	1.4×10^{-6}

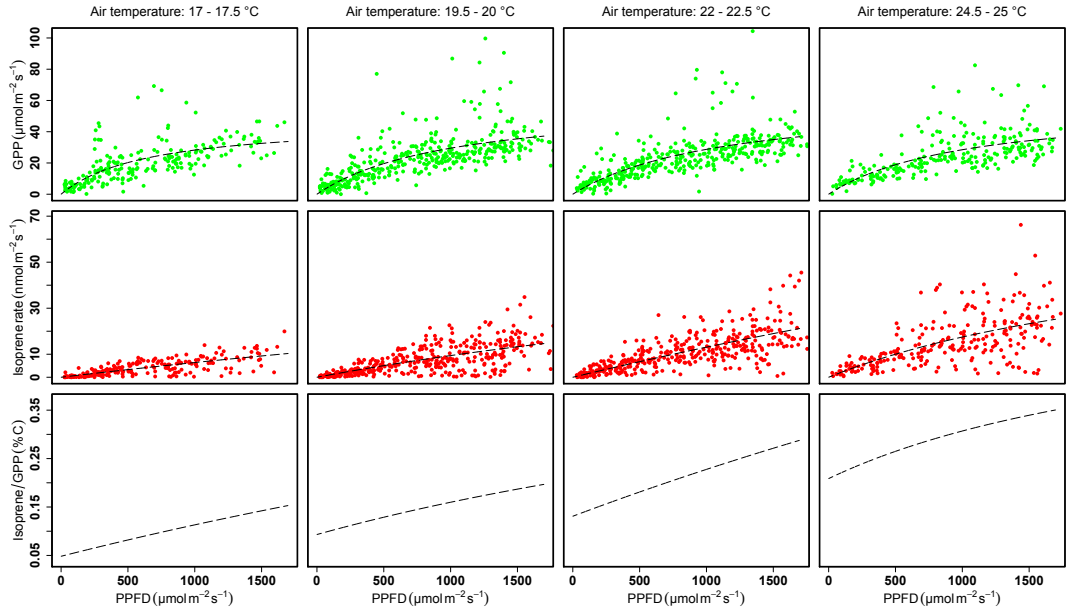


Figure 5.1: *GPP* (top panels, green symbols), isoprene emission rate (middle panels, red symbols) and ratio of isoprene to *GPP* (bottom panels) versus *PPFD* observed at the UBMS site. Data are shown for four air temperature 0.5 ˚C bins spanning the 15°C to 25°C full range analysed here. The relationships of *GPP* and isoprene emission rate to changes in *PPFD* were estimated by Michaelis-Menten type functions (dashed lines) fitted to the data. Ratios of isoprene to *GPP* displayed in the bottoms panel result from these fits.

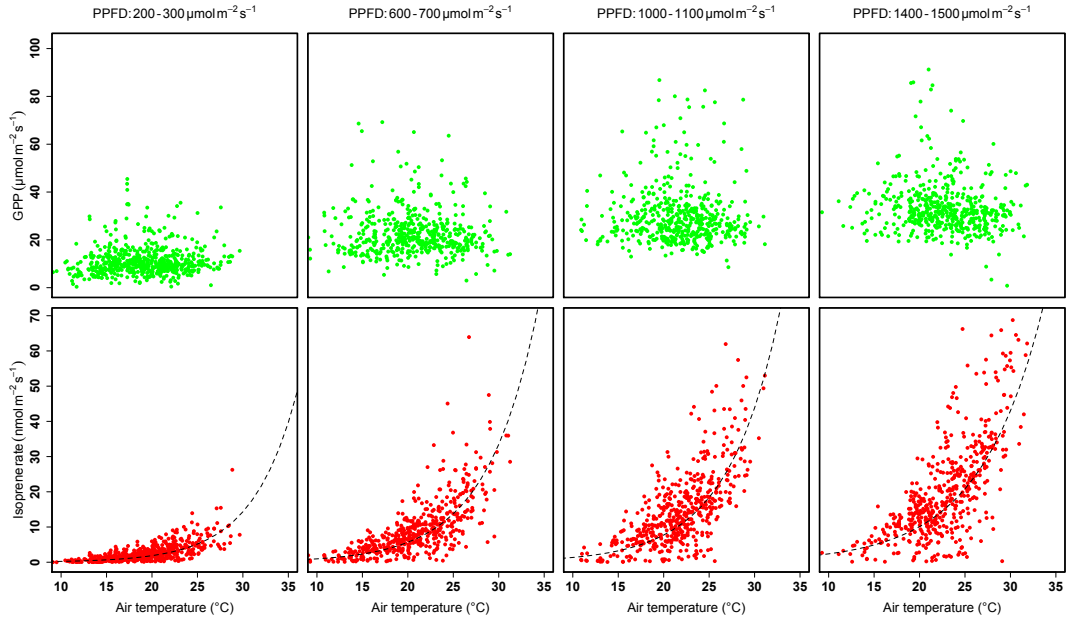


Figure 5.2 : *GPP* (top panels, green symbols), isoprene emission rate (bottom panels, red symbols) versus air temperature at the UMBS site. Data are shown for four *PPFD* 100 μmol m^{-2} s^{-1} bins spanning the 100 μmol m^{-2} s^{-1} to 1700 μmol m^{-2} s^{-1} full range analysed here. The relationships of *GPP* and isoprene emission rate to changes in air temperature were estimated with exponential functions (dashed lines) fitted to the data.

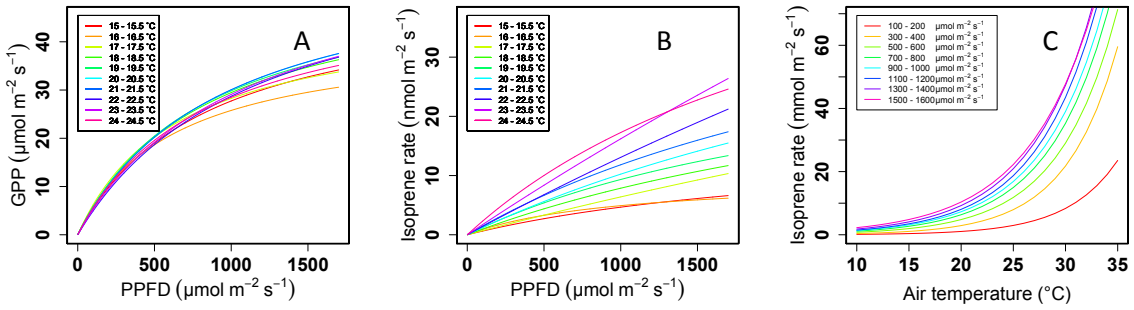


Figure 5.3: Responses of (A) *GPP* and (B) isoprene emission rate to changes in *PPFD* at air temperature ranging from 15 to 25 ˚C, and (C) responses of isoprene emission rates to changes in air temperature, at *PPFD* ranging from 100 to 1600 μmol m^{-2} s^{-1} at the UMBS site. *PPFD* response curves were fitted to the data using a Michaelis- Menten type functions. Air temperature response curves were fitted to the data using exponential functions.

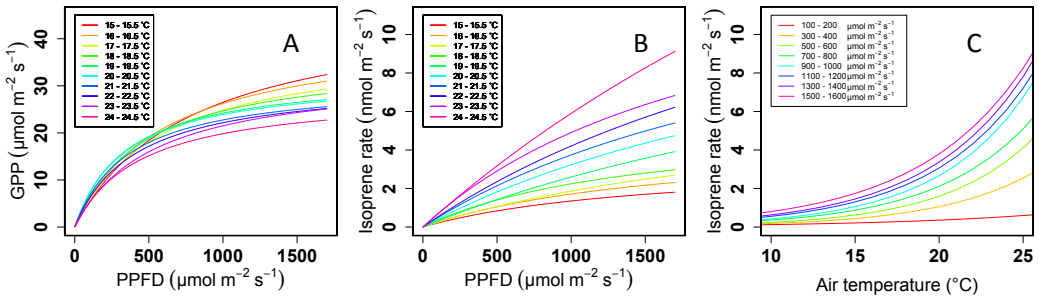


Figure 5.4: Responses of (A) *GPP* and (B) isoprene emission rate to changes in *PPFD* at air temperature ranging from 15 to 25 ˚C, and (C) responses of isoprene emission rates to changes in air temperature, at *PPFD* ranging from 100 to 1600 μmol m^{-2} s^{-1} at the Vielsalm site. *PPFD* response curves were fitted to the data using a Michaelis- Menten type functions. Air temperature response curves were fitted to the data using exponential functions.

Table 5.2: Evaluation statistics of Michaelis-Menten fits to observed *GPP* and isoprene emission versus *PPFD* at different air temperature at the UMBS and Vielsalm sites.

T_{max} (°C)	15.5	16	16.5	17	17.5	18	18.5	19	19.5	20	20.5	21	21.5	22	22.5	23	23.5	24	24.5	25	MEAN
UMBS																					
GPP																					
Explained variance (r^2)	0.54	0.56	0.56	0.61	0.46	0.64	0.47	0.51	0.52	0.50	0.51	0.48	0.54	0.55	0.50	0.49	0.42	0.40	0.55	0.44	**0.51**
Modelling efficiency (N_E)	0.53	0.56	0.56	0.61	0.46	0.63	0.47	0.51	0.52	0.50	0.51	0.48	0.54	0.55	0.50	0.49	0.42	0.39	0.55	0.44	**0.51**
Mean absolute error (σ_A)	5.47	5.34	5.40	5.70	6.23	5.49	6.70	6.20	6.18	6.61	7.00	7.24	6.32	6.02	6.04	6.31	7.12	7.81	5.84	6.92	**6.30**
Isoprene																					
Explained variance (r^2)	0.45	0.37	0.38	0.50	0.55	0.59	0.51	0.54	0.50	0.47	0.49	0.45	0.54	0.49	0.51	0.45	0.39	0.39	0.45	0.37	**0.47**
Modelling efficiency (N_E)	0.45	0.37	0.38	0.50	0.55	0.59	0.51	0.54	0.50	0.47	0.49	0.45	0.54	0.49	0.51	0.45	0.39	0.39	0.45	0.37	**0.47**
Mean absolute error (σ_A)	1.32	1.41	1.60	1.77	1.69	1.82	2.19	2.46	2.74	3.16	3.21	3.52	3.30	3.76	4.02	5.28	6.35	6.40	5.31	6.06	**3.37**
Vielsalm																					
GPP																					
Explained variance (r^2)	0.87	0.80	0.78	0.85	0.80	0.85	0.78	0.78	0.73	0.74	0.79	0.79	0.76	0.68	0.81	0.72	0.81	0.67	0.74	0.76	**0.78**
Modelling efficiency (N_E)	0.87	0.80	0.78	0.85	0.80	0.84	0.78	0.77	0.72	0.74	0.79	0.79	0.76	0.68	0.80	0.72	0.81	0.67	0.74	0.75	**0.77**
Mean absolute error (σ_A)	2.72	3.51	3.67	3.14	3.41	3.10	3.45	3.57	4.28	3.89	3.58	3.06	3.35	3.83	2.94	3.30	2.73	3.92	2.85	2.61	**3.35**
Isoprene																					
Explained variance (r^2)	0.63	0.62	0.68	0.71	0.71	0.67	0.70	0.67	0.69	0.68	0.70	0.74	0.66	0.72	0.73	0.76	0.72	0.66	0.84	0.76	**0.70**
Modelling efficiency (N_E)	0.63	0.61	0.68	0.71	0.70	0.67	0.70	0.67	0.69	0.68	0.70	0.74	0.66	0.72	0.73	0.76	0.72	0.66	0.84	0.76	**0.70**
Mean absolute error (σ_A)	0.28	0.30	0.37	0.39	0.36	0.44	0.47	0.60	0.64	0.70	0.82	0.70	0.82	0.89	0.94	0.95	1.01	1.27	0.97	0.97	**0.69**

Table 5.3: Evaluation statistics of exponential fits to observed isoprene emission versus T_a at different *PPFD* at the UMBS and Vielsalm sites

$PPFD_{max}$ (μmol m^{-2} s^{-1})	200	300	400	500	600	700	800	900	1000	1100	1200	1300	1400	1500	1600	1700	MEAN
UMBS																	
Isoprene																	
Explained variance (r^2)	0.36	0.51	0.53	0.61	0.60	0.53	0.62	0.54	0.61	0.50	0.59	0.58	0.51	0.54	0.42	0.37	**0.53**
Modelling efficiency (N_E)	0.30	0.48	0.48	0.58	0.58	0.51	0.60	0.51	0.59	0.46	0.56	0.55	0.48	0.50	0.36	0.34	**0.49**
Mean absolute error (σ_A)	0.93	1.21	1.76	2.29	2.75	3.60	3.84	4.61	4.61	5.64	5.68	6.09	6.83	7.28	7.28	8.76	**4.57**
Vielsalm																	
Isoprene																	
Explained variance (r^2)	0.29	0.55	0.66	0.75	0.72	0.76	0.74	0.79	0.72	0.64	0.73	0.69	0.76	0.76	0.65	0.69	**0.68**
Modelling efficiency (N_E)	1.00	1.00	1.00	1.00	1.00	1.00	1.00	1.00	0.99	1.00	0.99	1.00	0.99	0.99	0.99	0.99	**1.00**
Mean absolute error (σ_A)	0.22	0.27	0.38	0.47	0.57	0.68	0.72	0.59	1.10	0.85	1.11	1.04	1.29	1.02	1.24	1.28	**0.80**

The ratio of assimilated carbon lost in the form of isoprene ranges from 0.05% to 0.35% at UMBS and from 0.02% to 0.18% at Vielsalm. Ratios of isoprene emission to *GPP* tend to increase with increasing *PPFD* at both sites. However, if instead of T_a data are sorted by narrow ranges of canopy temperature (T_c) estimated from sensible heat fluxes, the systematic increase of the ratio *I*/*GPP* with increasing *PPFD* is markedly attenuated (data not shown).

Temperature-curves across PPFD

Figure 5.2 shows examples of T_a-curves of *GPP* and *I* at the site of UMBS. At both sites (UMBS and Vielsalm), *GPP* and *I* respond in a quite different manner to changes in T_a. *GPP* shows almost no response to T_a, as confirmed by high p-values calculated for *GPP* versus T_a (not shown). On the other hand, isoprene emission responds extremely strongly to changes in T_a. The response of both *GPP* and *I* to changes in temperature remains whether canopy or air temperature is used (data not shown).

Responses of isoprene emission to changes in T_a were approximated for both sites using exponential fits. Statistics for these fits are shown in Table 5.3. Exponential fits explain about 52% of observed variance in isoprene emission at UMBS and 68 % at Vielsalm. Figures 5.3C and 5.4C show exponential fits to isoprene emission T_a-curves under different *PPFD* regimes. At a T_a of 25˚C, *I* increases by 75% at UMBS and 138% at Vielsalm when *PPFD* increases from 100-to 1600 μmol m^{-2} s^{-1}.

5.3.2 Model evaluation

Parameters of the Farquhar and isoprene emission models, estimated from the *PPFD*-curves of *GPP* and isoprene emission at a T_a ranging from 24.5 to 25˚C, are reported in Table 5.1. For both sites, carbon assimilation was always found to be light-limited, whatever the canopy position. Also, for both sites, estimated quantum efficiencies for electron transport (α_{co2}) and the curvature parameter (θ) of the Farquhar model are rather small. At UMBS, the Farquhar model captures extremely well the estimates of *PPFD* responses of *GPP*, explaining almost 100% of the variance and showing a mean model efficiency of 0.97 and a mean absolute error of 1.3 μmol m^{-2} s^{-1} across all temperatures (Table 5.4, Figs. 5.5-5.6). As in the observations, the Farquhar model also shows a limited response to changes in T_a (Fig. 5.6). The picture is somewhat different at Vielsalm, where although the Farquhar model has a good (r^2) of 0.99 across all temperature and thus captures the observed pattern of variation in *GPP* versus *PPFD*, it fails to capture the observed increase in *GPP* with decreasing temperature as revealed by the poor modelling efficiency score of 0.2 and a mean absolute error of 5.38 μmol m^{-2} s^{-1} (Table 5.4). Here again, the Farquhar model upscaled to the canopy simulates almost no response of *GPP* to changes in T_a (data not shown).

Canopy-scale simulations, completed with the three isoprene models used in this study (G93, N99 and the energetic status model), are presented in Figs 5.5-5.6 (for UMBS) with associated model evaluation statistics summarised in Figs. 5.7-5.8. All models capture very well the isoprene emissions *PPFD*- and T_a-responses and explain on average more than 90% of the variance (r^2) in the (smoothed) data (not shown). For the emissions *PPFD*- responses, model efficiencies are good for all the isoprene models, with averaged values for respectively G93, N99 and the energetic status model of 0.84, 0.76, 0.92 at UMBS and 0.9, 0.65, 0.91 at Vielsalm. The energetic status model shows a slight improvement when compared to the N99 from which it originates, especially for *PPFD*- responses at low temperatures. Mean absolute errors of simulated *PPFD*-responses are low whatever the isoprene model, and do not exceed 3.1 nmol m^{-2} s^{-1} at UMBS and 1.1 nmol m^{-2} s^{-1} at Vielsalm.

The picture is different for isoprene emission T_a- responses. Model efficiencies are less good compared to the *PPFD*- responses and span over a large range of −21 to 0.97 across models and sites. For all isoprene models, mean absolute errors of simulated T_a-responses are larger when compared to *PPFD*- responses with averaged values across the range of *PPFD* of 5.62, 7.86, 5.54 nmol m^{-2} s^{-1} at UMBS and 2.98, 3.62, 2.52 nmol m^{-2} s^{-1} at Vielsalm for G93, N99 and the energetic status model respectively. Interpretation of these mean absolute errors would need further investigation, particularly the impact of large value of exponential fits at high temperature should be analysed. Nonetheless, the energetic model outperforms the original N99 model.

The behaviour of the *PPFD*-response of the ratio of isoprene emission to *GPP* is divergent among models (shown for UMBS in Fig. 5.5). For N99, this ratio is always constant across the whole range temperature, indicating that modelled carbon assimilation is always under light-limited regime; using G93, I found a systematic increase of *I*/*GPP* with *PPFD* at Vielsalm and a behaviour depending on T_a at UMBS with a decrease in *I*/*GPP* with increasing *PPFD* observed at higher temperatures; at both sites, the energetic status model consistently shows an increase in the ratio *I*/*GPP* with *PPFD*, as observed.

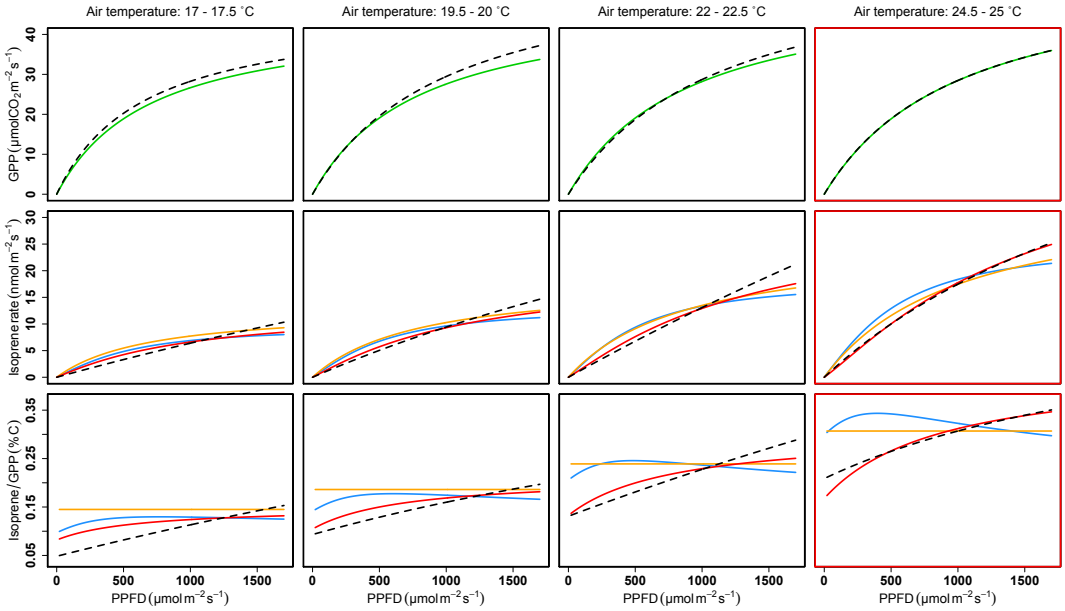


Figure 5.5 Modelled responses of *GPP* (top panels), isoprene emission rate (middle panels) and ratio of isoprene to *GPP* (bottom panels) to changes in *PPFD* at the UBMS site. Data are shown for four air temperature 0.5 ˚C bins spanning the 15°C to 25°C full range analysed here. Dashed black lines represent the fits to observations using Michaelis- Menten type functions; green solid lines represent the Farquhar model (top panels); blue, orange and red solid lines, in the middle and bottom panels, represent simulations made using respectively G93, N99, and the energetic status model. *GPP* modelled with the Farquhar model were used for the simulations of the isoprene on *GPP* ratio (bottom panels). Parameters of the models were estimated by minimising *RSS* on the estimates of *GPP* and isoprene rate at the temperature range of 24.5-25˚C (red box).

Table 5.4: Evaluation statistics of modelled *GPP PPFD*-curves against observations smoothed using Michaelis-Menten type functions fitted to data at the UMBS and Vielsalm sites.

Farquhar model																					
T_{max} (˚C)	**15.5**	**16**	**16.5**	**17**	**17.5**	**18**	**18.5**	**19**	**19.5**	**20**	**20.5**	**21**	**21.5**	**22**	**22.5**	**23**	**23.5**	**24**	**24.5**	**25**	**MEAN**
UMBS																					
Explained variance (r^2)	1.00	1.00	1.00	0.99	1.00	0.99	1.00	1.00	1.00	1.00	1.00	1.00	1.00	1.00	1.00	1.00	1.00	1.00	1.00	1.00	**1.00**
Modelling efficiency (N_E)	0.95	0.99	1.00	0.95	0.97	0.93	0.95	0.96	0.95	0.96	0.96	0.95	0.96	0.98	0.99	0.99	0.99	0.99	1.00	1.00	**0.97**
Mean absolute error (σ_A)	1.61	0.59	0.35	1.83	1.40	2.19	1.96	1.76	2.00	1.52	1.87	2.21	1.71	1.10	0.67	0.98	0.62	1.08	0.43	0.02	**1.30**
Vielsalm																					
Explained variance (r^2)	0.97	0.98	0.98	0.98	0.99	1.00	1.00	1.00	1.00	1.00	1.00	1.00	1.00	1.00	1.00	1.00	1.00	1.00	1.00	1.00	**0.99**
Modelling efficiency (N_E)	-0.38	-0.38	-0.38	-0.19	-0.07	-0.33	-0.07	-0.25	-0.06	0.02	0.08	0.26	0.40	0.39	0.59	0.85	0.76	0.84	0.93	1.00	**0.20**
Mean absolute error (σ_A)	8.95	8.40	8.55	7.70	7.06	7.99	6.83	7.20	6.39	6.03	5.88	4.86	4.61	4.49	3.80	2.13	2.89	2.23	1.43	0.18	**5.38**

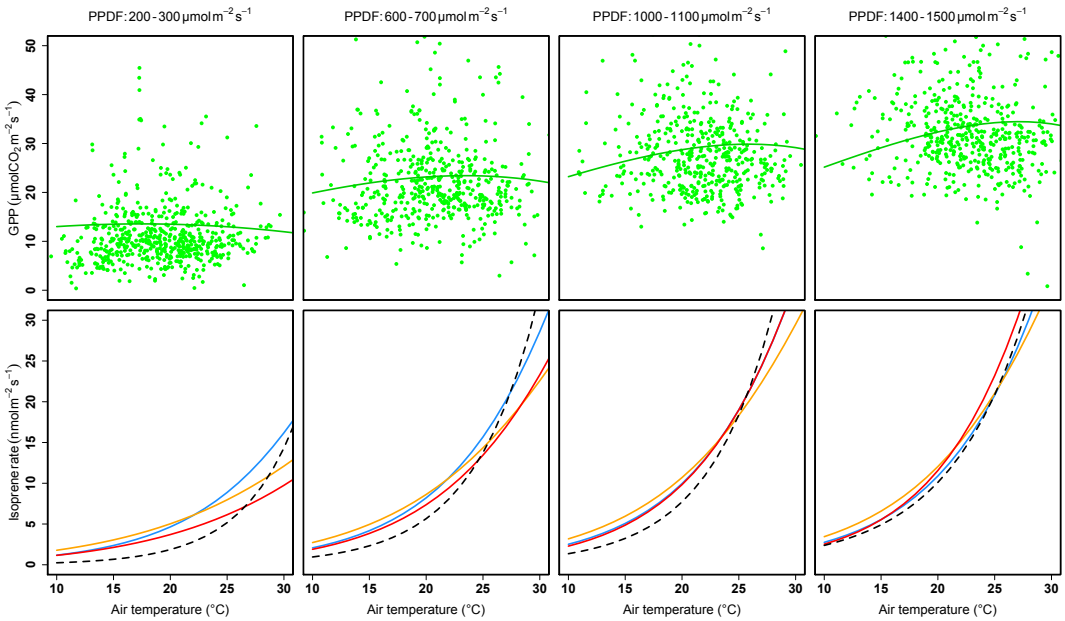


Figure 5.6: Modelled responses of *GPP* (top panels), isoprene emission rate (bottom panels) to changes in air temperature at the UMBS site. Data are shown for four *PPFD* 100 μmol m^{-2} s^{-1} bins spanning the 100 μmol m^{-2} s^{-1} to 1700 μmol m^{-2} s^{-1} full range analysed here. In the top panels, green dots represent the observed *GPP* and the green solid lines represent simulations using the Farquhar model. In the bottom panels dashed lines represent fits to observations using exponential functions; blue, orange and red solid lines represent isoprene emission simulated with respectively G93, N99, and the energetic status model.

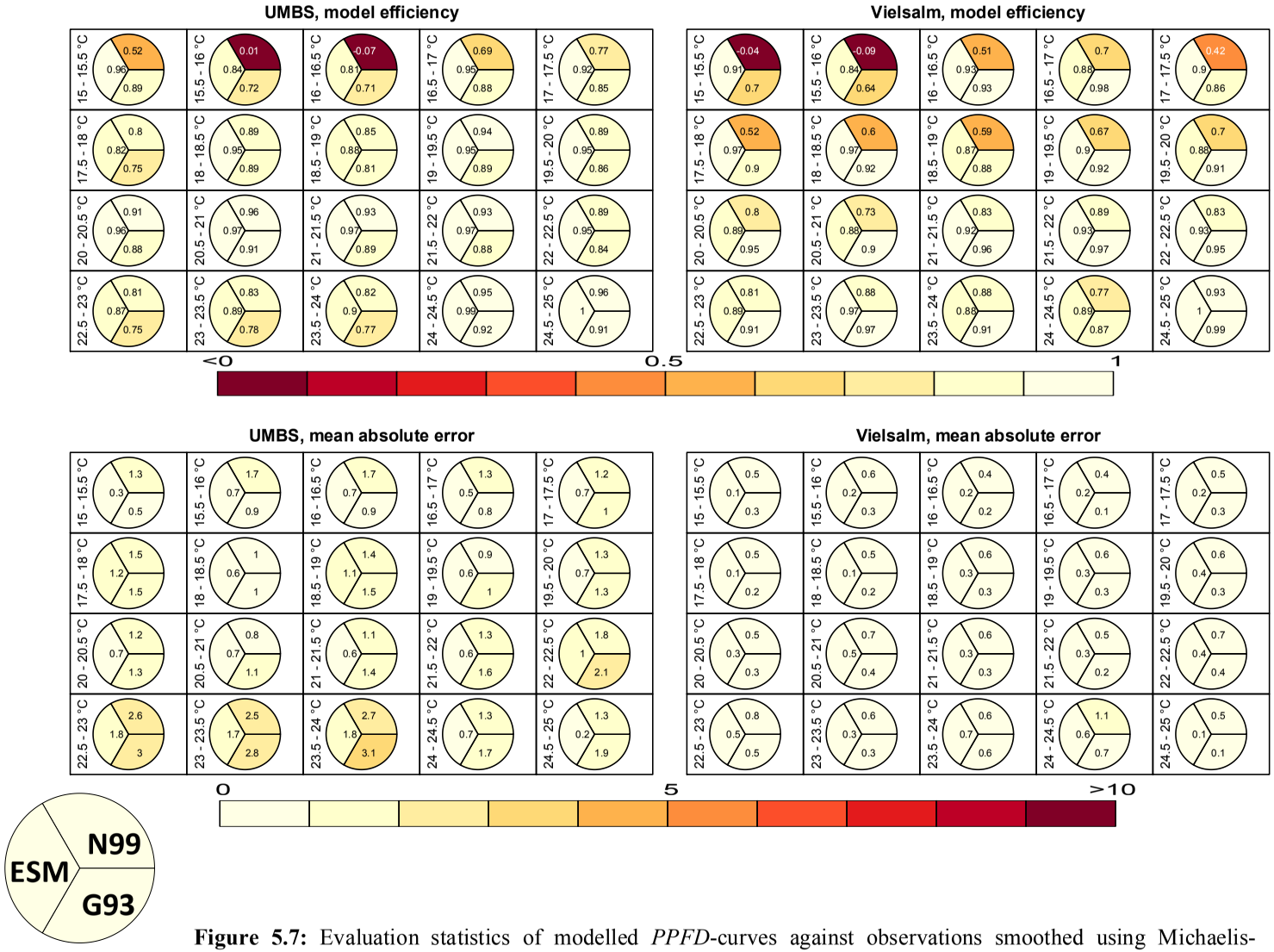


Figure 5.7: Evaluation statistics of modelled *PPFD*-curves against observations smoothed using Michaelis-Menten type functions fitted to data. Difference in model efficiency (N_E, top panels) and mean absolute error (σ_A in nmol $m^{-2}s^{-1}$, bottom panels) between isoprene models are shown at air temperature ranging from 15 to 25 °C for the UMBS site (left panels) and the Vielsalm site (right panels). For each circle, starting from top right and clockwise, sectors correspond to N99, G93, and the energetic status model (ESM). Actual values of N_E, and σ_A are given in each sector. For both panels red/white colours mean poor/good model behaviour.

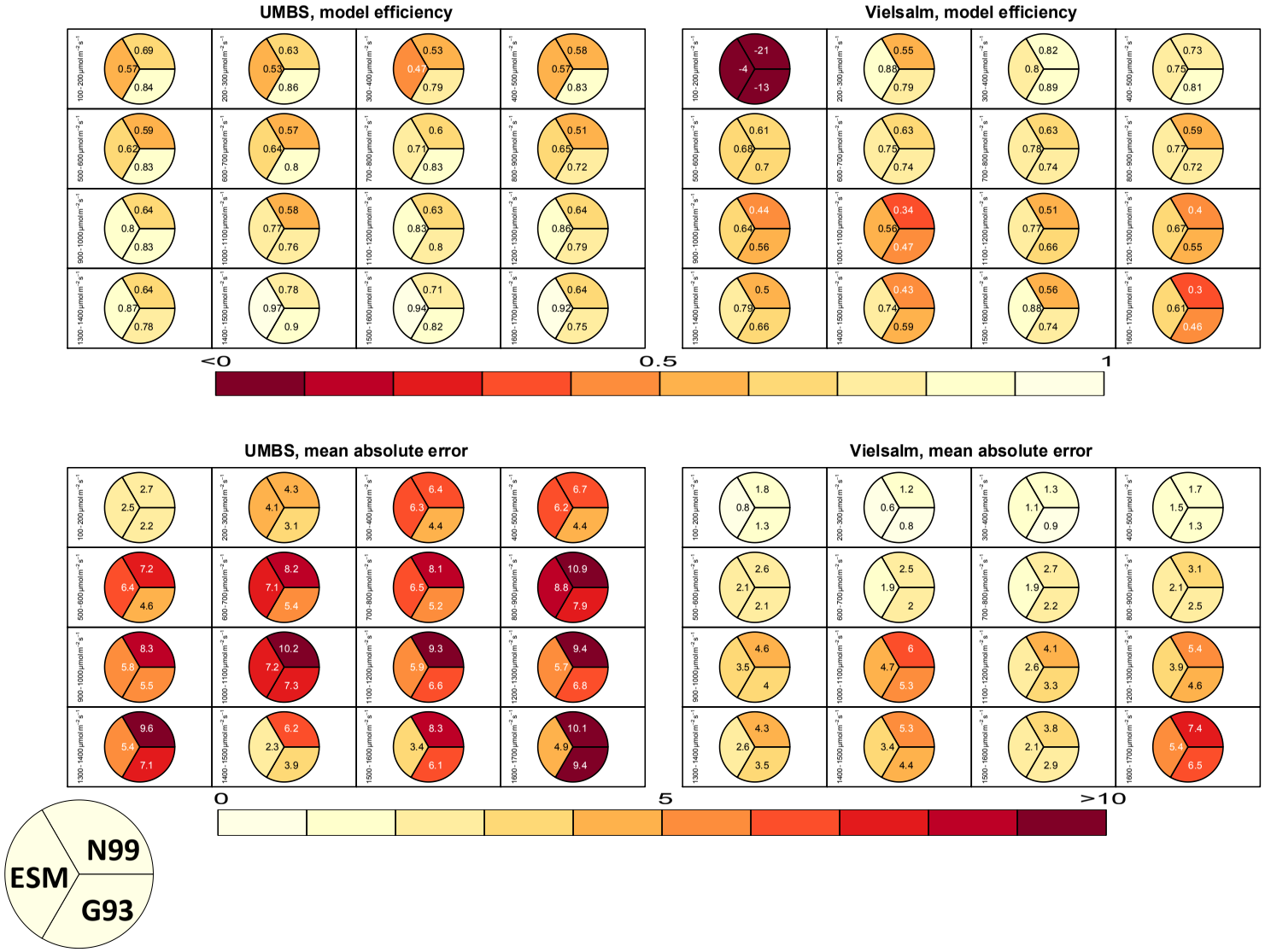


Figure 5.8: Evaluation statistics of modelled T_a-curves against observations smoothed using exponentials fitted to data. Difference in model efficiency (N_E, top panels) and mean absolute error (σ_A in nmol m^{-2} s^{-1}, bottom panels) between isoprene models are shown at *PPFD* ranging from 100-to 1600 μmol m^{-2} s^{-1} for the UMBS site (left panels) and the Vielsalm site (right panels). Starting from top right and clockwise, sectors correspond to N99, G93, and the energetic status model (ESM). Actual values of N_E, and σ_A are given in each sector. For both panels red/white colours mean poor/good model behaviour.

Canopy profiles

Figures 5.9 and 5.10 show the within-canopy extinction of modelled gross carbon assimilation, light-limited minus Rubisco-limited electron fluxes [$J - J_v$], and isoprene emission (computed from the energetic status model), at a T_a of 25˚C and a *PPFD* of 1000 μmol m^{-2} s^{-1} applied at the top of the canopy. Due to light extinction through the canopy, assimilation, [$J - J_v$] and I diminish from the top to the bottom of the canopy by (respectively) 61%, 25% and 64% at UMBS, and 74%, 200% and 79% at Vielsalm. At both sites, driven by the extinction of photosynthetic parameters through the canopy, 'standard' isoprene emission, computed from the energetic status model for T_a and *PPFD* standardized at 25˚C and a of 1000 μmol m^{-2} s^{-1}, decreases with canopy depth by 21% at UMBS and 47% at Vielsalm (Figs 5.9D and 5.10D).

Modelled carbon assimilation and isoprene emission *PPFD*-curves at the top, middle and bottom of the canopy are shown in Figs. 5.11 and 5.12. Both simulated assimilation and isoprene emission maxima decrease with canopy depth at both sites. Isoprene rate and carbon assimilation at UMBS show no clear saturation at higher *PPFD* whatever the position in the canopy. Carbon assimilation at Vielsalm is found to saturate at high *PPFD* suggesting that Rubisco-limited conditions are reached, with a *PPFD* transition threshold from light- to Rubisco- saturation decreasing with canopy depth.

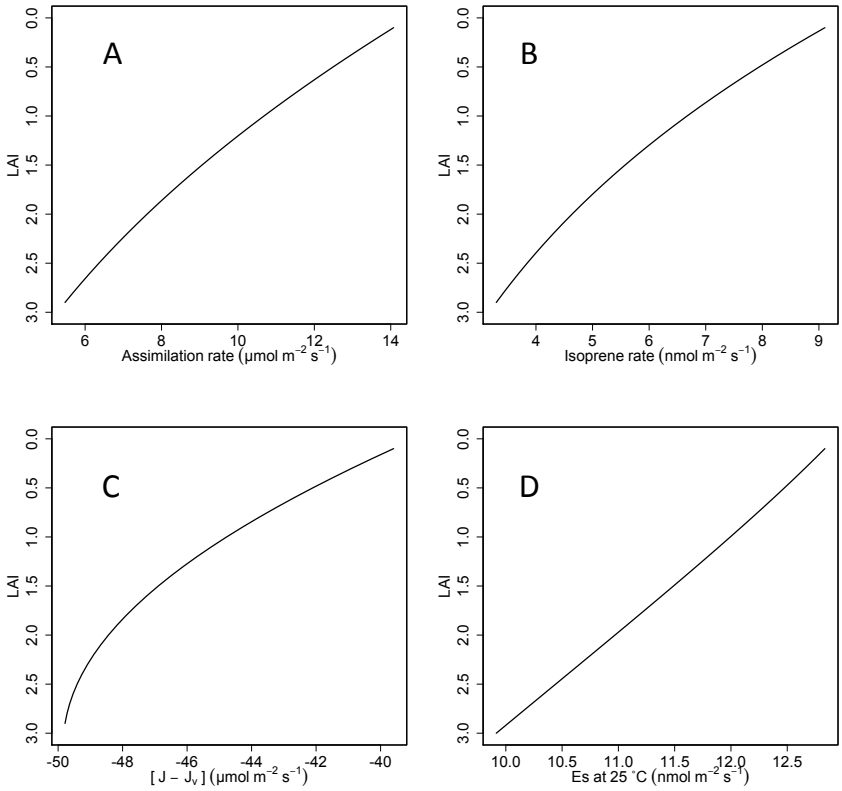


Figure 5.9: Canopy profiles of (A) carbon assimilation rate, (B) isoprene emission rate, (C) energetic status of the leaf approximated by $[J - J_v]$ and (D) isoprene emission rate (E_s) under standard conditions of temperature and *PPFD* at the UMBS site. Simulations of assimilation and isoprene emission rate were done using the Farquhar model and the energetic status model respectively. Simulations in panels (A), (B) and (C) were performed for air temperature at 25 ˚C and *PPFD* at 1000 μmol m^{-2} s^{-1} at the top of the canopy. The simulation in panel (D) was performed under standard conditions of an air temperature at 25 ˚C and *PPFD* at 1000 μmol m^{-2} s^{-1} kept constant across the canopy.

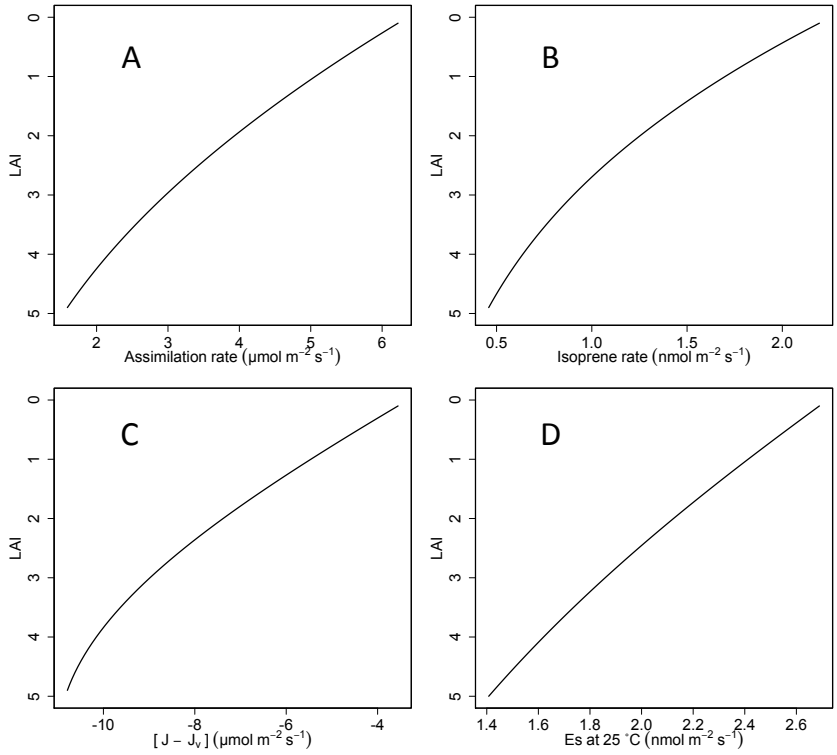


Figure 5.10: Canopy profiles of (A) carbon assimilation rate, (B) isoprene emission rate, (C) energetic status of the leaf approximated by $[J - J_v]$ and (D) isoprene emission rate (E_s) under standard conditions of temperature and *PPFD* at the Vielsalm site. Simulation of assimilation and isoprene emission rate were done using the Farquhar model and the energetic status model respectively. Simulations in panels (A), (B) and (C) were performed for air temperature at 25 ˚C and *PPFD* at 1000 μmol m^{-2} s^{-1} at the top of the canopy. The simulation in panel (D) was performed under standard conditions of an air temperature at 25 ˚C and *PPFD* at 1000 μmol m^{-2} s^{-1} kept constant across the canopy.

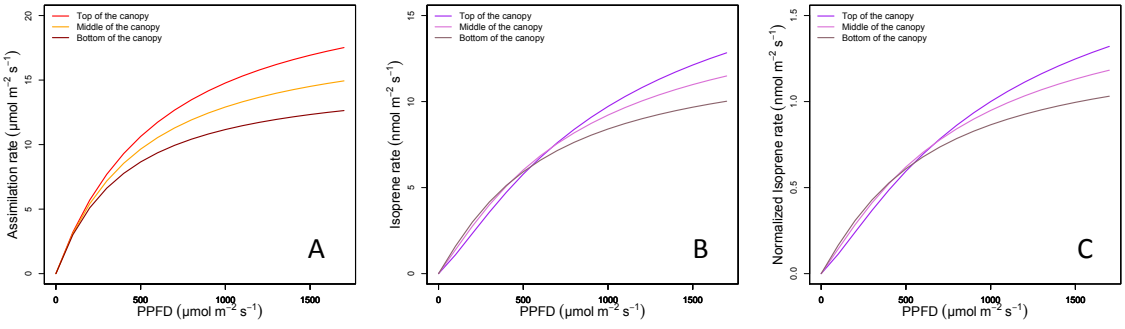


Figure 5.11: Modelled responses of (A) assimilation rate, (B) isoprene emission rate and (C) normalised isoprene emission rate to changes in *PPFD* at the top, middle and bottom of the canopy at air temperature 25 ˚C at the UMBS site. Assimilation and isoprene emission rates are modelled with the Farquhar model and the energetic status model respectively.

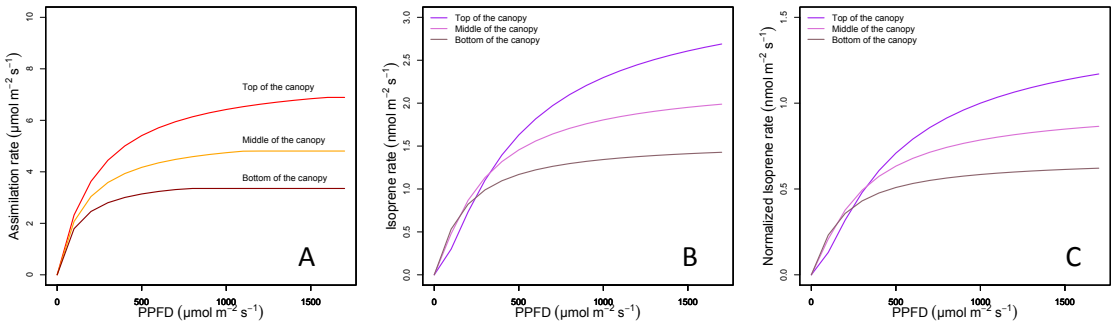


Figure 5.12: Modelled responses of (A) assimilation rate, (B) isoprene emission rate and (C) normalised isoprene emission rate to changes in *PPFD* at the top, middle and bottom of the canopy at air temperature of 25 ˚C at the Vielsalm site. Assimilation and isoprene emission rates are modelled with the Farquhar model and the energetic status model respectively.

5.4 Discussion

The simple multi-layer approach adopted here neglects many factors potentially influencing *GPP* and isoprene emission. Among these are the effects of sun position (diffuse *versus* direct radiation and variations in the extinction coefficient for *PPFD*), canopy structure, leaf orientation, true leaf temperature, interannual and seasonal variation of both photosynthetic and isoprene capacities, within-canopy gradient in isoprene emission capacity, and within- canopy chemistry. Any of these factors could influence above-canopy *GPP* and/or isoprene fluxes (Harley *et al.*, 1996; Sharkey *et al.*, 1996; De Pury & Farquhar, 1997; Huber *et al.*, 1999; Mayrhofer *et al.*, 2005; Grote, 2007; Niinemets *et al.*, 2010b; Keenan *et al.*, 2011; Bryan *et al.*, 2012; Laffineur *et al.*, 2013). Moreover, although the entire vegetation of the studied ecosystem influences *GPP* (all species participate in the CO_2 fluxes), only a few species contribute to the observed isoprene fluxes. Nonetheless, we can derive key conclusions from a simple approach, with has the benefits of transparency and tractability.

The first observation is that all the three isoprene models tested here are very similar in term of model efficiencies, as revealed by the model evaluation statistics (Figs 5.7-5.8). Niinemets *et al.* (2013) made the same observation for monoterpene predictions using a different 'canopy scaling' approach and comparing the simulations with flux measurement of *Quercus ilex* L. Although using a different approach, different measurements and to a certain extent different photosynthetic and isoprene emission

models, my approach thus yields the same conclusion reached by Niinemets and co-authors about the 'striking' similarity in the models' performances. In particular it appears that the three isoprene models (G93, N99 and the energetic status model) have very similar temperature and *PPFD* responses. The models overall capture about 50% of the signal in isoprene emissions.

If different models are found to perform equally well (in this study and in Niinemets *et al.*, 2013), the question can be raised as to how (and why) these models may diverge in future climate projections. To my knowledge only one study (Keenan *et al.*, 2009) reported future projections using different isoprene models at a regional scale. Keenan and co-authors showed that despite similar results for the present climate, isoprene emissions diverge strongly for predicted future climates due to the slight differences in the parameterisation of the emission responses to changes in temperature, *PPFD* and CO_2 concentrations.

The second observation concerns the *GPP* inferred from CO_2 flux measurement. The relative lack of responsiveness of above-canopy *GPP* to changes in temperature ranging from 10 to 30˚C is notable. As the assimilation was always under light limited conditions in my simulations, this lack of responsiveness seems to indicate stability with temperature in the functioning of the electron transport rate. This result also suggests that the temperature response of isoprene emission, at least between 10˚C and 30˚C, is primarily controlled by IspS and not by the electron transport rate. All models capture this response well.

The fact that assimilation was found to be always light-limited tends, within the limitation of my approach, to support the hypothesis that Rubisco capacity acclimates seasonally to light intensity. The capacity of the plant to regulate its capacity to assimilate CO_2 according the light intensity it receives is still debated. This theory is important for dynamic global vegetation models (DGVM). The BIOME3 biogeography model and the Lund-Postdam-Jena dynamic global vegetation model (Haxeltine & Prentice, 1996; Sitch *et al.*, 2003) assume acclimation of Rubisco capacity to light intensity; others don't. Solving the question of acclimation or not is crucial for accurate future predictions of carbon uptake by terrestrial vegetation.

Finally, at canopy scale the site with higher isoprene emissions rate (UMBS) was also the one with the larger *GPP* and V_{cmax}. Due these differences in V_{cmax}, modelled across-canopy assimilation *PPFD*-curves at UMBS do not saturate at any *PPFD* (Fig. 5.11A) while assimilation *PPFD*-curves at Vielsalm show saturation with increasing *PPFD,* indicating that Rubisco-limited conditions have been reached (Fig. 5.12A). This result along, with the measurements on *Populus nigra* at CREAF reported in chapter IV where Rubisco limited-condition were extremely hard to reach, seems to indicate that high isoprene emitters species might have developed an especially high capacity for electron transport.

Without any need to postulate within-canopy acclimation in the IspS capacity (i.e. parameter c_1 of the model, Eq. 5.11), the model manages to simulate a decrease in isoprene standard emission factor (here standardized at a T_a of 25˚C) with canopy depth of the type usually observed (Sharkey *et al.*, 1996; Niinemets *et al.*, 2010a). *PPFD*-curves at different canopy positions computed from the energetic status model are also promising, and resemble the first adjustment made by Guenther and co-authors when attempting to account for the within-canopy behaviour of emissions (Guenther *et al.*, 1999; Monson *et al.*, 2012).

This work presents the first attempt to upscale the energetic status model of Morfopoulos *et al.* (2013, 2014) from leaf to canopy. The model manages to predict changes in isoprene emission to changes in *PPFD* and T_a with a very good agreement when compared to general *PPFD*- and T_a isoprene curves inferred from observations. The ability of the model to reproduce the general responses of isoprene to T_a indicates that the newly introduced temperature function accounting for IspS activity (and tested against data for the first time here) is appropriate. The results show a slight improvement on the Niinemets *et al.* (1999b) model (N99); the new model succeeds in capturing the higher carbon investment in isoprene production at higher *PPFD*, while N99 doesn't. This signifies that improvements at the leaf level made by the new model on isoprene emission's responses to changes in *PPFD* and temperature (Chapter III, Chapter IV) still stand at the canopy scale.

Another difference between N99 and my model comes from the capacity of the latter to predict changes in isoprene emission with changes in C_i. It is possible that a more elaborate canopy model, taking into account water exchanges with the atmosphere,

would be able to perform even better through consideration of C_i variations through the canopy and through the seasons.

Annex 5A.1 – Supplementary figures to chapter V

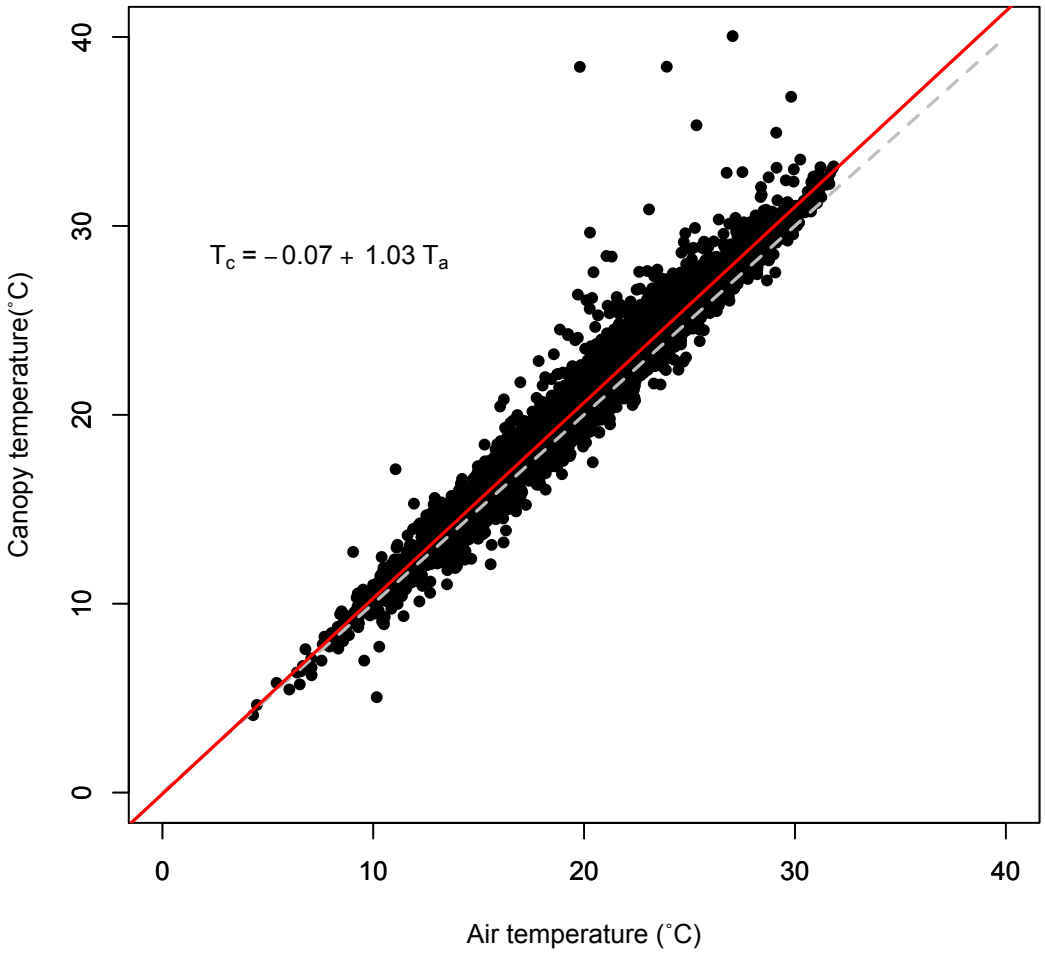


Figure 5A.1.1: Canopy temperature versus air temperature for the UMBS site.

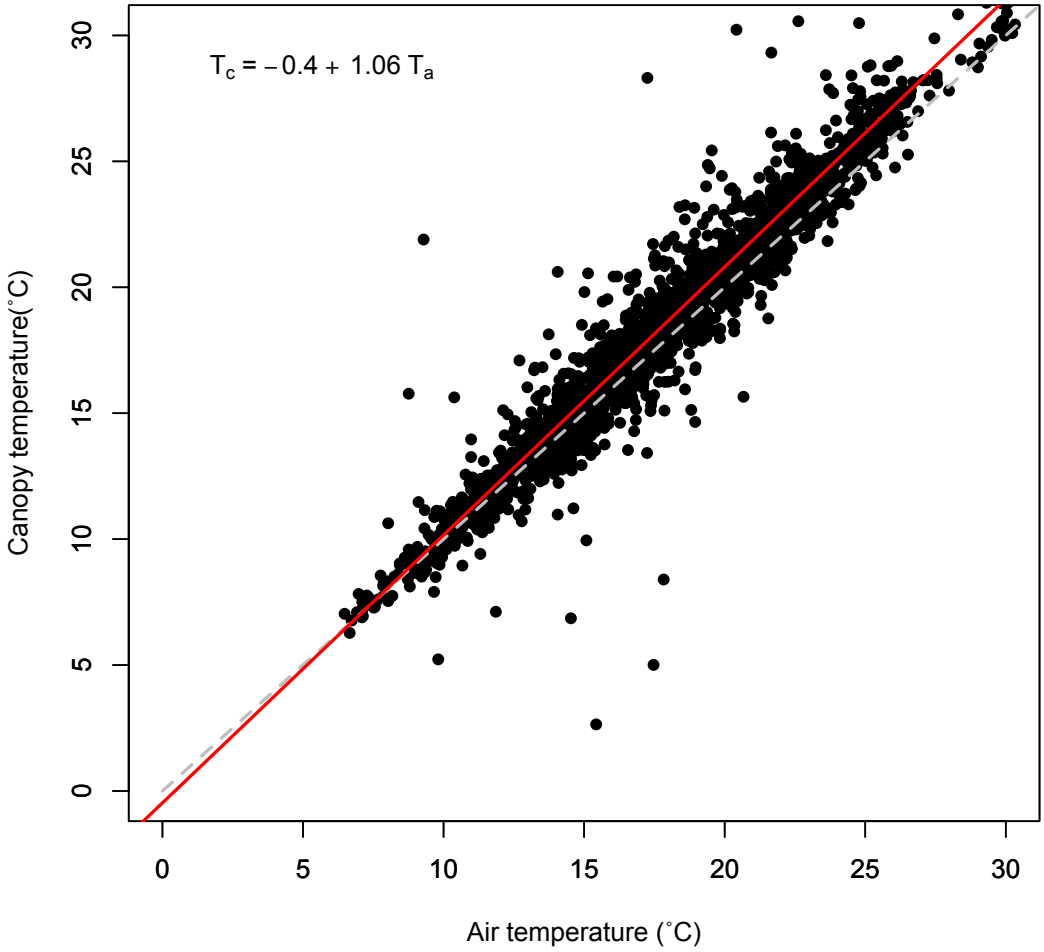


Figure 5A.1.2: Canopy temperature versus air temperature for the Vielsalm site

6 Conclusions

Quantitatively, isoprene is the most important BVOC released by terrestrial vegetation into the atmosphere (Laothawornkitkul *et al.*, 2009; Guenther *et al.*, 2012). Isoprene degradation to its oxidation products happens fast in the troposphere (Atkinson, 2000). This high chemical reactivity, combined with the large amount emitted, raises questions about potential impacts on atmospheric chemistry and physics that can result from isoprene emissions by plants, whether at the local, regional or global scale. At the local scale, the influence of isoprene on tropospheric ozone concentration is important both for human health and for the growth of plants, especially food crops. At larger scales, isoprene not only affects ozone production (or depletion, depending on the atmospheric background), but also the total oxidation capacity of the atmosphere. Isoprene thereby influences the abundances of other trace gases including methane, slowing down their degradation and increasing their lifetimes and concentrations. Isoprene thus indirectly affects the radiative forcing of the Earth's climate through its effect on the concentration of methane, a powerful greenhouse gas. Finally, products of isoprene oxidation can lead to the production of secondary organic aerosols (SOA) that act as cloud condensation nuclei (CNN), affecting the sky albedo and the fraction of diffuse radiation as well as the hydrological cycle (Arneth *et al.*, 2010; Peñuelas & Llusia, 2003).

Isoprene emission is primarily controlled by vegetation type, photosynthetic photon flux density (*PPFD*), leaf temperature (*T*) and CO_2 concentration. A warming climate and further changes in land use will affect the balance among different drivers of isoprene emission in ways that are non-trivial to predict. Robust, quantitative, process-based modelling is necessary, in order to investigate how isoprene emission may be expected to change and what the consequences might be for air quality and climate. It is therefore important to understanding the physiological processes that control isoprene emission by plants, and their response to changes in environmental drivers.

Isoprene is formed in chloroplasts though the 2-C-methyl-D-erythritol 4-phosphate (MEP) pathway, which combine glyceraldehyde 3-P (G3P) and pyruvate into the isoprene precursor dimethylallyl diphosphate (DMADP) (Lichtenthaler, 1999; Vickers *et al.*, 2009a). In the presence of the enzyme isoprene synthase (IspS), DMADP is transformed into isoprene, which promptly escapes from the leaf due to its high volatility. Thus isoprene synthesis is jointly driven by DMADP production and IspS

activity. The MEP pathway is also important for the formation of 'essential' isoprenoids such as carotenoids and tocopherol, which play photoprotective and antioxidant roles for the photosynthetic apparatus (Owen & Peñuelas, 2005).

Similarities in the responses of isoprene emission and CO_2 assimilation to *PPFD*, and in ^{13}C labelling experiments, show that isoprene emission and CO_2 assimilation are mechanistically linked (Delwiche & Sharkey, 1993; Loreto *et al.*, 2004). However, whereas the benefit of carbon assimilation is clear (the transformation of inorganic carbon to organic compounds used for plant growth and function), the adaptive significance of isoprene production is much less clear. It is now established nonetheless that isoprene protects the photosynthetic apparatus both from transient heat stress and from damage due to ROS, whether generated internally or externally to the leaf (Sharkey & Singsaas, 1995; Singsaas *et al.*, 1997; Fares *et al.*, 2006; Siwko *et al.*, 2007; Velikova *et al.*, 2005, 2011). Similarly Rubisco, an essential enzyme for carbon assimilation, is present in all leaves but this is not the case for IspS; only some species of plants have the capacity to produce isoprene, indicating that it is not essential to plant function in general. The challenge is to find an effective way of modelling the complex and incompletely understood metabolic pathway that leads to isoprene synthesis in the absence of a comprehensive explanation for its utility to plants, and with incomplete information about the distribution of isoprene emission ability at a global scale. At a minimum we need to define which are the key controllers of isoprene production, how isoprene responds to these key factors, and which ones really matter at larger spatio-temporal scales.

So far only one 'process-based' model has been used in global-scale studies investigating the impact of isoprene emission on the Earth system: the physiological model of isoprene emission developed by Niinemets and co-workers in 1999 (Niinemets *et al.*, 1999b). This model considers that production of isoprene is driven jointly by electron availability and IspS activity. I started my thesis work by analysing this model. My analysis revealed some inconsistencies between the authors' hypotheses concerning the controls of isoprene production, and the mathematical formulation of the model. In particular, Niinemets *et al.* (1999b) linked isoprene synthesis strongly to light limited carbon assimilation rather than to the part electron transport rate (ETR) engaged in the MEP pathway

In order to improve the Niinemets model, I asked how the specific part of the total ETR generated by Photosystem II (PSII) that is available to the MEP pathway could be represented in a model. This portion of the ETR is not very well known, mostly because of the difficulties in measuring it. I made the pragmatic assumption, based on available knowledge of the processes involved, that the magnitude of this electron flux should depend on the energetic status of the leaf, balancing the requirement of electrons for carbon assimilation against the maximum ETR as predicted by the Farquhar model. Approximating the energetic status of the leaf by the difference between light- (supply) and Rubisco (demand) electron fluxes, I developed a new, conceptually simple model and tested its predictions against published observations of isoprene emission variations in response to *PPFD*, temperature and leaf-internal CO_2 concentration (C_i). This first test was extremely promising, and indicated that my hypothesis has the major advantage of providing a unifying explanation for isoprene responses to all three environmental drivers. Moreover, it can explain the observed (and otherwise mysterious) lack of correlation between carbon assimilation and isoprene production responses to changes in C_i (Morfopoulos *et al.*, 2013).

In order to test the hypothesis further, I conducted leaf-scale experiments on *Populus nigra* L. during a secondment at Centre for Ecological Research and Forestry Applications (CREAF), Spain. The experimental protocol was designed to show how variations in the balance between electron supply and demand for carbon assimilation, driven by changes in the *PPFD* and CO_2 conditions of the experiment, combine to influence isoprene emission. Using the data that I collected at CREAF, and additional data on hybrid poplar from the study of Sun *et al.* (2012) (which followed a similar protocol), I tested my model and compared the results with those obtained using two pre-existing models: the empirical Guenther *et al.* (1993) algorithm, and the Niinemets model. Overall, my model reproduces the observations best of the three, without the need for any additional empirical functions. In particular, my model captures extremely well the response of isoprene to changes in C_i and gives an explanation for (otherwise unexplained) changes in the quantum efficiency of isoprene production at different concentrations of CO_2 (Morfopoulos *et al.*, 2014).

Finally, I tested my new model, along with the models of Guenther *et al.* (1993) and Niinemets *et al*. (1999b), at the canopy scale. I used a simple multi-layer approach and

compared the simulations against general *PPFD*- and air temperature isoprene-emission response curves, obtained using long-term measurements of both isoprene and CO_2 fluxes above canopy level in two mixed temperate forests. Differences between observed gross primary production (GPP) and isoprene emission highlighted the importance of temperature as a driver of isoprene emission. All models gave comparable results at this scale. Nevertheless, my model yielded better results than the Niinemets model from which it was developed.

To summarise, in comparison to the Niinemets *et al.* (1999b) model, my model improves:

1. The response of isoprene emission to C_i
2. The response of isoprene emission to *PPFD*
3. The respone of isoprene emission to *T*
4. The quantum efficiency of isoprene emission at different CO_2 concentrations.
5. The mismatch between carbon assimilation and isoprene emission in response to changes in *PPFD*, *T* and C_i.

An important future direction of research will be to try to upscale this new model to the global scale, in order to estimate changes in large-scale emissions induced by future climate changes, and how these changes in isoprene emission feed back on the climate system. This would be a non-trivial task and poses many challenges. First among these challenges is: what parameter values to apply to plant functional types (PFTs), which are the entities through which vegetation is represented in global vegetation models? Large datasets of the isoprene emission factor (I_s), (the isoprene emission rate measured at a leaf temperature of 30˚C and *PPFD* of 1000 μmol m^{-2} s^{-1}) are available, but the link between isoprene emission and photosynthetic parameters (J_{max}, V_{cmax}) is not represented in the current datasets.

My model accounts for instantaneous responses of isoprene emission to changes in its main drivers (*PPFD*, *T*, C_i), but acclimation processes in the plant capacity to emit isoprene may exist and are not described yet. We know that plants' capacity for emitting isoprene varies through ontogeny, and with prior conditions of temperature and *PPFD*, drought events, and CO_2 growth conditions. Understanding how and why the leaf acclimates its isoprene emission capacity (as also its photosynthetic capacity) to external

conditions is crucial to improve process-based modelling of isoprene emission. One particularly important task is to better understand (and include in models) the response of isoprene emission capacity to the CO_2 concentration at which the plants were grown. This point is essential. It is generally recognized now that increased atmospheric CO_2 concentration inhibits the capacity of the plant to emit isoprene. At the global scale, CO_2 inhibition seems (according to modelling studies performed so far) to effectively cancel the otherwise expected increase of emissions due to warming (Possell *et al.*, 2005; Young *et al.*, 2009; Heald *et al.*, 2009; Pacifico *et al.*, 2012). CO_2 inhibition is usually represented by downscaling I_s. But some recent studies, conducted by Z. Sun, Ü. Niinemets and co-workers, have shown that the long-term CO_2 inhibition effect also depends on the conditions of *PPFD*, temperature or C_i at which isoprene emission is measured (Sun *et al.*, 2013). As yet we have no comprehensive framework to predict such complexities.

I conclude this thesis with two isoprene-related 'wishes'. My first wish is to see, through a closer collaboration between experimentalists and modellers, the construction of a dataset exploring leaf-scale responses of isoprene emission to changes in *T*, *PPFD*, C_i, and growth CO_2 concentration measured together. Such a dataset would allow more systematic testing of alternative modelling hypotheses. My second wish is to see a renewed focus on large-scale modelling of isoprene emission, which would explicitly test the impact of alternative hypotheses on the amount and the spatial distribution of future isoprene emissions.

Bibliography

Affek HP, Yakir D. **2003**. Natural abundance carbon isotope composition of isoprene reflects incomplete coupling between isoprene synthesis and photosynthetic carbon flow. *Plant Physiology* **131**: 1727–1736.

Archibald AT, Levine JG, Abraham NL, Cooke MC, Edwards PM, Heard DE, Jenkin ME, Karunaharan A, Pike RC, Monks PS, *et al.* 2011. Impacts of HOx regeneration and recycling in the oxidation of isoprene: Consequences for the composition of past, present and future atmospheres. *Geophysical Research Letters* **38**: L05804.

Archer S, Zitser SF.**1994**. Land cover change and regional tropospheric chemistry. In: *National Institute for Global Environmental Change.* Annual Report to the US DoE, 168–171.

Arneth A, Harrison SP, Zaehle S, Tsigaridis K, Menon S, Bartlein PJ, Feichter J. **2010**. Terrestrial biogeochemical feedbacks in the climate system. *Nature geoscience* **3**: 525–532.

Arneth A, Miller PA, Scholze M, Hickler T, Schurgers G, Smith B, Prentice IC. **2007a**. CO_2 inhibition of global terrestrial isoprene emissions: Potential implications for atmospheric chemistry. *Geophysical Research Letters* **34**: L18813.

Arneth A, Monson RK, Schurgers G, Niinemets Ü, Palmer PI. **2008a**. Why are estimates of global terrestrial isoprene emissions so similar (and why is this not so for monoterpenes)? *Atmospheric Chemistry and Physics* **8**: 4605–4620.

Arneth A, Niinemets Ü, Pressley S, Bäck J, Hari P, Karl T, Noe S, Prentice I, Serça D, Hickler T, *et al.* 2007b. Process-based estimates of terrestrial ecosystem isoprene emissions: incorporating the effects of a direct CO_2-isoprene interaction. *Atmospheric Chemistry and Physics* **7**: 31–53.

Arneth A, Schurgers G, Hickler T, Miller PA. **2008b**. Effects of species composition, land surface cover, CO_2 concentration and climate on isoprene emissions from European forests. *Plant biology* **10**: 150–162.

Arneth A, Schurgers G, Lathiere J, Duhl T, Beerling DJ, Hewitt CN, Martin M, Guenther A. **2011**. Global terrestrial isoprene emission models: sensitivity to variability in climate and vegetation. *Atmospheric Chemistry and Physics* **11**: 8037–8052.

Ashworth K, Wild O, Hewitt CN. **2013**. Impacts of biofuel cultivation on mortality and crop yields. *Nature Climate Change* **3**: 492–496.

Atkinson R. **2000**. Atmospheric chemistry of VOCs and NOx. *Atmospheric Environment* **34**: 2063–2101.

Auble DL, Meyers TP. **1992**. An open path, fast response infrared absorption gas analyzer for H_2O and CO_2. *Boundary Layer Meteorology* **59**: 243–250.

Baker NR. **2008**. Chlorophyll fluorescence: a probe of photosynthesis in vivo. *Annual review of plant biology* **59**: 89–113.

Banerjee A, Wu Y, Banerjee R, Li Y, Yan H, Sharkey TD. **2013**. Feedback inhibition of deoxy-D-xylulose-5-phosphate synthase regulates the methylerythritol 4-phosphate pathway. *The Journal of biological chemistry* **288**: 16926–36.

Barkley MP, Kurosu TP, Chance K, De Smedt I, Van Roozendael M, Arneth A, Hagberg D, Guenther A. **2012**. Assessing sources of uncertainty in formaldehyde air mass factors over tropical South America: Implications for top-down isoprene emission estimates. *Journal of Geophysical Research* **117**: D13304.

Barkley MP, Palmer PI, Ganzeveld L, Arneth A, Hagberg D, Karl T, Guenther A, Paulot F, Wennberg PO, Mao J, *et al.* 2011. Can a "state of the art" chemistry transport model simulate Amazonian tropospheric chemistry? *Journal of Geophysical Research* **116**: D16.

Barkley MP, Palmer PI, Kuhn U, Kesselmeier J, Chance K, Kurosu TP, Martin R V., Helmig D, Guenther A. **2008**. Net ecosystem fluxes of isoprene over tropical South America inferred from Global Ozone Monitoring Experiment (GOME) observations of HCHO columns. *Journal of Geophysical Research* **113**: D20304.

Barkley MP, De Smedt I, Van Roozendael M, Kurosu TP, Chance K, Arneth A, Hagberg D, Guenther A, Paulot F, Marais E, *et al.* 2013. Top-down isoprene emissions over tropical South America inferred from SCIAMACHY and OMI formaldehyde columns. *Journal of Geophysical Research: Atmospheres* **118**: 6849–6868..

Behnke K, Ehlting B, Teuber M, Bauerfeind M, Louis S, Hänsch R, Polle A, Bohlmann J, Schnitzler J. **2007**. Transgenic, non-isoprene emitting poplars don't like it hot. *The Plant journal* **51**: 485–499.

Behnke K, Loivamäki M, Zimmer I, Rennenberg H, Schnitzler J, Louis S. **2010**. Isoprene emission protects photosynthesis in sunfleck exposed Grey poplar. *Photosynthesis research* **104**: 5–17.

Bernacchi CJ, Portis AR, Nakano H, von Caemmerer S, Long SP. **2002**. Temperature response of mesophyll conductance . Implications for the determination of Rubisco enzyme kinetics and for limitations to photosynthesis in vivo. *Plant Physiology* **130**: 1992–1998.

Bernacchi CJ, Singsaas EL, Pimentel C, Portis ARJ, Long SP. **2001**. Improved temperature response functions for models of Rubisco-limited photosynthesis. *Plant, Cell and Environment* **24**: 253–260.

Bloom AJ, Caldwell RM, Finazzo J, Warner RL, Weissbart J. **1989**. Oxygen and carbon dioxide fluxes from barley shoots depend on nitrate assimilation. *Plant physiology* **91**: 352–6.

Brilli F, Barta C, Fortunati A, Lerdau M, Loreto F, Centritto M. **2007**. Response of isoprene emission and carbon metabolism to drought in white poplar (*Populus alba*) saplings. *The New phytologist* **175**: 244–254.

Brooks A, Farquhar GD. **1985**. Effect of temperature on the CO_2/O_2 specificity o f ribulose- 1,5-bisphosphate carboxylase/oxygenase and the rate of respiration in the light. *Planta* **165**: 397–406.

Bryan AM, Bertman SB, Carroll MA, Dusanter S, Edwards GD, Forkel R, Griffith S, Guenther AB, Hansen RF, Helmig D, Jobson BT, Keutsch FN, Lefer BL, Pressley SN, Shepson PB, Stevens PS, Steiner AL. 2012. In-canopy gas-phase chemistry during CABINEX 2009: sensitivity of a 1-D canopy model to vertical mixing and isoprene chemistry. *Atmospheric Chemistry and Physics* **12**: 8829–8849.

Von Caemmerer S. **2000**. *Biochemical models of leaf photosynthesis.* (ACP Victoria, Ed.).

Calfapietra C, Wiberley AE, Falbel TG, Linskey AR, Mugnozza GS, Karnosky DF, Loreto F, Sharkey TD. **2007**. Isoprene synthase expression and protein levels are reduced under elevated O_3 but not under elevated CO_2 (FACE) in field-grown aspen trees. *Plant, cell and environment* **30**: 654–661.

Campbell WH. **1988**. Nitrate reductase and its role in nitrate assimilation in plants. *Physiologia Plantarum* **74**: 214–219.

Canvin DT, Atkins CA. **1974**. Nitrate , nitrite and ammonia assimilation by leaves : effect of light , carbon dioxide and oxygen. *Planta* **116**: 207–224.

Cen Y, Sage RF. **2005**. The regulation of Rubisco rctivity in response to variation in temperature and atmospheric CO_2 partial pressure in sweet potato. *Plant physiology* **139**: 979–990.

Carlton AG, Wiedinmyer C, Kroll JH. **2009**. A review of Secondary Organic Aerosol (SOA) formation from isoprene. *Atmospheric Chemistry and Physics* **9**: 4986–5005.

Carslaw KS, Boucher O, Spracklen D V., Mann GW, Rae JGL, Woodward S, Kulmala M. **2010**. A review of natural aerosol interactions and feedbacks within the Earth system. *Atmospheric Chemistry and Physics* **10**: 1701–1737.

Charon L, Pale-grosdemange C, Rohmer M. **1999**. On the reduction steps in the mevalonate independent 2-C-MethyI-D-erythritol 4-phosphate (MEP) pathway for isoprenoid biosynthesis in the bacterium *Zymomonas mobilis*. *Tetrahedron Letters* **40**: 7231–7234.

Claeys M, Graham B, Vas G, Wang W, Vermeylen R, Pashynska V, Cafmeyer J, Guyon P, Andreae MO, Artaxo P, *et al.* 2004. Formation of secondary organic aerosols through photooxidation of isoprene. *Science* **303**: 1173–1176.

Crafts-Brandner SJ, Salvucci ME. **2000**. Rubisco activase constrains the photosynthetic potential of leaves at high temperature and CO_2. *Proceedings of the National Academy of Sciences of the United States of America* **97**: 13430–13435.

Collins WJ, Derwent RG, Johnson CE, Stevenson DS. **2002**. The oxidation of organic compounds in the troposphere and their global warming potentials. *Climatic Change* **52**: 453–479.

Collins WJ, Sitch S, Boucher O. **2010**. How vegetation impacts affect climate metrics for ozone precursors. *Journal of Geophysical Research* **115**: D23.

Cornic G, Briantais J-M. **1991**. Partitioning of photosynthetic electron flow between CO_2 and O_2 reduction in a C3 leaf (*Phaseolus vulgaris* L.) at different CO_2 concentrations and during drought stress. *Planta* **183**: 178–184.

Dani KGS, Jamie IM, Prentice IC, Atwell BJ. **2014**. Evolution of isoprene emission capacity in plants. *Trends in plant science*.

Delwiche CF, Sharkey TD. **1993**. Rapid appearance of ^{13}C in biogenic isoprene when $^{13}CO_2$ is fed to intact leaves. *Plant, Cell and Environment* **16**: 587–591.

Dietz K-J, Schreiber U, Heber U. **1985**. The relationship between the redox state of Q_A and photosynthesis in leaves at various carbon-dioxide, oxygen and light regimes. *Planta* **166**: 219–226.

Edney E, Kleindienst T, Jaoui M, Lewandowski M, Offenberg J, Wang W, Claeys M. **2005**. Formation of 2-methyl tetrols and 2-methylglyceric acid in secondary organic aerosol from laboratory irradiated isoprene/NO/SO/air mixtures and their detection in ambient PM samples collected in the eastern United States. *Atmospheric Environment* **39**: 5281–5289.

Eichelmann H, Oja V, Peterson RB, Laisk A. **2011**. The rate of nitrite reduction in leaves as indicated by O_2 and CO_2 exchange during photosynthesis. *Journal of experimental botany* **62**: 2205–2215.

Evans RC, Tingey DT, Gumpertz ML, Burns WF. **1982**. Estimates of isoprene and monoterpene emission rates in plants. *Botanical Gazette* **143**: 304–310

Fan J., Zhang R. 2004. Atmospheric oxidation mechanism of isoprene. *Environmental Chemistry* **1**: 140-149.

Fang C, Monson RK, Cowling EB. **1996**. Isoprene emission, photosynthesis, and growth in sweetgum (*Liquidambar styraciflua*) seedlings exposed to short- and long-term drying cycles. *Tree physiology* **16**: 441–446.

Fares S, Barta C, Brilli F, Centritto M, Ederli L, Ferranti F, Pasqualini S, Reale L, Tricoli D, Loreto F. **2006**. Impact of high ozone on isoprene emission, photosynthesis and histology of developing *Populus alba* leaves directly or indirectly exposed to the pollutant. *Physiologia Plantarum* **128**: 456–465.

Farquhar GD, von Caemmerer S, Berry JA. **1980**. A biochemical model of photosynthetic CO_2 assimilation in leaves of C_3 Species. *Planta* **149**: 78–90.

Fortems-Cheiney A, Chevallier F, Pison I, Bousquet P, Saunois M, Szopa S, Cressot C, Kurosu TP, Chance K, Fried A. **2012**. The formaldehyde budget as seen by a global-scale multi-constraint and multi-species inversion system. *Atmospheric Chemistry and Physics* **12**: 6699–6721.

Foster PN, Prentice IC, Morfopoulos C, Siddall M, van Weele M. **2013**. Isoprene emissions track the seasonal cycle of canopy temperature, not primary production: evidence from remote sensing. *Biogeosciences Discussion* 10: 19571-19601

Fu T, Jacob DJ, Wittrock F, Burrows JP, Vrekoussis M, Henze DK. **2008**. Global budgets of atmospheric glyoxal and methylglyoxal , and implications for formation of secondary organic aerosols. *Journal of Geophysical Research* **113**: D15303.

Fuchs H, Hofzumahaus A, Rohrer F, Bohn B, Brauers T, Dorn H, Häseler R, Holland F, Kaminski M, Li X, *et al.* 2013. Experimental evidence for efficient hydroxyl radical regeneration in isoprene oxidation. *Nature geoscience*: 1023–1026.

Funk JL, Jones CG, Gray DW, Heather L., Hyatt LA, Lerdau MT. **2005**. Variation in isoprene emission from *Quercus rubra* : Sources, causes, and consequences for estimating fluxes. *Journal of Geophysical Research* **110**.

Greenberg JP, Guenther A, Turnipseed A, Jiang, X, Seco, R, Filella I, Estiraste M, Sardans J, Ogaya R, Llusia, J, Peñuelas J. **2104**. A tethered-balloon PTRMS sampling approach for rapid surveying of landscape-scale biogenic VOC fluxes. *Atmospheric Measurement Techniques Discussion* **7**: 979–999

Grote R. **2007**. Sensitivity of volatile monoterpene emission to changes in canopy structure: a model-based exercise with a process-based emission model. *The New phytologist* **173**: 550–561.

Grote R, Mayrhofer S, Fischbach RJ, Steinbrecher R, Staudt M, Schnitzler J-P. **2006**. Process-based modelling of isoprenoid emissions from evergreen leaves of *Quercus ilex* (L.). *Atmospheric Environment* **40**: 152–165.

Grote R, Monson RK, Niinemets Ü. 2013. Leaf-level models of constitutive and stress-driven volatile organic compound emissions. In: Niinemets Ü, Monson RK eds. *Biology, controls and models of tree volatile organic compound emissions*. Berlin: Springer, 315–355.

Grote R, Morfopoulos C, Niinemets Ü, Sun Z, Keenan TF, Pacifico F, Butler T. 2014. A fully integrated isoprenoid emissions model coupling emissions to photosynthetic characteristics. *Plant, Cell and Environment*. Published online.

Grote R, Niinemets Ü. **2008**. Modeling volatile isoprenoid emissions--a story with split ends. *Plant biology* **10**: 8–28.

Guenther AB. **1997**. Seasonal and spatial variations in natural volatile organic compound emissions. *Ecological Applications* **7**: 34–45.

Guenther A. **2008**. Are plant emissions green? *Nature* **452**: 701–702.

Guenther A, Baugh B, Brasseur G, Greenberg J, Harley P, Klinger L, Serça D, Vierling L. **1999**. Isoprene emission estimates and uncertainties for the Central African EXPRESSO study domain. *Journal of Geophysical Research* **104**: 30625–30639.

Guenther A, Hewitt CN, Erickson D, Fall R, Geron C, Graedel T, Harley P, Klinger L, Lerdau M, McKay W, *et al.* 1995. A global model of natural volatile organic compound emissions. *Journal of Geophysical Research* **100**: 8873–8892.

Guenther AB, Jiang X, Heald CL, Sakulyanontvittaya T, Duhl T, Emmons LK, Wang X. **2012**. The Model of Emissions of Gases and Aerosols from Nature version 2.1 (MEGAN2.1): an extended and updated framework for modeling biogenic emissions. *Geoscientific Model Development* **5**: 1471–1492.

Guenther A, Karl T, Harley P, Wiedinmyer C, Palmer PI, Geron C. **2006**. Estimates of global terrestrial isoprene emissions using MEGAN (Model of Emissions of Gases and Aerosols from Nature). *Atmospheric Chemistry and Physics* **6**: 3181–3210.

Guenther AB, Monson RK, Fall R. **1991**. Isoprene and monoterpene emission rate variability : Observations with eucalyptus and emission rate algorithm development. *Journal of Geophysical Research* **96**: 10799–10808.

Guenther AB, Zimmerman PR, Harley PC, Monson RK, Fall R. **1993**. Isoprene and monoterpene emission rate variability: model evaluations and sensitivity analyses. *Journal of Geophysical Research* **98**: 12609–12617.

Hardacre CJ, Palmer PI, Baumanns K, Rounsevell M, Murray-Rust D. **2013**. Probabilistic estimation of future emissions of isoprene and surface oxidant chemistry associated with land-use change in response to growing food needs. *Atmospheric Chemistry and Physics* **13**: 5451–5472.

Harley PC, Baldocchi D. **1995**. Scaling carbon dioxide and water vapour exchange from leaf to canopy in a deciduous forest. I. Leaf model parametrization. *Plant, Cell and Environment* **18**: 1146–1156.

Harley P, Guenther AB, Zimmerman P. **1996**. Effects of light, temperature and canopy position on net photosynthesis and isoprene emission from sweetgum (*Liquidambar styraciflua*) leaves. *Tree physiology* **16**: 25–32.

Harley PC, Thomas RB, Reynolds JF, Strain BR. **1992**. Modelling photosynthesis of cotton grown in elevated CO_2. *Plant, Cell and Environment* **15**: 271–282.

Harrison SP, Morfopoulos C, Dani KGS, Prentice IC, Arneth A, Atwell BJ, Barkley MP, Leishman MR, Loreto F, Medlyn BE, *et al.* 2013. Volatile isoprenoid emissions from plastid to planet. *The New phytologist* **197**: 49–57.

Hauglustaine DA, Lathière J, Szopa S, Folberth GA. **2005**. Future tropospheric ozone simulated with a climate-chemistry- biosphere model. *Geophysical Research Letters* **32**: L24807.

Haxeltine A, Prentice IC. **1996**. BIOME3: An equilibrium terrestrial biosphere model based on ecophysiological constraints, resource availability, and competition among plant functional types. *Global Biogeochemical Cycles* **10**: 693–709.

Hills AJ, Zimmerman PR. **1990**. Isoprene measurement by ozone-induced chemiluminescence. *Analytical chemistry* **62**: 1055–1060.

Heald CL, Henze DK, Horowitz LW, Feddema J, Lamarque J-F, Guenther A, Hess PG, Vitt F, Seinfeld JH, Goldstein a. H, *et al.* 2008. Predicted change in global secondary organic aerosol concentrations in response to future climate, emissions, and land use change. *Journal of Geophysical Research* **113**: D05211.

Heald CL, Wilkinson MJ, Monson RK, Alo CA, Wang G, Guenther A. **2009**. Response of isoprene emission to ambient CO_2 changes and implications for global budgets. *Global Change Biology* **15**: 1127–1140.

Hecht S, Eisenreich W, Adam P, Amslinger S, Kis K, Bacher a, Arigoni D, Rohdich F. **2001**. Studies on the nonmevalonate pathway to terpenes: the role of the GcpE (IspG) protein. *Proceedings of the National Academy of Sciences of the United States of America* **98**: 14837–42.

Hewitt C N, Ashworth K, Boynard A, Guenther A, Langford B, Mackenzie AR, Misztal PK, Nemitz E, Owen SM, Possell M, Pugh TAM, Ryan AC, Wild O. **2011**. Ground-level ozone influenced by circadian control of isoprene emissions. *Nature geoscience* **4**: 671–674.

Hewitt CN, Street RA. **1992**. A qualitative assessment of the emission of non-methane hydrocarbon compounds from the biosphere to the atmosphere in the U.K.: Present knowledge and uncertainties. *Atmospheric Environment.* **26A**: 3069–3077.

Hikosaka K, Murakami A, Hirose T. **1999**. Balancing carboxylation and regeneration of ribulose-1,5- bisphosphate in leaf photosynthesis: temperature acclimation of an evergreen tree, *Quercus myrsinaefolia*. *Plant, Cell and Environment* **22**: 841–849.

Holmes JJ, Weger HG, Turpin DH. **1989**. Chlorophyll a fluorescence predicts total photosynthetic electron flow to CO_2 or NO_3^-/NO_2^- under transient conditions. *Plant physiology* **91**: 331–7.

Hoyaux, J., Moureaux, C., Tourneur, D., Bodson, B., Aubinet, M. 2008. Extrapolating gross primary productivity from leaf to canopy scale in a winter wheat crop. *Agricultural and Forest Meteorology* **148**: 668–679.

Huber L, Laville P, Fuentes JD. **1999**. Uncertainties in isoprene emissions from a mixed deciduous forest estimated using a canopy microclimate model. *Journal of Applied Meteorology* **38**: 899–912.

Jardine KJ, Monson RK, Abrell L, Saleska SR. **2011**. Within-plant isoprene oxidation confirmed by direct emissions of oxidation products methyl vinyl ketone and methacrolein. *Global Change Biology* **18**: 973-984.

Jenkin ME, Clemitshaw KC. **2000**. Ozone and other secondary photochemical pollutants: chemical processes governing their formation in the planetary boundary layer. *Atmospheric Environment* **34**: 2499–2527.

Johnson FH, Eyring H, Williams RW. **1942**. The nature of enzyme inhibitions in bacterial luminescence: sulfanilamide, urethane, temperature and pressure.*Journal of Cellular and Comparative Physiology* **20**: 247–268.

Karl T, Fall R, Rosenstiel TN, Prazeller P, Larsen B, Seufert G, Lindinger W. **2002**. On-line analysis of the $^{13}CO_2$ labeling of leaf isoprene suggests multiple subcellular origins of isoprene precursors. *Planta* **215**: 894–905.

Kattge J, Knorr W. **2007**. Temperature acclimation in a biochemical model of photosynthesis: a reanalysis of data from 36 species. *Plant, cell and environment* **30**: 1176–1190.

Keenan TF, Grote R, Sabaté S. **2011**. Overlooking the canopy: The importance of canopy structure in scaling isoprenoid emissions from the leaf to the landscape. *Ecological Modelling* **222**: 737–747.

Keenan TF, Niinemets Ü. 2012. Circadian control of global isoprene emissions. *Nature geoscience* **5**: 435.

Keenan T, Niinemets Ü, Sabate S, Gracia C, Peñuelas J. **2009**. Process based inventory of isoprenoid emissions from European forests: model comparisons, current knowledge and uncertainties. *Atmospheric Chemistry and Physics* **9**: 4053–4076.

Kreuzwieser J, Graus M, Wisthaler A, Hansel A, Rennenberg H. **2002**. Xylem-transported glucose as an additional carbon source for leaf isoprene formation in *Quercus robur*. *New Phytologist* **156**: 171–178.

Kroll JH, Ng NL, Murphy SM, Flagan RC, Seinfeld JH. **2006**. Secondary organic aerosol formation from isoprene photooxidation. *Environmental Science and Technology* **40**: 1869–1877.

Kuhn U, Andreae MO, Ammann C, Araújo a. C, Brancaleoni E, Ciccioli P, Dindorf T, Frattoni M, Gatti L V., Ganzeveld L, *et al.* 2007. Isoprene and monoterpene fluxes from Central Amazonian rainforest inferred from tower-based and airborne measurements, and implications on the atmospheric chemistry and the local carbon budget. *Atmospheric Chemistry and Physics Discussions* **7**: 641–708.

Kuhn U, Rottenberger S, Biesenthal T, Wolf A, Schebeske G, Ciccioli P, Brancaleoni E, Frattoni M, Tavares TM, Kesselmeier J. **2004a**. Seasonal differences in isoprene and light-dependent monoterpene emission by Amazonian tree species. *Global Change Biology* **10**: 663–682.

Kuhn U, Rottenberger S, Biesenthal T, Wolf A, Schebeske G, Ciccioli P, Kesselmeier J. **2004b**. Strong correlation between isoprene emission and gross photosynthetic capacity during leaf phenology of the tropical tree species *Hymenaea courbaril* with fundamental changes in volatile organic compounds emission composition during early leaf development. *Plant, Cell and Environment* **27**: 1469–1485.

Laffineur Q, Aubinet M, Schoon N, Amelynck C, Müller J, Dewulf J, Van Langenhove H, Steppe K, Simpraga M, Heinesch B. **2011**. Isoprene and monoterpene emissions from a mixed temperate forest. *Atmospheric Environment* **45**: 3157–3168.

Laffineur Q, Aubinet M, Schoon N, Amelynck C, Müller J-F, Dewulf J, Steppe K, Heinesch B. **2013**. Impact of diffuse light on isoprene and monoterpene emissions from a mixed temperate forest. *Atmospheric Environment* **74**: 385–392.

Laothawornkitkul J, Taylor JE, Paul ND, Hewitt CN. **2009**. Biogenic volatile organic compounds in the Earth system. *The New phytologist* **183**: 27–51.

Lathière J, Hewitt CN, Beerling DJ. **2010**. Sensitivity of isoprene emissions from the terrestrial biosphere to 20th century changes in atmospheric CO_2 concentration, climate, and land use. *Global Biogeochemical Cycles* **24**.

Lawlor DW, Tezara W. **2009**. Causes of decreased photosynthetic rate and metabolic capacity in water-deficient leaf cells: a critical evaluation of mechanisms and integration of processes. *Annals of botany* **103**: 561–79.

Lehning A, Zimmer W, Steinbrecher R, Brüggemann N, Schnitzler J-P. **1999**. Isoprene synthase activity and its relation to isoprene emission in *Quercus robu*r L. leaves. *Plant, Cell and Environment* **22**: 495–504.

Lelieveld J, Butler TM, Crowley JN, Dillon TJ. **2008**. Atmospheric oxidation capacity sustained by a tropical forest. *Nature* **452**: 737–740.

Lelieveld J, Dentener FJ, Peters W, Krol MC. **2004**. On the role of hydroxyl radicals in the self-cleansing capacity of the troposphere. *Atmospheric Chemistry and Physics* **4**: 2337–2344

Lerdau M, Keller M. **1997**. Controls on isoprene emission from trees in a subtropical dry forest. *Plant, Cell and Environment* **20**: 569–578.

Lerdau MT, Throop HL. **1999**. Isoprene emission and photosynthesis in a tropical forest canopy: implications for model development. *Ecological Applications* **9**: 1109–1117.

Li Z, Ratliff EA, Sharkey TD. **2011**. Effect of temperature on postillumination isoprene emission in oak and poplar. *Plant Physiology* **155**: 1037–1046.

Li Z, Sharkey TD. **2012**. Metabolic profiling of the methylerythritol phosphate pathway reveals the source of post-illumination isoprene burst from leaves. *Plant, Cell and Environment* **36**: 429–437.

Li Z, Sharkey TD 2013. Molecular and pathway controls on biogenic volatile organic compound emissions. In: Niinemets Ü, Monson RK eds. *Biology, controls and models of tree volatile organic compound emissions*. Berlin: Springer, 119-151.

Lichtenthaler HK. **1999**. the 1-deoxy-d-xylulose-5-phosphate pathway of isoprenoid biosynthesis in plants. *Annual review of plant physiology and plant molecular biology* **50**: 47–65.

Lichtenthaler HK, Schwender J, Disch A, Rohmer M. 1997. Biosynthesis of isoprenoids in higher plant chloroplasts proceeds via a mevalonate-independent pathway. *FEBS letters* **400**: 271–274.

Lindinger W, Hansel A, Jordan A. 1998. On-line monitoring of volatile organic compounds at pptv levels by means of proton-transfer-reaction mass spectrometry (PTR-MS) medical applications, food control and environmental research. *International Journal of Mass Spectrometry and Ion Processes* **173**: 191–241.

Lloyd J, Grace J, Miranda AC, Meir P, Wong SC, Miranda HS, Wright IR, Gash JHC, McIntyre J. **1995**. A simple calibrated model of Amazon rainforest productivity based on leaf biochemical properties. *Plant, Cell and Environment* **18**: 1129–1145

Lloyd J, Patiño S, Paiva RQ, Nardoto GB, Quesada C A., Santos AJB, Baker TR, Brand WA, Hilke I, Gielmann H, *et al.* 2010. Optimisation of photosynthetic carbon gain and within-canopy gradients of associated foliar traits for Amazon forest trees. *Biogeosciences* **7**: 1833–1859.

Logan BA, Monson RK, Potosnak MJ. **2000**. Biochemistry and physiology of foliar isoprene production. *Trends in plant science* **5**: 477–81.

Long SP. **1991**. Modification of the response of photosynthetic productivity to rising temperature by atmospheric CO_2 concentrations: Has its importance been underestimated? *Plant, Cell and Environment* **14**: 729–739.

Loreto F. **2002**. Distribution of isoprenoid emitters in the *Quercus* genus around the world: chemo-taxonomical implications and evolutionary considerations based on the ecological function of the trait. *Perspectives in Plant Ecology, Evolution and Systematics* **5/3**: 185–192.

Loreto F, Pinelli P, Brancaleoni E. **2004**. ^{13}C labeling reveals chloroplastic and extrachloroplastic pools of dimethylallyl pyrophosphate and their contribution to isoprene formation. *Plant physiology* **135**: 1903–1907.

Loreto F, Sharkey TD. 1990. A gas-exchange study of photosynthesis and isoprene emission in *Quercus rubra* L. *Planta* **182**: 523–531.

Makkonen R, Asmi A, Kerminen V-M, Boy M, Arneth A, Hari P, Kulmala M. **2012**. Air pollution control and decreasing new particle formation lead to strong climate warming. *Atmospheric Chemistry and Physics* **12**: 1515–1524.

Marais EA, Jacob DJ, Kurosu TP, Chance K, Murphy JG, Reeves C, Mills G, Casadio S, Millet DB, Barkley MP, *et al.* 2012. Isoprene emissions in Africa inferred from OMI observations of formaldehyde columns. *Atmospheric Chemistry and Physics* **14**: 6219–6235.

Martin M, Stirling CM, Humphries SW, Long SP. **2000**. A process-based model to predict the effects of climatic change on leaf isoprene emission rates. *Ecological Modelling* **131**: 161–174.

Mayrhofer S, Teuber M, Zimmer I, Louis S, Fischbach RJ. **2005**. Diurnal and seasonal variation of isoprene biosynthesis-related genes in grey poplar leaves. *Plant physiology* **139**: 474–484.

McKinney KA, Lee BH, Vasta A, Pho T V., Munger JW. **2011**. Emissions of isoprenoids and oxygenated biogenic volatile organic compounds from a New England mixed forest. *Atmospheric Chemistry and Physics* **11**: 4807–4831.

Medlyn BE, Berbigier P, Clement R, Grelle A, Loustau D, Linder S, Wingate L, Jarvis PG, Sigurdsson BD, McMurtrie RE. **2005**. Carbon balance of coniferous forests growing in contrasting climates: Model-based analysis. *Agricultural and Forest Meteorology* **131**: 97–124.

Medlyn BE, Dreyer E, Ellsworth D, Forstreuter M, Harley PC, Kirschbaum MUF, Roux XLE. **2002**. Temperature response of parameters of a biochemically based model of photosynthesis . II . A review of experimental data. *Plant, Cell and Environment* **25**: 1167–1179.

Misson L, Limousin J-M, Rodriguez R, Letts MG. **2010**. Leaf physiological responses to extreme droughts in Mediterranean *Quercus ilex* forest. *Plant, Cell and Environment* **33**: 1898–910.

Monson RK. 2013. Metabolic and gene expression controls on the production of biogenic volatile organic compounds. In: Niinemets Ü, Monson RK eds. *Biology, controls and models of tree volatile organic compound emissions*. Berlin: Springer, 153–179.

Monson RK, Fall R. **1989**. Isoprene emission from aspen leaves : influence of environment and relation to photosynthesis and photorespiration. *Plant physiology* **90**: 267–74.

Monson RK, Grote R, Niinemets Ü, Schnitzler J-P. **2012**. Modeling the isoprene emission rate from leaves. *The New phytologist* **195**: 541–59.

Monson RK, Jaeger CH, Adams WW, Driggers EM, Silver GM, Fall R. **1992**. Relationships among isoprene emission rate, photosynthesis, and isoprene synthase activity as influenced by temperature. *Plant physiology* **98**: 1175–80.

Monson RK, Jones RT, Rosenstiel TN, Schnitzler J. **2013**. Why only some plants emit isoprene. *Plant, cell and environment* **36**: 503–516.

Monson RK, Lerdau MT, Sharkey TD, Schimel DS, Fall R. **1995**. Biological aspects of constructing volatile organic compound emission inventories. *Atmospheric Environment* **29**: 2989–3002.

Monson RK, Trahan N, Rosenstiel TN, Veres P, Moore D, Wilkinson M, Norby RJ, Volder A, Tjoelker MG, Briske DD, *et al.* 2007. Isoprene emission from terrestrial ecosystems in response to global change: minding the gap between models and observations. *Philosophical transactions of the Royal Society A: Mathematical, Physical and Engineering Sciences* **365**: 1677–1695.

Morfopoulos C, Prentice IC, Keenan TF, Friedlingstein P, Medlyn BE, Peñuelas J, Possell M. **2013**. A unifying conceptual model for the environmental responses of isoprene emissions from plants. *Annals of Botany* **112**: 1223–1238.

Morfopoulos C, Sperlich D, Peñuelas J, Filella Cubells I, Llusià J, Medlyn BE, Niinemets Ü, Possell M, Sun Z, Prentice IC. 2014. A model of plant isoprene emission based on available reducing power captures responses to atmospheric CO_2. *The New Phytologist* Accepted.

Moriasi DN, Arnold JG, Liew MW Van, Bingner RL, Harmel RD, Veith TL. **2007**. Model evaluation guidelines for systematic quantification of accuracy in watershed simulations. *transactions of the ASABE* **50**: 885–900.

Murchie EH, Lawson T. **2013**. Chlorophyll fluorescence analysis: a guide to good practice and understanding some new applications. *Journal of Experimental Botany* **64**: 3983–98.

Nash J, Sutcliffe J. **1970**. River flow forecasting through conceptual models. Part I. *Journal of Hydrology* **10**: 282–290.

Niinemets Ü. **2004**. Costs of production and physiology of emission of volatile leaf isoprenoids. *Advances in plant physiology* **7**: 233–268.

Niinemets Ü. **2010**. Mild versus severe stress and BVOCs: thresholds, priming and consequences. *Trends in plant science* **15**: 145–53.

Niinemets Ü, Cescatti A, Rodeghiero M, Tosens T. **2005**. Leaf internal diffusion conductance limits photosynthesis more strongly in older leaves of Mediterranean evergreen broad-leaved species. *Plant, Cell and Environment* **28**: 1552–1566.

Niinemets Ü, Ciccioli P, Noe SM, Reichstein M. 2013. Scaling BVOC emissions from leaf to canopy and landscape: how different are predictions based on contrasting emission algorithms? In: Niinemets Ü, Monson RK eds. *Biology, controls and models of tree volatile organic compound emissions*. Berlin: Springer, 357–390.

Niinemets Ü, Copolovici L, Hüve K. **2010a**. High within-canopy variation in isoprene emission potentials in temperate trees: Implications for predicting canopy-scale isoprene fluxes. *Journal of Geophysical Research* **115**: G04029.

Niinemets Ü, Monson RK .2013. State-of-the-art of BVOC research: what do we have and what have we missed? A synthesis. In: Niinemets Ü, Monson RK eds. *Biology, controls and models of tree volatile organic compound emissions*. Berlin: Springer, 509–528.

Niinemets Ü, Monson RK, Arneth A, Ciccioli P, Kesselmeier J, Kuhn U, Noe SM, Peñuelas J, Staudt M. **2010b**. The leaf-level emission factor of volatile isoprenoids: caveats, model algorithms, response shapes and scaling. *Biogeosciences* **7**: 1809–1832.

Niinemets Ü, Tenhunen JD, Canta NR, Chaves MM, Faria T, Pereira JS, Reynolds JF. **1999a**. Interactive effects of nitrogen and phosphorus on the acclimation potential of foliage photosynthetic properties of cork oak , *Quercus suber*, to elevated atmospheric CO_2 concentrations. *Global Change Biology* **5**: 455–470.

Niinemets Ü, Tenhunen JD, Harley PC, Steinbrecher R. **1999b**. A model of isoprene emission based on energetic requirements for isoprene synthesis and leaf photosynthetic properties for *Liquidambar* and *Quercus*. *Plant, Cell and Environment* **22**: 1319–1335.

Niinemets Ü, Valladares F. **2006**. Tolerance to shade, drought, and waterlogging of temperate northern hemisphere trees and shrubs. *Ecological Monographs* **76**: 521–547.

Ninyerola M, Pons X, Roure, JM. 2000. A methodological approach of climatological modelling of air temperature and precipitation. *International Journal of Climatology* **20**: 1823–1841.

Nozière B, González NJ. D, Borg-Karlson A-K, Pei Y, Redeby JP, Krejci R, Dommen J, Prevot ASH, Anthonsen T. **2011**. Atmospheric chemistry in stereo: A new look at secondary organic aerosols from isoprene. *Geophysical Research Letters* **38**: L11807.

Onoda Y, Hikosaka K, Hirose T. **2005**. The balance between RuBP carboxylation and RuBP regeneration: a mechanism underlying the interspecific variation in acclimation of photosynthesis to seasonal change in temperature. *Functional Plant Biology.* **32**: 903–910.

Owen SM, Peñuelas J. **2005**. Opportunistic emissions of volatile isoprenoids. *Trends in Plant Science* **10**: 420–426.

Paasonen P, Asmi A, Petäjä T, Kajos MK, Äijälä M, Junninen H, Holst T, Abbatt JPD, Arneth A, Birmili W, *et al.* 2013. Warming-induced increase in aerosol number concentration likely to moderate climate change. *Nature Geoscience* **6**: 438–442

Pacifico F, Folberth GA, Jones CD, Harrison SP, Collins WJ. **2012**. Sensitivity of biogenic isoprene emissions to past, present, and future environmental conditions and implications for atmospheric chemistry. *Journal of Geophysical Research* **117**: D22302.

Pacifico F, Harrison SP, Jones CD, Arneth A, Sitch S, Weedon GP, Barkley MP, Palmer PI, Serça D, Potosnak M, *et al.* 2011. Evaluation of a photosynthesis-based biogenic isoprene emission scheme in JULES and simulation of isoprene emissions

under present-day climate conditions. *Atmospheric Chemistry and Physics* **11**: 4371–4389.

Pacifico F, Harrison SP, Jones CD, Sitch S. **2009**. Isoprene emissions and climate. *Atmospheric Environment* **43**: 6121–6135.

Palmer PI, Abbot DS, Fu T-M, Jacob DJ, Chance K, Kurosu TP, Guenther A, Wiedinmyer C, Stanton JC, Pilling MJ, *et al.* 2006. Quantifying the seasonal and interannual variability of North American isoprene emissions using satellite observations of the formaldehyde column. *Journal of Geophysical Research* **111**: D12315.

Palmer PI, Jacob DJ, M. FA, Martin R V. 2003. Mapping isoprene emissions over North America using formaldehyde column observations from space. *Journal of Geophysical Research* **108**: 4180.

Peñuelas J, Marino G, Llusia J, Morfopoulos C, Farré-Armengol G, Filella I. **2013**. Photochemical reflectance index as an indirect estimator of foliar isoprenoid emissions at the ecosystem level. *Nature communications* **4**: 2604.

Peñuelas J, Llusia J. **2003**. BVOCs : Plant defense against climate warming? *Trends in plant science* **8**: 105–109.

Peñuelas J, Staudt M. **2010**. BVOCs and global change. *Trends in plant science* **15**: 133–144.

Pétron G, Harley P, Greenberg J, Guenther A. **2001**. Seasonal temperature variations influence isoprene emission. *Geophysical Research Letters* **28**: 1707–1710.

Pike RC, Young PJ. **2009**. How plants can influence tropospheric chemistry: the role of isoprene emissions from the biosphere. *Weather* **64**: 332–336.

Poisson N, Kanakidou M, Crutzen PJ. 2000. Impact of non-methane hydrocarbons on tropospheric chemistry and the oxidizing power of the global troposphere: 3-dimensional modelling results. *Journal of Atmospheric Chemistry* **36**: 157–230.

Possell M, Heath J, Nicholas Hewitt C, Ayres E, Kerstiens G. **2004**. Interactive effects of elevated CO_2 and soil fertility on isoprene emissions from *Quercus robur*. *Global Change Biology* **10**: 1835–1843.

Possell M, Hewitt CN. **2011**. Isoprene emissions from plants are mediated by atmospheric CO_2 concentrations. *Global Change Biology* **17**: 1595–1610.

Possell M, Nicholas Hewitt C, Beerling DJ. **2005**. The effects of glacial atmospheric CO_2 concentrations and climate on isoprene emissions by vascular plants. *Global Change Biology* **11**: 60–69.

Possell M, Loreto F .2013. The role of volatile organic compounds in plant resistance to abiotic stresses: responses and mechanisms. In: Niinemets Ü, Monson RK eds.

Biology, controls and models of tree volatile organic compound emissions. Berlin: Springer, 209–235.

Pressley S, Lamb B, Westberg H, Flaherty J, Chen J. **2005**. Long-term isoprene flux measurements above a northern hardwood forest. *Journal of Geophysical Research* **110**: D7.

Pressley S, Lamb B, Westberg H, Vogel C. **2006**. Relationships among canopy scale energy fluxes and isoprene flux derived from long-term, seasonal eddy covariance measurements over a hardwood forest. *Agricultural and Forest Meteorology* **136**: 188–202.

de Pury DGG, Farquhar GD. **1997**. Simple scaling of photosynthesis from leaves to canopies without the errors of big-leaf models. *Plant, Cell and Environment* **20**: 537–557.

Rajabi Memari H, Pazouki L, Niinemets Ü. 2013. The biochemistry and molecular biology of volatile messengers in trees. In: Niinemets Ü, Monson RK eds. *Biology, controls and models of tree volatile organic compound emissions*. Berlin: Springer, 47–93.

Rasulov B, Bichele I, Laisk A, Niinemets Ü. 2013. Competition between isoprene emission and pigment synthesis during leaf development in aspen. *Plant, Cell and Environment* **37**: 724–741.

Rasulov B, Copolovici L, Laisk A, Niinemets Ü. **2009a**. Postillumination isoprene emission: in vivo measurements of dimethylallyldiphosphate pool size and isoprene synthase kinetics in aspen leaves. *Plant physiology* **149**: 1609–1618.

Rasulov B, Hüve K, Bichele I, Laisk A, Niinemets Ü. **2010**. Temperature response of isoprene emission in vivo reflects a combined effect of substrate limitations and isoprene synthase activity: a kinetic analysis. *Plant physiology* **154**: 1558–1570.

Rasulov B, Hüve K, Laisk A, Niinemets Ü. **2011**. Induction of a longer term component of isoprene release in darkened aspen leaves: origin and regulation under different environmental conditions. *Plant physiology* **156**: 816–831.

Rasulov B, Hüve K, Välbe M, Laisk A, Niinemets Ü. **2009b**. Evidence that light, carbon dioxide, and oxygen dependencies of leaf isoprene emission are driven by energy status in hybrid aspen. *Plant physiology* **151**: 448–460.

Reichstein, M., Falge, E., Baldocchi, D., Papale, D., Aubinet, M., Berbigier, P., Bernhofer, C., Buchmann, N., Gilmanov, T., Granier, *et al.* 2005. On the separation of net ecosystem exchange into assimilation and ecosystem respiration: review and improved algorithm. *Global Change Biology* **11**: 1424–1439.

Rosenkranz M, Schnitzler J-P. 2013. Genetic engineering of BVOC emissions from trees. In: Niinemets Ü, Monson RK eds. *Biology, controls and models of tree volatile organic compound emissions*. Berlin: Springer, 95-118.

Rosenstiel TN, Ebbets a L, Khatri WC, Fall R, Monson RK. **2004**. Induction of poplar leaf nitrate reductase: a test of extrachloroplastic control of isoprene emission rate. *Plant biology* **6**: 12–21.

Rosenstiel TN, Potosnak MJ, Griffin KL, Fall R, Monson RK. **2003**. Increased CO_2 uncouples growth from isoprene emission in an agriforest ecosystem. *Nature* **421**: 256–259.

Sanderson MG, Jones CD, Collins WJ, Johnson CE, Derwent RG. **2003**. Effect of climate change on isoprene emissions and surface ozone levels. *Geophysical Research Letters* **30**: 10–13.

Sasaki K, Ohara K, Yazaki K. **2005**. Gene expression and characterization of isoprene synthase from *Populus alba*. *FEBS letters* **579**: 2514–2518.

Sasaki K, Saito T, Lämsä M, Oksman-Caldentey K-M, Suzuki M, Ohyama K, Muranaka T, Ohara K, Yazaki K. **2007**. Plants utilize isoprene emission as a thermotolerance mechanism. *Plant and cell physiology* **48**: 1254–1262.

Schmid HP, Su H-B, Vogel CS, Curtis PS. **2003**. Ecosystem-atmosphere exchange of carbon dioxide over a mixed hardwood forest in northern lower Michigan. *Journal of Geophysical Research* **108**: 4417.

Schnitzler J-P, Lehning A, Steinbrecher R. 1997. Seasonal pattern of isoprene synthase activity in *Quercus robur* leaves and its significance for modeling isoprene emission rates. *Botanica Acta* **110**: 1–4.

Schnitzler J-P, Zimmer I, Bachl a, Arend M, Fromm J, Fischbach RJ. **2005**. Biochemical properties of isoprene synthase in poplar (*Populus* x *canescens*). *Planta* **222**: 777–786.

Seemann M, Tse Sum Bui B, Wolff M, Miginiac-Maslow M, Rohmer M. **2006**. Isoprenoid biosynthesis in plant chloroplasts via the MEP pathway: direct thylakoid/ferredoxin-dependent photoreduction of GcpE/IspG. *FEBS letters* **580**: 1547–1552.

Sharkey TD. **2013**. Is it useful to ask why plants emit isoprene? *Plant, Cell and Environment* **36**: 517–520.

Sharkey TD, Chen X, Yeh S. **2001**. Isoprene increases thermotolerance of fosmidomycin-fed leaves. *Plant Physiology* **125**: 2001–2006.

Sharkey TD, Loreto F. **1993**. Water stress, temperature, and light effects on the capacity for isoprene emission and photosynthesis of kudzu leaves. *Oecologia* **95**: 328–333.

Sharkey TD, Singsaas EL. **1995**. why plants emit isoprene. *Nature* **374**: 769.

Sharkey TD, Singsaas E L, Vanderveer PJ, Geron C. **1996**. Field measurements of isoprene emission from trees in response to temperature and light. *Tree physiology* **16**: 649–654.

Sharkey TD, Wiberley AE, Donohue AR. **2008**. Isoprene emission from plants: why and how. *Annals of Botany* **101**: 5–18.

Sharkey TD, Yeh S. **2001**. Isoprene emission from plants. *Annual review of plant physiology and plant molecular biology* **52**: 407–436.

Silver GM, Fall R. **1991**. Enzymatic synthesis of isoprene from dimethylallyl diphosphate in aspen leaf extracts. *Plant physiology* **97**: 1588–1591.

Silver GM, Fall R. **1995**. Characterization of aspen isoprene synthase, an enzyme responsible for leaf isoprene emission to the atmosphere. *The Journal of Biological Chemistry* **270**: 13010–13016.

Singarayer JS, Valdes PJ, Friedlingstein P, Nelson S, Beerling DJ. **2011**. Late Holocene methane rise caused by orbitally controlled increase in tropical sources. *Nature* **470**: 82–85.

Singsaas L, Lerdau M, Winter K, Sharkey TD. **1997**. Isoprene increases thermotolerance of isoprene-emitting species. *Biochimica et Biophysica Acta (BBA)* **115**: 1413–1420.

Singsaas EL, Ort DR, DeLucia EH. **2001**. Variation in measured values of photosynthetic quantum yield in ecophysiological studies. *Oecologia* **128**: 15–23.

Sitch S, Smith B, Prentice IC, Arneth A, Bondeau A, Cramer W, Kaplan JO, Levis S, Lucht W, Sykes MT, *et al.* 2003. Evaluation of ecosystem dynamics, plant geography and terrestrial carbon cycling in the LPJ dynamic global vegetation model. *Global Change Biology* **9**: 161–185.

Siwko ME, Marrink SJ, de Vries AH, Kozubek A, Schoot Uiterkamp AJM, Mark AE. **2007**. Does isoprene protect plant membranes from thermal shock? A molecular dynamics study. *Biochimica et biophysica acta* **1768**: 198–206.

Stavrakou T, Müller J-F, De Smedt I, Van Roozendael M, van der Werf GR, Giglio L, Guenther A. **2009**. Evaluating the performance of pyrogenic and biogenic emission inventories against one decade of space-based formaldehyde columns. *Atmospheric Chemistry and Physics* **9**: 1037–1060.

St.Paul NKM, Limousin J-M, Rodríguez-Calcerrada J, Ruffault J, Rambal S, Matthew LG, Misson L. **2012**. Photosynthetic sensitivity to drought varies among populations of *Quercus ilex* along a rainfall gradient. *Functional Plant Biology* **39**: 25–37.

Sun Z, Hüve K, Vislap V, Niinemets Ü. **2013a**. Elevated [CO_2] magnifies isoprene emissions under heat and improves thermal resistance in hybrid aspen. *Journal of experimental botany* **64**: 5509–5523.

Sun Z, Niinemets Ü, Hüve K, Noe SM, Rasulov B, Copolovici L, Vislap V. **2012**. Enhanced isoprene emission capacity and altered light responsiveness in aspen grown under elevated atmospheric CO_2 concentration. *Global Change Biology* **18**: 3423–3440.

Sun Z, Niinemets U, Hüve K, Rasulov B, Noe SM. **2013b**. Elevated atmospheric CO_2 concentration leads to increased whole-plant isoprene emission in hybrid aspen (*Populus tremula* × *Populus tremuloides*). *The New phytologist* **198**: 788–800.

Tai APK, Mickley LJ, Heald CL, Wu S. **2013**. Effect of CO_2 inhibition on biogenic isoprene emission: Implications for air quality under 2000-to-2050 changes in climate, vegetation and land use. *Geophysical Research Letters* **40**: 3479–3483.

Tingey DT, Evans R, Gumpertz M. **1981**. Effects of environmental conditions on isoprene emission from live oak. *Planta* **152**: 565–570.

Trowbridge AM, Asensio D, Eller ASD, Way DA, Wilkinson MJ, Schnitzler J-P, Jackson RB, Monson RK. **2012**. Contribution of various carbon sources toward isoprene biosynthesis in poplar leaves mediated by altered atmospheric CO_2 concentrations. *PloS one* **7**: e32387.

Unger N, Harper K, Zheng Y, Kiang NY, Aleinov I, Arneth A, Schurgers G, Amelynck C, Goldstein A, Guenther A, *et al.* 2013. Photosynthesis-dependent isoprene emission from leaf to planet in a global carbon-chemistry-climate model. *Atmospheric Chemistry and Physics* **13**: 10243–10269.

Urbanski S, Barford C, Wofsy S, Kucharik C, Pyle E, Budney J, McKain K, Fitzjarrald D, Czikowsky M, Munger JW. 2007. Factors controlling CO_2 exchange on timescales from hourly to decadal at Harvard Forest. *Journal of Geophysical Research* **112**: G02020.

Valdes PJ, Beerling DJ, Johnson CE. 2005. The ice age methane budget. *Geophysical Research Letters* **32**: L02704.

Velikova V, Pinelli P, Pasqualini S, Reale L, Ferranti F, Loreto F. **2005**. Isoprene decreases the concentration of nitric oxide in leaves exposed to elevated ozone. *New Phytologist* **166**: 419–426.

Velikova V, Sharkey TD, Loreto F. **2012**. Stabilization of thylakoid membranes in isoprene-emitting plants reduces formation of reactive oxygen species. *Plant Signaling and Behavior* **7:**1.

Velikova V, Váarkonyi Z, Szabóo M, Maslenkova L, Nogues I, Kovács L, Peeva V, Busheva M, Garab G, Sharkey TD, *et al.* 2011. Increased thermostability of thylakoid membranes in isoprene-emitting leaves probed with three biophysical techniques. *Plant physiology* **157**: 905–916.

Vickers CE, Gershenzon J, Lerdau MT, Loreto F. **2009a**. A unified mechanism of action for volatile isoprenoids in plant abiotic stress. *Nature Chemical Biology* **5**: 283–291.

Vickers CE, Possell M, Cojocariu CI, Velikova VB, Laothawornkitkul J, Ryan A, Mullineaux PM, Hewitt CN. **2009b**. Isoprene synthesis protects transgenic tobacco plants from oxidative stress. *Plant, cell and environment* **32**: 520–531.

Vickers CE, Possell M, Hewitt CN, Mullineaux PM. **2010**. Genetic structure and regulation of isoprene synthase in Poplar (*Populus* spp.). *Plant molecular biology* **73**: 547–558.

Weise SE, Li Z, Sutter AE, Corrion A, Banerjee A, Sharkey TD. **2013**. Measuring dimethylallyl diphosphate available for isoprene synthesis. *Analytical biochemistry* **435**: 27–34.

Wiedinmyer C, Guenther A, Harley P, Hewitt N, Geron C, Artaxo P, Steinbrecher R, Rasmussen R. **2004**. Global organic emissions from vegetation. In *Emissions of atmospheric trace compounds*. Springer Netherlands: 115–170.

Wildermuth MC, Fall R. **1996**. Light-Dependent lsoprene Emission. *Plant Physiology* **112**: 171–182.

Wilkinson MJ, Monson RK, Trahan N, Lee S, Brown E, Jackson RB, Polley HW, Fay PA, Fall R. **2009**. Leaf isoprene emission rate as a function of atmospheric CO_2 concentration. *Global Change Biology* **15**: 1189–1200.

Williams C. **1860**. On isoprene and caoutchine. *Proceedings of the Royal Society of London* **10**: 516–519.

Wolfertz M, Sharkey TD, Boland W, Kühnemann F, Yeh S, Weise SE. **2003**. Biochemical regulation of isoprene emission. *Plant, Cell and Environment* **26**: 1357–1364.

Ye Z-P, Suggett DJ, Robakowski P, Kang H-J. **2013**. A mechanistic model for the photosynthesis-light response based on the photosynthetic electron transport of photosystem II in C_3 and C_4 species. *New Phytologist* **199**: 110–120.

Young PJ, Arneth A, Schurgers G, Zeng G, Pyle JA. **2009**. The CO_2 inhibition of terrestrial isoprene emission significantly affects future ozone projections. *Atmospheric Chemistry and Physics* **9**: 2793–2803.

Zimmer W, Brüggemann N, Emeis S, Giersch C, Lehning A, Steinbrecher R, Schnitzler J-P. **2000**. Process-based modelling of isoprene emission by oak leaves. *Plant, Cell and Environment* **23**: 585–595.

Zimmer W, Steinbrecher R, Körner C, Schnitzler J-P. **2003**. The process-based SIM – BIM model : towards more realistic prediction of isoprene emissions from adult *Quercus petraea* forest trees. *Atmospheric Environment* **37**: 1665–1671.

Supplementary material

S1. The Guenther *et al.* (1993) algorithm

In the Guenther *et al.* (1993) algorithm (G93) isoprene emission rate of isoprene (I) is calculated by multiplying a species-specific standard emission rate (I_S) by a set of empirical equations taking in account changes in environmental factors. The standard conditions for estimation of I_S are a leaf temperature of 30˚C and a *PPFD* of 1000 μmol m^{-2} s^{-1}. Guenther *et al.* (1993) solely considered changes in *PPFD* and temperature:

$$I = I_s C_L C_T, \tag{s1.1}$$

with

$$C_L = \frac{\alpha C_{L1} PPFD}{\sqrt{(1+\alpha^2 PPFD^2)}} \tag{s1.2}$$

and

$$C_T = \frac{\exp\left(\frac{C_{T1}(T_k - T_{ks})}{R T_k T_{ks}}\right)}{C_{T3} + \exp\left(\frac{C_{T2}(T_k - T_{ks})}{R T_k T_{ks}}\right)} \tag{s1.3}$$

where T_k (K) is the leaf temperature, T_{ks} is the temperature at standard conditions (= 303 K), R is the gas constant (= 8.314 J K^{-1} mol^{-1}), *PPFD* is the photosynthetic photon flux density. C_{L1}, α, C_{T1}, C_{T2}, C_{T3} and T_m are empirical coefficients:C_{L1} = 1.066, α = 0.027, C_{T1} = 95 000 J mol^{-1}, C_{T2} = 230 000 J mol^{-1}, C_{T3} = 0.961 J mol^{-1} and T_m = 314 K.

S2. Model of photosynthetic carbon assimilation (Farquhar *et al.,* 1980)

The model for photosynthetic carbon assimilation is based on the Farquhar model (Farquhar *et al.*, 1980). Temperature responses of the different parameters are described in Medlyn *et al*. (2002), and based on previous work from (Harley *et al*., 1986, 1992; Long, 1991; Harley & Baldocchi, 1995; Lloyd *et al*., 1995; Bernacchi *et al*., 2001).

Calculation of the light limited electron flux (J):

$$J = \frac{(\alpha\, PPFD + J_{\max}) - \sqrt{(\alpha\, PPFD + J_{\max})^2 - 4\alpha\,\theta\, PPFD\, J_{\max}}}{2\theta} \quad \text{(s2.1)}$$

$$J_{\max} = J_{\max 25} \exp\left(E_{\mathrm{aJ}} \left(\frac{1}{298.15} - \frac{1}{T_{\mathrm{k}}} \right) \right) \cdot \left(\frac{J_1}{J_2} \right) \quad \text{(s2.2)}$$

$$J_1 = 1 + \exp\left(\frac{\left(298.15 \cdot \Delta S - E_{\mathrm{dJ}} \right)}{298.15 \cdot R} \right) \quad \text{(s2.3)}$$

$$J_2 = 1 + \exp\left(\frac{\left(T_{\mathrm{k}}\, \Delta S - E_{\mathrm{dJ}} \right)}{R T_{\mathrm{k}}} \right) \quad \text{(s2.4)}$$

$J_{\max 25}$ is the value of $J_{\max}$ at 25˚C, α taken at 0.385 mol electron mol^{-1} photon (if not adjusted to data), θ is a curvature parameter for the light response and T_{k} is the temperature in K. Other symbols are summarized in Table S2.1

Calculation of the Rubisco capacity (V_{cmax})*, Γ*, k_{c}* and k_{o}:

$$V_{c\max} = V_{c\max 25} \exp\left(E_{\mathrm{a}} \left(\frac{1}{298.15} - \frac{1}{T_{\mathrm{k}}} \right) \right) \quad \text{(s2.5)}$$

$$k_{\mathrm{c}} = 404.9 \exp\left(79430 \frac{\left(T_{\mathrm{k}} - 298.15 \right)}{298.15\, R\, T_{\mathrm{k}}} \right) \quad \text{(s2.6)}$$

$$k_{\mathrm{o}} = 278.4 \exp\left(36380 \frac{\left(T_{\mathrm{k}} - 298.15 \right)}{298.15\, R\, T_{\mathrm{k}}} \right) \quad \text{(s2.7)}$$

$$\Gamma^* = 42.75 \exp\left(37830 \frac{\left(T_k - 298.15\right)}{298.15 R T_k} \right) \quad \text{(s2.8)}$$

V_{cmax25} is the value of V_{cmax} at 25˚C, k_c and k_o are the Michaelis coefficients of Rubisco for CO_2 and O_2 respectively and Γ^* is the CO_2 compensation point in the absence of dark respiration. Other symbols are summarized in Table S2.1

Table S2.1 Description and values of the parameters of Farquhar model used in standard simulations (Medlyn *et al.,* 2005)

Symbol	Definition	Unit	Value
E_{aJ}	Activation energy for J	kJ mol^{-1}	38.670
E_{dJ}	Deactivation energy for J	kJ mol^{-1}	200
E_a	Activation energy for V_{cmax}	kJ mol^{-1}	58. 520
E_d	Deactivation energy for V_{cmax}	kJ mol^{-1}	200
ΔS	Entropy term	kJ mol^{-1} K^{-1}	0.6381

S3. List of publications

Morfopoulos C., Sperlich D., Peñuelas J., Filella I., Llusià J., Medlyn B.E., Niinemets Ü., Possell M., Sun Z., Prentice I.C. 2014**.** A model of plant isoprene emission based on available reducing power captures responses to atmospheric CO_2. *The New Phytologist*. DOI: 10.1111/nph.12770. http://onlinelibrary.wiley.com/doi/10.1111/nph.12770/full

Grote R., **Morfopoulos C.**, Niinemets Ü., Sun Z., Keenan T.F., Pacifico F., Butler T. 2014. *Plant, Cell and Environment*. DOI: 10.1111/pce.12326. http://onlinelibrary.wiley.com/doi/10.1111/pce.12326/full

Morfopoulos C., Prentice I.C., Keenan T.F., Friedlingstein P., Medlyn B.E., Peñuelas J., Possell M. 2013. A unifying conceptual model for the environmental responses of isoprene emissions from plants. *Annals of Botany* 112 (7): 1223-1238. DOI: 10.1093/aob/mct206. http://aob.oxfordjournals.org/content/112/7/1223.full

Foster P. N., Prentice I. C., **Morfopoulos C.**, Siddall M., van Weele M.2013. Isoprene emissions track the seasonal cycle of canopy temperature, not primary production: evidence from remote sensing. *Biogeosciences Discussion* 10: 19571-19601. doi:10.5194/bgd-10-19571-2013. http://www.biogeosciences-discuss.net/10/19571/2013/bgd-10-19571-2013.html

Peñuelas J., Marino G., Llusia J., **Morfopoulos C.**, Farré-Armengol G., Filella I. 2013. Photochemical reflectance index as an indirect estimator of foliar isoprenoid emissions at the ecosystem level. *Nature Communications* 4: 2604. doi:10.1038/ncomms3604. http://www.nature.com/ncomms/2013/131010/ncomms3604/full/ncomms3604.html

Harrison, S. P., **Morfopoulos, C**., Dani, K. G. S., Prentice, I. C., Arneth, A., Atwell, B. J., Barkley, M. P., *et al*. 2013. Volatile isoprenoid emissions from plastid to planet. *The New phytologist*, 197 (1), 49-57. DOI: 10.1111/nph.12021. http://onlinelibrary.wiley.com/doi/10.1111/nph.12021/full

Morfopoulos, C., Foster, P. N., Friedlingstein, P., Bousquet, P., & Prentice, I. C. 2012. A global model for the uptake of atmospheric hydrogen by soils. *Global Biogeochemical Cycles*, 26 (3), GB3013. DOI: 10.1029/2011GB004248. http://onlinelibrary.wiley.com/doi/10.1029/2011GB004248/full

Bousquet, P., *et al*. [15 co-authors incl. **Morfopoulos C.**]. 2011. A three-dimensional synthesis inversion of the molecular hydrogen cycle: Sources and sinks budget and implications for the soil uptake, *Journal of Geophysical Research,* 116 (D1), D01302. DOI: 10.1029/2010JD014599. http://onlinelibrary.wiley.com/doi/10.1029/2010JD014599/full


I DID IT.!
I DID IT.!
SOMEHOW I IMAGINED THIS EXPERIENCE WOULD BE MORE REWARDING.